



HAL
open science

Modelling, control and supervision of multi-source system connected to the network with a buffer storage of electrical energy via hydrogen vector

Abdulkader Tabanjat

► **To cite this version:**

Abdulkader Tabanjat. Modelling, control and supervision of multi-source system connected to the network with a buffer storage of electrical energy via hydrogen vector. Electric power. Université de Technologie de Belfort-Montbéliard, 2015. English. NNT : 2015BELF0266 . tel-01619392

HAL Id: tel-01619392

<https://theses.hal.science/tel-01619392>

Submitted on 19 Oct 2017

HAL is a multi-disciplinary open access archive for the deposit and dissemination of scientific research documents, whether they are published or not. The documents may come from teaching and research institutions in France or abroad, or from public or private research centers.

L'archive ouverte pluridisciplinaire **HAL**, est destinée au dépôt et à la diffusion de documents scientifiques de niveau recherche, publiés ou non, émanant des établissements d'enseignement et de recherche français ou étrangers, des laboratoires publics ou privés.

SPIM

Thèse de Doctorat



école doctorale sciences pour l'ingénieur et microtechniques

UNIVERSITÉ DE TECHNOLOGIE BELFORT-MONTBÉLIARD

Modélisation, commande et supervision d'un système multi-sources connecté au réseau avec stockage tampon de l'énergie électrique via le vecteur hydrogène

■ Abdulkader TABANJAT

SPIM

Thèse de Doctorat



école doctorale sciences pour l'ingénieur et microtechniques
UNIVERSITÉ DE TECHNOLOGIE BELFORT-MONTBÉLIARD

Thèse présentée par

Abdulkader TABANJAT

Pour obtenir le

Grade de Docteur de

L'Université de Technologie de Belfort–Montbéliard

Spécialité : Génie Electrique

Modélisation, commande et supervision d'un système multi-sources connecté au réseau avec stockage tampon de l'énergie électrique via le vecteur hydrogène

Soutenue le 25 Septembre 2015 devant le jury :

M. Daniel HISSEL	Directeur	Professeur, Université de Franche–Comté
M. Mohamed BECHERIF	Co-Directeur	Maître de Conférences HDR, Université de Technologie de Belfort–Montbéliard
M. Seddik BACHA	Président	Professeur, Université de Grenoble, Laboratoire G2ELAB
M. Benoit ROBYNS	Rapporteur	Professeur, Ecole des Hautes Etudes d'Ingénieur, Laboratoire L2EP, Lille
M. Achour BETKA	Rapporteur	Professeur, Université de Biskra, Algérie
M. Haïtham RAMADAN	Examinateur	Maître de Conférences, Université de Zagazig, Egypte

PREFACE

The PhD. work, which is presented in this thesis, has been done at the FEMTO-ST laboratory – University of Technology of Belfort-Montbéliard – SPIM Doctoral School, from October 2011 to September 2015.

ACKNOWLEDGEMENTS

This dissertation is not only a result of my own dedication and perseverance, but is largely a credit to the patient and helpful people that I have worked with and to the supporting and understanding people that I have lived with over these past three years. I would like to take this opportunity to express my gratitude to everyone who contributed to this work.

My sincere thanks go to my supervisor Prof. Daniel HISSEL and my co-supervisor Dr. Mohamed BECHERIF, for their confidence in me throughout this thesis and for their valuable guidance during the study.

I would like to thank members of the jury, Prof. Daniel HISSEL, Dr. Mohamed BECHERIF, Prof. Benoit ROBYNS, Prof. Achour BETKA Prof. Seddik BACHA, and Dr. Haïtham RAMADAN for their valuable discussions and insightful comments during the writing of the manuscript.

I am equally indebted to Dr. Haitham RAMADAN for his generous cooperation during the writing of manuscript and papers.

Many thanks go also to Djelalli LARIOUMLIL for his enormous help on implementation of experimental test-bench.

I also extend thanks to Abdelmajid NAIMI for his providing with materials to assist me with test-bench performing.

I would like also to thank my colleagues in FCLab federation, FEMTO-ST laboratory and UTBM University especially Damien GUILBERT, Ali MOHAMMADI, Djafar CHABANE, Mona IBRAHIM, Laurence MARY, Zhixue ZHENG, Zhongliang LI, Simon MORANDO, Soichi FUKUHARA, Bilel HOSNI, Serge AGBLI, Joseba ASENSIO, Aicha SAADI, and to anyone and everyone else who has offer me encouragement, loving reproche, constructive criticism, quality time, a shoulder on which to lean, a place of rest, and/or avenue to be of doctor.

Finally, I am infinitely grateful to my family members for their moral support, especially to my mother for her continuous encouragement and my wife for her understanding during my thesis.

Special thank go to my little daughter Jana who gives my life new colours and different meaning.

Table of contents

Preface.....	i
Acknowledgements	i
General introduction.....	1
Nomenclature	5
1. Introduction.....	17
1.1. Renewable energy production.....	19
1.1.1. Hydropower plants	19
1.1.2. Solar power plants	19
1.1.3. Wind power plants.....	20
1.1.4. Fuel cells.....	21
1.2. Energy storage.....	22
1.2.1. Energy storage technologies.....	23
1.2.1.1. Pumped hydro energy storage.....	23
1.2.1.2. Compressed air energy storage	23
1.2.1.3. Flywheel energy storage	24
1.2.1.4. Supercapacitor energy storage	24
1.2.1.5. Superconducting magnetic energy storage	24
1.2.1.6. Lead acid battery energy storage	24
1.2.1.7. Nickel cadmium battery energy storage	25
1.2.1.8. Lithium ion battery energy storage	25
1.2.1.9. Sodium nickel chloride battery energy storage.....	25
1.2.1.10. Flow battery energy storage.....	26
1.2.2. Comparisons of energy storage techniques	26
1.3. Hydrogen production storage and carries.....	27
1.4. Hybrid power system	30
1.5. Control and energy management.....	30
1.5.1. Centralized control	31
1.5.2. Distributed control.....	32
1.5.3. Hybrid centralized and distributed control paradigm.....	32
1.5.4. Optimization techniques	32
1.6. Modelling methods.....	32

1.6.1.	Electric equivalent model	33
1.6.2.	Bond graph	33
1.6.3.	Causal ordering graph.....	34
1.6.4.	Energetic macroscopic representation	34
1.6.4.1.	Interaction principle	35
1.6.4.2.	Causality principle	35
1.6.4.3.	Inversion principle	36
1.7.	Literature review	36
1.7.1.	PV panels.....	37
1.7.2.	Energy storage systems	40
1.7.3.	Hybrid power systems	41
1.8.	Thesis orientation	43
1.9.	Thesis outline	44
2.	Multi-source system: Modelling and simulation	45
2.1.	Introduction	46
2.2.	PEM Electrolyser	46
2.2.1.	EMR electrical sub-model	46
2.2.2.	EMR electrochemical and thermodynamic sub-model	46
2.2.3.	EMR thermal sub-model	48
2.2.4.	EMR hydraulic sub-model.....	51
2.2.5.	Simulation results	52
2.3.	Fuel Cell	53
2.3.1.	EMR model of PEMFC	53
2.3.2.	EMR electrical sub-model	54
2.3.3.	EMR thermodynamic sub-model.....	54
2.3.4.	EMR thermal sub-model.....	55
2.3.5.	EMR fluidic sub-model.....	55
2.3.6.	PEMFC simulation	56
2.4.	Wind turbines	56
2.4.1.	EMR model of WT	57
2.4.2.	EMR aerodynamic sub-model	57
2.4.3.	EMR shaft sub-model.....	58
2.4.4.	EMR gearbox sub-model.....	58

2.4.5.	EMR induction machine sub-model	58
2.4.6.	Simulation results	60
2.5.	Photovoltaic source	61
2.5.1.	EMR radiometric/photometric sub-model	62
2.5.2.	EMR thermal sub-model	63
2.5.3.	EMR electrical sub-model	64
2.5.4.	PV panels control.....	64
2.5.5.	Simulation results	65
2.6.	Gas micro-turbine.....	65
2.6.1.	GMT control	68
2.6.2.	EMR GMT model.....	70
2.6.3.	Simulation results	70
2.7.	Multi-source EMR model.....	70
2.8.	Conclusion.....	71
3.	PV panels and hydrogen	73
3.1.	Introduction	74
3.2.	PV panel system under-study	74
3.2.1.	PV panel configuration	75
3.2.2.	Maximum power point tracking	76
3.2.3.	PV panel characteristics.....	77
3.2.4.	FL estimator for shaded PV modules control.....	80
3.2.5.	Switching methodology for shaded PV identification removal.....	82
3.2.6.	Control of switches	83
3.3.	PV-PEM electrolyser under-study	88
3.3.1.	PEM electrolyser operation	89
3.3.2.	Energetic macroscopic representation for PEM ELS	91
3.3.3.	FLC design	92
3.3.4.	Simulation results of hybrid PV-PEM ELS.....	92
3.4.	Conclusion.....	96
4.	Energy management of multi-source system.....	97
4.1.	Introduction	98
4.2.	System sizing.....	99
4.2.1.	Gas micro-turbine sizing	99

4.2.2.	PV sizing.....	100
4.2.3.	WTs sizing.....	101
4.2.4.	PEM ELS sizing	103
4.2.5.	FC sizing.....	104
4.2.6.	Energy storage sizing.....	105
4.3.	Energy management strategy	106
4.4.	Energy management using Neural Networks.....	110
4.4.1.	NN inputs.....	112
4.4.2.	NN training, validation and test.....	113
4.4.3.	NN outputs.....	114
4.5.	Energy storage simulation results	115
4.6.	FL for energy management	117
4.7.	Conclusion.....	120
	General conclusion.....	121
	Perspectives.....	122
	References	123
	Appendix	134
	My Publications.....	140
	Abstract	141
	Résumé.....	141

GENERAL INTRODUCTION

The limited reserves of fossil fuel and the pollution gases produced pave the way to promising alternative Renewable Energy Sources (RESs) such as Solar Energy Sources (SEs) and Wind Energy Sources (WESs). SEs and WESs are freely available and environmentally friendly. However, RESs are intermittent in nature. Therefore, the smoothing of power fluctuations by storing the energy during periods of oversupply and restore it to the grid when demand becomes necessary. Accordingly, Energy Storage Systems (ESSs) can be appropriately used for this purpose.

One of long-term ESSs is hydrogen. It is a renewable fuel and excellent energy carrier thanks to its reliability and relative high efficiency conversion. It can be stored in different forms gaseous, liquid or metal hydride. It is environmentally appropriate since there are no pollution gases or materials related to its production, storage, transportation and/or consumption. The importance of hydrogen use becomes a priority solution when the energy produced from RESs is injected with a big amount.

Aiming at solving the intermittence problem of RESs, Hybrid Power System (HPSs) are considered. Obviously, several RESs are considered to be combined with both ESSs and Back-up (BKU) power units or one of them only. Accordingly, several hybridization possibilities of power sources can be obtained: (i) BKU power units are integrated into RESs so that high level of local energy security can be achieved. (ii) Hybridization of primary RESs such as SE and WES: in this case SEs provide their power in the day time and WESs produce usually more powers with stronger wind in the night. (iii) Hybridization of RESs and ESSs: both reliability and security of power generation systems can be ensured. Obviously, the produced and stored energies can be optimised to increase the yield energy of HPSs. (iv) Both fast-dynamic ESS and long-term ESS are hybridized with RESs: This combination of ESSs leads to a more reliable power providing in HPSs for both dynamic and static cases.

Using several energy sources for constructing HPSs alongside with ESS will require an energy management strategy to achieve minimum HPS cost and optimal balance between energy generation and energy consumption. This energy management method is a mechanism to achieve an ideal energy production and to conveniently satisfy the load demand at relatively high efficiency.

PV panels, such as one of main HPS elements, have several operational problems especially shading problems. Numerous solutions have been presented until now. However, the high cost is still the hallmark of these solutions. Therefore, a new solution, making the equilibrium between the cost and the reliability, have been searched. In addition, the relatively PV panels low efficiency has been enhanced by cooling the PV panels.

In this thesis, a HPS including RESs such as main sources combined with GMT and hydrogen storage system such as BKUs has been presented. The aim of this hybridization is to build a reliable system, which is able to supply the load and having the ability to store the excess energy in hydrogen form and reuse it later when demanded. Consequently, the stored energy at the end of each cycle will be about zero and minimum generated power cost is achieved. In addition, partial shading problem of PV panels is comprehensively studied and a new solution based on simple switches and FLC integrated into dSPACE electronic card is created. Consequently, a real time PV panels reconfiguration and disconnecting shaded ones is performed and minimum power losses is achieved. Then, the PV panels are connected to a PEM ELS. The emitted temperature by the PV panels is transferred to the endothermic element PEM ELS. Consequently, an efficiency enhancement of the hybrid system PV- PEM ELS is realized.

The context of the thesis is introduced in the first chapter, and then the thesis work is presented in three chapters:

In the second chapter HPS comprises of PV, WTs, PEM ELS, PEMFC and Gas Micro-Turbine (GMT) has been studied. Each source has been presented using specific EMR model. Accordingly, different equations necessary to realize the different models have been comprehensively illustrated. Consequently, a global model presented the HPS has been obtained.

In the third chapter, HPS comprises 72 kW PV panels and 59 kW PEM ELS has been studied. Accordingly, a new shaded PV panel's solution based on simple switches reconfiguration and dSPACE electronic card has been achieved. In addition, PEM ELS efficiency enhancement based on FL-PI controls has been performed. Consequently, the obtained HPS is able to provide the hydrogen at relatively high efficiency.

In the fourth chapter, sizing and energy management strategies have been applied on a HPS comprising PV, WTs, GMT and FCs sources. Obviously, both NN and FL methods have been applied to achieve an optimal solution with minimum energy production cost. Consequently, a comparison between the two approaches has been performed and economic study has been presented.

The conclusion and the perspectives of this thesis are finally presented in the fifth chapter.

NOMENCLATURE

PEM ELS parameters

A	Cell surface.
A	PEM ELS active surface, (cm^2).
A_{cd}	Nernst potential coefficient, (V/K).
B_{cd}	Nernst potential coefficient (V/K).
C_{dl}	Double layer capacity, (F).
C_h	Hydraulic capacity, $2.7228 \times 10^{-8} \times (N_{cell}/7)$.
C_P	Module heat capacity, ($J kg^{-1} K^{-1}$).
$C_{P_{H_2O}}$	Calorific water capacity, $4180 (J K^{-1} C^{-1})$.
$C_{th-stack}$	Heat capacity of the stack, (J/K).
E	Reversible potential, (V).
$E_{act-anod}$	The anode activation overvoltage.
$E_{act-cath}$	The cathode activation overvoltage.
E_{Nernst}	Nernst potential, (V).
E_{ohm}	Ohmic overvoltage.
F	Faraday constant, $96\,485 (C/mol)$.
I	Rated stack current, $j \times S_{cell} = 300 (A)$.
I_{ELS}	Electrolyser current, (A).
j	Nominal stack current, $0.5 \times 10^4 (A/m^2)$.
$j_{0,A}$	Exchange of anodic current density, (A/cm^2).
$j_{0,C}$	Exchange of cathode current density, (A/cm^2).
M_{H_2}	Hydrogen molar mass, (g/mol).
M_{H_2O}	Water molar mass, (g/mol).
M_{O_2}	Oxygen molar mass, (g/mol).
n	Number of electrons participating in reaction.
\dot{n}	Molar flow.
$\dot{n}_{cathode}$	Molar flow at the cathode.
\dot{n}_{H_2}	Hydrogen molar flow.
\dot{n}_{H_2O}	Water molar flow.
\dot{n}_{losses}	Molar flow of losses.
\dot{n}_{O_2}	Oxygen molar flow.
N_{cell}	Number of cells in series, 90.
P_{atm}	Atmosphere pressure, $1 (Atm) = 1 \times 10^5 (Pa)$.
P_{H_2}	Pressure of hydrogen production, $1.09 \times 10^5 (Pa)$.
P_{O_2}	Pressure of oxygen production, $10^5 (Pa)$.
P_{in_A}	The inlet water pressure at the anode side, (Atm).
P_{out}	The outlet water pressure, (Atm).
P_{stack}	The stack water pressure, (Atm).
Q_{m-H_2, O_2}	Mass flow of hydrogen and oxygen.
$Q_{V-H_2O-outa}$	Volume flow of water to the anode.
$Q_{V-H_2O-outc}$	Volume flow of water at the cathode.
Q_{Vin-H_2O}	Volume flow of water into the reservoir for $N_{cell} = 7$, $3 \times 10^{-6} \times (S_{cell}/S_0) (m^3/s)$.
$Q_{V-H_2O_mem}$	Water volume flow of membrane.

$Q_{V-H_2O_reat}$	Water volume flow of reacting.
R	Perfect gas constant, $8.3144 (JK^{-1}mol^{-1})$.
R_{ej}	Ohmic overvoltage.
Rh_1, Rh_2	Hydraulic resistance, $1.01 \times 10^{10} \times (N_{cell}/7) (Pa sm^3)$.
R_m	Ohmic resistance of a cell, (Ω) .
R_t	Charges transfer resistance, (Ω) .
R_{th}	Thermal resistance parameter adjustment for variation of temperature, $0.2 \times 10^{10} \times (N_{cell}/7), (K/W)$.
S	Laplace variable.
S_{cell}	Cell surface, $600 \times 10^{-4} (m^2)$.
S_0	Active area, $16 \times 10^{-4} (m^2)$.
T	The stack temperature, (K) .
T_{amb}	The ambient temperature, (K) .
T_{in-H_2O}	The water temperature, (K) .
V_{ELS}	Electrolyser voltage, (V) .
$\eta(I_{ELS})$	Activation overvoltage, (V) .
η_{diff}	Diffusion overvoltage, (V) .
α_A	Charge transfer coefficient of the anode.
ΔG	Gibbs free energy variation, (J/mol) .
ΔH	Enthalpy (J) .
ΔH_0	Standard change in enthalpy, (J/mol) .
ΔS	Change in Entropy, $(J/(K.mol))$.
$\Delta S_{cathode}$	Change in Entropy at the cathode, $(J/(K.mol))$.
ΔS_{H_2}	Hydrogen entropy change, $(J/(K.mol))$.
ΔS_{H_2O}	Water entropy change, $(J/(K.mol))$.
ΔS_{losses}	Entropy change of losses, $(J/(K.mol))$.
ΔS_{O_2}	Oxygen entropy change, $(J/(K.mol))$.
ΔS_0	Standard entropy variation, $(J/(K.mol))$.
ΔS_q	Entropy flow, (W/K) .
α	Charge transfer coefficient.
α_C	Charge transfer coefficient of the cathode.
\emptyset	The membrane thickness, $130 \times 10^{-6} (\mu m)$.
σ_m	Membrane conductivity, (s/cm) .
ρ_{H_2O}	Water density, $1 \times 10^3 (Kg/m^3)$.

Fuel cell parameters

$A_{cd}(T_{fc})$	Nernst potential coefficient.
$B_{cd}(T_{fc})$	Nernst potential coefficient.
E_N	Nernst potential variation, (V) .
I_{fc}	Fuel cell current, (I) .
I_{nfc}	Current nominal value of PEMFC system, (A) .
i_{cell}	The cell nominal current, (A) .
j_{cell}	Current density of one cell.
N	Number of cells.
n_{cellp}	The number of stacks in parallel.
P_{fc}	Fuel cell power, (W) .
P_{SCH_2}	Hydrogen partial pressure.

P_{SCO_2}	Oxygen partial pressure.
q_{cH_2}	The volume flow of hydrogen.
q_{cO_2}	The volume flow of oxygen.
R_{dx1}	Fluidic resistance on the supply side.
R_{dx2}	Fluidic resistance on the exhaust side.
R_m	Ohmic resistance of a cell, (Ω).
R_t	Charges transfer resistance, (Ω).
S_{cell}	Cell surface.
V_{fc}	Fuel cell voltage, (V).
ΔE	Potential variation, (V).
ΔS_{qn}	The entropy flow.
ΔV_{act}	Activation voltage drop, (V).
ΔV_{conc}	Concentration voltage drop, (V).
ΔV_{ohm}	Ohmic voltage drop, (V).

Wind turbine parameters

C	Concordia matrix (conservation P): $v_{dq} = [C] \times v_{123}$.
C_{blade}	Torque at blades.
C_{gear}	Torque at gearbox.
C_{inv}	Current transformation matrix from $i = [i_1, i_2]$ to $i = [i_{sa}, i_{sb}, i_{sc}]$.
C_m	The torque at induction machine.
C_p	The power coefficient which represents the aerodynamic efficiency of the wind turbine, it depends on the characteristic of the turbine.
f_{sh}	Coefficient of viscous friction of the shaft.
$F i_{rd}$	Rotor flux.
F_{tg}	Tangential force.
G_{blade}	A gain has been used in the Simulink model to facilitate the calculation of P.
i_{inv}	Current flowing through the inverter.
i_{IM}	Current flowing through the induction machine.
i_{sq}	Stator current.
J_{sh}	Equivalent inertia of the shaft.
K_i	The transfer function static gain of i_{sd} and i_{sq} .
K_{ii}	Current transformation matrix from $i = [i_{s1}, i_{s2}, i_{s3}]$ to $i = [i_{s1}, i_{s2}]$.
K_{uv}	Transformation matrix from u to v ($v = [K_{uv}] * u$) with $u = [u_{13}, u_{23}]$ and $v = [v_{s1n}, v_{s2n}, v_{s3n}]$.
L_r	Self-inductance of rotor, 1.99 (mH).
L_s	Self-inductance of stator, 2.5 (mH).
m_{gear}	Reduction ratio of the gearbox.
m_{inv}	Duty cycle.
M_{sr}	Mutual-inductance between stator and rotor, 2.2 (mH).
P	Nominal power, 900 (kW).
p	Number of pole pairs, 2.
R_{blade}	Blade radius, 24 (m).
R_r	Rotor's resistance, 5 (m Ω).

R_s	Stator's resistance, 6 ($m\Omega$).
$R(\theta)$	Rotation matrix for transforming the current reference frame (dq) to reference frame (ab).
S_{blade}	The circular area scanned by the turbine.
T_i	The transfer function constant time of is_d and is_q .
T_r	The rotor time constant.
T_s	The stator time constant.
u_{inv}	Output voltage of the inverter.
V_{blade}	Nominal speed of blades, 25 (Tr/min).
V_{dc}	DC bus-bar voltage, 1500 (V).
V_{wind}	Nominal speed of wind, 12 (m/s).
ω	The rotation speed of the blade.
ω_{blade}	Nominal speed of blades.
W_{blade}	Rated power of blades, 2.61 (rad/s).
ω_{gear}	Rotation speed of gearbox.
ω_r	Rotor pulsation.
ω_s	Stator pulsation.
ω_{sh}	Rotation speed of the equivalent shaft.
ρ_{air}	The air density.
λ	The relative speed representing the ratio between the linear speed at the extremity value of the wind blades and wind speed.

PV parameters

A	Module surface.
α	Duty cycle.
C_p	Thermal capacity of the module.
E_e	Irradiance, (W/m^2).
E_{ref}	Reference irradiance, (W/m^2).
G_{ref}	Irradiance, 1000 (W/m^2).
I_0	Diode saturation current, (A).
I_{ph}	Module photocurrent, (A).
$I_{ph,ref}$	Reference module photocurrent, (A).
I_{PV}	Module current, (A).
I_{SC}	Short circuit current of the array, $n_p \times I_{SC_{ref}} = 626.4$ (A).
$I_{SC_{ref}}$	Reference value of module short circuit current, 5.4 (A).
K	Boltzmann constant, 1.38×10^{-23} (JK^{-1}).
$MPPT$	Maximum Power Point Tracking.
n	Ideality factor.
n_m	Number of modules (696), $n_s \times n_p$.
n_p	Number of modules in parallel, 116.
n_s	Number of modules in series, 6.
N_p	Number of cells in parallel, $n_p \times 1$.
N_s	Number of cells in series, 36.
$P\&O$	Perturb and Observe algorithm.
P_{PV}	Array power under STC, $n_m \times 18 * 5 = 62640$ (W).
PV	Photovoltaic.
q	Electron initial charge, 1.602×10^{-19} (C).

$R_{atm/PV}$	Convective thermal resistance.
R_s	The series module resistance, $2.6449 \times 10^{-1} (\Omega)$.
R_{sh}	The parallel module resistance, $10^5 (\Omega)$.
T_a	Ambient temperature.
T_{PV}	Module temperature.
$T_{PV,ref}$	Module temperature at STC, 298 (K).
V_{OC}	Open circuit voltage of the array, $n_s \times V_{OC,ref} = 133.2 (V)$.
$V_{OC,ref}$	Reference value of module open circuit voltage, 22.2 (V).
V_{PV}	Module voltage, (V).
V_{sp}	Wind velocity, (ms^{-1}).
$\sum \dot{Q}_{in}$	Sum of incoming heat flux.
$\sum \dot{Q}_{out}$	Sum of outgoing heat flux.
μ_{ISC}	Coefficient of variation of short-circuit current with respect to temperature, (A/K).
η_{PV}	Module coefficient.

Gas micro-turbine parameters

C_{em}	The electromagnetic torque of the synchronous machine.
C_m	Turbine torque.
D_{tur}	Friction coefficient.
E_1	The output of the valve positioner.
F_d	The input of the valve positioner.
f	The viscous friction coefficient.
J	The total inertia.
K_f	Gain of the actuator.
K_{HHV}	Coefficient depends on the enthalpy.
K_i	Integral gain, 0.50.03.
K_P	Proportional gain, 7.
K_t	Gain of temperature controller, 1.
K_v	Gain of the valve positioner.
L_{max}	Maximal load, 1.2 (p.u.).
N	The value of the current speed.
P_{rate}	Nominal power, 150 (kW).
P_{ref}	Reference power, 1 (p.u.).
T_1	Constant of fuel system, 1, 10 (s).
T_2	Constant of fuel system, 2, 0.1 (s).
T_3	Limit time constant of the load, 3 (s).
T_f	Time constant of the actuator.
T_r	Limited temperature.
T_v	Time constant of the valve positioner.
V_{max}	Maximal position of the valve, 1.2 (p.u.).
V_{min}	Minimal position of the valve, -0.1 (p.u.).
W_f	Requested fuel flow.

Control symbols

<i>FLC</i>	Fuzzy Logic Control.
------------	----------------------

PI	Proportional-Integral.
Q_{H_2}	Hydrogen flow, (m^3/s).
t	Time of electrolyser operation at maximum temperature, (s).
T	Water temperature, (K).
T_{inH_2O}	Electrolyser input water temperature, (K).
$T_{inH_2O_F}$	Electrolyser input water temperature using water temperature FLC controller, (K).
$T_{inH_2O_ELS}$	Water temperature provided to PEM electrolyser, (K).
$T_{inH_2O_P}$	Electrolyser input water temperature considering the pressure changes, (K).
ΔQ_{H_2}	The difference between hydrogen flow at the electrolyser output at two different temperatures, (m^3/s).
$\partial \Delta Q_{H_2}$	The difference between two values of ΔQ_{H_2} , (m^3/s).

General abbreviations

AI	Artificial Intelligence.
AMS	Analog and Mixed-Signal.
ANN	Artificial Neural Networks.
BG	Bond Graph.
BKU	Backup.
BKUS	Back-up Source.
CAES	Compressed Air Energy Storage.
COG	Causal Organic Graph.
DG	Distribution Generation.
EEQ	Electrical Equivalent.
ELS	Electrolyser.
EMR	Energetic Macroscopic Representation.
ESC	Energy Supervisory Control.
ESSs	Energy Storage System.
EWEA	European Wind Energy Association.
FBES	Flow Battery Energy Storage.
FC	Fuel Cell.
FES	Flywheel Energy Storage.
FL	Fuzzy Logic.
FLC	Fuzzy Logic Control.
GA	Genetic Algorithm.
GHS	Green House Gases.
GMT	Gas Micro-Turbine.
GO	Genetic Optimizer.
GUI	Graphical User Interface.
HESS	Hydrogen Energy Storage System.
HPS	Hybrid Power System.
HS	Harmony Search.
IEC	Internal Combustion Engine.
IM	Induction Machine.
LABES	Lead Acid Battery Energy Storage.
LIES	Lithium Ion Energy Storage.
LUT	Lookup Table.

MCS	Maximum Control Structure.
MPPT	Maximum Power Point Tracking.
NiCd	Nickel Cadmium.
NN	Neural Networks.
PEM	Proton Exchange Membrane.
PEM ELS	Proton Exchange Membrane Electrolyser.
PEMFC	Proton Exchange Membrane Fuel Cell.
PHES	Pumped Hydro power Energy Storage.
P&O	Perturb and Observe.
PSO	Particle Swarm optimization.
PV	Photovoltaic.
RE	Renewable Energy.
RESs	Renewable Energy Sources.
SA	Simulated Annealing.
SAO	Simulated Annealing Optimizer.
SES	Supercapacitor Energy Storage.
SMES	Superconducting Magnetic Energy Storage.
SNCES	Sodium Nickel Chloride Energy Storage.
SoC	State of Charge.
SSE	Sum of Squared Errors.
SSSR	State Space Search Reference.
TPEC	Total Produced Energy Cost.
TS	Tabu Search.
VHDL	Hardware Distribution Language.
WE	Wind Energy.
WTs	Wind Turbines.

List of Figures

Fig. 1.1: A Schematic diagram of a hydrogen FC and half-cell reactions.....	21
Fig. 1.2: Energy storage technologies.	23
Fig. 1.3: Comparisons of energy storage techniques.....	27
Fig. 1.4: Global hydrogen production sources in percent.	28
Fig. 1.5: Data communication and power flow in HPSs.	31
Fig. 1.6: Centralized, distributed and hybrid energy management categories.....	31
Fig. 1.7: COG representation of a permanent magnet DC machine	34
Fig. 1.8: Inversion-based control.....	36
Fig. 1.9: Different interconnection schemes in passive techniques.....	38
Fig. 1.10: Fixed and adaptive parts of PV reconfiguration proposed by Nguyen et al	39
Fig. 1.11: Optimal PV array reconfiguration presented by Shams El-Dein et al.	40
Fig. 2.1: EMR of electrical sub-model.	46
Fig. 2.2: EMR of electrochemical and thermodynamic sub-model.....	47
Fig. 2.3: EMR of thermal sub-model.....	48
Fig. 2.4: EMR of hydraulic sub-model.....	51
Fig. 2.5: The EMR model of overall PEM ELS.....	52
Fig. 2.6: ELS current as function of voltage.	53
Fig. 2.7: EMR of PEMFC.	54
Fig. 2.8: V–I characteristics for different number of cells and stacks configurations.....	56
Fig. 2.9: WT with the batteries pack connection.....	57
Fig. 2.10: The EMR model of WT.....	57
Fig. 2.11: EMR induction machine model.	59
Fig. 2.12: wind and power profiles of WT.....	61
Fig. 2.13: EMR model of PV panels.	61
Fig. 2.14: I-V and P-V curves under different irradiance levels.	65
Fig. 2.15: General block diagram of GMT.....	66
Fig. 2.16: Block diagram of fuel supply system.....	66
Fig. 2.17: Block diagram of the combination compressor/turbine.....	67
Fig. 2.18: The GMT power as a function of fuel flow.	67
Fig. 2.19: Block diagram of GMT controllers.....	68
Fig. 2.20: Speed control using two different methods.....	68
Fig. 2.21: GMT speed controller.....	69
Fig. 2.22: Simplified model of GMT.	69
Fig. 2.23: Simplified GMT model.....	69
Fig. 2.24: EMR GMT model.....	70
Fig. 2.25: Simulation and reference values for mechanical power.	70
Fig. 2.26: global EMR model of multi sources system.	71
Fig. 3.1: Equivalent circuit of a solar cell.	76
Fig. 3.2: Synoptic of the PV panel and the boost converter controller.....	76
Fig. 3.3: I-V and P-V curves under different irradiance levels.	77
Fig. 3.4: PV panel experimental and simulation characterization curves.....	77

Fig. 3.5: Experimental test-bench of PWX500 PV panel.....	78
Fig. 3.6: I-V characteristics considering irradiance and temperature variations.....	78
Fig. 3.7: Shading nine cells from: (i) two different lines (9 cells/ P),.....	79
Fig. 3.8: Experimental I-V and P-V characteristics for shaded PWX500 PV panel.....	79
Fig. 3.9: Different power losses estimation in case of shading.....	81
Fig. 3.10: FL and dSPACE control of the proposed system.....	82
Fig. 3.11: Experimental test–bench of the new switches reconfiguration.....	83
Fig. 3.12: FL estimator inputs and outputs.....	84
Fig. 3.13: U, I, P results and current flow for the four PV panels (normal mode).....	86
Fig. 3.14: U, I, P results, and current flow for four PV panels connection (shaded PV1 and PV2).....	86
Fig. 3.15: Online PV panels reconfiguration.....	88
Fig. 3.16: The overall system under-study with the proposed water heating control.....	89
Fig. 3.17: Internal structure of the PEM electrolyser.....	90
Fig. 3.18: Physical interactions within an electrolyser.....	90
Fig. 3.19: EMR model of the PV panel.....	91
Fig. 3.20: EMR model of PEM electrolyser.....	91
Fig. 3.21: Inputs and outputs membership functions.....	92
Fig. 3.22: Polarization curves for different water temperature.....	93
Fig. 3.23: Current-Temperature relation and the error based on LUT and curve fitting approaches....	94
Fig. 3.24: LUT with water temperature input and current electrolyser output.....	94
Fig. 3.25: H ₂ flow versus water temperature.....	94
Fig. 3.26: Controlled and uncontrolled hydrogen flow at PEM electrolyser.....	95
Fig. 3.27: FLC for instantaneous water temperature reference control.....	96
Fig. 4.1: Multi-source system under study.....	99
Fig. 4.2: Graphical illustration of cell/module/array photovoltaic.....	100
Fig. 4.3: WT components.....	101
Fig. 4.4: Batteries charging from IM.....	102
Fig. 4.5: WT operation curve.....	102
Fig. 4.6: Pitch control and stall control in WT.....	103
Fig. 4.7: I–V characteristics of PEM electrolyser and PV module.....	104
Fig. 4.8: Experimental FC output power.....	105
Fig. 4.9: Flowchart for energy storage methodology and energy management strategy.....	107
Fig. 4.10: Energy management strategy at different load power values.....	109
Fig. 4.11: NN general structure.....	110
Fig. 4.12: Two layers feed-forward network for energy management.....	111
Fig. 4.13: NN inputs and outputs.....	112
Fig. 4.14: Output power of RESs when MPPT is considered.....	112
Fig. 4.15: The daily load of one village in region of Belfort.....	113
Fig. 4.16: NN GUI for system energy management.....	113
Fig. 4.17: Training, validation and test data fitting for a target.....	114
Fig. 4.18: Sources and ELS power for one cycle of 24 hours.....	115
Fig. 4.19: Load tracking by the multi-source power generation.....	115
Fig. 4.20: Power and energy stored in the hydrogen tank from RESs.....	116
Fig. 4.21: Energy consumption at maximum load values.....	116
Fig. 4.22: Energy stored in/consumed from the tank and the sum of both during daily operation....	117
Fig. 4.23: GUI tools of FL.....	118

Fig. 4.24: Energy management methodology based on FL..... 119
Fig. 4.25: Load tracking by the multi–source power generation using FL. 119
Fig. 4.26: Stored and consumed energies using FL..... 120

List of Tables

Table 1.1: Compliance of different modelling approaches to the needs.	35
Table 1.2: EMR pictogram.	35
Table 1.3: Hydrogen ESS compared with other ESS technologies	40
Table 2.1: Entropy constant values of PEM ELS.....	47
Table 2.2: Enthalpy constant values of PEM ELS.	47
Table 2.3: CP values for water, hydrogen and oxygen.....	50
Table 2.4: EMR and MCS equations.....	65
Table 3.1: Experimental power losses in function of shading percentage.	81
Table 3.2: FL estimator inputs.	85
Table 3.3: FL estimator outputs.	85
Table 3.4: All possibilities of PV panel shading.	87
Table 3.5: FLC inference rules.....	92
Table 3.6: The current values as a function of temperature.	93
Table 4.1: PEMFC operation conditions.....	105
Table A.1: PEMFC operation conditions.....	134
Table A.2: PEM electrolyser EMR sub-models.	134
Table A.3: Fuzzy logic rules used for the energy management.	135
Table A.4: Inputs and outputs of the proposed FLC.	138

1. INTRODUCTION

The Green House Gases (GHGs) emitted by the traditional energy production and consumption negatively impact the world environment. Accordingly, the Kyoto protocol, signed by the 37 industrialized countries, has entered into force on February 2005. This protocol imposes reducing the GHGs below the levels of 1990 during an initial commitment of 2008 through 2012 [Sant 05].

Carbone dioxide (CO₂) is the primary GHGs emitted through human activities. About 72% of the totally emitted GHG is CO₂. It has been created by burning fossil fuels such as coal, natural gas, and oil which are requested for numerous human activities including electricity production, transportation and industry. Heavy uses of fossil fuels since the industrial revolution have increased the CO₂ in the atmosphere. Accordingly, an increasing rate of CO₂ of about one part of million per year has been produced. Consequently, an expected average earth temperature increase of 2.5 °C will be achieved in the near future. That may lead to glaciers melt and coastal flooding.

Zero carbon sustainable alternative energy sources are required to avoid fossil energies problems of limitation, unsustainability and injected carbon dioxide in the air causing planet pollution. The interest in environment-friendly Renewable Energy (RE) has increased in recent years due to environmental concerns about global warming and air pollution, reduced costs of the technologies, besides the improved efficiency and reliability. RE can be generated from solar, wind, ocean, hydropower, biomass, geothermal resources, biofuels and hydrogen derived from renewable resources. RE technologies are essential contributors to sustainable energy due to their general contribution to world energy security, reducing dependence on fossil fuel resources, and providing opportunities for mitigating GHGs. Renewable Energy Sources (RESs) are interesting for creating new jobs, its life quality, decreasing dependence on fossil fuels, and reducing operating costs [Stig 14].

The sun is one of RESs. It delivers 100,000 TW of energy to the earth. Whereas, the world energy consumption in 2012 was 12,476.6 million tonnes of oil equivalent of 145,103 TWh. Consequently, it is dazzling that the global energy consumption by the world can be produced by solar energy in every 88 minutes. In other words, 6000 times' annual energy consumption can be produced by received solar energy at the earth surface [Ohun 14] [Shah 13].

Despite its intermittency, Wind Energy (WE) is a promising source of RE widely used and considered to be the cleanest RE with no environment impact [Abba 14]. The European Wind Energy Association (EWEA) has adopted an energy production policy. This strategy aims at 20% of RE production percentage of total produced energy. In addition, an installed capacity of WE at 80000 MW in EU-27 by 2020 should be reached. Obviously, this WE capacity represents 5% of total produced energy [EWEA 09].

In this chapter, the energy production from different RESs will be presented. The hybridization among the different sources will be studied. Then, the energy storage technologies will be highlighted. Therefore, the different existing energy management control approaches for hybrid systems will be discussed. A comprehensive literature review presenting the recent studies on hybrid systems including hydrogen storage technologies will be presented. In addition, the proposed solutions for PV panels' problems especially shading will be explained. Finally, the orientation of the thesis will be illustrated at the end of the chapter.

1.1. RENEWABLE ENERGY PRODUCTION

RESs refer to the sustainable natural energy sources, such as the sun and the wind. RESs convert these natural energy sources into consumable energy forms (electricity and heat), which are easy to transport and to use. According to the European directive on RES for production of electricity [Dire 01], RESs include: (i) hydropower plants; (ii) solar (photovoltaic, thermal electric); (iii) wind; (iv) geothermal; (v) wave and tidal energy; (vi) biodegradable waste; (vii) biomass (solids, biofuels, landfill gas, sewage treatment plant gas and biogas).

1.1.1. HYDROPOWER PLANTS

Hydropower is a process in which the force of flowing water is used to spin a turbine connected to a generator to produce electricity. Most hydroelectric power comes from the potential energy of dammed water driving a turbine and generator. The power extracted from the water depends on the volume and the amount of potential energy in water proportional to the head, which is difference in height between the source and the water's outflow. A simple formula for approximating electric power production of a hydroelectric plant is:

$$P = Q \rho g \Delta Z = mg \Delta Z \quad (1.1)$$

where P is the power, ρ is the density of water, ΔZ is the height, Q is the volumetric flow rate, \dot{m} is the mass and g is the acceleration due to gravity. The annual electric energy production depends on the available water supply. In some installations, the water flow rate can vary by a factor of 10:1 over the year.

Hydropower eliminates the use of fossil fuels and hence carbon dioxide emission. Hydroelectric plants also tend to have longer economic lives (50 years or longer) than fuel-fired power production. The sale of hydroelectricity may cover the construction costs after 5–8 years of full operation [Mark 07]. Operating labour cost is also usually low, as plants are automated. The hydroelectric capacity is either the actual annual energy production or by installed capacity. A hydroelectric plant rarely operates at its full capacity over a full year. The ratio of annual average power output to installed capacity is the capacity factor for a hydroelectric power plant. There are large, small, and micro hydropower plant operations.

1.1.2. SOLAR POWER PLANTS

Solar power is derived from the energy of sunlight. Average daily insolation changes from 150 to 300 W/m² or 3.5 to 7.0 kWh/m² day. There are two main types of technologies for converting solar energy to electricity: Photovoltaic (PV) and solar–thermal electric [Pica 09].

- PV conversion produces electricity directly from sunlight via a solar cell. There are many types of PV cells, such as thin film, mono-crystalline silicon, polycrystalline silicon, and amorphous cells, as well as multiple types of concentrating solar power. PV power can be used either in small- or in medium-sized applications.
- Solar–thermal electric production based on concentrating solar power systems use lenses or mirrors and tracking systems to focus a large area of sunlight into a small beam. The concentrated solar energy heat is used for producing steam to drive turbines and produce electricity. A parabolic trough consists of a linear parabolic reflector that concentrates light onto a receiver positioned along the reflector's focal line. The receiver is a tube positioned right above the middle of the parabolic mirror and is filled with a working fluid. The reflector is made to follow the sun during the daylight hours by tracking along a single axis [Tyag 07].

Recently, solar installations are expanded into residential areas, with governments offering incentive programs to make renewable green energy sources more economic options [Demi 06].

1.1.3. WIND POWER PLANTS

The Earth is unevenly heated by the sun and the differential heating drives a global atmospheric convection system leading to the wind. Wind power is the conversion of WE into electricity by using Wind Turbines (WTs). A WT is a device for converting the kinetic energy in wind into the mechanical energy of a rotating shaft. The generator is usually connected to the turbine shaft through gears which turn the generator at a different speed than the turbine shaft. Power electronic devices convert the electricity into the ideal frequency and voltage to be fed into the power grid at 60 or 50 Hz.

The power produced by a WT is proportional to the kinetic energy of the wind captured by WTs. The kinetic energy of the wind is equal to the product of the kinetic energy of air per unit mass and the mass flow rate of air through the blade span area, then:

Wind power = (efficiency) (kinetic energy) (mass flow rate of air)

$$\dot{W}_{Wind} = \eta_{Wind} \frac{v^2}{2} (\rho A v) = \eta_{Wind} \frac{v^2}{2} \rho \frac{\pi D^2}{4} v \quad (1.2)$$

therefore,

$$\dot{W}_{Wind} = \eta_{Wind} \rho \frac{\pi v^3 D^2}{8} = k_{Wind} v^3 D^2 \quad (1.3)$$

where $k_{Wind} = \frac{\eta_{Wind} \rho \pi}{8}$

where ρ is the density of air, v is the air velocity, D is the diameter of the WT blades, and η_{Wind} is the WT efficiency. Therefore, the power produced by WTs is proportional to the cube of the wind velocity and the square of the blade span diameter. The strength of wind varies, and an average value for a given location does not alone indicate the amount of energy produced by WT. To assess the frequency of wind speeds at a particular location, a probability distribution function is often fit to the observed data. In addition, other factors include the availability of transmission lines, value of energy, cost of land acquisition, land use considerations, and environmental impact of construction and operations should be considered. Wind power density is a calculation of the effective power of the wind at a particular location. A map showing the distribution of wind power density is a first step in identifying possible locations for WTs [Dai 15].

At the end of 2013, the worldwide capacity of wind-powered generators was 318.105 GW [Dai 15]. Large-scale wind farms are connected to the electric power transmission network, while the smaller facilities are used to provide electricity to isolated locations. WE, as an alternative to fossil fuels, is plentiful, renewable, widely distributed, clean and produces no GHGs emissions during operation. Wind power is an intermittence RES, and for economic operation, all of the available output must be taken when it is available. Problems of wind speed variability can be mitigated by grid energy storage, batteries, pumped-storage hydroelectricity and energy demand management. Although high WT capital cost, wind power has negligible fuel costs and life of the equipment in more than twenty years [Arch 07] [Manw 10].

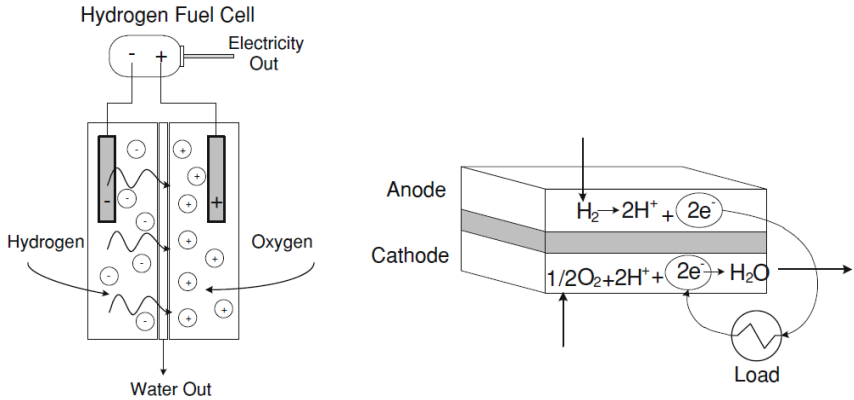
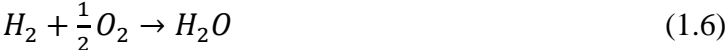
WE penetration refers to the fraction of energy produced by wind compared with the total available production capacity. There is no generally accepted maximum level of wind penetration. An interconnected electricity grid usually includes reserve production and transmission capacity to allow for equipment failures. This reserve capacity can also serve to regulate for the varying power production by wind plants. At present, a few grid systems have penetration of WE above 5% such as Denmark (values over 19%), Spain and Portugal (values over 11%), Germany and the Republic of Ireland (values over 6%) [Kasi 13]. Despite the available power forecasting methods, predictability of wind plant output remains low for short-term operation. Pumped-storage hydroelectricity or other forms of grid energy storage can be developed for storing energy during high-wind periods and releasing it when needed.

1.1.4. FUEL CELLS

A Fuel Cell (FC) oxidizes a fuel, such as hydrogen or methane, electrochemically to produce electric power. It consists of two electrodes separated by an electrolyte. The fuel and oxygen are continuously fed into the cell and the products of reaction are withdrawn continuously. The fuel makes intimate contact with the anode which is called fuel electrode. Oxygen, usually in air, makes intimate contact with the cathode which is called oxygen electrode. Half-cell reactions take place at each electrode. The sum of the half-cell reactions is the overall reaction. The type of electrolyte characterizes the type of FC. Schematic FC using hydrogen as fuel is illustrated in Fig. 1.1. When the electrolyte is acidic, the half-cell reactions occurring at the hydrogen electrode (anode) and at the oxygen electrode (cathode) are [Luci 14]:



The electrons with negative charge (e^-) are released at the anode. These electrons produce an electric current which is used by the reaction occurring at the cathode. The electric current is carried out by an external circuit. The cation (H^+) migrates from anode to cathode through the electrolyte. The sum of the half-cell reactions is the overall reaction taking place at the FC:



(a) Schematic of a hydrogen FC. (b) Half-cell reactions for a hydrogen/oxygen FC with acidic electrolyte.

Fig. 1.1: A Schematic diagram of a hydrogen FC and half-cell reactions.

A thin solid polymer known as Proton Exchange Membrane (PEM) serves as an acid electrolyte in the hydrogen/oxygen FC. Each side of the membrane is bonded to a porous carbon electrode impregnated with platinum which serves as a catalyst. The porous electrode provides a very large interface area for the reaction and facilitates the diffusion of hydrogen and oxygen into the cell and the water vapour out of it. Cells can be connected in series to make a compact unit with a required level of energy output and operate at a temperature near 60 °C.

For each mole of hydrogen consumed, 2 mole of electrons pass to the external circuit. Therefore, the electrical energy (work), W_e , is the product of the charge transferred and the voltage V of the cell:

$$W_e = -2FV = \Delta G \quad (1.7)$$

where F is the Faraday's constant ($F = 96485$ coulomb/mole) and ΔG is the Gibbs energy. The electric work of reversible and isothermal FC is:

$$W_e = \Delta H - q = \Delta G \quad (1.8)$$

where ΔH is the Enthalpy and q is the caloric energy.

In practice, the operating voltage of hydrogen/oxygen FC is around 0.6-0.7 volts, because of the internal irreversibilities which reduce the electric work produced and increase the heat transfer to the surroundings.

FCs are very efficient, but expensive to build. Small FCs can power electric cars. Large FCs can provide electricity in remote places with no power lines. Portable FCs are being manufactured to provide longer power for laptop computers, cell phones, and military applications [Larm 03] [Viel 09]. FC is relatively new technology, has no moving parts, has no emissions and is light and reliable. Hydrogen has a higher energy density per weight but lower per volume than a gasoline. These features provide more of FC in the future particularly with renewable applications.

1.2. ENERGY STORAGE

Energy storage is a key element for the growth of REs when the energy source is intermittent and located in an isolated area which cannot be connected to the distribution network. Indeed, with the new energy markets, many delocalized sources- usually intermittent renewable ones- will be connected to the network, which may result in destabilization. To overcome this problem, Energy Storage Systems (ESSs) and appropriate management of these resources are the best solutions.

Electrical energy can be stored in form of different kinds: mechanical, electro-chemical, electromagnetic and thermal. Fig. 1.2 presents the classification of energy technologies. The red, blue and green colours represent the long, medium and short energy storage technologies respectively.

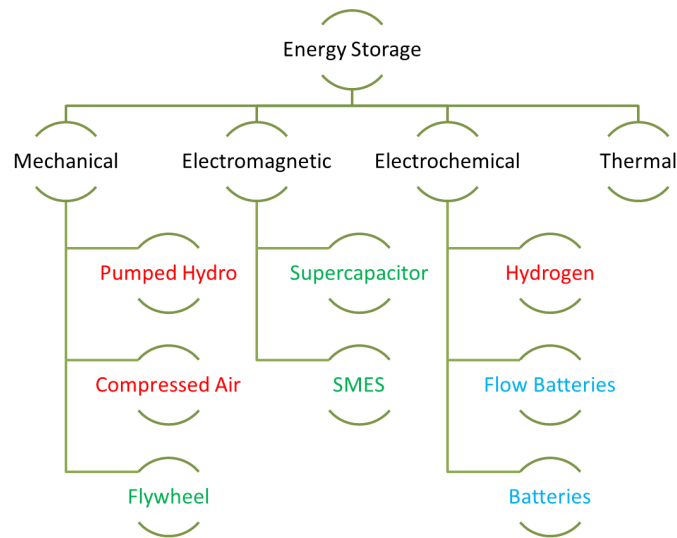


Fig. 1.2: Energy storage technologies.

1.2.1. ENERGY STORAGE TECHNOLOGIES

1.2.1.1. PUMPED HYDRO ENERGY STORAGE

Pumped Hydro Energy Storage (PHES), the largest and the most mature technology available, consists of two reservoirs and a body of water at a relatively high elevation represents potential or stored energy [Luim 09] [Scho 96]. It is similar to hydroelectric power plant. During the “charging” process, water from lower reservoir is pumped up to the upper one. In “discharging” process, water from upper reservoir is released and flows through hydro turbines which are connected to generators, producing electrical energy [Scho 96]. In case of hydro power plants, pumping is irrelevant. In most cases, the hydro facility could be used as storage without any pumping because it has a supply of water from a river.

PHES is adequate solution for wind farms that can ideally be applied for load levelling [Luim 09]. However, the lack of suitable places and the impact in the nature environment are still the main drawbacks [DOE 01]. This technology can be placed in ideal locations to function with wind farms [Luim 09]. Despite high technical immaturity, hydro power plants are still one of the best storage solutions for damping fluctuations caused by WPP.

1.2.1.2. COMPRESSED AIR ENERGY STORAGE

Compressed Air Energy Storage (CAES) systems deal with compressing air via electrical compressors in underground cavities (salt cavern, abandon mines, rock structures... etc.,) and store it in a high pressure. When energy is needed, compressed air is released through a turbine, but the operating units worldwide incorporate combustion prior to turbine expansion in order to increase the overall efficiency [DOE 01] [Gonz 04].

If favour of the high power and energy capacities, CAESs are convenient storage solution for wind farms. CAES can be used for frequent start up and shutdowns. Current research in CAES is mainly focused on the development of systems with fabricated storage tanks. Such approach will remove the geological dependency and compressed air will be stored in tanks with a higher pressure. System rating will be smaller (several MW) because of the tank cost. The possible lack of geological dependence might make CAES an interesting solution for the integration into wind farms.

1.2.1.3. FLYWHEEL ENERGY STORAGE

Flywheels Energy Storage (FES) are energy storage devices where energy is stored in the form of kinetic energy (rotating mass). Flywheels are made up of shaft that rotates on two magnetic bearings in order to decrease friction [Gyuk 04]. Whole structure is placed in a vacuum to reduce windage losses. During “charging” process rotor is accelerated to a very high speed by a motor and energy is maintained in a system as kinetic energy [Gyuk 04]. In “discharge” process, flywheels are releasing energy and driving the machine which is working as a generator.

Flywheels are not very well suited for wind farm support. Their ability to suppress fast wind power fluctuations is limited to small time scale. They can be considered as a support for WTs in combination with battery system rather than stand alone. However, energy density is low and self-discharge ratio is high. Unerco Power Technologies Company has demonstrated the application of kinetic energy storage to the smoothing of the output of WT systems. Most FES researches deal with high speed flywheels which are able to rotate with a speed up to 100 000 rpm.

1.2.1.4. SUPERCAPACITOR ENERGY STORAGE

In Supercapacitor Energy Storage (SES), the energy is stored in electric field. Its principle of operation is similar to that of conventional capacitors. However, supercapacitors use polarized liquid layers between conducting ionic electrolyte and conducting electrode to increase the capacitance. Due to the fact that capacitance is dependent also on the surface area of electrodes, highly porous material is used in order to increase the area. Consequently, supercapacitors can be rated up to 5000 F [DOE 01].

SES has response characteristics and small energy density similar to FES. However, there are no moving parts and the self-discharge ratio is relatively small. It can be considered a proper solution for WTs support in combination with a battery system rather than stand-alone ones.

1.2.1.5. SUPERCONDUCTING MAGNETIC ENERGY storage

Superconducting Magnetic Energy Storage (SMES) stores energy in magnetic field. SMES consists of superconductive coil, power conditioning system, refrigerator and vacuum [Luim 09]. Magnetic field is produced by DC current circulating through a superconducting coil [DOE 01]. In order to get rid of the resistive losses caused by current flow, the coil is kept in superconducting state. Cooling medium is liquid helium or nitrogen.

SMES are unlikely to be used for integrating renewable [Luim 09]. Superconductive coil is relatively very sensitive to temperature changes and has small energy density and power capacity up to 2 MW. SMES is usually utilized in industrial power quality market.

1.2.1.6. LEAD ACID BATTERY ENERGY STORAGE

Lead Acid Battery Energy Storage (LABES) is the most mature commonly used battery storage technology at present [Luim 09] [DOE 01]. Two kinds of LABESs can be distinguished: Flooded (FLA) and Valve-Regulated (VRLA). FLA batteries are constructed from two lead plates which are immersed in a mixture of sulphuric acid and water. In case of VRLA batteries, the operational principle is similar to FLA. However, they are sealed with a pressure-regulating valve which prevents venting of the hydrogen generated during the chemical reaction and eliminates the air from the cell. VRLA has higher initial cost and shorter lifetime, however they smaller weight, volumes and lower cost of maintenance than FLA.

LAES can be considered for wind power support. There exist stationary applications of LAES in the world rated in MW for power system applications. However, LAES usually lose with other batteries when it comes to wind power integration, mainly because of the relative small power density, low depth of discharge, life cycle capability and extreme sensitivity to temperature changes. Depth cycles decrease the life time of LABES. The current research in LABES is to minimize its charging/discharging time [Luim 09]. It is rather unlikely that this technology will be playing important role in a future as a large scale storage device, mainly due to very limited number of cycles. Moreover, an interesting solution seems to be an ultra-battery composed of LABES integrated to supercapacitor in one unit cell developed by CSIRO. Ultra battery can provide high power charge/discharge with both long and low-cost life [Site 01].

1.2.1.7. NICKEL CADMIUM BATTERY ENERGY STORAGE

Nickel Cadmium (NiCd) Energy Storage (NCES) is a mature solution like LA batteries [Site 02]. NCES consists of positive electrode (nickel hydroxide) and negative one (metallic cadmium). Electrodes are separated by nylon divider and the aqueous potassium hydroxide is the electrolyte. During discharging process, nickel oxyhydroxide reacts with water and produces nickel hydroxide and a hydroxide ion. At the negative electrode, cadmium hydroxide is produced. During charging process, the battery is reversed. NiCd batteries can operate in wider temperature range in comparison with LA. NiCd batteries are operated with small depth of discharge for more cycles. However, this technology suffers from memory effect besides its negative environmental impact. Cadmium is a toxic heavy metal and there are concerns related to disposal.

1.2.1.8. LITHIUM ION BATTERY ENERGY STORAGE

Lithium Ion Energy Storage (LIES) technology was first commercially available in 1990 [DOE 01]. The cathode is lithiated metal oxide while anode is graphic carbon with layer structure [Site 03]. The electrolyte is a lithium salt in organic solvent. During discharging, lithium migrates from anode to cathode in this case. During charging, reverse process occurs. The weight of LIES is approximately one half compared to NCES of similar capacity and its volume is 40 to 50% smaller than NCES [Site 02].

This technology can be sized in MW and therefore become a serious invention in large scale applications. LIES seems to be relevant for wind power plants. The main characteristic features of this technology are its small weight, high efficiency, high cell voltage and power density. LIES can be shaped into a wide variety of shapes and sizes. Moreover, this technology does not have a memory effect. Other features include the small self-discharge (0.1% per month) and long life for deep cycles.

1.2.1.9. SODIUM NICKEL CHLORIDE BATTERY ENERGY STORAGE

Sodium Nickel Chloride Energy Storage (SNCES) battery, popularly called ZEBRA belongs to the family of high temperature batteries. The negative electrode consists of liquid sodium and positive electrode is nickel chloride. There is a second liquid electrolyte (sodium chloroaluminate) to allow fast transport of sodium ions from the solid nickel chloride electrode to and from ceramic electrolyte [Sudo 01]. The best performance of a cell results in a temperature range 250 – 350 °C.

ZEBRA batteries can play a role in the future with renewables thanks to the higher energy density than LA and the resistant to short circuits [DOE 01].

1.2.1.10. FLOW BATTERY ENERGY STORAGE

Flow Batteries Energy Storage (FBES) principle of operation differs from conventional batteries. Energy is stored as a potential chemical energy by means of reversible reaction between two electrolytes in the electrolyte solutions. This makes the power and energy capacity decoupled. The size of the cell stack determines the power capacity, while the volume of electrolyte determines energy capacity [DOE 01]. Two charged electrolytes are pumped to the cell stack. In the cell stack, a chemical reaction occurs [Luim 09]. For each technology charge to discharge ration is 1:1 and batteries do not suffer from depth discharge. The three common kinds of flow batteries are: Vanadium Redox (VR), Polysulphide Bromide (PSB) and Zinc Bromine (ZnBr).

The operation of Polysulphide Bromide (PSB) is similar to VR. The characteristic feature is its relative fast reaction time. PSB batteries can be used for frequency response and voltage control. The disadvantage is the fact that small quantities of bromine, hydrogen and sodium sulphate are produced what imposes some maintenance [Luim 09].

In case of ZnBr technology, the operation principle is different than in the VR and PSB batteries. However, it contains the same components during the process of charging the electrolytes of zinc and bromine ions flow to the cell stack. The electrolytes are separated by a micro-porous membrane. Obviously, the electrodes in a ZnBr flow battery act as substrates to the reaction. As the reaction occurs, zinc is electroplated on the negative electrode and bromine is evolved at the positive electrode (similar to conventional battery operation).

The FBES technology capacity can be in MW which makes it convenient to wind power plants. There are already existing applications of VR with wind power plants.

1.2.2. COMPARISONS OF ENERGY STORAGE TECHNIQUES

The different energy sources have been compared in terms of their cost and their specific power and energy ranges.

As depicted in Fig. 1.3 [Ibra 08], the key element is the lowest possible self-discharge for low-power permanent applications. Based on the technical criteria alone, the lithium-ion unit is the best candidate.

For small systems of few kWh in isolated areas relying on intermittent RE, the key element is autonomy. The LAES remains the best compromise between performance and cost. LIES has better performance but is relatively still expensive.

For larger systems of few 100 kWh, LAES is still preferred compared to lithium. The alternative solutions are either less efficient or too expensive: compressed air (self-discharge problems), FCs (expensive and low energy efficiency), and flow batteries (high maintenance costs).

In the third category, concerning peak-hour load levelling requiring high-energy storage of several MWh, CAES and FBES are the best choices, with a definite cost advantage for CAES. However, these technologies have not yet been tested in the field.

For the fourth category, concerning power quality, the key criteria are energy release capacity and cycling capacity. Therefore, FES and SES are better adapted than LIES.

Among the choices, LAES satisfy the technical criteria of all the categories, but have limited durability and are unreliable. Nickel-based and metal-air batteries are still of reliable low

performance and high cost. FCs are still a young technology. Finally, certain technologies are able to fulfil the needs of storage for intermittent energy supplies: hydraulic and thermal storage for large-scale applications, and SMES for small-scale applications.

To answer to the future needs of delocalized production, energy storage should be technologically improved on the short to mid-term. LIES are very performant, but are relatively too expensive for application to remote area systems. The recycling and waste management of these batteries still need R&D work. LAES has the best cost-performance compromise. However, it has a weak link in an isolated system, as their life expectancy needs to be improved to be better answer to the needs. For network applications, the mid-term needs are ever growing. The most appropriate technologies (FBES, CAES, SES and FES) are more or less mature technologies and could be made more cost effective, more reliable and more efficient [Ren 15] [Kous 14].

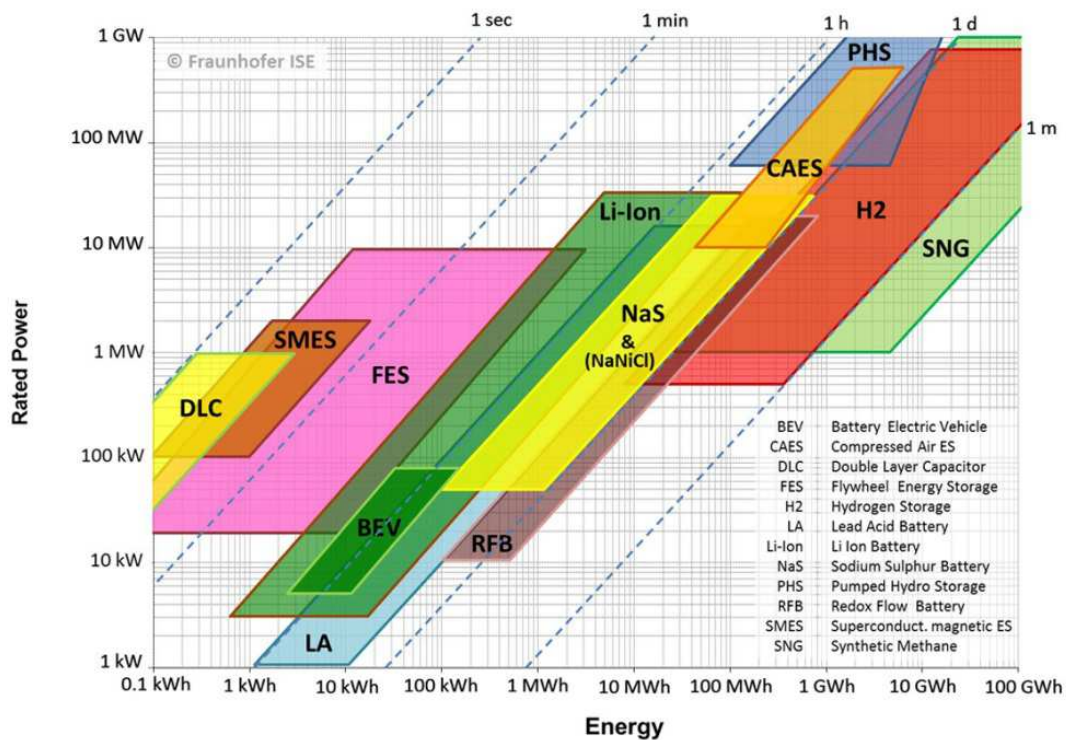


Fig. 1.3: Comparisons of energy storage techniques [Site 04].

1.3. HYDROGEN PRODUCTION STORAGE AND CARRIES

Hydrogen is an ideal energy carrier because: (i) it can be produced from and converted into electricity at relatively high efficiencies; (ii) its raw materials for production is water; (iii) it is a renewable fuel; (iv) it can be stored in gaseous, liquid or metal hydride form; (v) it can be transported over large distances through pipelines or via tankers; (vi) it can be converted into other forms of energy in more ways and more efficiently than any other fuel; (vii) it is environmentally compatible since its production, storage, transportation and end use do not produce pollutants, greenhouse gases or any other harmful effects on the environment (except in some cases the production of nitrous oxides). Unfortunately hydrogen currently suffers from high production costs.

Hydrogen does not occur naturally and thus it must be generated from other energy sources. Fig. 1.4 shows the global hydrogen production sources. Most hydrogen on earth is bonded to oxygen in water. Hydrogen is an energy carrier like electricity, and not a primary energy

source like natural gas. Hydrogen burns cleanly, producing little or no harmful emissions or CO₂. It has the highest energy content per unit of weight of any known fuel. When hydrogen is used in a FC, its only waste is water.

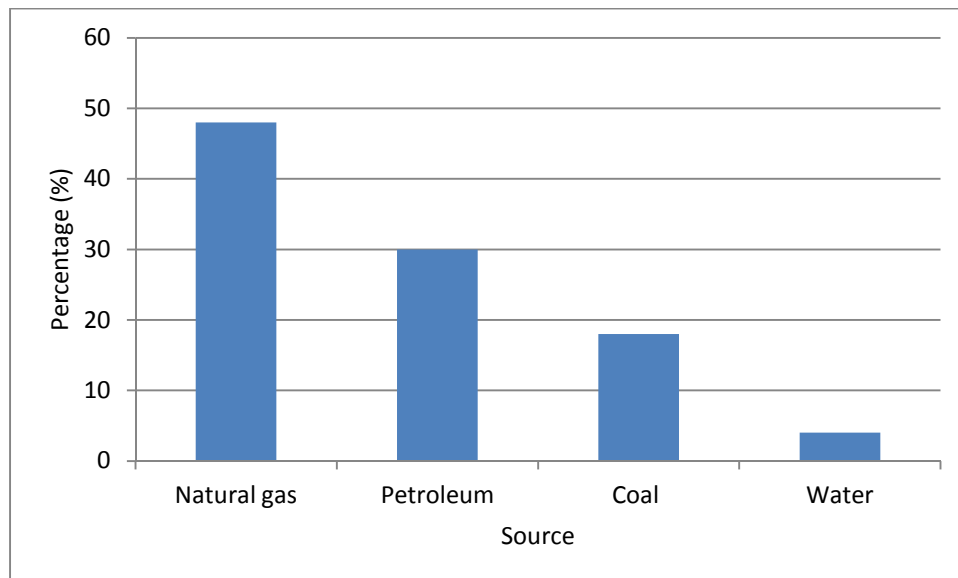


Fig. 1.4: Global hydrogen production sources in percent.

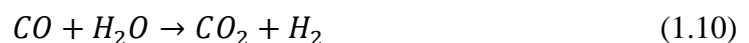
To make hydrogen a renewable fuel, it should be produced via RES, such as wind power or solar power. About half of the hydrogen produced is used for ammonia (NH₃) synthesis by the Haber process. The ammonia is used directly or indirectly as fertilizer. The other half hydrogen is used for converting heavy petroleum sources into lighter fractions to be used as fuels.

Steam reforming of natural gas, the least expensive method, is the most common method of producing commercial bulk hydrogen. At high temperatures and in presence of a metal-based catalyst (nickel), steam reacts with methane to yield carbon monoxide and hydrogen. These two reactions are reversible in nature.



the reaction is done at 750-800 °C, endothermic

Additional hydrogen can be recovered by a lower temperature gas-shift reaction



the reaction is performed at low temperature shift at 190-210 °C, exothermic

Hydrogen can also be produced by electrolysis of water, in which the water is split into hydrogen and oxygen, thus:



The current water-electrolysis processes have a maximum efficiency of 50–80%, so that 1 kg of hydrogen requires 50–80 kWh of electricity. Using electricity produced by PV systems may offer the cleanest way to produce hydrogen. Photo electrochemical light harvesting systems may generate sufficient voltage to split water.

Hydrogen can also be produced via pyrolysis or gasification of biomass resources such as agricultural residues like peanut shells, consumer wastes including plastics and waste grease, or biomass specifically grown for energy uses. Biomass pyrolysis produces bio oil that contains a wide spectrum of valuable chemicals and fuels, including hydrogen. Highly concentrated sunlight can be used to generate the high temperatures needed to split methane into hydrogen and carbon in a solar-driven thermochemical process.



The produced hydrogen can be recycled to the Sabatier process.

Producing hydrogen from electrolysis is the most economical solution among the others. Hydrogen production from fossil fuels is four times more expensive than using the fuel itself [DOE 01]. The production of hydrogen from reaction of steam with methane produces pollution. During the process of electrolysis, hydrogen produced from water and oxygen is dissipated into atmosphere. Latest advances increased the efficiency of hydrogen production to 85%.

Hydrogen energy storage is one of the most immature technologies [DOE 01]. Hydrogen electric energy storage process is divided into three parts: (i) hydrogen production, (ii) hydrogen storage and (iii) energy production.

Storing of hydrogen can be done by compressing it, by liquefying it or by metal hydride [DOE 01]. The most often used option is to compress hydrogen (65-75% efficiency). Hydrogen can be also stored in liquefied form by pressuring and cooling it. However, keeping the hydrogen liquid is energy demanding because of the very low temperature that has to be maintained. To create energy from hydrogen two methods have been used: (i) Internal Combustion Engine (ICE) and (ii) FC.

The common storage container for electrical energy is the battery. In single use batteries, chemical energy has been converted into electrical energy and cannot be recharged from the grid. In multiple use storage batteries, the electrical energy input has been converted into an active chemical within the battery. The chemicals have been stored within the battery for later regeneration of electricity. One of the biggest problems of batteries is their tendency to accept less total charge each recharge time. The LA batteries store modest amounts of energy, with a battery lifetime of 2 to 5 years. The lead used in the batteries is toxic, and care is needed for disposal. NiCd batteries store comparatively more energy but are far more expensive than LA batteries, and cadmium is toxic. Sodium-sulfur batteries can handle more power and recharge cycles without significant loss of capacity but they should be operated at 350 °C. Very long heating and cooling times are a shortcoming, and if damaged the hot sulfur and molten sodium burns. A rechargeable battery must store all the chemicals involved in the reaction within the confines of the battery case. This requirement, to carry all the reactants at all times, is the primary reason that batteries cannot store as much energy per unit mass as can chemical fuels that generate energy by reacting with air.

Hydrogen can be utilized directly for ICEs, as well as utilized as a chemical feed stock for almost all the things that are presently being manufactured using fossil fuels. The production of hydrogen from RESs can be used for the intermittent availability of the energy from these sources, with the stored hydrogen later used when needed. An approximate comparison of hydrogen-electricity total losses: Transmission line loss is 8%; pipeline energy consumption is 12%. Hydrogen requires additional conversion steps, with electrolysis consuming 10-15% of the original electricity. Re-converting H₂ to electricity takes 30-40% of remaining energy.

Storing hydrogen, then using it to generate electricity provides only 45–55% of the original energy compared to 92% if transmitted directly as electricity [Grim 08]. Hence, RE sent as electricity provides roughly twice the end use benefits as RE delivered as H₂.

1.4. HYBRID POWER SYSTEM

Because of the intermittent and fluctuant availability of the RESs, Hybrid Power Systems (HPSs) provide a high level of energy security through the mix of various generation systems and often incorporate energy storage systems to ensure maximum reliability of power supply. Several kinds of hybridization of power sources are presented as:

- Hybridization of RESs and Backup (BKU) power units: Because of the intermittent availability of renewable energy sources, BKU power units are usually integrated for a high level of local energy security. For example, diesel generator, micro gas turbine and FCs are usually used as uninterrupted power supplies [Chen 03].
- Hybridization of renewable primary sources: Two or more renewable primary sources can be associated for complementary advantages. For example, the PV-Wind system are often proposed, because the PV panels provide powers only in the day time and wind generators produce usually more powers with stronger wind in the night. [Ahme 06].
- Hybridization of RESs and ESSs: The association of ESSs with RESs can ensure reliability and security of the distributed power generation system while maximizing the benefit from REs. For these systems, the excess and deficit of energy production can be optimally adjusted by the energy storage units to increase the energy efficiency [Abbe 05].
- Hybridization of different kinds of energy storage devices: In this case, ESSs have to be classified into two categories: fast-dynamic storage devices and long-term storage devices. The association of these two kinds of device brings their complementary advantages to the RE based generator for the power supply improvement [Zhou 07].

In this PhD thesis, a hybrid power system has been proposed to assess the energy management procedure of an active wind generator–PV panels with BKU sources such as Gas Micro-Turbine (GMT) and FCs. When combined with an energy storage as hydrogen vector.

1.5. CONTROL AND ENERGY MANAGEMENT

The growth in supply and demand in the next decades indicates steady disinvestments for new transmission lines [GRID 03] [Drog 09]. As a result, the need for developing smart distribution systems becomes a necessity. Energy management is one of the most important approaches of enabling smart grids operation, efficiency and reliability. The objective of a typical energy management is to optimize energy utilization, to minimize energy costs/waste without affecting production and quality and to minimize environmental effects [Pers 14] [Sema 13] [Riff 09].

Proper control of HPS with multiple RE/conventional-Distributed Generation (DG) and energy storage is critical to achieve highest system reliability and operation efficiency [Dime 05] [Cimu 06]. Controller plays a vital role in monitoring and regulating the required power necessary to mitigate the load demand as depicted in Fig. 1.5. Typically, a control (or energy management) system has been required to determine and assign, active and reactive output power dispatch from each energy source while keeping its output voltage and frequency at desired levels. Generally, the control systems can be classified into three categories; centralized, distributed and hybrid control paradigms. In all cases, each energy

source should have its local controller that can determine optimal operation of the corresponding unit based on current information. If multiple objectives are to be met, and all energy sources cannot operate optimally, a compromised (global optimal) operating decision should be reached.

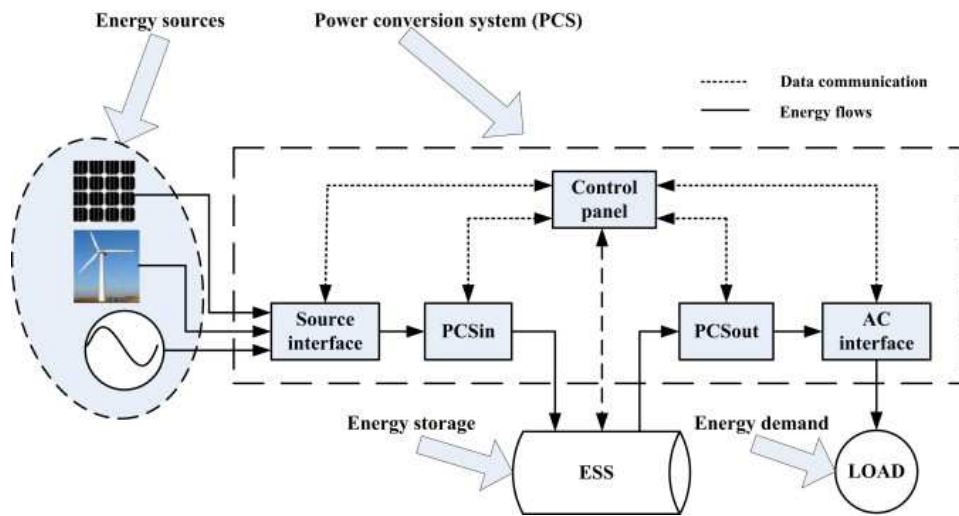
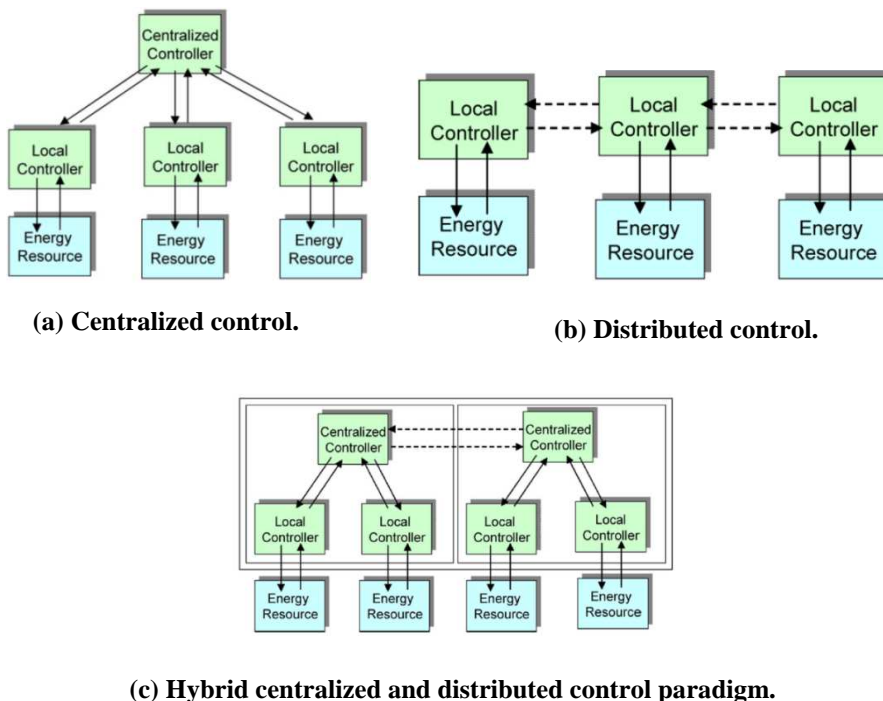


Fig. 1.5: Data communication and power flow in HPSs.

1.5.1. CENTRALIZED CONTROL

In the centralized control paradigm, the measurement signals of all energy units in a group, i.e., a micro-grid, are sent to a centralized controller, as shown in Fig. 1.6(a).

The centralized controller acts as an energy supervisor [Wang 08], [Miet 98] and makes decisions on control actions based on all measured signals and a set of predetermined constraints and objectives. It will prioritize and manage energy utilization among the various energy sources of the micro-grid [Miet 98] [Azmy 05] [Abid 03].



(a) Centralized control.

(b) Distributed control.

(c) Hybrid centralized and distributed control paradigm.

Fig. 1.6: Centralized, distributed and hybrid energy management categories.

1.5.2. DISTRIBUTED CONTROL

In a fully distributed control paradigm, the measurement signals of the energy sources of the hybrid system are sent to their corresponding local controller, as shown in Fig. 1.6(b) [Lago 09] [Haji 09] [Ko 07]. The controllers communicate with one another to make compromised (Pareto) operating decisions and achieve global optimization. The advantage of this scheme is the ease of “plug and play” operation. With this control structure, the computation burden of each controller has been greatly reduced, and there are no single-point failure problems. Its main disadvantage is still the complexity of its communication system. Intelligent model-free algorithms, such as Fuzzy Logic (FL), Neural Networks (NNs), Genetic Algorithms (GAs) and their hybrid combinations are potential tools for solving such problems [Lago 09] [Haji 09] [Ko 07].

1.5.3. HYBRID CENTRALIZED AND DISTRIBUTED CONTROL PARADIGM

A more practical scheme, hybrid control paradigm, combines centralized and distributed control schemes, as shown in Fig. 1.6(c) [Torr 08] [Jian 08].

The distributed energy sources are grouped within a micro-grid. Centralized control is used within each group, while distributed control has been applied to a set of groups. With such a hybrid energy management scheme, local optimization has been achieved via centralized control within each group, while global coordination among the different groups has been achieved through distributed control. By this way, the computational burden of each controller has been reduced, and single-point failure problems have been mitigated.

1.5.4. OPTIMIZATION TECHNIQUES

As the number of optimization variables increase, the number of simulations rises exponentially, with a consequent increase in time and effort. It is therefore important to find a feasible optimization technique to select the optimum system configurations quickly and accurately. Various optimization techniques for hybrid solar–wind system have been invested such as graphic construction methods, probabilistic approach, iterative technique, Artificial Intelligence (AI) methods, and multi-objective design [Yang 07] [Yang 08].

The main problem for the hybrid PV/wind system is related to the control and supervision of the energy distribution. The dynamic interaction between the RESs and the load demand can lead to critical problems of stability and power quality that are not common in conventional power systems. Managing the flow of energy throughout the proposed hybrid system to assure continuous power supply for the load demand is essential. In conventional energy management approaches, power electronics based DC–DC converters have been used for extracting maximum energy from PV and WE resources and controlling the complete hybrid system. Other advanced controlling techniques can remove the power fluctuations caused by the variability of the RESs and guarantee the quality of the power delivered to the load. Multi-sources system, provided an isolated area with the necessary power, has been discussed in this thesis.

1.6. MODELLING METHODS

Models are used for describing the behaviour of systems [Bahe 06]. An effective way to describe a system is by representing it in form of thermodynamic system. The thermodynamic system is a well-defined area that has been separated from the outside by a real or imaginary boundary. A system can then be classified by its boundary and quantities which enter and exit. Work, energy, heat and enthalpy flow through the boundary. If there is no matter flow

through the boundary, like in a light bulb, the system is called closed system. If there is matter flowing through the boundary, like in a pump, the system is called open system. A thermodynamic system can be described using the first law of thermodynamics, equation (1.13) with E the energy of the material, Q the heat energy and W the mechanical energy:

$$dE = dE_{in} - dE_{out} + \Delta Q + \Delta W \quad (1.13)$$

The change of internal energy depends on the internal energy of the matter flowing into and out of the system, the heat crossing the system border and the work done. When an open system is regarded, the energy balance can be transformed into an energy flow balance. A large fraction of system models are based on the first law of thermodynamics for open systems. Normally, a complex system has been divided in multitude small units, each unit represents an individual thermodynamic system. The subsystems can be divided into continuous systems which show stationary behaviour over time even if mass or energy flows enter the systems and open systems that consider time dependent behaviour. The subsystems are connected by quantities representing an energy flow. This approach is named energetic.

The causality of the system, the physical relation between cause and effect, is considered [Iwas 94] [Form 05]. As a subsystem represents a stationary conversion, the causality and therefore the definition of input and output is not fixed. For time dependent systems, this is not the case. The energy accumulated inside the system cannot change instantaneously. If the input value undergoes a step change, the output value will vary. However, it will take a certain time to reach the new stationary condition (transient behaviour). This transient behaviour has been represented by integration. Therefore, time dependent behaviours have to be represented in integral form, respecting the causality and thus defining the input and the output quantity.

Electric Equivalent (EEQ) Bond Graph (BG) and Energetic Macroscopic Representation (EMR) models use a combination of two different variables to describe the energy flow. Those two quantities represent the extensive variable related to the size of the system and the intensive variable independent on the system size. Those variables are labelled differently in the approaches, such as: action and reaction flow in EMR and effort and flow (BG) or through and across of Analog and Mixed-Signal (AMS) extensions that is a derivative of the Hardware Description Language VHDL (VHDL-AMS)

1.6.1. ELECTRIC EQUIVALENT MODEL

The EEQ model is based on the idea that systems from different domains can be reduced to few basic elements. In different energetic domains, there is not time dependent elements representing losses due to electrical or flow resistance (friction). There are time depending energy storage elements such as springs and capacitors/conductors. In the electric domain, the extensive variable is the current; the intensive variable is the voltage. Different accumulation elements have been used if kinetic energy is stored (inductor) or potential energy has been stored (capacitor). The approach using electric equivalence has been applied for FCs and FC systems by Hernandez [Hern 05], Chnani [Chna 05] and others [Famo 03] [Yu 04] [Bech 10].

1.6.2. BOND GRAPH

BG is an approach to describe systems graphically using a limited number of standardized blocks connected by power bonds [Site 05]. It is a causal explicit graphical tool. BG is based on the first law of thermodynamics for open systems using energy flows. Furthermore, it implies causalities to a large extent, helping to understand the systems working principle and to facilitate the controllability, observability and fault diagnosis. BG has been developed

during the 1960s by Payner [Payn 06] with main contributions of Karnopp, Rosenberg [Karn 90] and Thoma [Thom 06] [Sama 06].

1.6.3. CAUSAL ORDERING GRAPH

The Causal Ordering Graph (COG) is a graphic, functional and causal approach for system description [Haut 04] [Haut 96]. It is the basis of inversion based control because the causality is exclusively represented in integral form. A system has been divided into subsystems (represented by ovals) having an input and an output. The notation represents the causality. If the connection between the input and the output is static, the subsystem is labelled with a double arrow. If the system incorporates energy storage, this has to be described in integral form. It cannot be inverted keeping integral causality. Therefore, such systems are labelled with a single arrow. Furthermore, there can be coupling elements connecting two inputs to an output. Based on those three basic blocks, it is possible to describe a multitude of different systems. As only one quantity is used, it cannot be an energetic representation. To introduce the energetic aspect a secondary system description has to be used, describing the reaction variable as shown in Fig. 1.7 [Form 05].

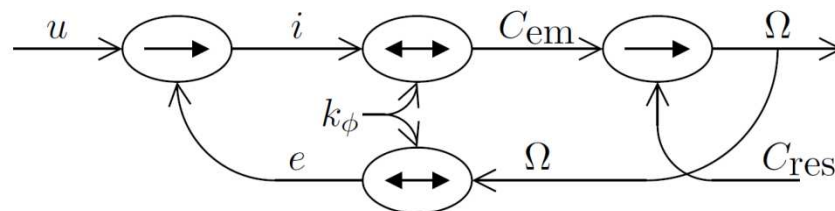


Fig. 1.7: COG representation of a permanent magnet DC machine [Form 05].

1.6.4. ENERGETIC MACROSCOPIC REPRESENTATION

The COG shows considerable potential for control structure development, but its application is still somewhat bulky complex for multi-physical systems. Therefore, another approach has been developed at the electrotechnic and power electronic laboratory of the University of Lille, France since the year 2000. The EMR tries to combine the needs regarding causality and energetic aspect for inversion based control development regarding adaptability [Form 05]. The EMR combines the advantages of the control structure development for COG and energetic approach in a commercial software [Bous 00] [Bous 03a].

The EMR is an easy to read graphic approach for system modelling. It incorporates the functional aspects with an integral causality and a choice of input and output keeping the energetic aspect based on the first principle of thermodynamic. As the EMR of a system is defined, the control structure can be developed using the GOC approach.

The EMR has been developed to describe electro-mechanical systems [Bous 00] [Bous 03b] [Bous 06]. It is based on energy flows, it is possible to adapt it to different energetic domains. In addition, it has been used for describing train system [Bous 05a], wind power [Bous 05b], paper machines [Sica 06], subway traction [Verh 04], hybrid vehicle [Lhom 08] and FC stack [Chre 08].

The compliance of different modelling approaches to the different demands has been presented in Table 1.1. The EMR is the most adapted to the problem, even though the methodology is relatively recent. It comprises as well the multi-domain aspect as the inversion based block wise control structure developed for the COG. Furthermore, it can be adapted to the use of multiple variables. Therefore, EMR has been chosen for applications on multi-source systems.

Table 1.1: Compliance of different modelling approaches to the needs.

Approach	Electric Equivalent Model	Bond Graph	COG	EMR
Domains	All simplified to electrical model	Different	Different	Different
Modular	Yes	Yes	No	Yes
Energetic	Implicit	Yes	No	Yes
Causality	No	Mostly	Yes	Yes
Visualization	Electric representation	Graphic	Graphic	Graphic
Software	PSPice	20-sim	Matlab-Simulink	Matlab-Simulink
Control	Electric approach	Overall transfer function needed	Yes	Yes

The different EMR elements, their causality and inversion principles have been comprehensively listed in [Site 06].

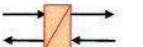
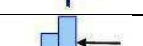
1.6.4.1. INTERACTION PRINCIPLE

The system can be decomposed into subsystems in interactions using 4 basic EMR elements as shown in Table 1.2:

- energy sources (green ovals, terminals of the systems);
- accumulation elements (orange rectangles with diagonal line, energy storage);
- conversion element without energy accumulation (various orange pictograms, energy conversion);
- coupling elements for energy distribution (orange overlapped pictograms, energy distribution).

The elements are connected by a quantity pair indicating action and reaction using exchange variable (arrows), as depicted in Table 1.2. Those quantity pairs reflect the causality of the system. The product of action and reaction variables between two elements leads to the instantaneous power exchanged. The choice of quantities is based on the first law of thermodynamics. Therefore, the methodology has been called EMR.

Table 1.2: EMR pictogram.

	Source element (energy source)		Accumulation element (energy storage)		Indirect inversion (closed-loop control)
	Mono-physical conversion element		Mono-physical coupling element (energy distribution)		Direct inversion (open-loop control)
	Multi-physical conversion element		Multi-physical coupling element (energy distribution)		Coupling inversion (energy criteria)
	Amplification element		Switching element		Inversion of a switching element

1.6.4.2. CAUSALITY PRINCIPLE

As in COG [Haut 96] [Haut 04], the integral causality only is considered in EMR. This property leads to define accumulation element by the time-dependent relationship between variables. The output is an integral function of its inputs. Other elements are described using

relationships without time dependence. In order to respect the integral causality specific association rules are defined.

1.6.4.3. INVERSION PRINCIPLE

This inversion methodology is an alternative way to locate controllers, measurements or estimations. The inversion based control theory has been initiated by COG [Haut 96]. The control structure of a system is considered as an inversion model because the control has to define the appropriated inputs to the system from the desired output as depicted in Fig. 1.8.

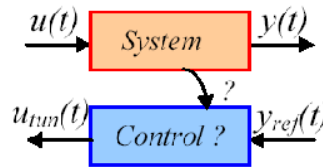


Fig. 1.8: Inversion-based control.

In this method, relationships without time-dependence are directly inverted (with neither control nor measurement).

Because the derivative causality is forbidden, the direct inversion of time-dependence relationships is not possible. An indirect inversion is thus performed using a controller and measurements. These inversion rules have been extended to EMR, therefore:

- conversion elements are directly inverted;
- accumulation elements are inverted using a close-loop control;
- inversions of coupling element require a criteria inputs, which lead an organization of the energy distribution.

Hence, these modelling methods are used to present the HPSs and control them. In this thesis, EMR is used to present the different elements of the studied HPS.

1.7. LITERATURE REVIEW

RESs can be defined as sustainable resources available over the long term at a reasonable cost that can be used without negative effect. RESs include biomass, hydropower, geothermal, solar, wind and marine energies. Renewable energy in 2011 supplied about 19% of the global final energy demand and 9.7% came from modern renewable sources, including hydropower, wind, solar, geothermal and biofuels [Alem 14]. The RESs sector is expected to continue growing in the future, especially in solar and wind equipment production. Technologies for the RES will also show a decrease in production costs as a result of accelerated technology developments, an increase in green equipment manufacturing and the degree of investment worldwide. However, PV sources are intermittent in nature. Therefore, the smoothing of power fluctuations by storing the energy during periods of oversupply and restore it to the grid when demanded becomes necessary. Accordingly, ESSs can be appropriately used for this purpose.

ESSs can be divided into two essential categories [Mass 15] [Kusa 15]: (i) capacity-oriented technologies such as hydroelectric and hydrogen systems; (ii) access-oriented technologies such as batteries, flywheels and supercapacitors. The cost and the power response time are the most considerable criteria to distinguish among the ESSs.

Hydrogen, as a long-term ESSs, is a renewable fuel and excellent energy carrier thanks to its reliability and relative high efficiency conversion. It can be stored in different forms gaseous, liquid or metal hydride. It is environmentally appropriate since there is no pollution gases or materials related to its production, storage, transportation and/or consumption. The importance of hydrogen use becomes a priority solution when the energy produced from RESs is injected with large amounts. For grid balance and power quality enhancement, the need to the high capacity HSS will be significantly increased as explained by Arnone et al. [Arno 14]. Therefore, hydrogen has been introduced as storage medium in HPSs such as [Taba 15] [Trif 14].

Aiming at solving the intermittency problem of RESs, HPSs with HSS are considered. Obviously, several RESs can be combined with both ESSs and Back-up (BKU) power units or at least one of them. Accordingly, several hybridization possibilities of power sources can be noticed [Torr 15]: (i) BKU power units integration into RESs increase the level of local energy security. (ii) Hybridization of primary RESs of SES and WES: SESs provide their power in the day time and WESs produce usually more powers with stronger wind in the night. (iii) Hybridization of RESs and ESSs to ensure both reliability and security of power generation systems. The produced and stored energies can be optimised to increase the energy yield of HPSs. (iv) Both fast-dynamic ESS and long-term ESS are hybridized with RESs to obtain more reliable HPSs for both dynamic and static cases. Many studies have been realized by using different hybridization systems. SES-WES have been combined by Bitterlin et al., Bansal et al. and by Moriana et al. [Bitt 06] [Bans 11] [Mori 10]. The difference among the existing studies is the different percentage participation of each source. Other combination solutions of HPSs have been applied to meet the requested load such as WES-SES-diesel [Shaa 10], WES-diesel [Bowe 03] and WES-hydropower [Beni 08].

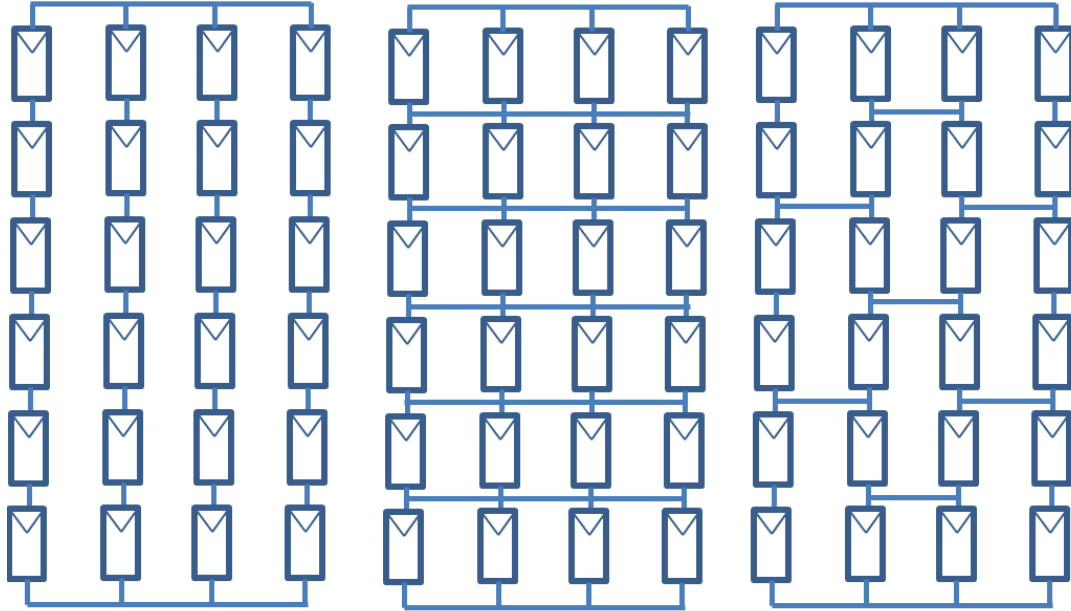
1.7.1. PV PANELS

The PV power system becomes popular in this new era because the solar energy is renewable and environmental friendly. Although research and development on solar cell design and fabrication is carried out continuously to reduce the high capital cost, the improvement of overall PV system performance is equally important. One of the interesting areas is by implementing suitable shading solution to ensure the maximum power can be extracted regardless changes of environmental conditions.

PV panels have different operating points depend mainly on the solar radiation density. Hence, strategies for selecting the maximum power operating point are requested. Accordingly, Maximum Power Point Tracking (MPPT) technique is largely proposed as a solution for the shaded PV panels [Ahma 08] [Chow 10]. When shading is partial, there will be a new problem where the MPPTs are different for the various PV panel groups connected to one MPPT controller. Therefore multi-MPPT can be proposed. Nevertheless, in this case, all PV panels have a MPPT controller which is far from being economically optimal. In general, passive and active techniques have been introduced as solutions for this problem [Sham 13] [Bidr 12]:

- I. Passive techniques: two solutions are used here for reducing partial shading losses; the first one is by-Pass diodes [Hayo 10], which have been invested to protect shading panels from hot spot effects and to increase the overall PV partial shading panel's efficiency. However, the main disadvantage of these diodes is preventing PV panels from producing maximum possible power in case of partial shading [Sham 13]. The other solution is changing PV array interconnection using one of the following

configuration types: Series-Parallel (SP) (Fig. 1.9(a)), Total-Cross-Tied (TCT) (Fig. 1.9(b)) and Bridge-Linked (BL) (Fig. 1.9(c)). It has been shown that BL and TCT configurations result in increase in MPPT configuration. However, the higher number of interconnections slightly increases the loss of the PV system due to the additional cable loss. In this approach, the large adaptive bank significantly rises installation cost and requires a complicated control algorithm [Sham 13] [Bidr 12].



(a) Series-Parallel

(b) Total-Cross-Tied

(c) Bridge-Linked

Fig. 1.9: Different interconnection schemes in passive techniques [Sham 13].

II. Active techniques: three categories have been noticed in this technique:

- Multi-tracker Inverter

The shading effect in one module or a group of modules will considerably affect the overall power production. This problem can be solved with a multi-tracker inverter [Hayo 10]. The presence of a multi-tracker inverter is therefore justified when several parts of a PV array do not have the same electrical properties. For example, when a part of the field is likely to be subjected to shading, it is connected to a MPPT of a dedicated inverter. Similarly, when two parts of a field do not have the same orientation and inclination (for example double bridge east-west), each part can be connected to a singular MPPT. The multi-tracker is a technical solution that increases the overall cost of the installation.

- A tracker per module

It is now clear that when there are power disparities (especially because of the shade or dust), the ideal solution would be to have a MPPT for each module [Kara 07] [Kara 08] [Sara 10]. Thus, the available power of each module would be obtained. Some manufacturers offer this option in their pack. This solution is ten times more expensive than the multi-tracker solution [Hayo 10].

- Photovoltaic array reconfiguration

This technique depends on using poles and switches for obtaining an optimal PV reconfiguration. This technique has been developed as following:

- Simplified form of PV array reconfiguration was started by Salameh et al. [Sala 90a] [Sala 90b]. In these studies, PV array reconfiguration has been applied to supply DC motor coupled with water pump by required power.
- The second using was to provide electrical cars with necessary power [Autt 98]. The real use of PV cells reconfiguration has been started by Sherif and Boutros [Sher 02]. In their solution, PV reconfiguration has been realized using transistors and switches between cells.
- The PV array reconfiguration, which has been achieved by Nguyen et al. [Nguy 08], has been divided into fix and adaptive parts with switching matrix between them as depicted in Fig. 1.10. However, the mathematical formula for the optimal reconfiguration has not been presented. In [Vela 05] [Vela 08] [Vela 09], a new PV reconfiguration has been reached taking into account the mathematical formula requested for optimal solution. But with 280 possibilities of configuration for just nine PV modules, it will be difficult to determine the optimal configuration. Therefore, this solution is suitable for a small number of PV modules. In [Sham 13], Shams El-Dein et al. have founded an optimal PV array reconfiguration in addition to mathematical formulation. This solution is so complicated and needs a lot of poles and switches for each module as shown in Fig. 1.11. Moreover, it requests an optimal solution to realize the suitable reconfiguration.

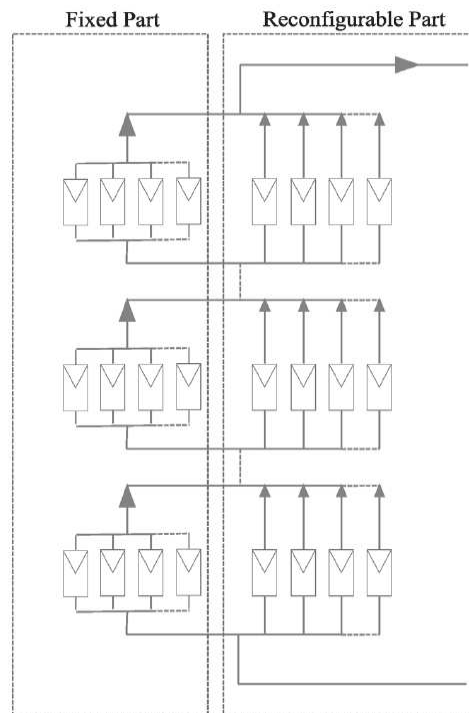


Fig. 1.10: Fixed and adaptive parts of PV reconfiguration proposed by Nguyen et al [Nguy 08].

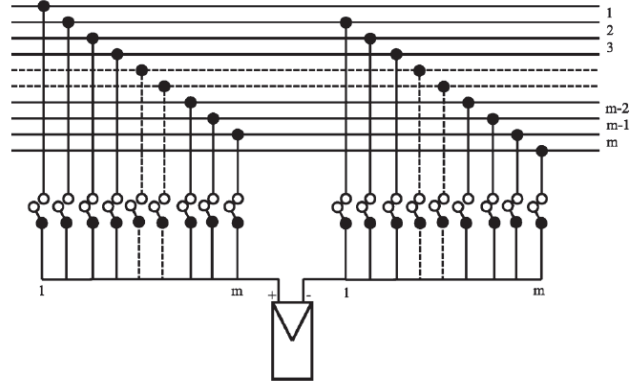


Fig. 1.11: Optimal PV array reconfiguration presented by Shams El-Dein et al.

The production of energy is becoming increasingly decentralized [Salm 10]. For small and medium generation purposes, RE systems can be conveniently used. Although decentralized systems can be favourably used in order to reconcile the different forms of energy, to create synergies between them, and to accomplish supply/demand equilibrium, still their main disadvantage is the energy fluctuations increase in power grids. Consequently, the need for ESS has obviously risen [Mash 09] [Mahm 03]. ESS is among the possible solutions for smoothing power fluctuations by storing the system energy surplus during overproduction periods and reusing this energy excess when requested. For this purpose, the following ESSs have been used: compressed-air, pumped hydro, flywheel, super-capacitors, hydrogen and batteries [Kare 14] [Vina 08] [Subk 11] [Huan 09] [Taba 12]. Table 1.3, introduced by Barin et al. [Bari 09], presents the main features of each ESS.

1.7.2. ENERGY STORAGE SYSTEMS

To decide which ESS technology is more appropriate, five ESSs qualitative criteria are considered: load management, technical maturity, power quality, efficiency and cost. Owing to hydrogen ESS low mass density and low self-discharges [Bari 09] shown in Table 1.3, it becomes a promising means of electrochemical storage that attracts huge interest despite its immature technology, and relative high cost. Since hydrogen is not a primary energy source, its energy storage is based on an electrolyser to split water into hydrogen and oxygen. Hydrogen ESS is suitable for storing electrical energy for a long term. It is one of the most suitable technologies and reliable options for load shifting applications. On the other side, batteries' banks are largely used as solution for PV energy storage. However, the demerits of this technology are its relative low energy density, self-discharge, and leakage characteristics. Unlike hydrogen storage systems, batteries are not the best ESS solution for long-term energy storage purposes [Meen 14] [Parr 14].

Table 1.3: Hydrogen ESS compared with other ESS technologies [Bari 09] [Medi 14].

ESS Criteria	Compressed air	Pumped hydro	Hydrogen	Flywheel	Super-capacitor
Quantitative	Rated data				
Costs (US\$/kW)	450	750	1200	300	1300
Quantitative	Weights – “the higher the better”				
Load management	0.65	0.60	0.80	0.40	0.25
Power quality	0.40	0.40	0.85	0.80	0.65

In order to balance the energy network in HPSs, Ehteshami et al. [Ehte 14] have compared a numerous energy storage techniques based on their energy/power density, ease of integration,

cost effectiveness, durability, efficiency and safety. The study has proved that the hydrogen is the most appropriate storage medium among the other existing storage methods in favour of its low capital cost and high energy density. Another comparison on the energy storage technologies has been adopted by Meena et al. [Meen 14], Hydrogen Energy Storage System (HESS) is stated to be a promising technology for load shifting applications. Another comparison has been achieved using small scale application of HPSs. Accordingly, Parra et al. [Parr 14] has tested a single grid-connected house that has been provided with PV energy source for a cycle of day. This system has been combined with two storage mediums, LABES and hydrogen. The authors have noticed that both LABES and hydrogen have a system efficiency enhancement of about 1.5 times for each. Consequently, an equal performance for both types of storage technologies has been illustrated.

Hydrogen is a good storage carries thanks to its clean, light and efficient fuel. In favour of its positives aspects, HESS has been used for different RE systems especially PV and wind systems. In [Gao 14], Gao et al. have shown the importance of energy storage as a solution for the RESs intermittence using WE. A comparison between hydrogen production from RESs and non-RESs has been examined by Acar et al. [Acar 14]. Based on the global warning potential beside the social cost of carbon criteria, the results have shown the optimal hydrogen production from wind as well as from nuclear sources. In [Riha 14], two energy sources, PV panels and WT have been used by Riahy et al. to overcome RESs intermittence problem, to enhance the reliability of the system and to minimize hydrogen production. Ural et al. [Ural 14] have only proposed PV array to produce the hydrogen at surplus energy production and to re-provide it by means of FCs to eliminate instability in case of lack of power.

1.7.3. HYBRID POWER SYSTEMS

In recent years, many improvements have been provided to hybrid PV-Hydrogen systems to increase their efficiency such as modifying the electrolyser connection with PV, using special chemical compounds, controlling water temperature and finding solutions for some negative internal physical phenomena. Talin et al. [Tali 13] have studied a PV-hydrogen system combined with photo-electrochemical junction cells that directly convert sunlight into oxygen and hydrogen. As this technology is in its early stage studies, its low efficiency should be improved. Furthermore, in another proposed solution, PV-Electrolyser (ELS) system efficiency can be increased using direct connection between PV and Proton Exchange Membrane Electrolyser (PEM ELS) as discussed by Rau et al. [Rau 14]. Special chemical compounds have also been used to affect the system efficiency. Cadmium Sulfide nanoparticles as photosensitizers have been developed to promote the electrolyser hydrogen production. As a result, PV efficiency has been increased as explained by Zou et al. and by Zhu et al. [Zou 14] [Zhu 14]. Polonsky et al. [Polo 14] have proved the effect of temperature on electrolyser efficiency. Temperature has been increased from 373K to 933K in pressurized Alkaline. In this case, temperature has non-significant impact on the system efficiency in thermo-neutral mode. In operation mode (operation at temperature below 373K) and endothermic mode (operation at temperature more than 933K) any temperature-rise has an effect on electrolyser efficiency as shown by Petipas et al. [Peti 14].

Although alkaline electrolysers are available with MW class for industrial applications, PEM ELSs are preferred in RE storage due to their very fast response time which makes them suitable for the fluctuating behaviour of RESs as illustrated by Arico et al. [Aric 13].

Energy management is a necessary method for achieving an economic HPS solution which will be applied in this thesis [Kanc 11]. The use of hybrid system with RESs and no RESs as

well as the RESs intermittency guide to a non-controlled HPS output that needs an ESS to meet the requested load [Riff 09] [Mult 13]. However, this ESS requests an energy management system able to produce convenient orders to store/restore the energy at ESS. Consequently, an economic HPS will be obtained.

In order to achieve an optimal power generation from different RESs and the reliability of the power system, many studies have been realized [Jose 14]. PV-WE have been combined by Bitterlin et al., Bansal et al. and by Moriana et al. [Bitt 06] [Bans 11] [Mori 10]. The difference among the existing studies is the different percentage participation of each source. Other combination solutions of HPSs have been applied to meet the requested load such as WE-PV-diesel [Shaa 10], WE-diesel [Bowe 03] and WE-hydropower [Beni 08]. As the RESs have the intermittence problems, it is necessary to combine these systems with ESSs. Many energy management solutions have been introduced for this objective. Monnerie et al. [Monn 14] have used a hybrid WT and high temperature steam electrolyser. The investigation of energy balance has been achieved for a plant capacity of 10 MW. This combination aims at efficiency enhancement of the plant. Consequently, a plant efficiency of 38% has been obtained and the power penetration has been overcome. PV-WT system has been also treated by Cau et al. [Cau 14]. This system has been combined with storage elements such as batteries and hydrogen. In this case, the energy management has considered the uncertainty of batteries instead of State of Charge (SoC) and the load demand for taking into account RESs intermittency. A reduction in cost of 15% has been noticed in comparison to the conventional SoC method. As presented by Rau et al. [Rau 14], direct connection of PV panels with a PEM ELS has been used. Accordingly, this system has an optimal efficiency at higher current-lower voltage. Moreover, Choudar et al. [Chou 15] have introduced a HPS of grid connected active PV system consisting of PV-batteries-ultra-capacitors. The presented strategy was considered the weather prediction and load forecasting. The results have shown smooth power providing, fast power compensation and optimum investing of storage elements.

Energy management is becoming a priority for HPSs regularity as well as to reduce the energy generation costs. For finding the most proper approach, to achieve the optimal energy management strategy, one of existing optimizers can be applied such as (i) random optimizer; (ii) gradient optimizer; (iii) random minimax optimizer; (iv) gradient minimax optimizer; (v) quasi-newton optimizer; (vi) least Pth optimizer; (vii) minimax optimizer; (viii) random max optimizer; (ix) hybrid optimizer; (x) discrete optimizer; (xi) Genetic Optimizer (GO); (xii) State Space Search Reference (SSSR); (xiii) Simulated Annealing Optimizer (SAO) and (xiv) sensitivity analysis [Site 07]. Generally, for global solution, GO and SAO have been used. Velik et al. [Veli 14] have selected the SAO to search for the optimal energy management strategy. Accordingly, the two methods SSSR and SAO have been compared and the optimization error results have shown the preference of SAO methodology.

After choosing the appropriate optimizer, system sizing has to be applied for achieving the minimum cost power generation of HPSs-satisfied loads demand. Accordingly, Maleki et al. [Male 14] have applied multi-AI techniques on PV-WT-FC. This combination aims at optimum sizing for satisfying the load demand and minimum annual cost. Particle Swarm optimization (PSO), Tabu Search (TS), Simulated Annealing (SA) and Harmony Search (HS) methodologies have been applied on the proposed system. An economic comparison has been performed among the mentioned methods. As a result, PSO is the most economic method and promising one. In addition, using historical data of climate and the load demands, Feroldi et al. [Fero 14] have applied the GA for finding the optimum sizing of the HPSs. Furthermore, Brka et al. [Brka 14] have used GA to choose the best stand-alone hydrogen system among three proposed systems such as WT-H₂, WT-PV-H₂ and PV-H₂. The comparison has been

performed based on three criteria: minimising net present cost, whole life cycle emission and dumped excess energy at low demand.

When the energy produced from RESs is injected with a big amount, the need to the high capacity hydrogen-based will increase significantly for grid balance and power quality enhancement as explained by Arnone et al. [Arno 14]. Accordingly, some researchers have used different conventional controlling technique [Redd 07] for different combination of HPSs. Park et al. [Park 04] have presented the power compensation system for controlling the energy flow through HPSs according to load demand. Valenciaga and Puleston [Vale 05] and Onar et al. [Onar 06] have developed controller for HPSs. Accordingly, three modes of operation have been developed using sliding mode control methods for controlling the hybrid system. Trifkovic et al. [Trif 14] have developed a HPS consisting of WE–PV–FC–ELS with hydrogen storage. Predictive control has been designed for better power management in comparison with the case where no predictive control has been applied. Garcia et al. [Garc 14] constructed three Energy Supervisory Control (ESC) for both batteries and hydrogen storage mediums. In this study, the SoC of batteries and the hydrogen tank levels have been maintained at optimal levels. A comparison among the three ESCs has been performed to reduce the ESS devices' costs.

The techno-economic study of the HPSs is required for optimal efficient utilisation. This study can be investigated using software tools. Sinha et al. [Sinh 14] have found 19 software tools that have been used for this aim. Consequently, suitable method based on the capability, limitation and availability of each software tool has been searched for. Accordingly, HOMER software tool which has been widely used due to its easiest and fastest evaluation capacity for many maximum combinations of RESs has been found as appropriate software. In addition, HOMER has been used by Mohammed et al. [Moha 14] for dealing with the energy management of hybrid PV–FC system in the city of Brest in France. A special Matlab–Simulink[®] model for the energy management controlled the energy flow between HPSs and load has been constructed by Abdelkafi et al. [Abde 14]. This hybrid system composed of WT–ELS–FC and super-capacitor. Different scenarios have been treated alongside with optimal and reliable energy management algorithm has been obtained. Furthermore, Zhang et al. [Zhan 14a] have exercised an energy management on HPS consisting of micro-grids that has the structure PV–ELS. Obviously, this study has been applied for both stand-alone and grid-tied. The load prediction has led to an enhancement in electricity consumption by (5.7% and 25%) for (stand-alone and grid-tied) systems respectively. El-Shater et al. [El-Sh 01] discussed the energy flow and management of a hybrid PV–wind–fuel system. Each of the three energy sources has been controlled so as to deliver energy at optimum efficiency by FL control technique which is employed to achieve MPPT for both solar and wind energies and to deliver is maximum power to a fixed DC voltage bus. Chedid and Rahman [Ched 97] have presented controller design that monitors the operation of the stand-alone or grid-connected systems. The controller determines the available energy from each of the system components and environmental credit of the system. The developed model can give production cost, unmet and spilled energies, and battery charged and discharged losses. Some new approaches based on FL and GA techniques [Senj 06] [Ched 00] have been proposed for the scheduling of the battery and the diesel generator of a hybrid PV–WE–diesel system.

1.8. THESIS ORIENTATION

In this thesis RESs consisting of PV-WE have been selected as principle sources and they have backed up by another sources that have dynamic production feeding such as GMT and FCs. This combination of sources has an over generation at low load. However, they have a lack of power at peak load. Therefore, an energy management strategy has been proposed to

overcome the difference between generation and consumptions. This energy management based on hydrogen storage and uses the electrolyzers for the energy storage and FCs for energy restoring. In addition, FLC and NN have been used such as energy management methods. A comparison of these two methods has been introduced. The problem of hydrogen flow at electrolyser output has been studied as well as the problem of PV panel shading has been detailed. Consequently, an increasing in hydrogen flow has been obtained and a new PV panels reconfiguration overcome the problem of PV panel shading has been achieved.

In this thesis, the main contributions are thus to propose:

- A relatively cheap and simple PV panel's configuration to overcome the partial shading PV panels using switches and dSPACE electronic card. The shaded PV panels, if any, have caused minimum power losses in comparison of existing solutions.
- A methodology for increasing the electrolyser water temperature of input by internally using a percentage of the energy produced by PV panels via FL control and PI control. Therefore, the positive effect of water temperature rise in PEM ELS has been demonstrated. The desirable impact of water temperature control on the PEM ELS efficiency using PV panels has been clearly highlighted.
- An energy management methodology for the proposed HPS. This energy management has been achieved using two methods Fuzzy Logic Control (FLC) and NN. Consequently, a comparison between the two methodologies has been performed.

1.9. THESIS OUTLINE

In the second chapter HPS comprises of PV, WTs, PEM ELS, PEMFC and Gas Micro-Turbine (GMT) has been studied. Each source has been presented using specific EMR model. Accordingly, different equations necessary to realize the different models have been comprehensively illustrated. Consequently, a global model presenting the HPS has been obtained.

In the third chapter, HPS comprises 72 kW PV panels and 59 kW PEM ELS has been studied. Accordingly, a new shaded PV panel's solution based on simple switches reconfiguration and dSPACE electronic card has been achieved. In addition, PEM ELS efficiency enhancement based on FL-PI controls has been performed. Consequently, the obtained HPS is able to provide the hydrogen at relatively high efficiency.

In the fourth chapter, sizing and energy management strategies have been applied on a HPS comprising PV, WTs, GMT and FCs sources. Obviously, both NN and FL methods have been applied to achieve an optimal solution with minimum energy production cost. Consequently, a comparison between the two approaches has been performed and economic study has been presented.

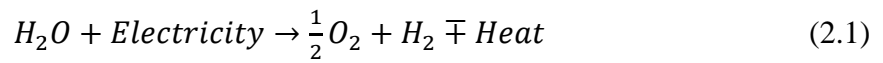
2. MULTI-SOURCE SYSTEM: MODELLING AND SIMULATION

2.1. INTRODUCTION

In this chapter, EMR modelling of multi-source system has been proposed. Obviously, PEM ELS, PEMFC, WT, PV panels and GMT models have been introduced. The mathematical equations presenting the sub-models have been comprehensively explained. In addition, simulation result has been shown to present sources' outputs for each model. The global HPS model will serve for the energy management study in case of multi-source system.

2.2. PEM ELECTROLYSER

EMR model for PEM ELS has been developed by Agbli [Agbl 11a] using EMR methodology in Femto-ST/FCLab laboratories. The PEM ELS uses the electricity as a fuel alongside with water and heat as endothermic nature elements. As a result of reaction in the PEM ELS, oxygen and hydrogen have been produced at the anode and the cathode respectively as given in equation (2.1).



The PEM ELS model comprises four sub-models: electrical, electrochemical-thermodynamic, thermal and hydraulic models.

2.2.1.EMR ELECTRICAL SUB-MODEL

The terminal voltage of the electrolyser can be divided into two parts: the first (E) that is assigned to the Gibbs free energy change, while the second part is related to over-voltages. The sum of the over-voltages is related to the current flowing through the electrolyser $\eta(I_{ELS})$. Electrical variables of the electrolyser, I_{ELS} and V_{ELS} , follow the relationship:

$$V_{ELS} = E + \eta(I_{ELS}) \quad (2.2)$$

Experimentally, it is possible to use the electrolyser with either imposed current or voltage configuration.

This sub-model consists of one EMR source and coupling blocks. The coupling block has served in the connection between the provided power at the electrolyser input and both powers providing the electrochemical sub-model $E I_{ELS}$ and covering power loss in thermal model $I_{ELS} \eta(I_{ELS})$. The EMR of electrical sub-model is shown in Fig. 2.1.

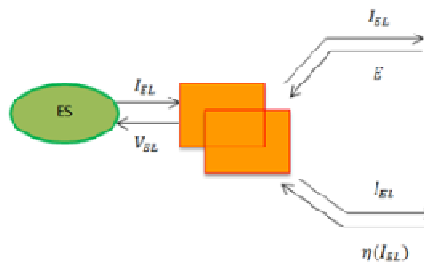


Fig. 2.1: EMR of electrical sub-model.

2.2.2.EMR ELECTROCHEMICAL AND THERMODYNAMIC SUB-MODEL

The EMR of the electrochemical and thermodynamic sub-model is depicted in Fig. 2.2.

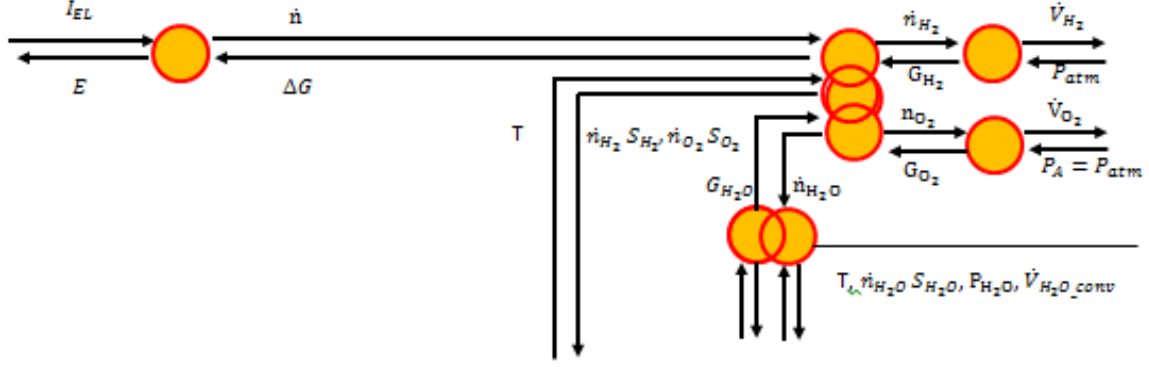


Fig. 2.2: EMR of electrochemical and thermodynamic sub-model.

Fig. 2.2 summarizes the principle of water separation into oxygen and hydrogen in presence of electric and thermal energy dissipated by the PEM ELS over-potential and needed in the environment of electrolysis. The losses in the stack combined of activation, diffusion and ohmic losses have been converted to heat. Therefore, thermal energy has been generated from the electrical source and/or the electrolytic environment.

When water is electrolysed, electrical and heat energies ($\Delta G_{(1)}$ and $T\Delta S_{(1)}$ respectively) related to the equation (2.1) will be required to complete the reaction [Onda 04].

Gibbs energy stated in equation (2.3) can be obtained by finding the values of enthalpy variation ΔH and free entropy variation ΔS :

$$\Delta G_{(H_2O, H_2, O_2)} = \Delta H + T\Delta S \quad (2.3)$$

Entropy variation for water electrolysis in equation (2.1) is:

$$\Delta S_{(H_2O, H_2, O_2)} = A \cdot \ln(T) + B \cdot T + C \left(\frac{T^2}{2}\right) + D \left(\frac{T^3}{2}\right) - \left(\frac{E}{2T^2}\right) + G \quad (2.4)$$

The constant A , B , C , D , E and G are listed in Table 2.1:

In addition, the enthalpy variation for equation (2.1) is presented as:

$$\Delta H_{H_2O, H_2, O_2} = AT + B \left(\frac{T^2}{2}\right) + C \left(\frac{T^3}{3}\right) + D \left(\frac{T^4}{4}\right) - \left(\frac{E}{T}\right) + F - H + H_0 \quad (2.5)$$

where, the constants A , B , C , D , E , F , H and H_0 are given in Table 2.2:

Table 2.1: Entropy constant values of PEM ELS.

	$A[K]$	$B[K]$	$C[K^2]$	$D[K^3]$	$E[K^{-2}]$	$G[J/Kmol]$
H_2O	-203.60	1523.29	-3196.41	2474.45	3.8553	-488.72
H_2	33.07	-11.36	11.43	-2.77	-0.1586	172.71
O_2	30.32	-20.24	57.87	-36.51	-0.0074	246.79

Table 2.2: Enthalpy constant values of PEM ELS.

	$A[K]$	$B[K^2]$	$C[K^3]$	$D[K^4]$	$E[K^{-1}]$	$F[J/mol]$	$H[J/mol]$	$H_0[J/mol]$
H_2O	-203.6	1523.29	-3196.41	2474.4	3.8553	-256.55	-285.83	-285.83
H_2	33.07	-11.36	11.43	-2.77	-0.1586	-9.98	0	0
O_2	31.32	-20.24	57.87	-36.51	-0.0074	-8.90	0	0

Based on equation (2.1), the Gibbs energy and the entropy variations are respectively:

$$\Delta G_{(2.1)} = G_{H_2} + \frac{1}{2}G_{O_2} - G_{H_2O} \quad (2.6)$$

$$\Delta H_{(2.1)} = H_{H_2} + \frac{1}{2}H_{O_2} - H_{H_2O} \quad (2.7)$$

The Gibbs energy is related to the electrolysis voltage as expressed in equation (2.8):

$$E_{(2.1)} = \frac{\Delta G_{(2.1)}}{nF} \quad (2.8)$$

where, n is the number of electrons participating in the reaction according to water electrolysis:



The electrolyser current is directly proportional to the amount of the produced gas and the consumed water as depicted in equation (2.11).

$$\dot{n} = \dot{n}_{H_2O} = \dot{n}_{H_2} = 2\dot{n}_{O_2} = \left(\frac{I_{ELS}}{2F}\right) N_{cell} \eta_F \quad (2.11)$$

Gibbs energy and entropy expressions as function of liquid water, hydrogen and oxygen for a given temperature can be expressed by equations (2.4) and (2.5) [Onda 04] [Pier 07].

The value of the reversible potential E depends on the reactants concentration. Consequently, the reversible potential E , called the Nernst potential, is calculated as [Pier 07] [Ni 07]:

$$E = E_{Nernst} = \left(\frac{\Delta G}{nF}\right) = E_{(2.1)} + \left(\frac{RT}{2F}\right) \ln \left(\frac{P_{H_2} P_{O_2}^{0.5}}{a_{H_2O}}\right) \quad (2.12)$$

where, the water electrolysis occurs at atmosphere pressure (1 atm).

The gas flow is expressed by:

$$\dot{V}_{gas} = \dot{n}_{gas} \left(\frac{RT}{P_{atm}}\right) \quad (2.13)$$

2.2.3.EMR THERMAL SUB-MODEL

The EMR of thermal sub-model is depicted in Fig. 2.3:

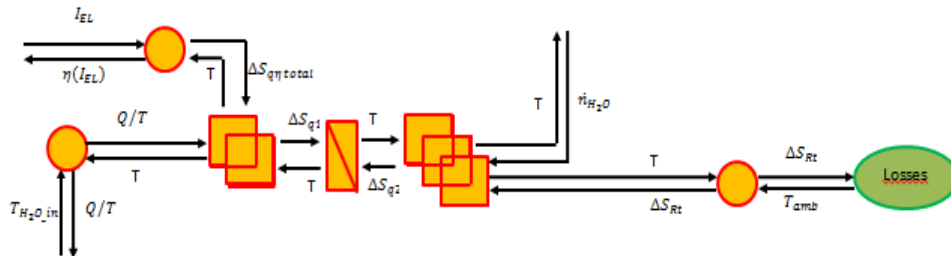


Fig. 2.3: EMR of thermal sub-model.

The thermal model has two degrees of freedom. The first describes the temperature of the stack and the other is concerned with the temperatures evaluation of the tank.

When electrochemical reaction takes place, there will be a power loss related to temperature loss which represents the output of the thermal sub-model. The requested energy for temperature loss cover obtained from electrical sub-model is shown in Fig. 2.3. The stack of the electrolyser may be considered as a heat accumulation element. Considering all thermal fluxes at inputs and outputs, the thermal model can be presented as equation (2.14) [Ni 07] [Lebb 09] [Biak 08] [Shin 07] [Bous 02] [Bous 00] [Pére 10] [Roy 06] [Four 06] [Ulle 03]:

$$C_{th-stack} \left(\frac{dT}{dt} \right) = T \left[\sum(\Delta S_q)_{in} - \sum(\Delta S_q)_{out} \right] \quad (2.14)$$

Equation (2.14) presents the heat balance in the electrolyser stack taking into account all losses and sources of thermal energy. Therefore, the sum of entropies related to both heat sources $\sum(\Delta S_q)_{in}$ and heat losses $\sum(\Delta S_q)_{out}$ have to be calculated.

The entropy variation of input $(\Delta S_q)_{in}$ can be calculated considering the entropy flow for the electro-thermic and hydro-thermic exchangers.

a. Entropy flow for the exchanger electro-thermic

The main source of heat comes from the conversion of all heat over-voltages η_{tot} as expressed in equation (2.15):

$$T\Delta S = 2F \eta_{tot} = 2F(\eta_{EL} + \eta_{diff} + R_e j) \quad (2.15)$$

The obtained entropy can be given by:

$$\dot{n} \Delta S = \dot{n} \left(\frac{2F(\eta_{ELS} + \eta_{diff} + R_e j)}{T} \right) = \left(\frac{I_{ELS}}{2F} \right) N_{cell} \left(\frac{2F(\eta_{ELS} + \eta_{diff} + R_e j)}{T} \right) \quad (2.16)$$

Due to the work conditions and devices used in the experimental test [Agbl 11a], it is not possible to measure considerable value of current. Therefore, the diffusion overvoltage η_{diff} has been neglected. Moreover, the activation overvoltage η_{ELS} and ohmic overvoltage E_{ohm} have been calculated from equations (2.17) and (2.18) [Biak 08] [Harr 05] [Dale08] [Garc 08]:

$$\eta_{ELS} = E_{act-anod} + E_{act-cath} = \left(\frac{RT}{2\alpha_{AF}} \right) \sinh^{-1} \left(\frac{I_{ELS}}{2j_{0,AA}} \right) + \left(\frac{RT}{2\alpha_{CF}} \right) \sinh^{-1} \left(\frac{I_{ELS}}{2j_{0,CA}} \right) \quad (2.17)$$

$$E_{ohm} = R_e j = \left(\frac{\phi}{\sigma_m} \right) I_{ELS} \quad (2.18)$$

b. Entropy flow for the exchanger hydro-thermic

The entropy flow for the exchanger hydro-thermic is given by:

$$\dot{n}_{H_2O} \Delta S_{H_2O} = \frac{C_{P-H_2O}(T - T_{in-H_2O}) Q_{V in-H_2O} \rho_{H_2O}}{T} \quad (2.19)$$

where, the water density is calculated using:

$$\rho_{H_2O} = (T_{in-H_2O} - 273.15) (-0.0038) + (T_{in-H_2O}) (-0.0505) + 1002.6 \quad (2.20)$$

C_P values are function of the three parameters listed in Table 2.3 according to equation (2.21):

$$C_{P-(H_2O, H_2, O_2)} = \frac{[a + bT + cT^2 + dT^3 + eT^{-2}]}{1000 M_{(H_2O, H_2, O_2)}} \quad (2.21)$$

Table 2.3: CP values for water, hydrogen and oxygen.

Equation	a	$b[K]$	$c[K^2]$	$d[K^3]$	$e[K^2]$
C_{P-H_2O}	-203.60	1523.29	-3196.41	2474.46	3.8553
C_{P-H_2}	33.07	-11.36	11.43	-2.77	-0.1586
C_{P-O_2}	31.32	-20.24	57.87	-36.51	-0.0073

As a result, the input entropy variation representing all heat losses is equal to the sum of equations (2.16) and (2.19) respectively, then:

$$(\Delta S_q)_{in} = \left(\frac{I_{ELS}}{2F}\right) N_{cell} \left(\frac{2F(\eta_{ELS} + \eta_{diff} + R_{ej})}{T}\right) + \left(\frac{C_{P-H_2O}(T-T_{in-H_2O})Q_{V_{in-H_2O}} \rho_{H_2O}}{T}\right) \quad (2.22)$$

The entropy variation of output $(\Delta S_q)_{out}$ related to heat sources is composed of:

i. The entropy variation of hydrogen given by:

$$\dot{n}_{H_2} \Delta S_{H_2} = \frac{C_{P-H_2}(T-T_{in-H_2O})Q_{m-H_2}}{T} \quad (2.23)$$

where, the mass flow of hydrogen is:

$$Q_{m-H_2} = \dot{n}_{H_2} M_{H_2} \quad (2.24)$$

ii. The entropy flow of oxygen $0.5\dot{n}_{O_2} \Delta S_{O_2}$ can be expressed as:

$$\dot{n}_{O_2} \Delta S_{O_2} = \frac{C_{P-O_2}(T-T_{in-H_2O})Q_{m-O_2}}{T} \quad (2.25)$$

The mass flow of oxygen Q_{m-O_2} is:

$$Q_{m-O_2} = \dot{n}_{O_2} M_{O_2} \quad (2.26)$$

iii. The entropy flow of consumed water is:

$$\text{Consumed water entropy} = \dot{n}_{H_2O} \Delta S_{H_2O} \quad (2.27)$$

iv. The entropy flow of anode is:

$$\begin{aligned} \dot{n}_{anode} \Delta S_{anode} &= \dot{n}_{H_2O} \Delta S_{H_2O} + \dot{n}_{O_2} \Delta S_{O_2} \\ &= \left(\frac{C_{P-H_2O}(T-T_{in-H_2O}) \rho_{H_2O} Q_{V-H_2O-outc}}{T}\right) + \left(\frac{C_{P-O_2}(T-T_{in-O_2})Q_{m-O_2}}{T}\right) \end{aligned} \quad (2.28)$$

v. The entropy flow of cathode is:

$$\begin{aligned} \dot{n}_{cathode} \Delta S_{cathode} &= \dot{n}_{H_2O} \Delta S_{H_2O} + \dot{n}_{H_2} \Delta S_{H_2} \\ &= \left(\frac{C_{P-H_2O}(T-T_{in-H_2O}) \rho_{H_2O} Q_{V-H_2O-outc}}{T}\right) + \left(\frac{C_{P-H_2}(T-T_{in-H_2})Q_{m-H_2}}{T}\right) \end{aligned} \quad (2.29)$$

vi. The entropy flow of losses is:

$$\dot{n}_{losses} \Delta S_{losses} = \left[\frac{(T-T_{amb})}{Rt}\right] / T \quad (2.30)$$

The total output entropy variation is the sum of the entropy variations of hydrogen, flow of oxygen, the entropy flow of consumed water, the entropy flow of anode, the entropy flow of cathode and the entropy flow of losses, so that:

$$\begin{aligned}
(\Delta S_q)_{out} = & \frac{C_{P-H_2}(T-T_{in-H_2O})Q_{m-H_2}}{T} + \frac{C_{P-O_2}(T-T_{in-H_2O})Q_{m-O_2}}{T} + \dot{n}_{H_2O} \Delta S_{H_2} + \\
& \left(\frac{C_{P-H_2O}(T-T_{in-H_2O} \rho_{H_2O})Q_{V-H_2O-outa}}{T} \right) + \left(\frac{C_{P-O_2}(T-T_{in-O_2})Q_{m-O_2}}{T} \right) + \\
& \left(\frac{C_{P-H_2O}(T-T_{in-H_2O} \rho_{H_2O})Q_{V-H_2O-outc}}{T} \right) + \left(\frac{C_{P-H_2}(T-T_{in-H_2})Q_{m-H_2}}{T} \right) + \left(\frac{(T-T_{amb})}{\frac{Rt}{T}} \right)
\end{aligned} \quad (2.31)$$

2.2.4.EMR HYDRAULIC SUB-MODEL

The EMR of PEM ELS hydraulic sub-model is shown in Fig. 2.4:

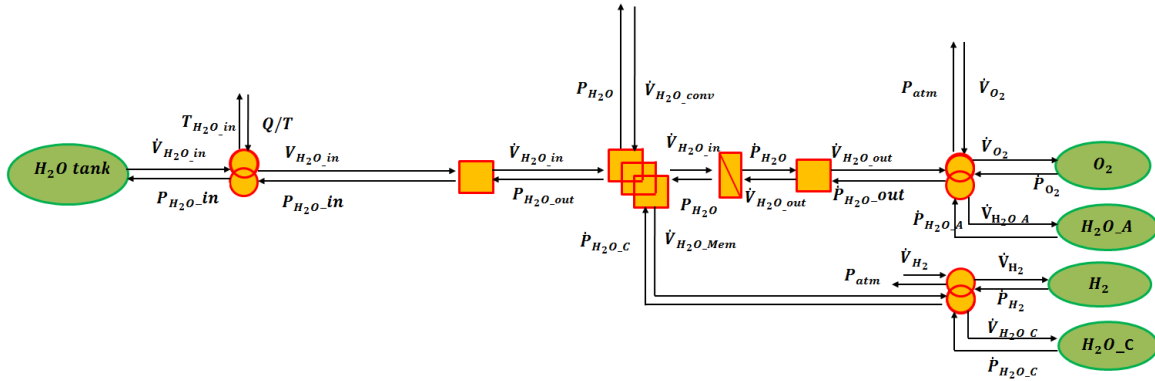


Fig. 2.4: EMR of hydraulic sub-model.

In the hydraulic sub-model, water is provided from the tank as input. In addition, hydrogen and oxygen are produced at the output. Moreover, temperature is exchanged between both hydraulic and thermal sub-models.

From Fig. 2.4, there is an element of energy conversion (without changing domain) for materializing pressure losses before entering the confines of the stack. In addition, an element of coupling which allows recognizing both the entering reaction water at the reaction sites and transferred water to the cathode via the membrane. A storage element, just after the coupling element, allows evaluating the profile of the pressure within the stack. The homogeneous fluid transfers, in its flow, the heat from the source of heat storage of stack. It is related to the water and the exhaust gases. At the end, the water is separated from the gas before being fed back into the same tank. To simplify the diagram, the source element that models the tank is presented by a single and not two water tanks as in the beginning and the end of the hydraulic circuit for achieving the closed loop.

On the anode side of the electrolyser, the balance among the water flow at the input $Q_{Vin_{H_2O}}$, the reacting water flow $Q_{V_{H_2O}reat}$ and evacuation water flow via the membrane $Q_{V_{H_2O}mem}$ have to be taken into account, so that:

$$Q_{V_{H_2O}} = Q_{Vin_{H_2O}} - (Q_{V_{H_2O}reat} + Q_{V_{H_2O}mem}) \quad (2.32)$$

At the cathode side, equation (2.32) is:

$$Q_{V_{H_2O}-outc} = Q_{Vin_{H_2O}cath} + Q_{V_{H_2O}mem} \quad (2.33)$$

If the cathode side of the electrolyser is not supplied with water, the amount of water discharged from the electrode will be only that passes through the membrane $Q_{V_{H_2O}mem}$.

The pressure profile at the crossing of the stack, with reference to the anode (the same principle to the cathode) can be modelled as:

$$P_{in_A} = \int \frac{Q_{vin_H_2O} - Q_{v_H_2O_outa}}{C_h} dt \quad (2.34)$$

The global EMR model of PEM ELS is depicted in Fig. 2.5. The EMR formalism has several advantages: representation of multi-physic systems, systematic deduction of control structures, and the implementation can be easily performed under common commercial software environments, such as Matlab-Simulink.

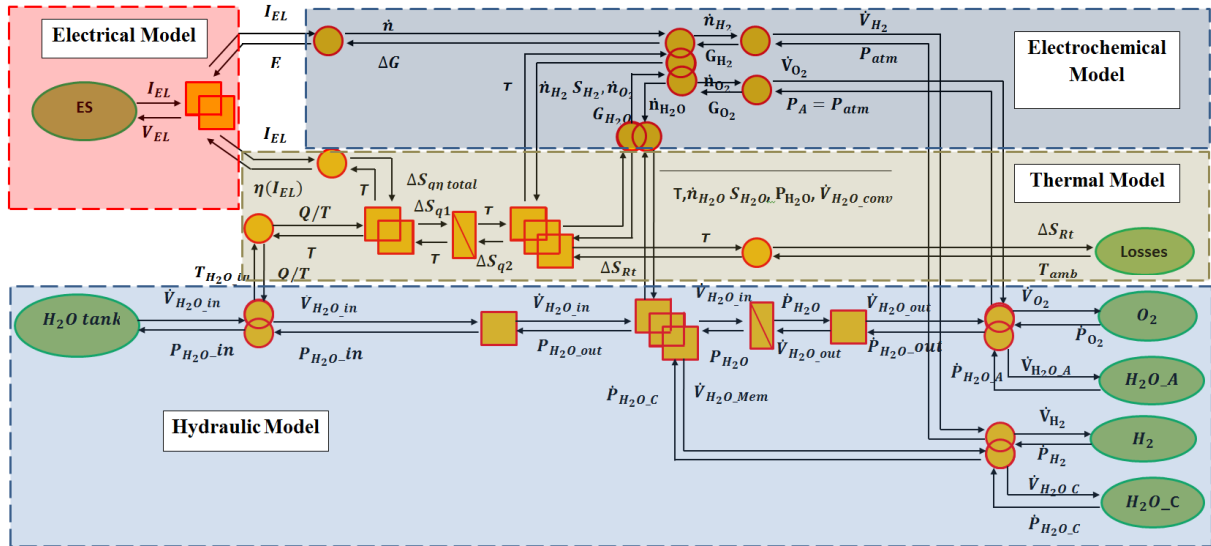


Fig. 2.5: The EMR model of overall PEM ELS.

2.2.5. SIMULATION RESULTS

The electrolyser in the system under study is staXX7 of H-TEC with an active area of 16 cm² and a membrane thickness of 130 μm. Tests have been performed on this small electrolyser. Then, for the simulation purpose the 59 kW PEM ELS model was extrapolated for realistic parameter values. It is possible to impose voltage or current to the PEM ELS model. However, in the simulation, the current is imposed. Consequently, the voltage is deduced at the ELS terminals. Then, the current value has been varied and the corresponding voltage values have been obtained. Therefore, the polarization curve of PEM ELS at 353 K stack temperature is reached as in Fig. 2.6. As depicted in Fig. 2.6, there is a proportional relation between electrolysers' voltage and current.

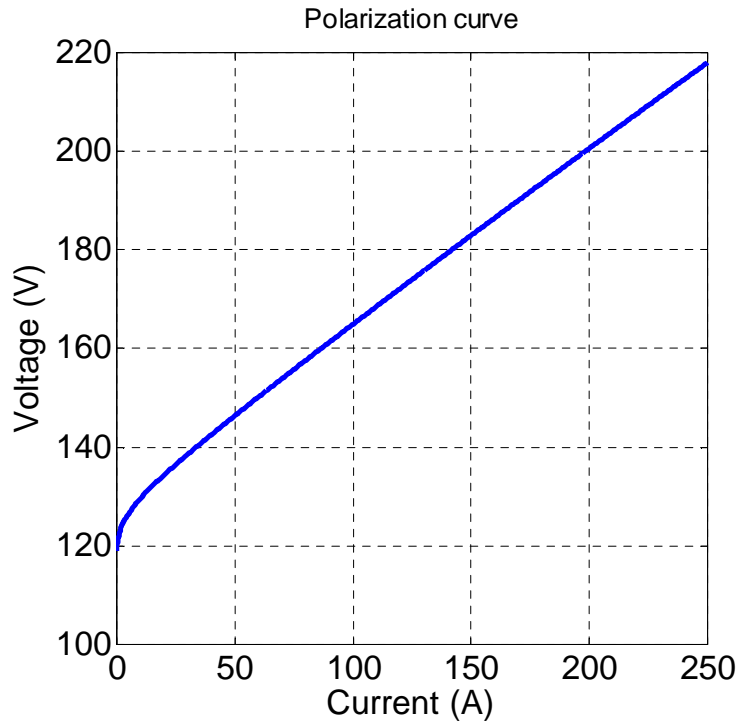
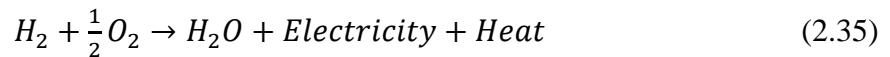


Fig. 2.6: ELS current as function of voltage.

2.3. FUEL CELL

The FC uses hydrogen as a fuel at the anode and oxygen as an oxidant at the cathode to generate both electrical energy and heat due to the exothermic nature of the overall reaction in PEMFC as in equation (2.35). In the PEMFC, as a source of energy, the reaction product of chemical reaction is pure water then:



2.3.1.EMR MODEL OF PEMFC

EMR model of PEMFC, developed by Hissel [Hiss 08], was used for hybrid vehicle applications [Boul 08] [Sola 09]. In addition, it can be integrated to fit other stationary applications [Agbl 11c]. Fig. 2.6 shows the EMR model of PEMFC [Hiss 08]. The corresponding EMR model consists of four sub-models: electrical, thermodynamic, thermal and fluidic models. The studied FC model is ZSW 20-cell stack of nominal power of 500 watt. Each cell has an active area of 100 cm² (nominal current I_{fc} of 50A).

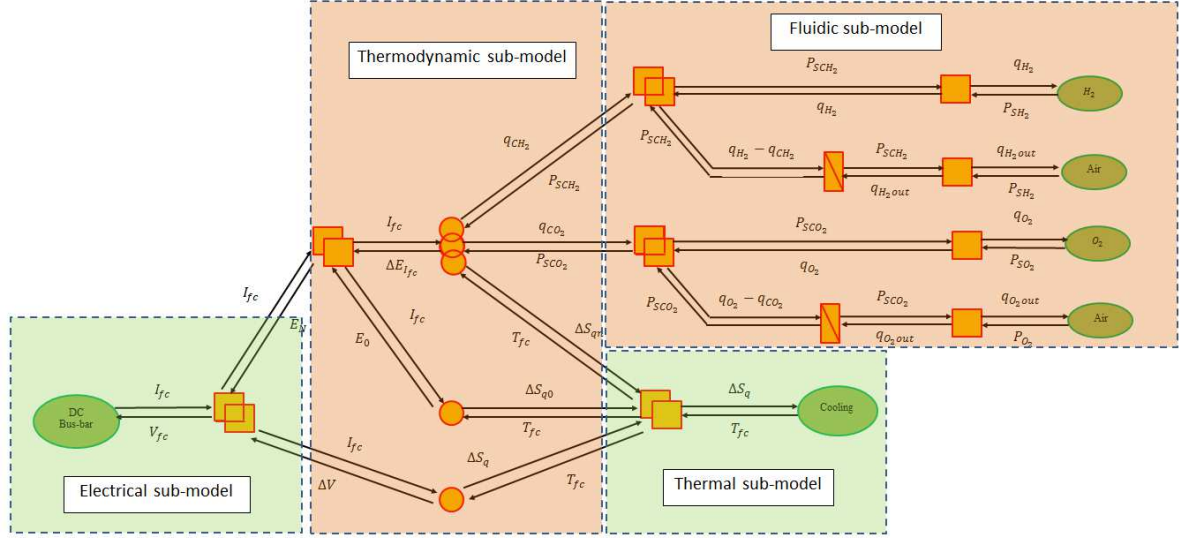


Fig. 2.7: EMR of PEMFC.

2.3.2.EMR ELECTRICAL SUB-MODEL

In the electrical sub-model, the stack voltage V_{fc} is the cell voltage multiplied by the number of cells inside the coupling element, thus:

$$V_{fc} = N(E_N + \Delta V) \quad (2.36)$$

where, N is the number of cells in the stack, E_N is the Nernst potential and ΔV is the sum of activation, concentration and ohmic over-voltages.

2.3.3.EMR THERMODYNAMIC SUB-MODEL

Thermodynamic model has two input variables, the FC temperature T_{fc} and the FC current I_{fc} , in addition to two output variables such as the thermodynamic potential E_0 and the entropy flow ΔS_{q0} which is function of the entropy variation ΔS_0 and I_{fc} :

$$E_0 = - \frac{(\Delta H_0(T_{fc}) - T_{fc} \Delta S_0(T_{fc}))}{2F} \quad (2.37)$$

$$\Delta S_{q0} = \frac{\Delta S_0 I_{fc}}{2F} \quad (2.38)$$

Nernst potential is the sum of potential variation ΔE and standard potential E_0 , then:

$$E_N = E_0 + \Delta E \quad (2.39)$$

where, the potential variation ΔE is a function of the partial pressures on catalytic sites P_{SCH_2} and P_{SCO_2} respectively, thus:

$$\Delta E = A_{cdT_{fc}} \ln\left(\frac{P_{SCH_2}}{P_0}\right) + B_{cdT_{fc}} \ln\left(\frac{P_{SCO_2}}{P_0}\right) \quad (2.40)$$

where, $A_{cdT_{fc}}$ and $B_{cdT_{fc}}$ are the Nernst potential coefficients.

The entropy flow ΔS_{q_n} represents the emission of heat during the electrochemical reactions, so that:

$$\Delta S q_n = \frac{\Delta E I_{fc}}{T_{fc}} \quad (2.41)$$

The gases flow q_{cH_2} and q_{cO_2} are calculated according to the perfect gas law, then:

$$q_{cH_2} = \frac{1}{2F} \left(\frac{RT_{fc}}{P_{SCH_2}} \right) \quad (2.42)$$

$$q_{cO_2} = \frac{1}{2F} \left(\frac{RT_{fc}}{P_{SCO_2}} \right) \quad (2.43)$$

Therefore, the FC voltage is equal to:

$$V_{fc} = N[E_N - (\Delta V_{act} + \Delta V_{conc} + \Delta V_{ohm})]$$

where, the voltage drop, caused by the activation, concentration and ohmic are ΔV_{act} , ΔV_{conc} and ΔV_{ohm} respectively. They are given by:

$$\Delta V_{act} = \left(\frac{R}{2\alpha F} \right) T_{fc} \ln \left(\frac{I_{fc} + I_n}{I_0} \right) \quad (2.44)$$

$$\Delta V_{conc} = \left(\frac{R}{2F} \right) T_{fc} \ln \left(1 - \frac{I_{fc}}{I_l} \right) \quad (2.45)$$

$$\Delta V_{ohm} = R_m I_{fc} \quad (2.46)$$

2.3.4.EMR THERMAL SUB-MODEL

In this sub-model, the ohmic and transfer resistances, R_m and R_t respectively, cause losses in the form of heat. Consequently, the entropy ΔS_q will be:

$$\Delta S_q = \left(\frac{(R_m + R_t) I_{fc}^2}{T_{fc}} \right) \quad (2.47)$$

where, ΔS_q is a function of the current I_{fc} , and the $(R_m + R_t)I_{fc}$ which corresponds to the overall activation, concentration and ohmic over-potentials.

2.3.5.EMR FLUIDIC SUB-MODEL

In the fluidic model, hydrogen and oxygen are obtained and the air is an atmospheric exhaust. Hydrogen and oxygen have been provided with their special tanks. Obviously, the mono-physical conversion elements represent the charge losses, therefore:

$$P_x = P_{scx} + R_{dx1} q_x \quad (2.48)$$

$$q_{xout} = \frac{(P_{scx} - P_{sx})}{R_{dx2}} \quad (2.49)$$

where, $x = O_2$ and/or H_2 , R_{dx1} and R_{dx2} are the fluidic resistance on the supply and exhaust sides respectively of the anodic/cathodic compartment, P_x , P_{sx} and P_{scx} are partial pressures, q_x and q_{xout} are volume flows.

Furthermore, the accumulation elements represent the buffer volume in the diffusion layers and the coupling elements have been used for the output gas calculation, then:

$$\frac{dP_{scx}}{dt} = \left(\frac{1}{C_{dx}} \right) (q_x - q_{cx} - q_{xout}) \quad (2.50)$$

where, C_{dx} is the fluidic capacity of the anodic/cathodic compartment.

2.3.6. PEMFC SIMULATION

The requested power can be obtained by increasing the number of PEMFCs in the stack. The cell nominal current i_{cell} depends on the cell surface s_{cell} , therefore:

$$i_{cell} = s_{cell} j_{cell} \quad (2.51)$$

where, j_{cell} is the current density of the PEMFC cell, n_{cell} is the number of cells connected in series to provide the stack voltage V_{fc} for which the desired power P_{fc} will be:

$$P_{fc} = V_{fc} I_{fc} \quad (2.52)$$

The larger the surface of the cell, the greater the current delivered by the PEMFC will be. The nominal value of PEMFC system I_{nfc} obtained by connecting a number of stacks in parallel n_{stp} is:

$$I_{nfc} = n_{stp} I_{fc} \quad (2.53)$$

The model can be adjusted for wide power range applications. Simulation results for one, twenty cells and two stacks of twenty cells in parallel are depicted in Fig. 2.8. These curves present the current as function of voltage. Higher number of cells leads to an increase in stack voltage. The PEMFC considered parameters are listed in the Appendix (Table A.1)

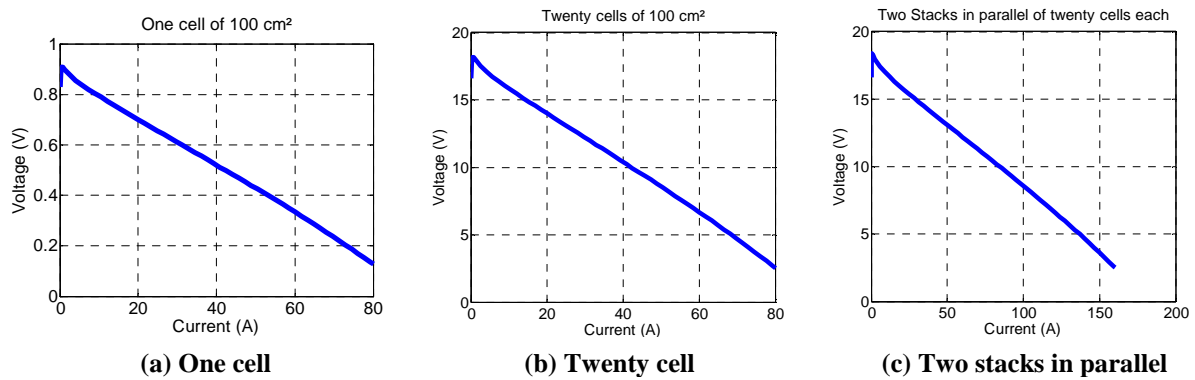


Fig. 2.8: V-I characteristics for different number of cells and stacks configurations.

2.4. WIND TURBINES

WTs convert the kinetic energy of wind into mechanical energy. The most of this energy is transferred into electrical energy.

The system of WT nacelle is composed of an 800 kW WT recharging batteries, the wind pod contains all elements which convert mechanical energy produced by the wind into electrical energy such as the blades, the shaft, the gear box, the Induction Machine (IM) and the electrical energy elements such as the inverter and the batteries as depicted in Fig. 2.9.

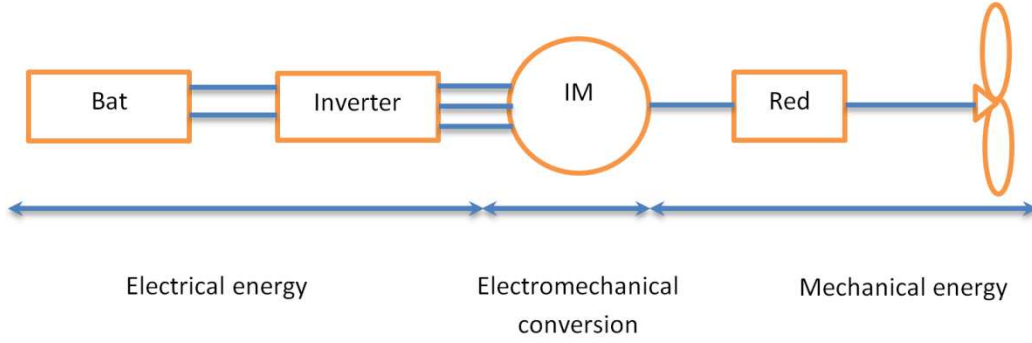


Fig. 2.9: WT with the batteries pack connection.

2.4.1.EMR MODEL OF WT

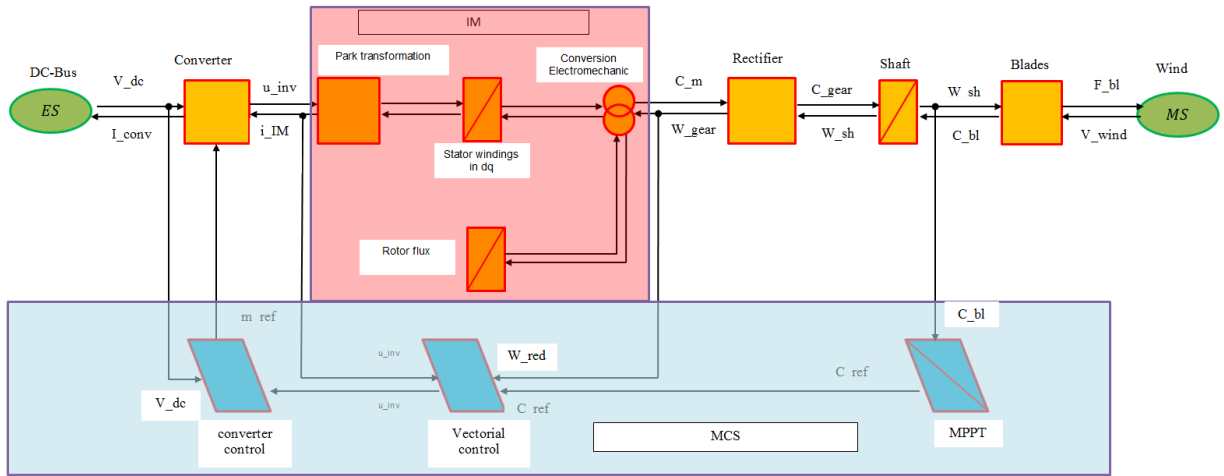


Fig. 2.10: The EMR model of WT.

As shown in Fig. 2.10, the EMR model of the WT consists of seven blocks such as:

- **The wind:** is the movement in an atmosphere gas mass at the surface of the planet. It is the source of the kinetic energy which drives the turbine blades modelled by a power source block.
- **The blades:** convert kinetic energy of winds into rotational movement.
- **The shaft:** this element transmits the rotational movement of the blades, which is modelled by a block of energy storage, and has provided adaptation between the blades and the gear element.
- **Rectifier:** converts AC electrical quantities to DC ones.
- **Induction machine:** is an electromechanical conversion element that ensures the conversion of the mechanical energy produced by the wind to electrical energy.
- **DC/DC converter:** adapts the voltage and current to be used at the DC bus terminal and allows WT control application.
- **Batteries:** modelled by electrical source elements.

2.4.2.EMR AERODYNAMIC SUB-MODEL

The wind speed V_{wind} applied on the blades of the WT, causes its rotation and creates a mechanical shaft power, denoted by P , such that:

$$P = \frac{\left(\frac{C_p}{\lambda}\right) \rho_{air} S_{blade} V_{wind}^3}{2} = \left(\frac{C_p}{\lambda}\right) G_{blade} V_{wind}^3 \quad (2.54)$$

The variables λ , S_{blade} and G_{blade} are calculated by:

$$\lambda = \frac{V_{blade}}{V_{wind}} \quad (2.55)$$

where, $V_{blade} = R_{blade} \omega$

$$S_{blade} = \pi R_{blade}^2 \quad (2.56)$$

$$G_{blade} = \frac{\rho_{air} S_{blade}}{2} \quad (2.57)$$

The tangential force can be estimated as:

$$F_{tg} = \frac{P}{V_{wind}} = \frac{\left(\frac{C_p}{\lambda}\right) \rho_{air} S_{blade} V_{wind}^2}{2} = \left(\frac{C_p}{\lambda}\right) G_{blade} V_{wind}^2 \quad (2.58)$$

2.4.3.EMR SHAFT SUB-MODEL

The shaft is expressed by:

$$J_{sh} \frac{d\omega_{blade}}{dt} + f_{sh} = C_{gear} - C_{blade} \quad (2.59)$$

where, ω_{blade} is the nominal speed of blades, J_{sh} is the equivalent inertia of the shaft, f_{sh} is the Coefficient of viscous friction of the shaft, C_{gear} is the torque at gearbox, C_{blade} is the torque at blades. Hence, the equivalent shaft is:

$$W_{blade} = (C_{gear} - C_{blade}) F(s) \quad (2.60)$$

where, W_{blade} is the rated power of blades and $F(s)$ is the transfer function of the equivalent shaft will be presented by:

$$F(s) = \frac{K_{sh}}{\tau_{sh} s + 1} \quad (2.61)$$

where $K_{sh} = \frac{1}{f_{sh}}$, $\tau_{sh} = \frac{J_{sh}}{f_{sh}}$.

2.4.4.EMR GEARBOX SUB-MODEL

The gearbox inside the WT is modelled by:

$$\omega_{gear} = m_{gear} \omega_{sh} \quad (2.62)$$

$$C_{gear} = m_{gear} C_m \quad (2.63)$$

where, ω_{gear} is the rotation speed of gearbox, m_{gear} is the reduction ratio of the gearbox, ω_{sh} is the rotation speed of the equivalent shaft and C_m is the torque at the induction machine.

2.4.5.EMR INDUCTION MACHINE SUB-MODEL

The electrical energy can be transformed into mechanical energy using IM composed of four EMR blocks as depicted in Fig. 2.11. Obviously, Park transformation has been used in order to simplify the calculations of IM as a mono-physical coupling element. In addition, two accumulation elements have been applied to present the rotor and stator energies. The

conversion of electrical energy into mechanical one has been performed using multi-physical coupling element.

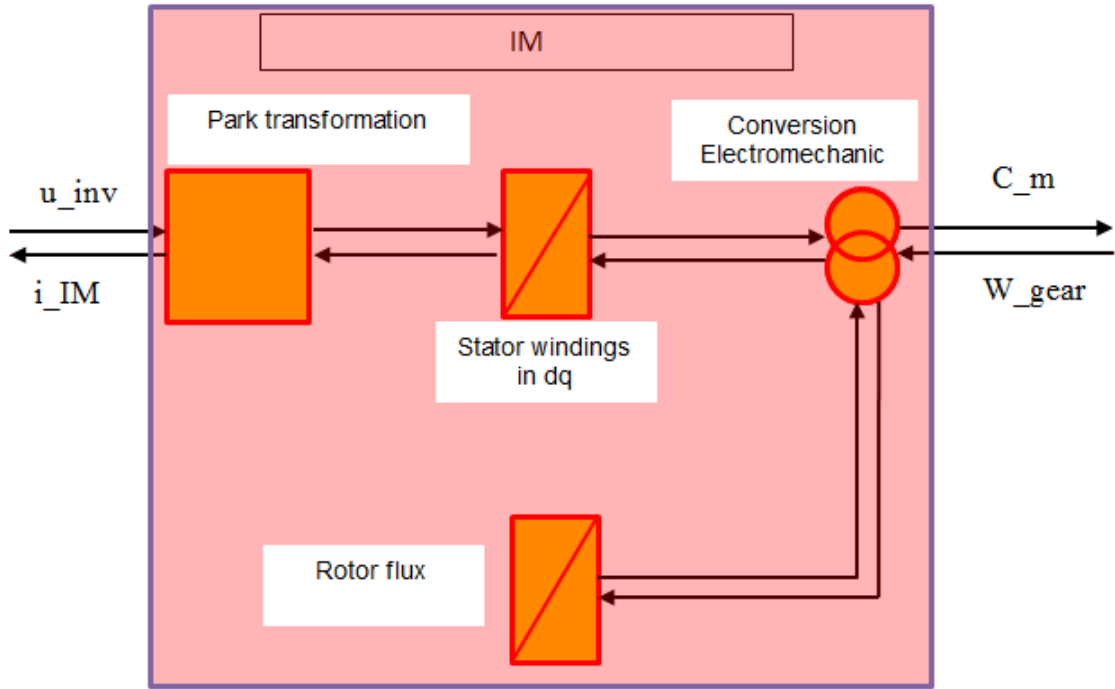


Fig. 2.11: EMR induction machine model.

- **Electromechanical conversion:** the block electromechanical conversion allows obtaining the output torque of the machine, such as:

$$C_m = p * \left(\frac{M_{sr}}{L_r} \right) F_{ird} i_{sq} \quad (2.64)$$

Rotor and stator pulsations respectively can be expressed by:

$$\omega_r = \left(\frac{M_{sr}}{(F_{ird} * T_r)} \right) i_{sq} \quad (2.65)$$

where, ω_r is the rotor pulsation, $T_r = \frac{L_r}{R_r}$, $F_{ird} = \left(\frac{M_{sr}}{T_r S + 1} \right) i_{sd}$, M_{sr} is the mutual-inductance between stator and rotor, T_r is the rotor time constant, F_{ird} is the rotor flux, L_r is the self-inductance of rotor and R_r is the rotor's resistance,

$$\omega_s = p \omega_{gear} + \omega_r \quad (2.66)$$

where, $\theta = \left(\frac{1}{s} \right) \omega_s$, ω_s is the stator pulsation and p is the number of pole pairs.

The disturbance in the electromechanical conversion block serves to determine the e_{sdq} vectors, then:

$$e_{sd} = F_{ird} \left(\frac{M_{sr}}{L_r T_r} \right) + \sigma L_s i_{sq} \omega_s \quad (2.67)$$

$$e_{sq} = F_{ird} \left(\frac{M_{sr}}{L_r} \right) p \omega_{gear} - \sigma L_s i_{sd} \omega_s \quad (2.68)$$

where $\sigma = 1 - \frac{M_{sr}^2}{(L_s * L_r)}$ is the dispersion coefficient and L_s is the self-inductance of the stator.

- **Rotor flux:** the rotor flux on the d axis is calculated by:

$$T_r \left(\frac{dF_{ird}}{dt} \right) + F_{ird} = M_{sr} i_{sd} \quad (2.69)$$

- **Stator voltage in (dq):** the stator voltage is expressed by:

$$V_s = \sigma L_s \left(\frac{di_s}{dt} \right) + \left(R_s + R_r \frac{M_{sr}^2}{L_r^2} \right) i_s \quad (2.70)$$

The stator voltage comprises two voltage components V_{sdq} and e_{sdq} , then:

$$i_{sdq} = (V_{sdq} - e_{sdq}) \left(\frac{K_i}{T_i s + 1} \right) \quad (2.71)$$

where $K_i = \frac{(T_s T_r)}{(L_s T_r + L_s T_s (1 - \sigma))}$, $T_i = \sigma L_s K_i = \sigma L_s \left(\frac{(T_s * T_r)}{(L_s T_r + L_s T_s (1 - \sigma))} \right)$, $T_s = \frac{L_s}{R_s}$

- **Park transformation:** allows moving to reference frame related to the stator as:

$$V_{sdq} = u_{inv} K_{uv} C R(\theta) \quad (2.72)$$

$$i_{IM} = \frac{i_{sdq} K_{ii}}{R(\theta) C} \quad (2.73)$$

The parameters of equation (2.72) and equation (2.73) are given by:

$$K_{uv} = \frac{1}{3} \begin{bmatrix} 2 & -1 \\ -1 & 2 \\ -1 & -1 \end{bmatrix}, K_{ii} = \begin{bmatrix} 1 & 0 & 0 \\ 0 & 1 & -1 \end{bmatrix}, C = \sqrt{\frac{2}{3}} \begin{bmatrix} 1 & -\frac{1}{2} & -\frac{1}{2} \\ -1 & \sqrt{\frac{3}{2}} & -\sqrt{\frac{3}{2}} \end{bmatrix}, C_{inv} = \sqrt{\frac{2}{3}} \begin{bmatrix} 1 & 0 \\ \frac{1}{2} & \sqrt{\frac{3}{2}} \\ -\frac{1}{2} & -\sqrt{\frac{3}{2}} \end{bmatrix},$$

$$R(\theta) = \begin{bmatrix} \cos(\theta) & \sin(\theta) \\ -\sin(\theta) & \cos(\theta) \end{bmatrix}, u_{inv} = m_{inv} V_{dc}, i_{inv} = m_{inv} i_{IM}$$

2.4.6. SIMULATION RESULTS

From Fig. 2.12, the wind speed in Belfort region and its corresponding power profiles are shown. It is clear that any change in wind speed causes a considerable change in wind power. Obviously, the wind speed related to the turbine power with a cubic proportional relationship. This relationship is expressed by equation (2.54). In detail, two wind increasing periods have been observed. Accordingly, the increase of power in period (1) is mainly depending on the starting current of IM and partially on the wind speed rise. In addition, the increase in power in period (3) is completely relating to the wind speed increase. Period (2) has constant output power corresponding to a relatively stable wind speed. These results validate the EMR WT model.

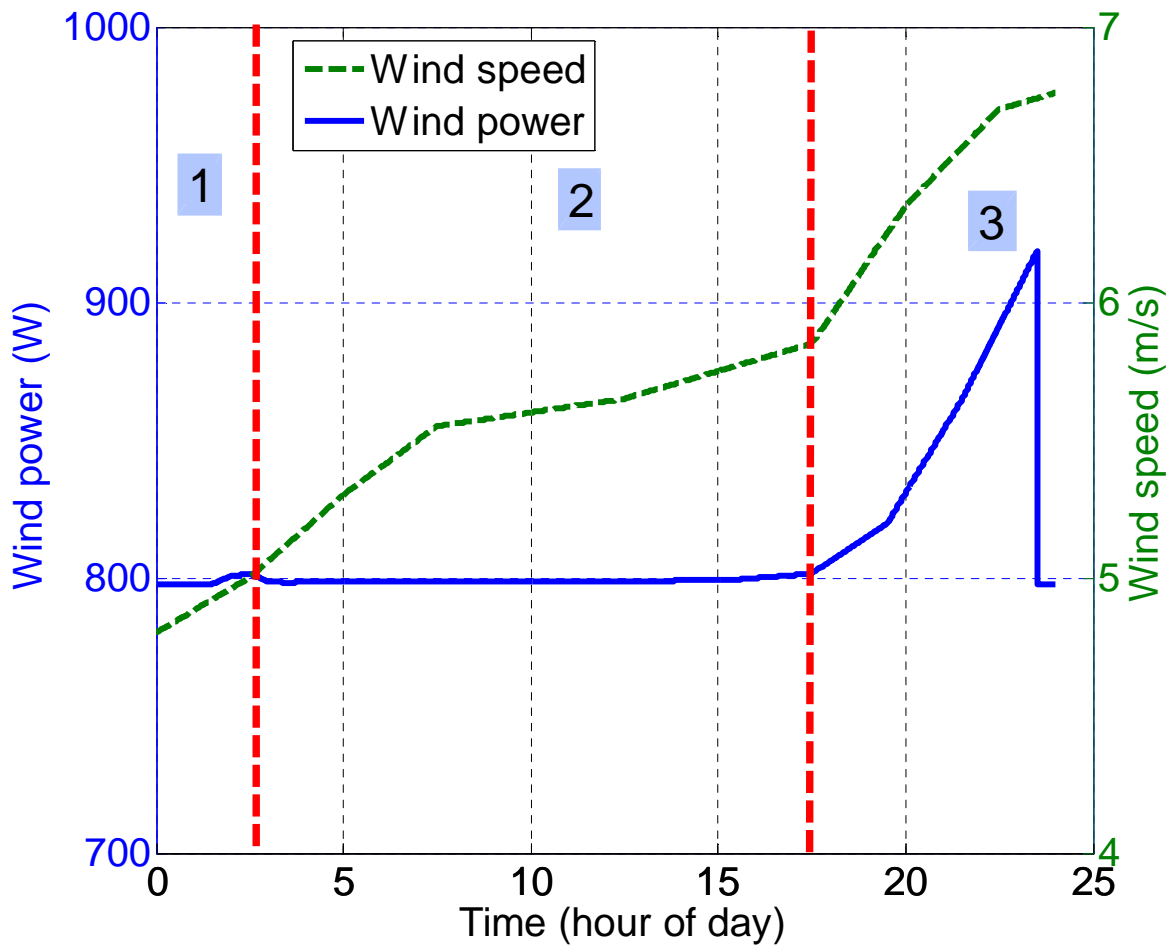


Fig. 2.12: wind and power profiles of WT.

2.5. PHOTOVOLTAIC SOURCE

The conversion of solar energy from the light flux until the electrical power of the PV generator is modelled. Photovoltaic panels are presented in EMR model as depicted in Fig. 2.13. This model is divided into three essential sub-models: radiometric/photometric sub-model, thermal sub-model and electrical sub-model.

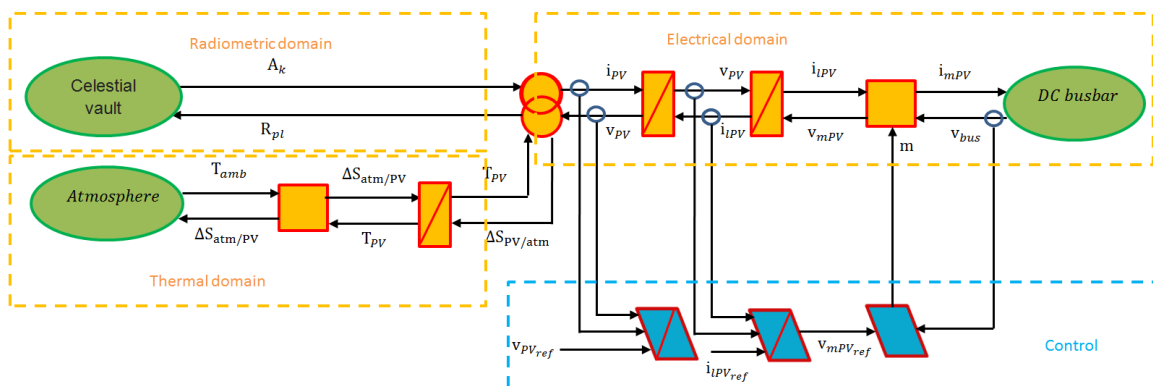


Fig. 2.13: EMR model of PV panels.

2.5.1.EMR RADIOMETRIC/PHOTOMETRIC SUB-MODEL

The luminous flux received at the surface of the PV converter is measured by W/m². The sun energy has an EMR model using a single action quantity as presented in [Pank 04]. Clearly, no reaction quantity has been considered. The modelling approach proposed for the solar energy captured by the surface of the PV converter is the quantities of both action and reaction.

For a monochromatic source, there is a flow of emitted photons as:

$$D_{ph} = \frac{dn_p}{dt} \quad (2.74)$$

Unlike the electric field in which the electron flow multiplied by the Faraday number gives the current intensity which is a kinetic magnitude, the photons flow is multiplied by its granular value in terms of energy: $E_P = h\nu$. So that, it directly results in an energy flow as:

$$\Phi = E_P D_{ph} = h\nu \left(\frac{dn_p}{dt} \right) \quad (2.75)$$

The photon is the basic unit of energy when it is represented by an energy grain without mass and load. The distribution of photons in a given area can be considered as a potential magnitude. Therefore, photonic energy state (for a monochromatic spectrum) distributed over a surface has been treated as a potential magnitude.

The number of photons arriving on that surface per area unit and per time unit will be a kinetic variable. So that, the Φ [W] becomes:

$$\Phi = A_k R_{pl} \quad (2.76)$$

The photons flux, emitted by the sun and reached the surface of solar modules, is the physical phenomenon which influences the physical properties of PV conversion materials. Thus, the action variable is defined as the kinetic variable (photons flux). The response variable is then the real distribution of these photons on the module surface.

The rate of photons n_p arriving the module surface is expressed as:

$$A_k = \frac{d}{dt} \left(\frac{n_p}{S} \right) = \frac{dn_p}{dt} \quad (2.77)$$

If a tie with the causal approach and quantities used in photometry or radiometry, it would exploit the radiation or irradiance E_e , then the action variable as a kinetic variable is:

$$A_k = \frac{E_e}{h\nu} \quad (2.78)$$

Knowing that the product of the action and reaction variables has a power unit, then:

$$\Phi = \left(\frac{E_e}{h\nu} \right) R_{pl} \quad (2.79)$$

As the received power of the solar source on a given surface is:

$$\Phi = E_e S \quad (2.80)$$

then, the size of the potential variable is therefore:

$$R_{pl} = hv S \quad (2.81)$$

Equation (2.81) involves a constant potential whatever sunlight, which is incoherent in terms of physics viewpoint. To consider the photons distribution on the associated surface, a dimensionless coefficient k related to proton flow arriving on the surface of the module is introduced such that:

$$k = f(n_p, \dot{n}_p) \quad (2.82)$$

where,

$$R_{pl} = k hv S \quad (2.83)$$

therefore,

$$\Phi = E_e S = k hv S \frac{d}{dt} \left(\frac{n_p}{S} \right) \quad (2.84)$$

2.5.2.EMR THERMAL SUB-MODEL

A part of the solar radiation received by the module is converted into electricity while the other part is released as heat in the environment [Krau 06] [Agbl 11b]. Due to the thermal inertia of the module where the reflection coefficient of materials is less than 1, the heat accumulation element can be considered. The module has a heat exchange with its surroundings environment. The dynamics of thermal activity within the module can assess the temporal evolution of the module temperature. Then, the heat storage of the module is considered by making an inventory of all modules incoming and outgoing heat flux as illustrated by [Krau 06] [Garc 08] [Agbl 11c]:

$$C_p \frac{\partial T_{PV}}{\partial t} = \sum \dot{Q}_{in} - \sum \dot{Q}_{out} \quad (2.85)$$

where, C_p is the thermal capacity of the module, T_{PV} is the module temperature, $\sum \dot{Q}_{in}$ is the sum of incoming heat flux and $\sum \dot{Q}_{out}$ is the sum of outgoing heat flux.

In the solar module, three types of heat flow can be identified: first, the thermal energy flux income, the thermal energy stored in the module and the heat flow dissipated into the surrounding environment.

The main source of the incoming thermal energy comes from the solar radiation and did not convert into electricity. It can be expressed as [Krau 06] [Agbl 11c]:

$$\dot{Q}_{in} = P_{in}(1 - \eta_{PV}) = A E_e(1 - \eta_{PV}) \quad (2.86)$$

where, A is the module surface and η_{PV} is the module coefficient.

The exchange of heat flow between the module and the atmosphere can be considered as a steady flow (convective flux), so the heat flux can be expressed as [Krau 06]:

$$\dot{Q}_{atm/PV} = \left(\frac{1}{R_{atm/PV}} \right) (T_{PV} - T_a) \quad (2.87)$$

where, $R_{atm/PV}$ is the convective thermal resistance and T_a is the ambient temperature.

According to the causal principle and considering that the entropic flow in the thermal domain is the kinetic magnitude while the temperature is the potential magnitude, the entropic flux can be deduced as:

$$\Delta S_{q_{in}} = \frac{\dot{Q}_{in}}{T_{PV}} \quad (2.88)$$

$$\Delta S_{q_{atm/PV}} = \frac{\dot{Q}_{atm/PV}}{T_{PV}} \quad (2.89)$$

Then, equation (2.85) becomes:

$$C_P \frac{\partial T_{PV}}{\partial t} = T_{PV} [\sum (\Delta S_{q_{in}} - \Delta S_{q_{out}})] \quad (2.90)$$

The integral form with EMR modelling of equation (2.90) is:

$$T_{PV} = \exp \left[\frac{1}{C_P} \int [\sum (\Delta S_{q_{in}} - \Delta S_{q_{out}})] dt \right] \quad (2.91)$$

Technically, an access to the internal environment of the solar module cannot be achieved. Consequently, the static temperature expression has been used for the experimental validation phase.

There are several correlations to estimate the temperature of the module. These correlations greatly depend on experimental conditions and assumptions set [Skop 09]. The following equation corresponds to the generic current experimental conditions [Chen 07]:

$$T_{PV} = 0.943 T_a + 0.028 E_e - 1.528 V_{Sp} + 277.3 \quad (2.92)$$

where, T_a is the ambient temperature, E_e is the irradiance and V_{Sp} is the wind velocity.

In equation (2.92), the impacts of the wind speed, light and radiation on the module temperature have been either explicitly or implicitly considered.

2.5.3.EMR ELECTRICAL SUB-MODEL

To get rid of the voltage ripple of the PV source, a capacitor has been connected across its terminals. Furthermore, an inductor for current ripple limiting has been connected at the static converter terminals. In addition, a control signal has been injected using DC/DC converter.

The electrical energy produced is then injected into the DC bus as shown in Fig. 2.13. Equations (2.93) and (2.94) reflect these two EMR storage elements in EMR model:

$$v_{PV} = \left(\frac{1}{C_{PV}} \right) \int (i_{PV} - i_{LPV}) dt \quad (2.93)$$

$$i_{LPV} = \left(\frac{1}{L_{PV}} \right) \int ((v_{PV} - v_{lm}) - r_{PV} i_{LPV}) dt \quad (2.94)$$

2.5.4.PV PANELS CONTROL

Thanks to the calculated open circuit voltage and the deduced maximum power point, two controllers have been used. Obviously, the first has concerned with the maximum voltage point V_{MPPT} obtained from MPPT controller injected in a voltage controller in order to obtain the PV current reference i_{LPVref} . In addition, the second deals with the current control that provides the voltage reference v_{lmref} [Dali 08] [Locm 10]. Consequently, the duty cycle

obtained from the two controllers has been injected into the DC/DC converter as shown in Fig. 2.13.

In Table 2.4, the equations present the Maximum Control Structure (MCS) elements and their correspondings in EMR model have been illustrated.

Table 2.4: EMR and MCS equations.

EMR model	MCS model
$i_{PV} - i_{lPV} = C_{V(PV)} \left(\frac{\partial v_{PV}}{\partial t} \right)$	$i_{lPV_{ref}} = -C_{V(PV)}(V_{MPPT} - v_{PV}) + i_{PV}$
$v_{PV} - v_{lm} = L_{PV} \left(\frac{\partial i_{PV}}{\partial t} \right) + r_{PV} i_{lPV}$	$v_{lm_{ref}} = -C_{I(PV)} (i_{lPV_{ref}} - i_{lPV}) + v_{PV}$
$v_{lm} = m_{PV} \cdot v_{bus}$	$m_{PV} = \frac{v_{lm_{ref}}}{v_{bus}}$

2.5.5. SIMULATION RESULTS

Because of the complex relationship between solar irradiation, temperature and resistance in solar cells, a non-linear output I-V curve has been reached. Current-voltage and power-voltage curves of sized PV array for the module are shown in Fig. 2.14 for different solar irradiance levels (400-1000 W/m²). As obviously illustrated in Fig. 2.14, the current has constant value while increasing the voltage until reaching the voltage at which the maximum power exists (V_{MPPT}). At this voltage, the current significantly decreases until attaining its zero value at the PV maximum voltage (V_{PVmax}). From the P-V curve, the power-increase leads to a significant voltage-rise until reaching V_{MPPT} . Then, an inverse relation appeared between the power and voltage at the voltages V_{MPPT} .

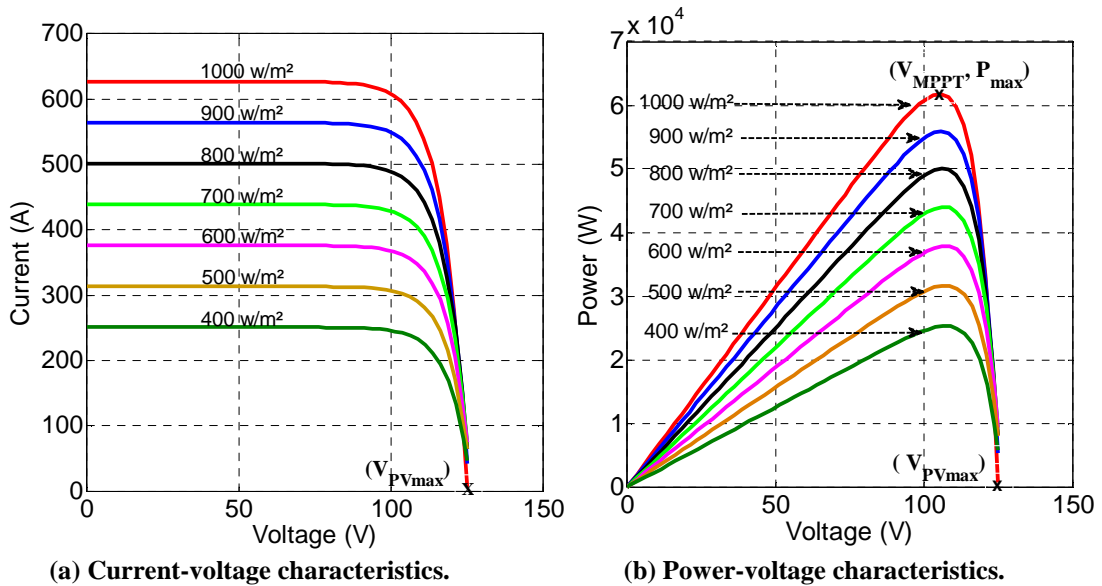


Fig. 2.14: I-V and P-V curves under different irradiance levels.

2.6. GAS MICRO-TURBINE

The model of the GMT includes synchronous machine and power converter (called back-to-back topology). Model components of the GMT have been summarized in the fuel supply and the group of compressor/turbine as in Fig. 2.15.

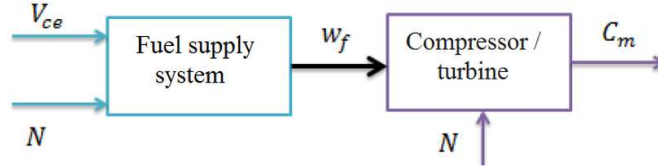


Fig. 2.15: General block diagram of GMT.

The fuel supply system consists of a controlled actuator to adjust the valve positioner. The fuel flow is the result of the inertia of the actuator and the valve positioner. The dynamic model of the valve positioner is given by:

$$E_1 = \left(\frac{K_v}{T_v s + 1} \right) F_d \quad (2.95)$$

where the valve positioner parameters: E_1 is the output, K_v is the gain, T_v is the time constant and F_d is the input.

The transfer function of the actuator is:

$$W_f = \left(\frac{K_f}{T_f s + 1} \right) E_1 \quad (2.96)$$

where, W_f is the requested fuel flow, K_f is the gain of the actuator and T_f is the time constant of the actuator.

The input of the fuel supply system V_{ce} is the output of the control system. V_{ce} represents the flow rate of fuel at considered operation point. The other input is the speed of the turbine in per unit (p.u.) (limited by the acceleration control). The fuel flow rate V_{ce} corresponds to the value of the per unit mechanical power of the turbine in steady state [Rowe 83]. Fig. 2.16 shows the block diagram of the fuel supply system.

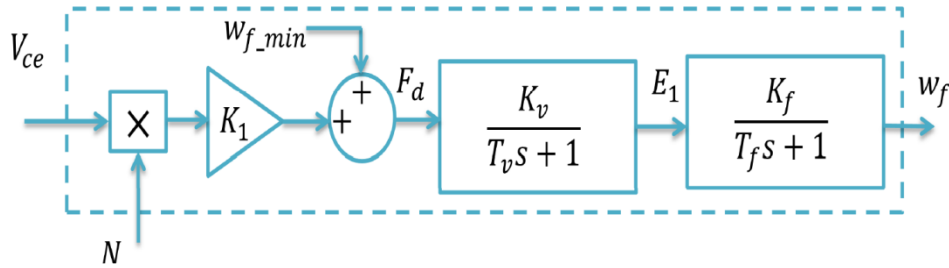


Fig. 2.16: Block diagram of fuel supply system.

The value of V_{ce} is scaled by K_1 ($K_1 = 1 - W_{f-min}$). Then, the minimum amount of fuel has been added to enable continuing combustion process in the combustion chamber. Obviously, W_{f-min} is the minimum fuel flow which allows running the GMT at a nominal speed when it works in open circuit (without load).

The combination compressor/turbine is the heart of the GMT. Its block diagram has been depicted in Fig. 2.17. A small delay T_{CR} related to combustion reaction time has been introduced. In addition, a delay T_{TD} requested to transfer gas from the combustion system by the turbine has been considered. Moreover, the constant time T_{CD} linked to discharge the compressor has been proposed.

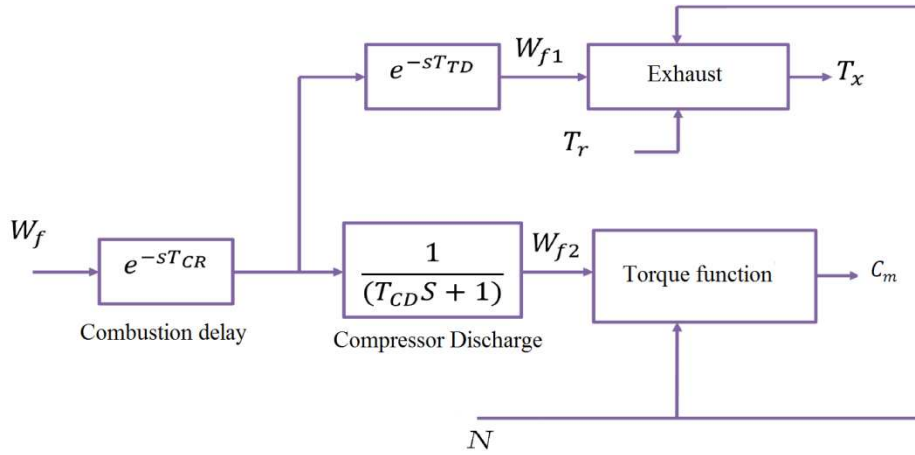


Fig. 2.17: Block diagram of the combination compressor/turbine.

There is a linear relationship between the ratio of the torque and the fuel flow as well as between the ratio of torque and the turbine speed in the speeds between 95-107%. Torque is expressed by [Hann 93]:

$$C_m = K_{HHV} (W_{f2} - 0.23) + 0.5 (1 - N) \quad (2.97)$$

where, K_{HHV} is the coefficient depends on the enthalpy and N is the value of the current speed.

Typical power/fuel flow characteristic increases linearly from zero power (23% of fuel flow) to the rated power (100% fuel flow) as shown in Fig. 2.18.

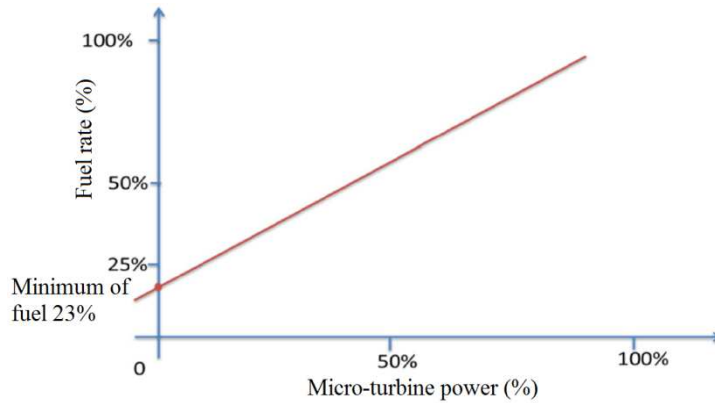


Fig. 2.18: The GMT power as a function of fuel flow.

The exhausted gas temperature in F (Fahrenheit) has been given by:

$$T_x = T_r - 700 (1 - W_{f1}) + 550 (1 - N) \quad (2.98)$$

where, T_r is the limited temperature.

The simplified model of the mechanical part is given by:

$$J \left(\frac{\partial \Omega}{\partial t} \right) = C_m - C_{em} - fN \quad (2.99)$$

where, J is the total inertia, C_m is the turbine torque and C_{em} is the electromagnetic torque of the synchronous machine.

In normal operation, the model accounts only the slow dynamics of the GMT. The fast dynamics of the GMT is (for example: start, stop, internal faults and power losses).

2.6.1. GMT CONTROL

The control structure of the GMT comprises the speed, temperature and acceleration controllers. The voltage regulator acts on the machine-side converter. The voltage or power regulator, depending on the operating mode of the generator, acts therefore on the network-side converter as depicted in Fig. 2.19.

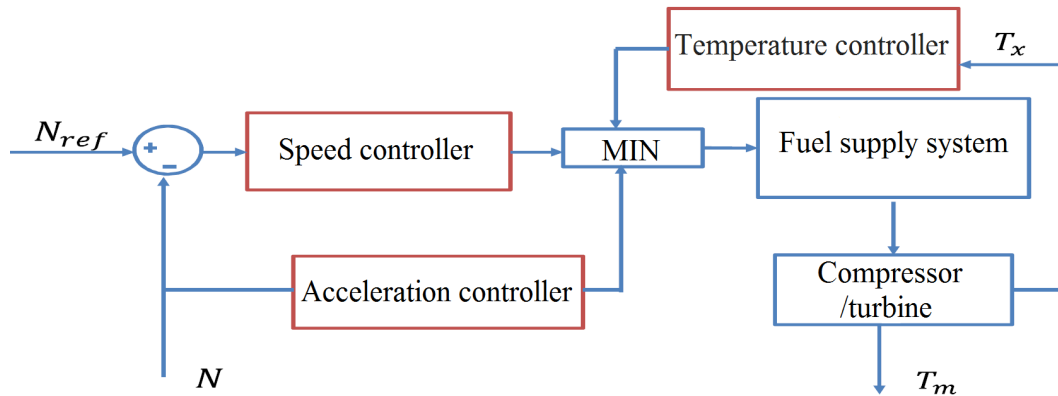


Fig. 2.19: Block diagram of GMT controllers.

Speed regulation: The speed controller allows controlling the GMT below rated power values. Depending on the characteristics of the regulator, speed control has been realized using either the droop curves or isochronous mode shown in Fig. 2.20. If the controller uses a droop curve, it will be a proportional one. Therefore, the output is proportional to the speed error. Like the droop curve behaviour, in an isochronous controller, the variation rate of the output is proportional to the speed error [Rowe 83].

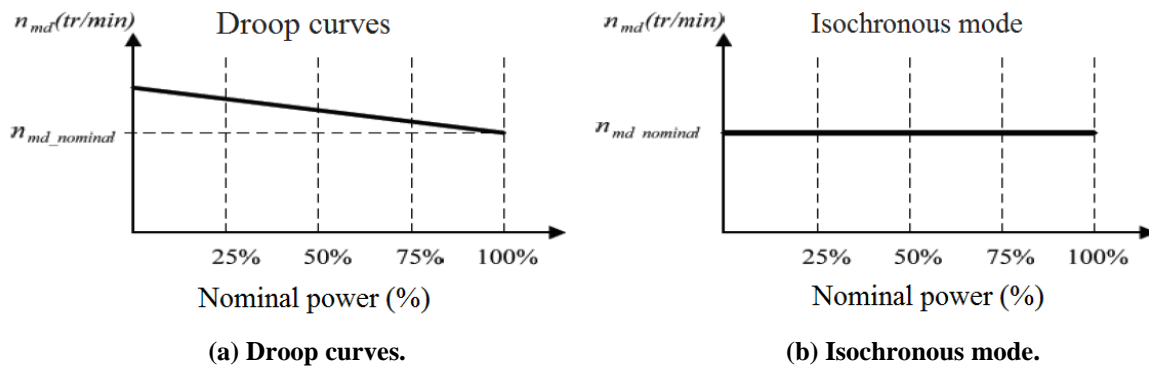


Fig. 2.20: Speed control using two different methods.

Fig. 2.21 shows the structure of the speed controller. The controller gain (T_I) is the time constant of the *lead-lag* regulator and (T_2/Z) is the time constant that represents the controller mode (droop or isochronous).

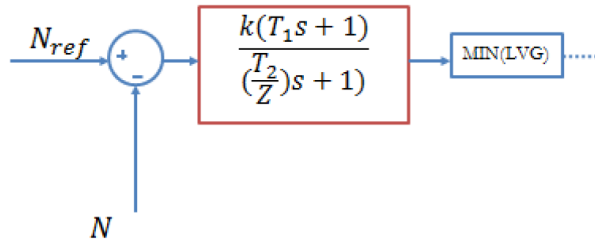


Fig. 2.21: GMT speed controller.

Simplified model of the GMT: If the changes in the speed is very low (parallel operation), several simplifications can be performed. The acceleration control becomes active only in case of sharp variations in load and it can be neglected. Since the GMT control is dominated by the speed controller, temperature control can be neglected as shown in Fig. 2.22.

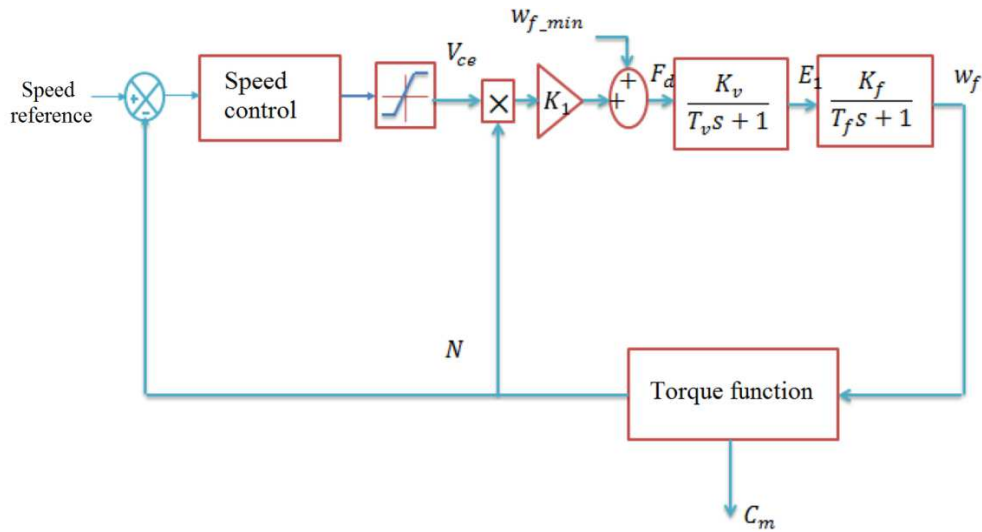


Fig. 2.22: Simplified model of GMT.

The proposed GMT model is shown in Fig. 2.23 [Zhu 02]. The model is limited for studying slow dynamics. The GMT has been supposed to work under normal conditions. Therefore, fast dynamics related to start-up and shutdown, internal faults and losses have not been considered. This model does not include the temperature and acceleration controls. These controllers do not intervene in the case of normal operation. The recovery is not included in the model because it only serves to increase the efficiency of GMT.

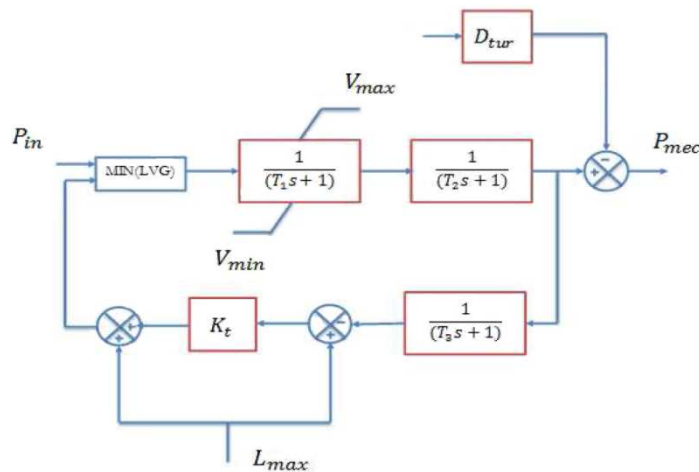


Fig. 2.23: Simplified GMT model.

2.6.2.EMR GMT MODEL

The GMT, presented by EMR model depicted in Fig. 2.24, includes the fuel supply system illustrated in Fig. 2.16 alongside with the compressor/turbine in Fig. 2.17. The fuel supply system and compressor/turbine have been modelled using two accumulation elements. The input of this system is the fuel valve and its output is the mechanical power that is transferred into electrical one by means of generator.

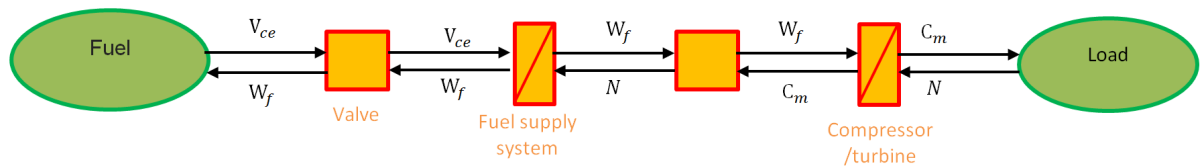


Fig. 2.24: EMR GMT model.

2.6.3.SIMULATION RESULTS

The simulation results have been presented in Fig. 2.25. During 300 seconds, both simulated mechanical and reference powers have been shown. The values of mechanical power reference have been varied between 0 and 150 kW. The simulation result has proved that the GMT response adequately towards reaching the reference power.

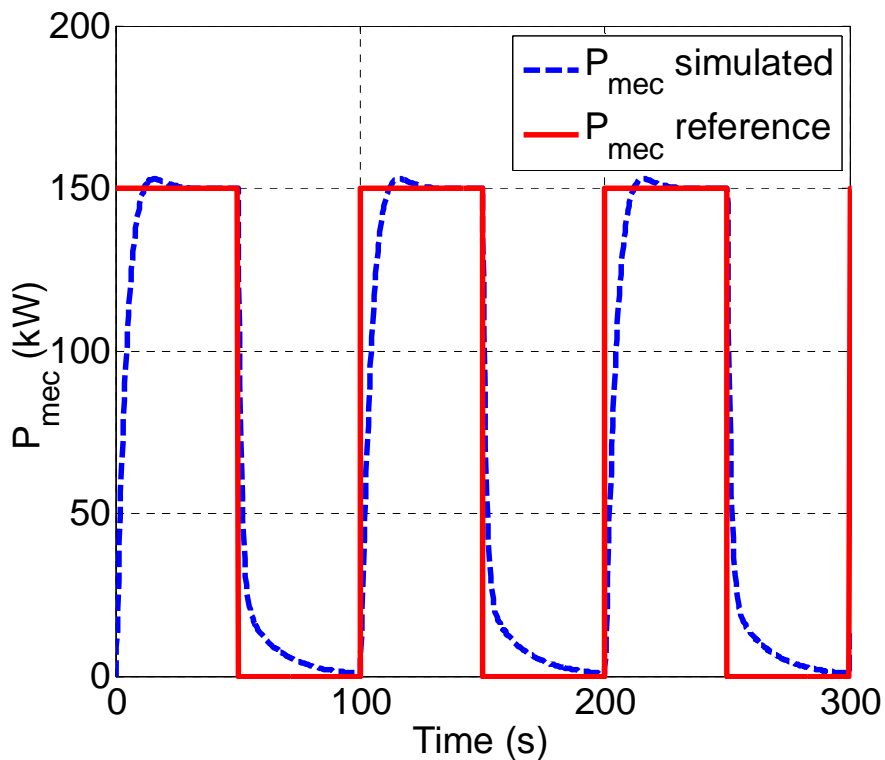


Fig. 2.25: Simulation and reference values for mechanical power.

2.7. MULTI-SOURCE EMR MODEL

In such model, all models of different sources are connected together as shown in Fig. 2.26. These models have been divided into two groups: loads and sources. In the sources, four elements are considered: PV panels, WTs, PEMFC and GMT. In loads, the electrical load as well the PEM ELS have been accounted for. It is required to provide the load by its

power all time for all possible source operating conditions. Sizing and energy management associating with this global model will be discussed in details in the fourth chapter.

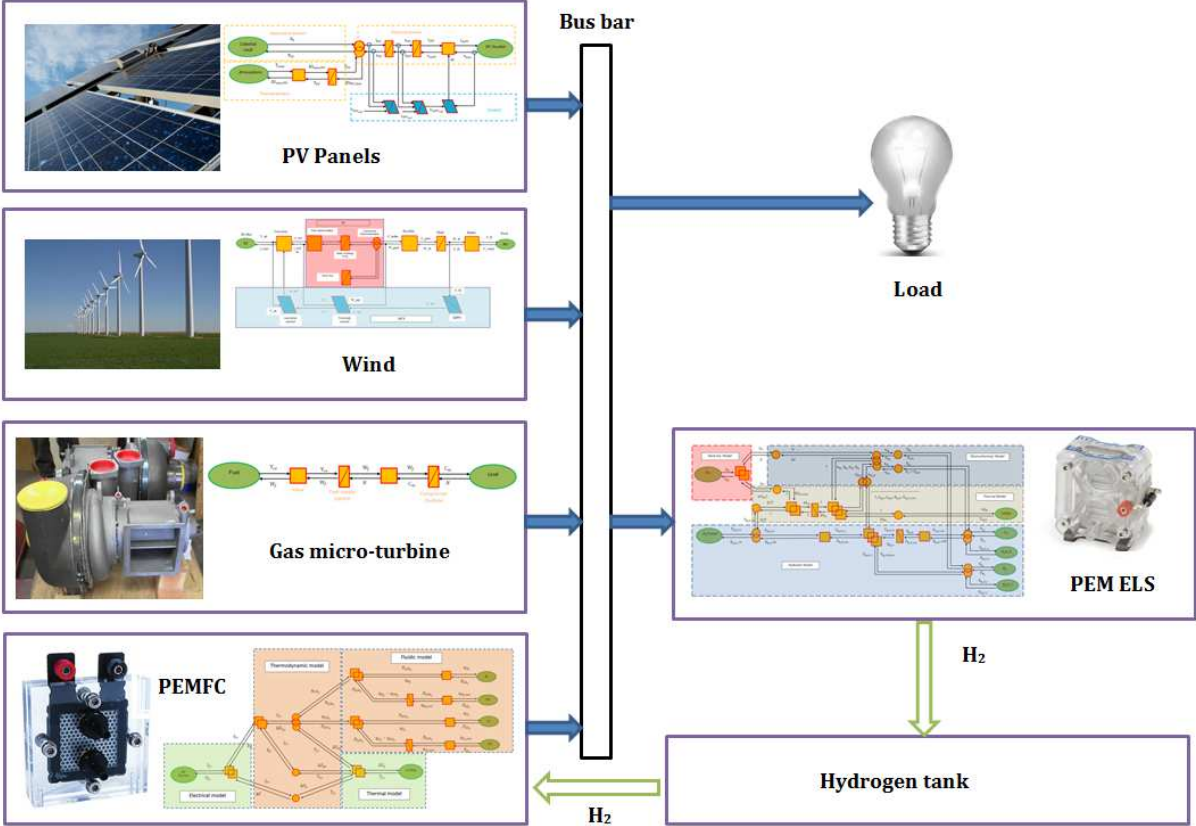


Fig. 2.26: global EMR model of multi sources system.

For multi-source energy management, PV panel and WTs have the priority provide their maximum power. Furthermore, GMT and PEMFC will be entered in service if supplementary power is required. Obviously, RESs have been invested as main sources and BKU by traditional one (GMT). In addition, PEM ELS works if further additional energy will be produced. In this case the energy will be stored such as hydrogen form in large tanks. Subsequently, stored hydrogen can be reused by the PEMFC.

2.8. CONCLUSION

In this chapter a multi-source system including RESs such as PV and WTs as principal source as well as GMT as Back-up Source (BKUS) has been shown. In addition, ESS consisting of PEM ELS, tank and PEMFC has been injected for enhancing the BKU system. EMR methodology has been used for presenting the different sources' models. Different mathematical equations representing the PEM ELS, PEMFC, GMT, PV and WTs models have been presented. Moreover, the simulation of each source model has been realized. Consequently, the validation of different models is achieved. Then, the global model of multi-source system has been shown. This last one will be useful for energy management treating in chapter four.

3. PV PANELS AND HYDROGEN

3.1. INTRODUCTION

This chapter deals with PV-PEM ELS system consisting of 59 kW PEM ELS connected to PV generator through a boost converter for H₂ production. The PV panels have been sized to 74 kW for providing requested energy to one part of Belfort region. The MPPT approach has been proposed for maximizing the energy captured by the PV panels. MPPT is mainly considered as a solution to overcome the problem of solar irradiance of PV panels [Ahma 08] [Chow 10]. In case of partial shading, the maximum power points vary for different PV panel groups when connected to MPPT controller. Consequently, the effect of the temperature and the irradiance on the PV characteristics (i.e., output power, voltage and efficiency) are presented. Therefore, new PV panel reconfigurations can be assumed to solve this problem. Practical tests for shading and dust cases are applied. Finally, experimental validation for the proposed shading effect solution are performed.

In addition, the efficiency enhancement of the hybrid PV-PEM ELS system is achieved. The PV panel characteristics have been experimentally validated. As the produced H₂ flow is dependent on the input water heating, the instantaneous reference PEM ELS input water temperature is determined using FLC. The optimal input water temperature is estimated in order to maximize H₂ production considering the physical constraints, especially the temperature limitation to avoid evaporation. The water temperature is optimally governed to its instantaneous reference value by the PI control. The produced H₂ flow would expand if the input water is heated. The effectiveness of the proposed FLC methodology towards improving the hybrid PV-PEM ELS system efficiency is verified through the maximization of both the PEM ELS produced H₂ flow and the PV captured energy.

3.2. PV PANEL SYSTEM UNDER-STUDY

The pollution caused by fossil energy gives the priority to the use of RESs in different regions worldwide. Solar energy is one of the most important sources energy. It can be well distributed, is renewable and has no hazard for atmosphere. However, PV panel has a problem when it is shaded by clouds, dust or other obstacles [Brec 11] [Ghaz 14a] [Diaz 11] [Char 13] [Adin 13] [Lim 14]. Shaded PV panels cause voltage drop at its terminals. Consequently, the extracted power is reduced. Shaded or dirty PV panels can directly affect the unshaded or clean ones. Even in presence of MPPT, the problem of partial shading effect decreases the overall PV panels' efficiency as explained in [Kako 11] [Vaid 13] [Doun 13] [Garr 07] [Goun 09] [Sala 09] [Syaf 09]. It is proven that shading and dust cause the same effect on the considered PV panel. To be concise, only the shading effect has been mentioned and practically applied in the chapter, but the result is valid for both without a lost in generality.

Many solutions have been proposed to partial shading effect, some of them have been interested in multi tracker and tracker per module such as [Kara 08] [Kara 08] [Sara 10] and others have dealt with photovoltaic array reconfiguration as explained in [Sala 90a] [Sala 90b] [Autt 98] [Sher 02] [Nguy 08] [Vela 05] [Veal 08] [Vela 09]. In the PV panels' reconfiguration proposed by [Sham 13], the complexity of PV array switches is still the main disadvantage in spite of all efforts to simplify its structure and to create optimization solutions. Moreover, multi-tracker inverters and a tracker per module solutions have cost problems [Kara 07] [Kara 08] and are insufficient to extract the maximum power.

Here, a new dynamical electrical array reconfiguration strategy of PV panels has been applied. This reconfiguration depends on FLC integrated in a dSPACE and only $n+6$ switches to make the configuration, where n is the number of PV panels. In this solution, any shaded PV panel can be switched off to avoid the overall power decrease. Therefore, all possible PV

panels' connection reconfiguration has been considered to provide the requested 24 V at load terminals and to minimize the power losses. If one of the PV panels or more is shaded, the connection of others in the same group will be automatically modified to maintain the requested 24 V for each PV panel row. This dynamical reconfiguration reduces the power losses, due to the shaded panel, by recovering an equivalent power from the reconfiguration of the other panels.

As a result, a real time switch position has been modified to ensure a constant voltage at 24 V and minimum number of PV panels has been switched off by isolating the effect of shaded panels. Similarly, the proposed solution can also be applied to dirty, shaded, dusty and faulty panels.

Two important phenomena affect shaded PV module: (i) Hot spot where the PV modules are equipped with bypass diodes [Chen 13] [Ubis 09] [Qi 14] [Zhen 14]. The role of bypass diodes is to protect the cells against the phenomenon of hot spot and improve the performance of modules subject to shading. (ii) Returning current: which result when two different modules (or chains of different modules) are connected in parallel [Alon 06]. Consequently two significant effects such as power losses and module damage can occur. To avoid this phenomenon, each PV panel has been provided with a diode connected in series.

All PV panel characteristics of the considered PWS500 module have been studied and the effect of shading has been experimentally verified. Then, a new cost effective solution has been proposed considering online operation, easy implementation and efficiency. This solution has been applied on a group of PV panels and experimentally validated.

3.2.1. PV PANEL CONFIGURATION

The solar cell has been presented by the equivalent circuit depicted in Fig. 3.1. The solar module is an association of series and parallel cells denoted by n_s and n_p respectively [Bech 11]. The conversion of solar energy into electrical energy is expressed by a non-linear relation between the module current I_{PVm} and its voltage V_{PVm} as given in equation (3.1):

$$I_{PV} = I_{ph} - I_0 \left[\exp \left(\frac{V_{PV} + I_{PV} R_s}{n V_T} \right) - 1 \right] - \frac{V_{PV} + I_{PV} R_s}{R_{sh}} \quad (3.1)$$

where I_{PV} : the module current, (A); I_{ph} : the module photocurrent, (A); I_0 : the diode saturation current (A); V_{PV} : the module voltage, (V); R_s : the series module resistance, 2.6449×10^{-1} (Ω); n : the ideality factor; $V_T = K T_{PV}$; K : Boltzmann constant, 1.38×10^{-23} ($J K^{-1}$); T_{PV} : the module temperature; and R_{sh} : the parallel module resistance, 10^5 (Ω).

The relation between the photocurrent and illumination is:

$$I_{ph} = \frac{E_e}{E_{ref}} \left(I_{ph,ref} + \mu_{ISC} (T_{PV} - T_{PV,ref}) \right) \quad (3.2)$$

where, E_e : the irradiance, (W/m^2); E_{ref} : the reference irradiance, (W/m^2); μ_{ISC} : the coefficient of variation of short-circuit current with respect to temperature, (A/K); $I_{ph,ref}$: the reference module photocurrent, (A); and $T_{PV,ref}$: the module temperature at STC, 298 (K).

Based on module model expressed by the equation (3.1), the PV array model can be constructed.

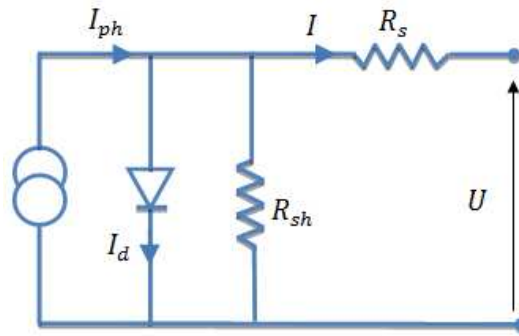


Fig. 3.1: Equivalent circuit of a solar cell.

3.2.2. MAXIMUM POWER POINT TRACKING

MPPT is a technique that inverters use to enable maximum power generation of solar panels. The aim of using MPPT algorithm is to maintain a PV maximum power point operation [Bech 11]. For this purpose, grid-tie inverters, solar battery chargers and similar devices are typically integrated into an electric power converter system that provides voltage or current conversion, filtering, and regulation for driving the electrolyser. Therefore, different MPPT algorithms based on Perturb and Observe (P&O), incremental conductance, parasitic capacitance and constant voltage can be used [Hohm 03]. For the PV model, the MPPT P&O algorithm has been considered due to its simplicity, robustness and ease of implementation as shown in Fig. 3.2.

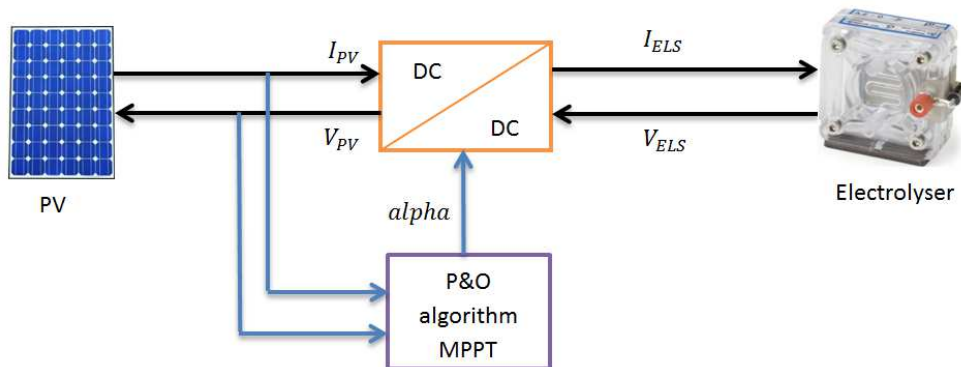


Fig. 3.2: Synoptic of the PV panel and the boost converter controller.

According to the “PWX500” double glass PV module characteristics system, it is capable of providing higher mechanical strength and greater electrical protection especially for marine applications, tropical environment or isolated areas. The solar irradiance and the ambient temperature are considered 1000 W/m^2 and 298K respectively.

Because of the complex relationship in solar cells between solar irradiation, temperature and total resistance, a non-linear output I-V curve has been reached. Current-voltage and power-voltage curves of sized PV array for the studied module have been shown in Fig. 3.3 for different solar irradiance levels ($400\text{-}1000 \text{ W/m}^2$). As obviously illustrated in Fig. 3.3, the current has constant value while increasing the voltage until reaching the voltage at which the maximum power exists (V_{MPPT}). At this voltage, the current significantly decreases until attaining its zero value at the PV maximum voltage (V_{PVmax}). From the P-V curve, the power-increase leads to a significant voltage-rise until reaching V_{MPPT} . Then, an inverse relation is appeared between the power and voltage at the voltages higher than V_{MPPT} .

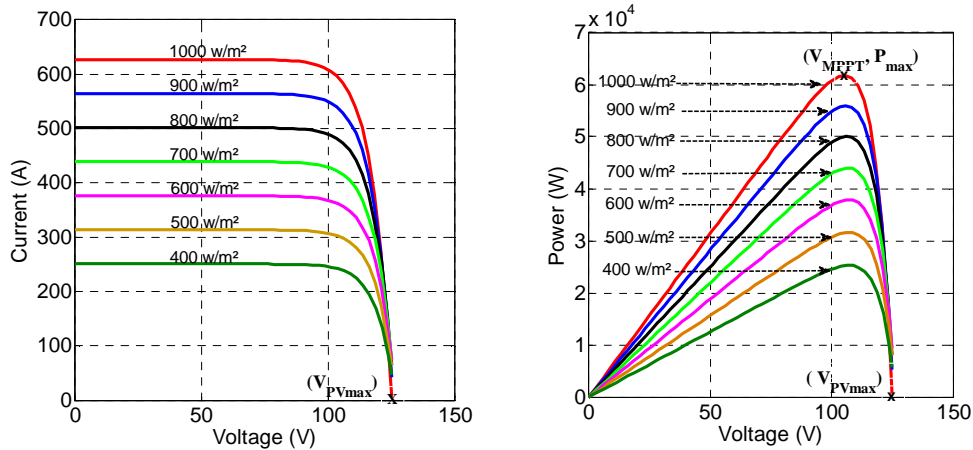


Fig. 3.3: I-V and P-V curves under different irradiance levels.

3.2.3. PV PANEL CHARACTERISTICS

The simulation and experimental results (the I-V and P-V curves) of the PV module have been performed as shown in Fig. 3.4 via Matlab-Simulink. The Sum of Squared Errors (SSE), the coefficient of determination (Rsquare) and the adjusted degree of freedom (Adjrsquare) data have been estimated in order to demonstrate the degree of vicinity between the simulation and the experimental curves. The SSE, Rsquare and Adjrsquare values are 0.0488, 0.9721, and 0.9696 respectively. These values are considered adequate to verify the closeness of both simulation and experimental curves. Accordingly, the experimental curves have been validated.

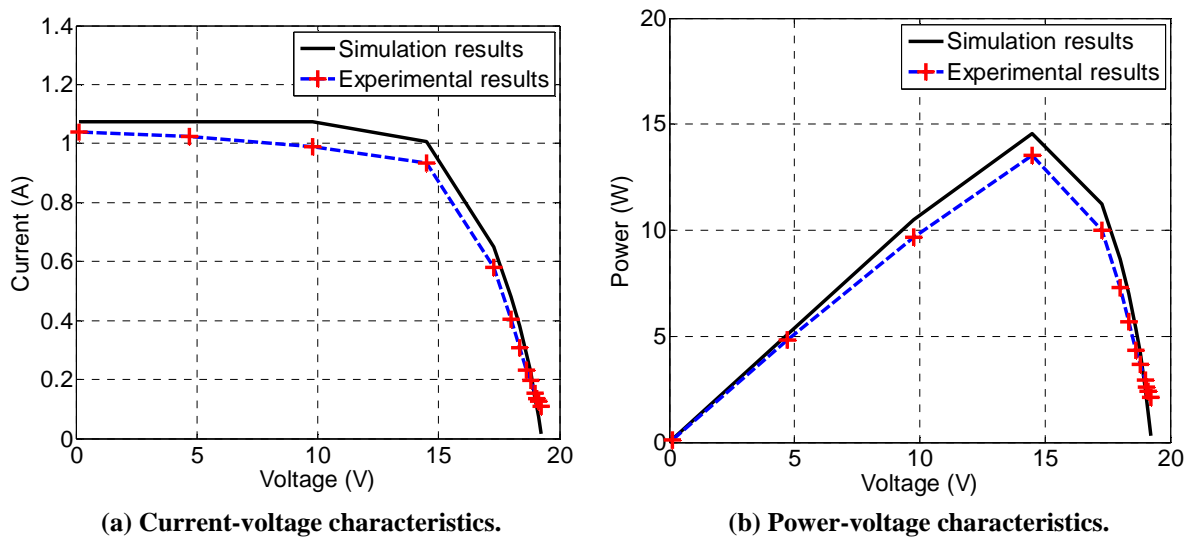


Fig. 3.4: PV panel experimental and simulation characterization curves.

The influences of temperature and irradiance have been studied using the test bench composed of 6 projectors of 500W each as illustrated in Fig. 3.5. Two tests have been accomplished. In the first, the projector irradiance has been fixed to 368 W/m² while the temperature has been risen gradually from 314K to 347K.

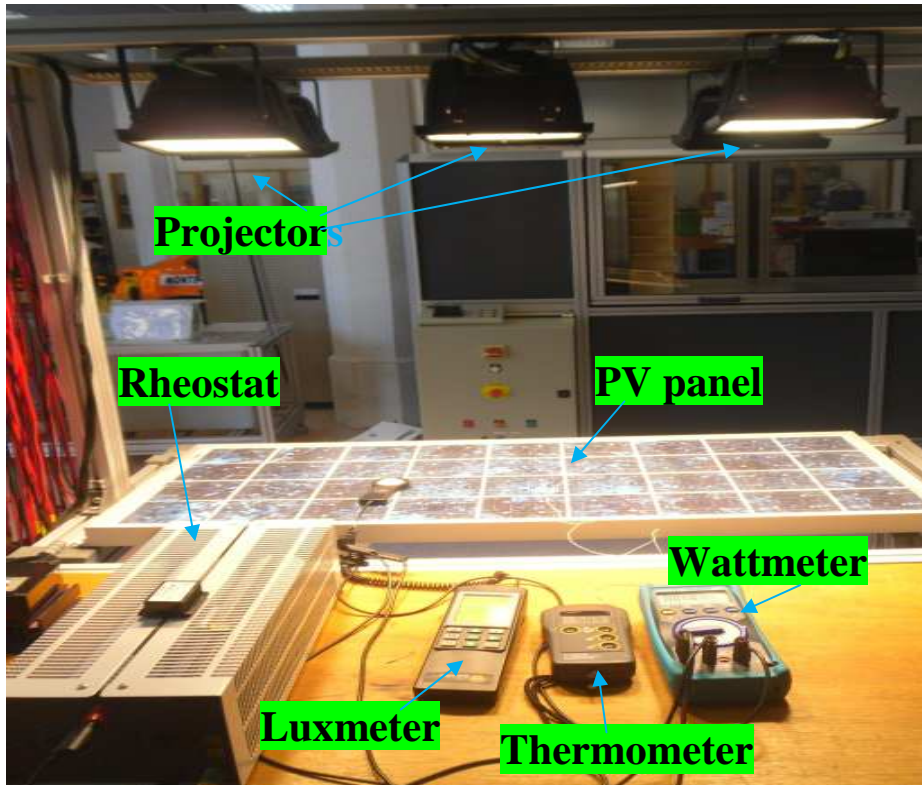


Fig. 3.5: Experimental test-bench of PWX500 PV panel.

In the second, the temperature has been fixed to be around 298K and the irradiance has been risen gradually from 175 W/m² to 407 W/m² as depicted in Fig. 3.6. It is difficult to perform this test at an exact temperature because of the significant relation between both temperature and irradiance. Therefore, multi on/off switching of the projector –as the source of irradiance– has been considered to approximately fix the temperature at the proposed degree. At this temperature, the irradiance has been changed between 175 and 404 W/m². The experimental results have been presented in Fig. 3.6.

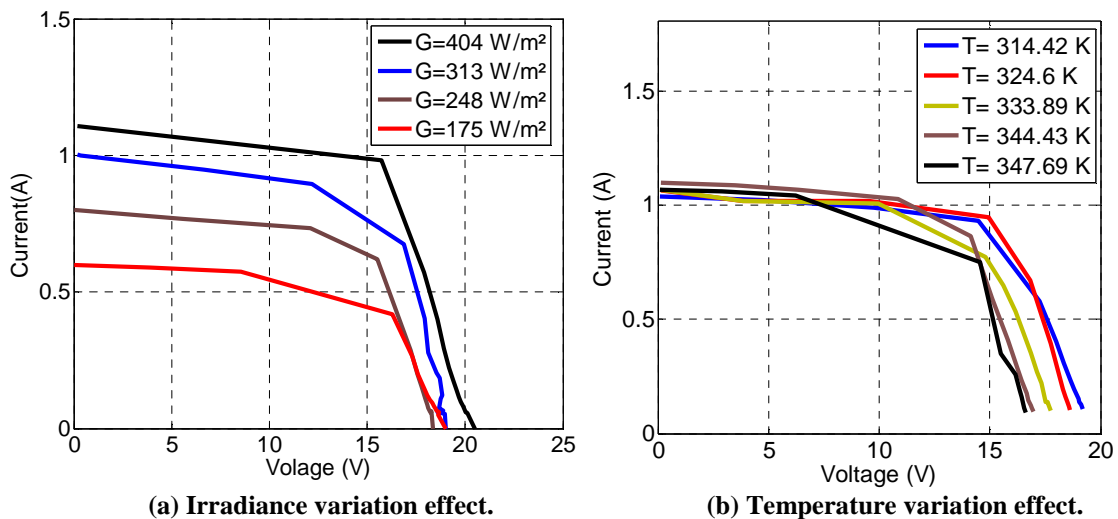


Fig. 3.6: I-V characteristics considering irradiance and temperature variations.

Obviously, Fig. 3.6 has illustrated the negative effect of shading and PV temperature rising. Considering PV irradiance variation, the I-V curves depicted in Fig. 3.6 have been considered approximately constant -with relative negligible decrease- until reaching the voltage point at

which maximum power attained. Then, the PV currents have decreased rapidly with the voltage rise until reaching the zero current at V_{MPPT} . Explicitly, different irradiation values result in various initial currents produced by PV panel. At constant temperature and voltage operating points, the current-irradiation relationship is proportional. Indeed, the shading leads to PV output current decrease. Assuming a temperature rise, insignificant variations on the PV panel I-V curves have been illustrated until reaching the maximum voltage point. Hereby, slight differences among the I-V curves have been reached by temperature change. To obtain the same current from the PV panel at higher temperatures, smaller PV terminal voltage could be necessary for the same irradiation as demonstrated in Fig. 3.6.

Although this increase in temperature is considered useless for PV panels, it can be desirably exploited by PEM ELS in case of hybrid PV-PEM ELS systems. Accordingly, the temperature variation can be assigned to a beneficial heat exchange process between the exothermic PV panels and the endothermic PEM ELS by means of water. The temperature exchange can lead to the hybrid PV-PEM ELS system efficiency rise if properly controlled. In this case, a water pump has been requested to exchange the heated water between PV and PEM ELS. Therefore, 20 % of the overall PV output energy has been considered for providing water pump with necessary energy. Consequently, heating the input water of the PEM ELS during simulation will be achieved. The energy source used for the water heating can be also obtained by using the unutilized long wavelength radiation incident from the sun.

Electrical PV module characteristics present substantial variations in case of partial shading, resulting in considerable reductions of the output power [Vela 09] [Hayo 10]. The principle of shaded series and parallel cells has been illustrated in Fig. 3.7. The PV module characteristics have been depicted considering the cells (1,2, and 9) shaded as shown in Fig. 3.8: (i) 2 cells/P: two cells are shaded from two different lines (parallel); (ii) 2 cells/S: two cells are shaded from the same line (series); (iii) 9 cells/P: nine cells are shaded from two different lines (parallel); (iv) 9 cells/S: nine cells are shaded from the same line (series).



Fig. 3.7: Shading nine cells from: (i) two different lines (9 cells/ P), and (ii) nine cells from the same line (9 cells/ S).

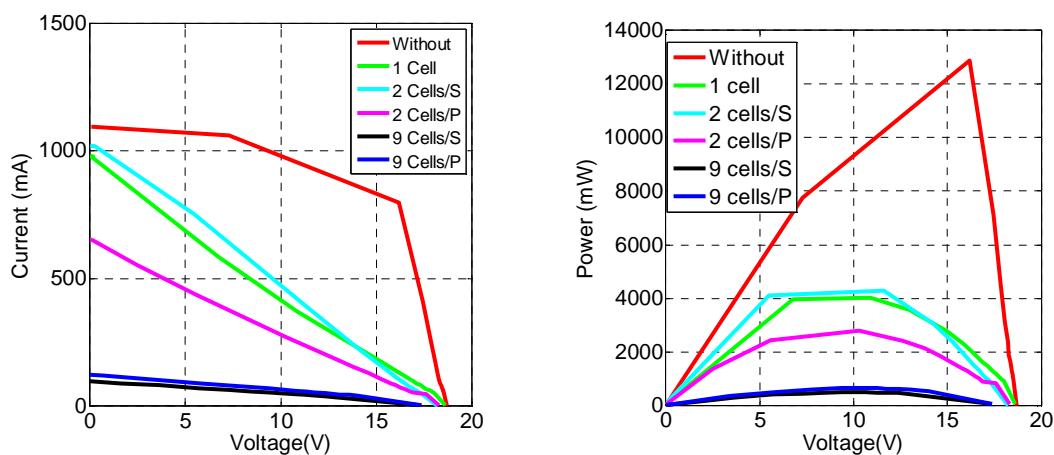


Fig. 3.8: Experimental I-V and P-V characteristics for shaded PWX500 PV panel.

From Fig. 3.8, it is clear that the point of maximal power in presence of shading is very far from the one obtained without shading. Obviously, one shaded cell is enough to decrease the

point of maximum power from about 13 W to about 4 W. Consequently, a solution has to be searched when using many PV panels. Using MPPT for group of PV panels which have different shading percentage shows the problem of extracting the maximum power regarding to each PV panel [Kara 07] [Kara 08] [Dept 11] [Walk 04] [Koba 06] [Boui 13] [Heyd 13] [Lali 13]. Therefore, a new series/parallel topology reconfiguration has been presented in this chapter which is suitable for the connection of a large number of PV without a change in the overall topology. As a result, new PV modules can be easily connected to the generator in a kind of plug and play process.

3.2.4.FL ESTIMATOR FOR SHADED PV MODULES CONTROL

This type of control approaches the human reasoning. It makes use of the tolerance, uncertainty, imprecision and fuzziness in the decision-making process. It offers a satisfactory performance without system detailed mathematical model need. However, the incorporation of the experts' knowledge into fuzzy rules is necessary. In addition, imprecise or noisy data can be treated by using FL. Consequently, it is able to control even those operating conditions where linear control techniques fail (i.e., large parameter variations). This system has four main parts. First, using input membership functions, inputs are fuzzified, then based on inference rules, outputs are produced and finally the fuzzy outputs are defuzzified and applied to the main control system. Fuzzy sets can describe vague concepts [Ross 10].

Fuzzification is the process where the crisp quantities are converted to fuzzy (crisp to fuzzy). Obviously, fuzzy values are formed by identifying some of the uncertainties present in the crisp values. The conversion of fuzzy values is introduced by the membership function. In practical application, there might be a negligible error that produces imprecision in the data. This last can be presented by the membership function. Consequently, fuzzification has been achieved. Fuzzification process may include membership values for the given crisp quantities [Ross 10].

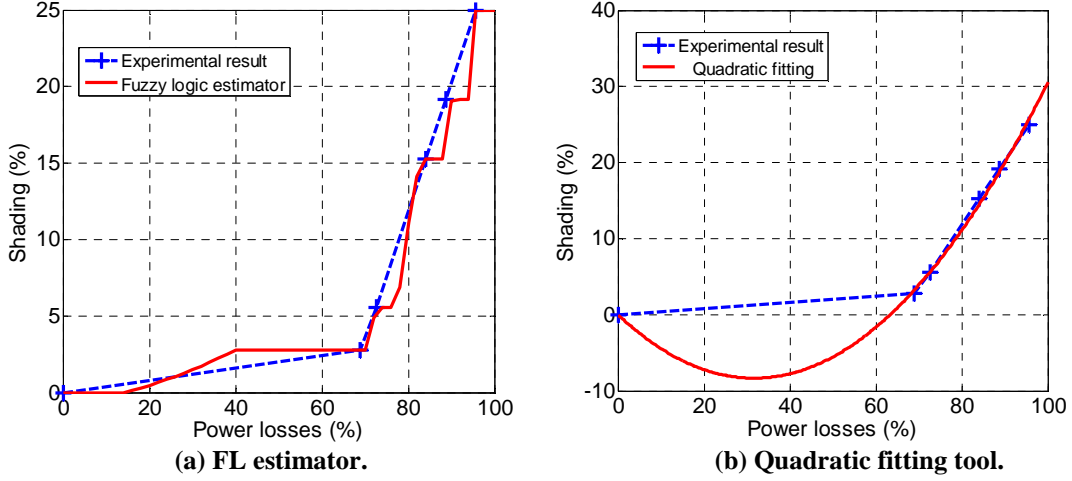
The generated fuzzy results cannot be directly used in the applications. Therefore, fuzzy quantities have been converted into crisp quantities. This can be achieved by using defuzzification process. Defuzzification reduces the collection of membership function values into a single scalar quantity [Ross 10].

The dust accumulation on PVs surfaces is a natural phenomenon that significantly reduces the PV panels' efficiency up to 70–80% [Ghaz 14a] [Ghaz 14b]. For example, in the United Kingdom, dust reduces the PVs efficiency by 5-6% if they are not cleaned after one month [Ghaz 14b]. This percentage becomes 40% in Sudan. Cleaning is the solution of dust particles, its frequency differ from one place to another. For the United Kingdom, two times of cleaning per year are enough to keep the PVs clean. The presence of heavy industry nearby, bird droppings, water stains, traffic pollutants or agricultural dust may warrant more frequent cleaning to assure optimal output and maintenance of solar modules [Ghaz 14a]. The cleaning cost increases with its frequency.

There is a proportional relationship between the shading amount and power losses of PV panels. This relationship has been practically studied for different shading conditions as demonstrated in Table 3.1. Then, the power losses as a function of shading has been depicted in Fig. 3.9. FL estimator has been used for obtaining the power losses estimation at any shading percentage as shown in Fig. 3.9(a).

Table 3.1: Experimental power losses in function of shading percentage.

Shading (%)	P_{max} (W)	Power losses (%)
0	12.89	0
2.78	4	68.97
5.56	3.53	72.61
15.28	2.05	84.1
19.168	1.46	88.69
25	0.57	95.58

**Fig. 3.9: Different power losses estimation in case of shading.**

FL estimator, used to predict the percentage of shading, can identify the shaded, dirty or faulty panel. FL provides a solution to obtain the shading or dust percentage for any unknown data of power losses. Therefore, this technique allows taking a decision if the PV panel has been shaded or not according to certain shading limits as shown in Fig. 3.9(a).

Another solution for estimating power losses in case of shading PV panel is by using the fitting tool in MatlabTM as depicted in Fig. 3.9(b). In this case, the suitable solution has been obtained using the following function:

$$y = -8.8833 * 10^{-5} x^3 + 0.0230 x^2 - 1.1212 x + 0.0001 \quad (3.3)$$

where, y represents the shading/dust percentage and x represents the power losses percentage. There is a proportional linear relationship between shading and power losses in PV modules. Obviously, this relationship has two significant parts. In the first one, there is a slight increase in power losses with shading percentage increase until 70%. Then, in the second part for shading percentage more than 70%, the power losses become much more important as illustrated in Fig. 3.9. Then, FL estimator has been selected to do the estimation of power losses or the percentage of shading/dust besides the location of the considered panel.

In order to optimize the power losses/ concerning (cleaning frequency and cost), the cleaning frequency should be calculated. The FL estimator of Fig. 3.9(a) allows obtaining the percentage of dust. Discrimination between shading and dust can be achieved by: (i) knowing the weather data, (ii) the shading is a temporary phenomenon while the dust is permanent if not cleaned. So, FL decides on the limit $V_{PV(min,max)}$ to switch on or off, locates the

shaded/dusty or faulty panel, gives the percentage of shading or dust and consequently suggests to proceed with cleaning of the considered panels or not.

As shown in Fig. 3.10 depending on the PV panel voltages V_{PV1} , V_{PV2} , V_{PV3} and V_{PV4} acting as FL inputs, FL estimator can: (i) warn about the shaded, dirty or faulty panel and locate it, (ii) determine the shading/dust percentage and (iii) estimate the maximum and minimum voltage values (V_{PVmin} and V_{PVmax}). Consequently, switches can change their status, on or off, depending on switching rules. According to this result, the incriminate panel is either disconnected or not (regarding the percentage of the lost power), the operator is warned to clean the panel or to check if there is a shadow on the identified panel.

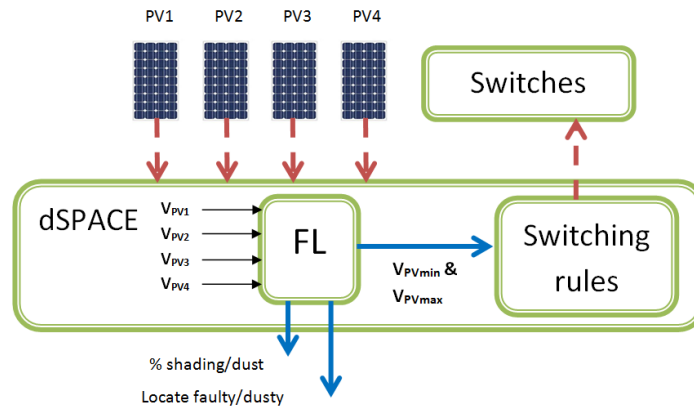


Fig. 3.10: FL and dSPACE control of the proposed system.

The switching rule base allows the representation of the relation between inputs and outputs and has the following structure:

If power losses (which is also the image of voltage drop) percentage condition is observed then the corresponding percentage of shading or dust is calculated. Consequently, the topology reconfiguration can be decided by switching off or on the PV panels.

If four PV panels are used, as shown in Fig. 3.10, the FL estimator has four inputs that are the PV output voltage (images of the four PV powers). The FL estimator has also four outputs: (i) minimal voltage V_{PVmin} ; (ii) maximal voltage V_{PVmax} ; (iii) the percentage of shading/dust of the four PV panels; (iv) and the location of the faulty/dusty PV panels if exist. Accordingly, switching rules compare each PV voltage drop with the voltage thresholds V_{PVmin} and V_{PVmax} . Consequently, connecting or disconnecting PV panels is decided on the basis of the shading/dust FL estimation.

3.2.5.SWITCHING METHODOLOGY FOR SHADED PV IDENTIFICATION REMOVAL

According to the high cost of MPPT dedicated to each module (which is about 100 \$ per each from Sian Sonic corporation), the insufficient tracker per module solution and the complexity of PV array switches reconfiguration solutions which have been presented until now, a new switches combination using FL estimator has been proposed as shown in Fig. 3.11.

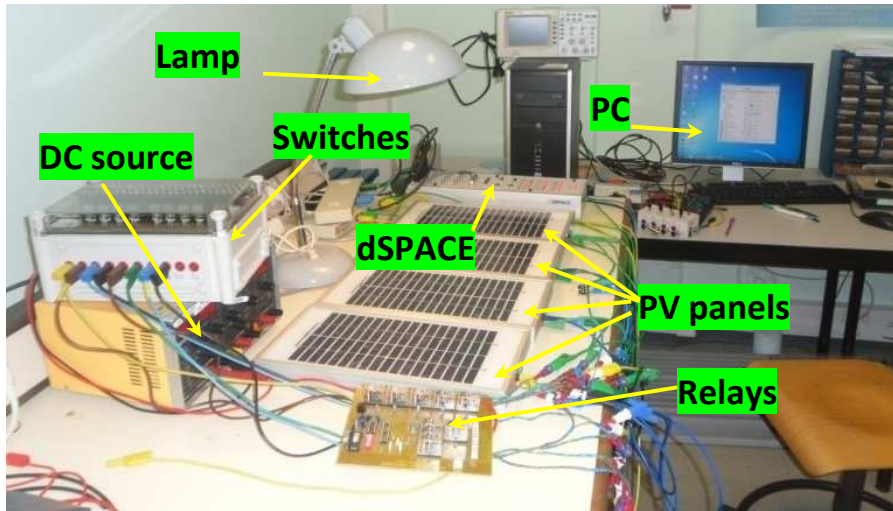


Fig. 3.11: Experimental test-bench of the new switches reconfiguration.

Experimentally, the test bench includes the following devices: (i) 4 PV panels with max power 5W for each and nominal voltage of 12V; (ii) dSPACE control hardware; (iii) 10 switches; (iv) 10 relays; (v) 4 A meters; (vi) DC source feeding power to the relays (relays can be fed directly by PV); (vii) cables; (viii) lamp; (ix) PC; (x) rheostat as a load; (xi) diodes.

The goal is to obtain 24 V output with minimized power loss on the shaded PV panels. Consequently, minimum cost can be reached due to the reduced number of MPPT controllers used.

PV panels have been divided into two strings (PV_1 and PV_2) and (PV_3 and PV_4) respectively connected in series electrical arrangement. To meet the 24 V requirements at the load terminals, each string contains two PV panels of 12 V output each. If more than four PV panels are considered, the other PV panels can be connected in parallel on the existing PVs. As a result 24 V output has been obtained at the load terminals. The 4 main PV modules, series/parallel reconfiguration, of the PV buses can be performed to reach the requested 24 V output as depicted in the general solution of Fig. 3.15.

The controlled switches have been used as follows:

Own switches: each PV module has its own switch allowing its disconnection under shaded or faulty conditions.

Reconfiguration switches: six switches are needed to perform the reconfiguration in series/parallel arrangement of the four PV modules.

Consequently, for the connection of (n) PV modules, the number of requested switches (own and reconfiguration switches) would be ($n+6$).

In this work, two types of switches have been used, normally opened such as $TSP12$ and $TSP34$ and the others switches will be closed.

3.2.6. CONTROL OF SWITCHES

As shown in Fig. 3.8, the shading affects the current and the voltage at the output of the PV module. In order to avoid additional sensors, the shading effect has been detected based on the voltage drop at the output of each PV module. Consequently, sensors have not been used and output voltage of each module has been directly connected as an input to the dSPACE card.

The effect of temperature on the PV characteristics has been included experimentally. Obviously, the temperature changes affect the PV panel voltage. It has been experimentally noticed that each PV panel voltage is also the image of the temperature. Consequently, there is no need to add any temperature sensor. The output panel voltage is then taking into account different variables and phenomena (temperature, hotspot, shading, dust, failure, ...etc.). Thus, the FL estimator has been proposed for the on/off switching decision, based on the output voltage drop on each module. The shaded or faulty PV module will be disconnected according to the output voltage drop at each module. In case of more PV modules, they can be disconnected or reconfigured in order to capture the requested 24 V at the PV panel output. Inputs of this switching control are PV panels' voltages as well as minimum and maximum voltage values (V_{PVmin} and V_{PVmax}) estimated by FL estimator and the outputs are the switches control in Boolean values as shown in Fig. 3.10.

If four PV panels are used, as show below in practical work Fig 3.12, in this case FL estimator has four inputs representing the percentage of voltage drop (instead of power), as well as FL estimator has ten outputs representing the situation of ten switches to apply the decision of switching on or off the four PV panels depending on their shading/dust situation estimated by FL.

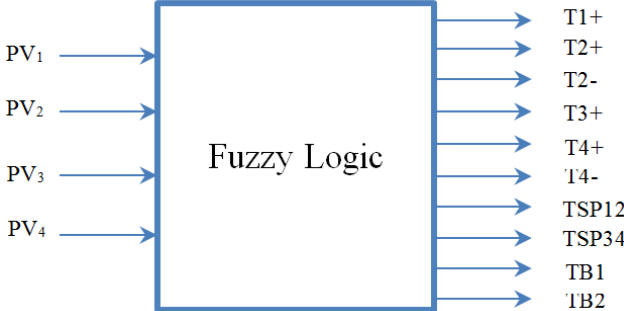


Fig. 3.12: FL estimator inputs and outputs.

The PV module voltage drop disconnection decision V_{PVmin} can be chosen by an expert or automatically set by FL on the basis of the overall power production losses. If the shaded PV module becomes unshaded, its reconnection is automatically done as depicted in Fig. 3.14. A hysteresis with a defined bandwidth (+1V) has been used on the PV module voltage in order to avoid chattering phenomenon between switching on and switching off. Then, $V_{PVmax} = V_{PVmin} + 1 V$.

In the studied scenario, either one or couple of PV modules have been shaded. Indeed, if more PV modules are shaded, the requested 24 V cannot be reached. Therefore, the PV modules will be automatically disconnected from the system in order to secure the overall installation and the PV module health.

FL rules for inputs and outputs are explained in Table 3.2 and Table 3.3. If the PV panels are in normal mode, there is no action. This situation is presented by (V_{PVmax}). Inversely, if the PV panels are switched off, this state of the selected PV module will be (V_{PVmin}) as shown in Fig. 3.14.

Table 3.2: FL estimator inputs.

INPUTS									
Rule	PV ₁	PV ₂	PV ₃	PV ₄	Rule	PV ₁	PV ₂	PV ₃	PV ₄
1	V _{PVmin}	V _{PVmin}	V _{PVmin}	V _{PVmin}	9	V _{PVmin}	V _{PVmax}	V _{PVmax}	V _{PVmin}
2	V _{PVmax}	V _{PVmin}	V _{PVmin}	V _{PVmin}	10	V _{PVmin}	V _{PVmax}	V _{PVmin}	V _{PVmax}
3	V _{PVmin}	V _{PVmax}	V _{PVmin}	V _{PVmin}	11	V _{PVmin}	V _{PVmin}	V _{PVmax}	V _{PVmax}
4	V _{PVmin}	V _{PVmin}	V _{PVmax}	V _{PVmin}	12	V _{PVmax}	V _{PVmax}	V _{PVmax}	V _{PVmin}
5	V _{PVmin}	V _{PVmin}	V _{PVmin}	V _{PVmax}	13	V _{PVmax}	V _{PVmax}	V _{PVmin}	V _{PVmax}
6	V _{PVmax}	V _{PVmax}	V _{PVmin}	V _{PVmin}	14	V _{PVmax}	V _{PVmin}	V _{PVmax}	V _{PVmax}
7	V _{PVmax}	V _{PVmin}	V _{PVmax}	V _{PVmin}	15	V _{PVmin}	V _{PVmax}	V _{PVmax}	V _{PVmax}
8	V _{PVmax}	V _{PVmin}	V _{PVmin}	V _{PVmax}	16	V _{PVmax}	V _{PVmax}	V _{PVmax}	V _{PVmax}

The normal mode presented by rule 16 in Table 3.2 and Table 3.3 corresponds to the absence of shading on any PV panels. All PV panels are in service and its output voltage is more than (V_{PVmax}). Thereby, all switches are in normal position (open or closed by fault). Therefore, $TSP12$ and $TSP34$ are normally opened and all others switches are normally closed. The connection will be parallel for both groups of switches (PV_1 and PV_2) and (PV_3 and PV_4) respectively as depicted in Fig. 3.13. In this case, the captured power is 16 W, and the voltage at each PV panel output is about 12 V.

Table 3.3: FL estimator outputs.

OUTPUTS										
Rule	T1+	T2+	T2-	T3+	T4+	T4-	TSP12	TSP34	TB1	TB2
1	1	1	1	1	1	1	1	1	1	1
2	0	1	1	1	0	1	1	1	1	0
3	1	1	0	1	0	1	1	1	1	0
4	1	0	1	0	1	1	1	1	0	1
5	1	0	1	1	1	0	1	1	0	1
6	0	1	0	1	0	1	1	1	1	0
7	0	0	1	0	0	1	0	0	0	0
8	0	0	1	1	0	0	0	0	0	0
9	1	0	0	0	0	1	0	0	0	0
10	1	0	0	1	0	0	0	0	0	0
11	1	0	1	0	1	0	1	1	0	1
12	0	0	0	0	0	1	0	0	0	0
13	0	0	0	1	0	0	0	0	0	0
14	0	0	1	0	0	0	0	0	0	0
15	1	0	0	0	0	0	0	0	0	0
16	0	0	0	0	0	0	0	0	0	0

In Fig. 3.13, each PV panel provides about 4 W, in normal operating condition. In case of a faulty PV panel, the power loss should be recovered (or its effect has to be minimized) from the other panels via the automatic switching PV reconfiguration of the topology. Compared to the classical and fixed series/parallel connection, the PVs in series are forced to produce the same current. Consequently, if one panel in series has been shaded or becomes faulty, the output current of the all PV in series has been fixed to the lowest produced current and affects directly the overall power generated.

To clarify the functionality of the proposed reconfiguration, the condition related to rule 11 will be explained. In rule 11, considered shaded PV_1 and PV_2 , as these two PV panels are from the same string while both (PV_3 and PV_4) are healthy, PV_3 and PV_4 should be

reconfigured in series in order to obtain the 24 V at load terminals. Therefore, PV_1 and PV_2 have to be disconnected by opening switches $T1+$ and $T2-$ and keeping the switch $TSP12$ closed (for series/parallel between PV_1 and PV_2) as depicted in Fig. 3.14.

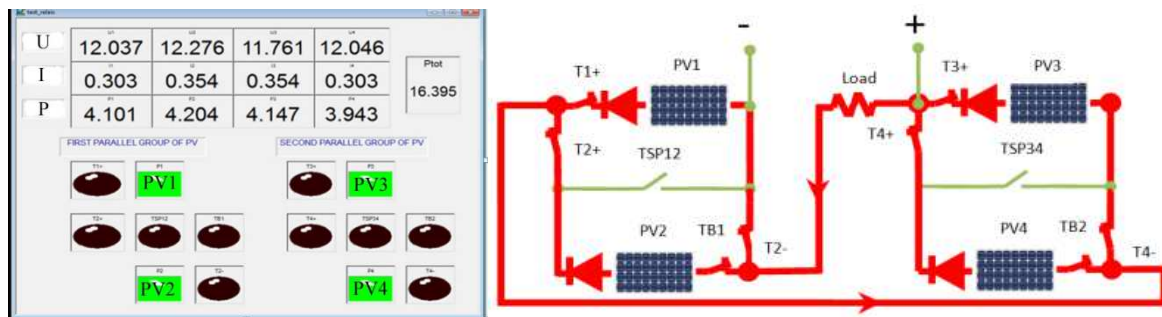


Fig. 3.13: U, I, P results and current flow for the four PV panels (normal mode).

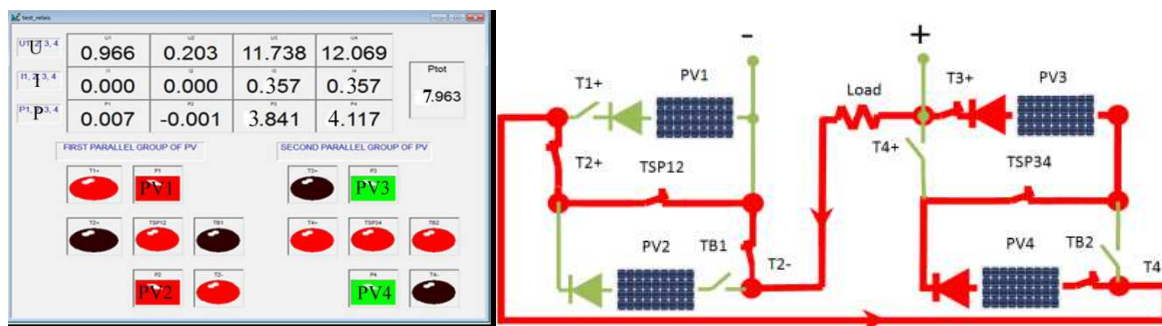


Fig. 3.14: U, I, P results, and current flow for four PV panels connection (shaded PV1 and PV2).

The all possibilities of shaded PV are:

- Case (1): No shaded PV panel (normal condition);
- Case (2): One shaded PV panel;
- Case (3): Two shaded PV panels from the same string;
- Case (4): Two shaded PV panels from different strings.

Otherwise, if three or four PV panels are shaded, all PV modules should be disconnected because the 24 V could not be reached.

All the possibilities of having one, two or no shaded PV are listed in Table 3.4 and have been experimentally tested.

Table 3.4: All possibilities of PV panel shading.

Case	PV Power value (W)		Electrical current flow path
(1)	PV ₁	4.1	
	PV ₂	4.2	
	PV ₃	4.15	
	PV ₄	3.94	
	P _{tot}	16.4	
(2)	PV ₁	0	
	PV ₂	4.13	
	PV ₃	3.91	
	PV ₄	3.97	
	P _{tot}	12.03	
(3)	PV ₁	0	
	PV ₂	0	
	PV ₃	3.84	
	PV ₄	4.12	
	P _{tot}	7.96	
(4)	PV ₁	0	
	PV ₂	4.03	
	PV ₃	0	
	PV ₄	4.01	
	P _{tot}	8.05	

From the experimental results reported in Table 3.4, in case of shaded, dusty or faulty panel, the lost power is the one of the switched off panel only without affecting the other panels. The reconfiguration rules allow guaranteeing the requested load voltage (of 24 V). Generally, when multi PV panels exist, any shaded PV panel will be switched off by its own switch if the

lack of power is no more possible to be recovered by the other PV panels. Hence, the most shaded PV string will be switched off as shown in Fig. 3.15.

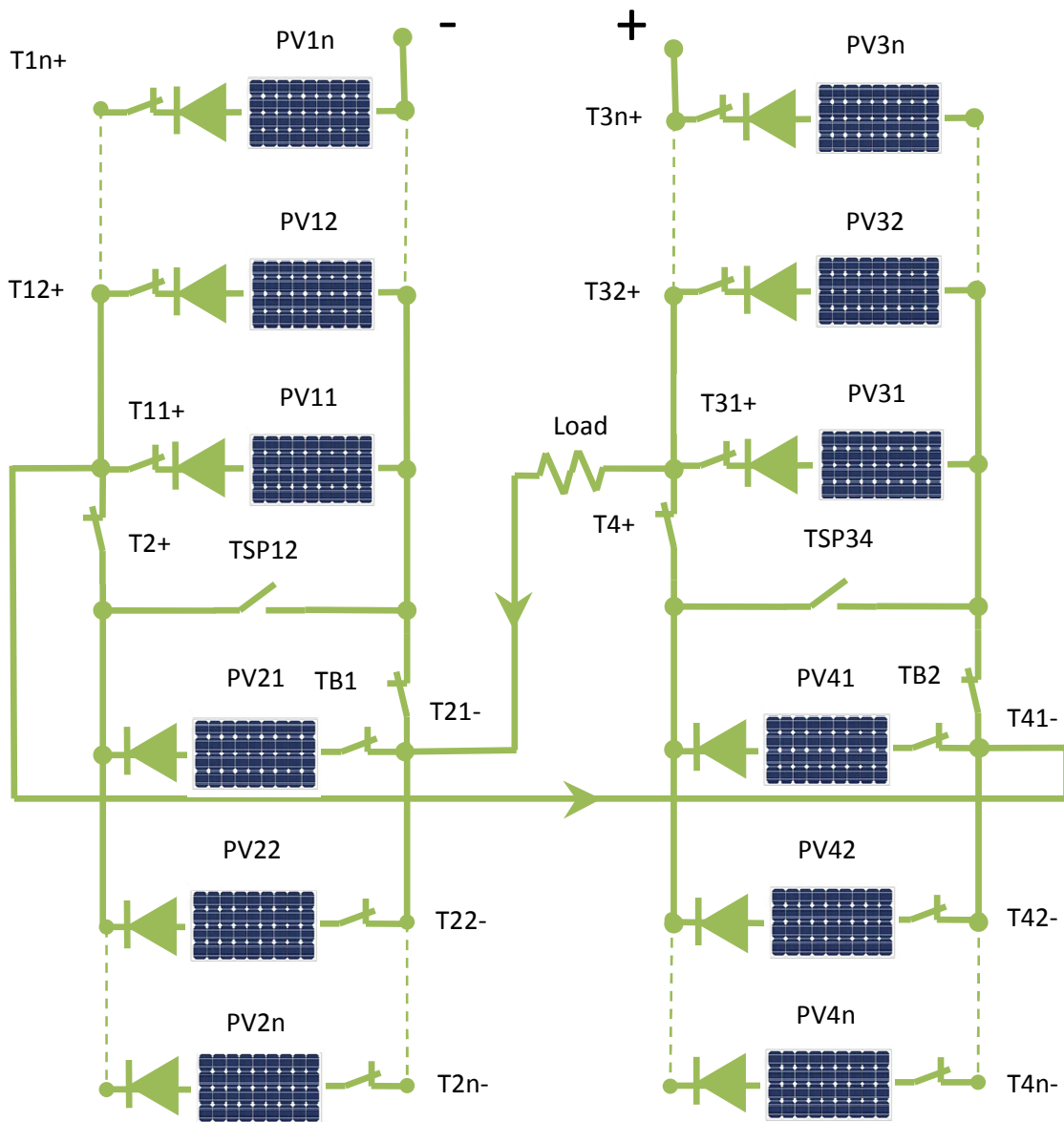


Fig. 3.15: Online PV panels reconfiguration.

3.3. PV–PEM ELECTROLYSER UNDER–STUDY

The system under-study, shown in Fig. 3.16, consists of PV panels of 74 kW rated power which are employed to provide the requested energy to PEM ELS of the 59 kW rated power. The MPPT approach is considered to extract the maximum power form the PV panels. In addition, a boost DC/DC converter is used to elevate the PV voltage to suite the electrolyser input. To ensure PV–PEM ELS energy equilibrium, any decrease in hydrogen flow at PEM ELS output results in water temperature reduction and vice versa. Therefore, water temperature has to be controlled to its reference value by FLC at each hydrogen flow value. The PI controller instantaneously governs the water temperature to its optimal value. The PV panels' energy generation is divided into two parts of 80% and 20% respectively to provide the corresponding necessary electrical and thermal energy to the PEM ELS [Taba 13]. The two parts of energy sources work at splitting water into its components hydrogen and oxygen.

The 80% represents the total energy fed to the PEM ELS. The 20% of the energy is used to run the heated water pump that transfers the heat from the PV panel's surface to the PEM ELS inlet water. Practically, the assumed percentages depend on the operating conditions. This division provides a positive influence on the PEM ELS efficiency. The proposed water temperature control at PEM ELS input has been used for two different temperature thresholds in order to maximize the hydrogen flow at the PEM ELS output and to cool the PV panels.

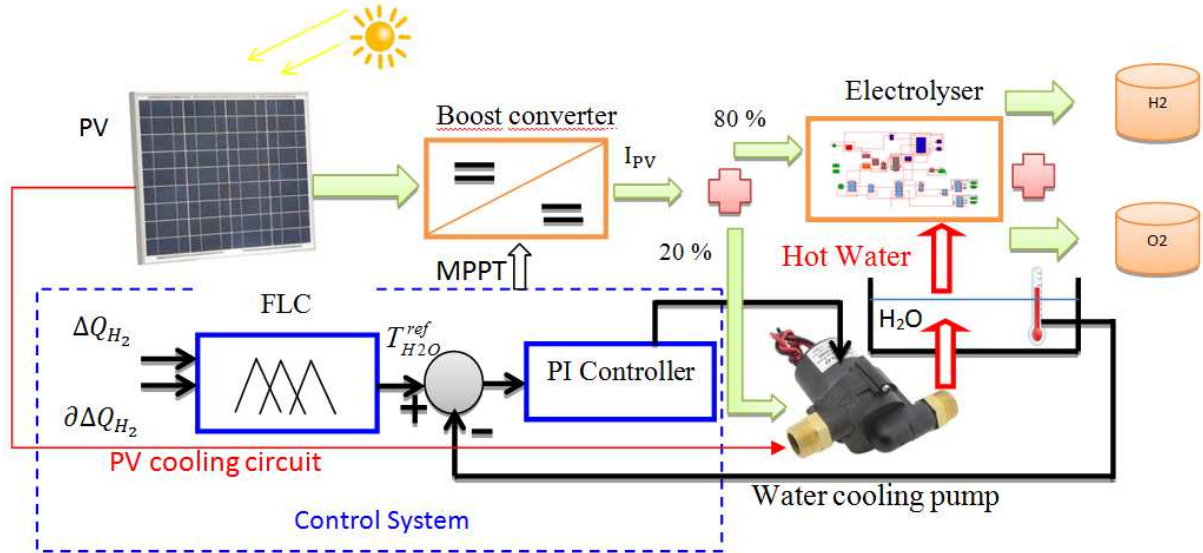


Fig. 3.16: The overall system under-study with the proposed water heating control.

3.3.1. PEM ELECTROLYSER OPERATION

In PEM ELS, water is supplied through water pipes at the anode reaction interface [Ghri 13], [Agbl 11a]. Oxygen and hydrogen are produced at the anode and cathode sides respectively as explained in equation (3.4). The most commonly used membrane material is Nafion (perfluorinated sulfonic acid membrane) proposed by DuPont [Scib 83]). Nafion has received a considerable amount of attention as a proton conductor for PEMFC and PEM ELS because of its better thermal and mechanical stability than cerium (IV) oxide and platinum. To function, the membrane conducts hydrogen ions (protons) and not electrons. When applying a DC voltage on the ELS terminals, oxygen, hydrogen protons and electrons are produced as illustrated in equation (3.4). At the cathode side, hydrogen is formed by the recombination of electrons and protons as presented in equation (3.5). The overall chemical reaction of the water electrolysis is given by equation (3.6).



The internal structure of PEM ELS and the synoptic of its internal phenomena are presented in Fig. 3.17 and Fig. 3.18 respectively.

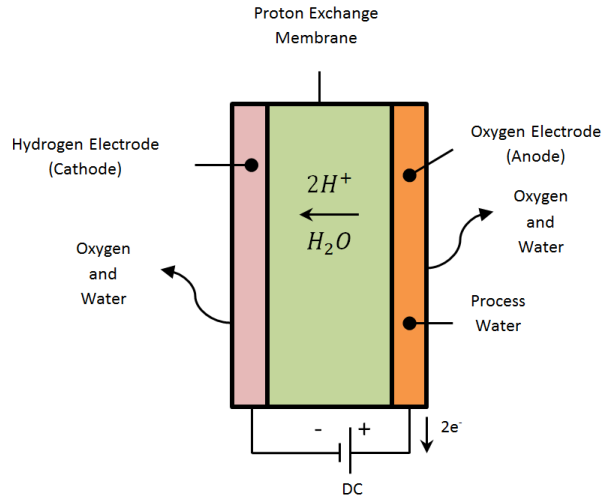


Fig. 3.17: Internal structure of the PEM electrolyser [Taba 12].

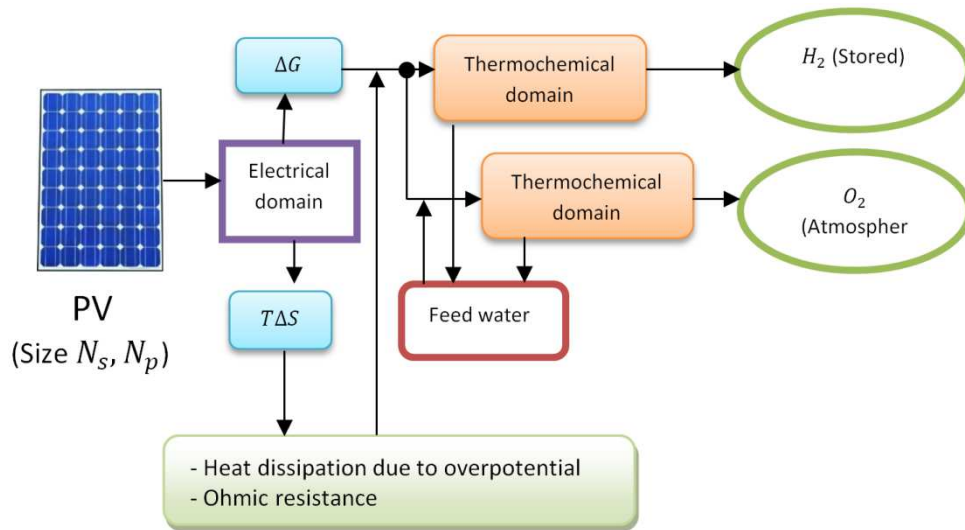


Fig. 3.18: Physical interactions within an electrolyser [Taba 12] and [Agbl 11a].

As the electrochemical reaction is mostly endothermic, the requested heat energy can be either taken from the environment or supplied by an electrical energy source. From Fig. 3.18, the PV energy produced is used in the electrolyser to split the water molecules into hydrogen and oxygen. This energy is supplied by applying a DC voltage between the stack terminals expressed by $V_{ref} = \Delta G/nF$ at Standard Test Conditions (STC) ($T = 298K$, and $P=101.325kPa=1 \text{ atm}$). At this voltage, the required heat energy from the surrounding environment equals to $T\Delta S$ where S is the entropy and T the temperature [Taba 13]. The total energy needed is expressed by the enthalpy $\Delta H = \Delta G + T\Delta S$. The voltage requested for splitting the water molecule is: $V_{tn} = \Delta H/nF = 1.482 \text{ V}$, where n is the number of transferred electrons and F is the Faraday constant $96\,485 \text{ C/mol}$. Two classic PEM ELSs can be considered: low-pressure alkaline electrolyte water electrolyser below 30 bars, and high pressure Solid Polymer Electrolyte electrolyser (SPE ELS) above 30 bars and up to 135 bars [Ghri 13].

The FC system can be used to convert the stored hydrogen back to electricity according to the demand. Obviously, the ELS and the FC efficiencies do not exceed 75% and 50% respectively. Thus, the overall system efficiency is about 35% which is considerably low compared to batteries. However, the battery self-discharge makes it unsuitable for long storage periods.

In this study, the model of the electrolyser prototype proposed by Agbli et al. [Agbl 11a] (type staXX7 of H-TEC, with an active area of 16 cm² and a membrane thickness of 130 μm) has been resized to fit the electrolyser under consideration (59 kW, 300A). Experimentally [Chre 09], the voltage has been imposed and the current has been obtained.

3.3.2. ENERGETIC MACROSCOPIC REPRESENTATION FOR PEM ELS

The EMR blocks of both PV module and PEM ELS are respectively depicted in Figs. 3.19–3.20 [Hohm 03], [Boss 07]. The two models and their equations are previously comprehensively explained in chapter 2. Radiometric field contains the sun as the energy source and the PV unit. A part of the solar radiation (G) was transferred into energy received at the PV surface represented by I_{PV} . The production of electrical energy is the result of coupling between the electric and radiometric fields. A part of the solar energy (R) is reflected from the PV surface towards the source. The DC/DC converter sub-model attenuates the current from I_{PV} to I_{ELS} to conveniently enter the electrolyser. Consequently, the voltage at electrolyser terminals V_{ELS} is estimated and thereafter amplified to properly entered the PV module.

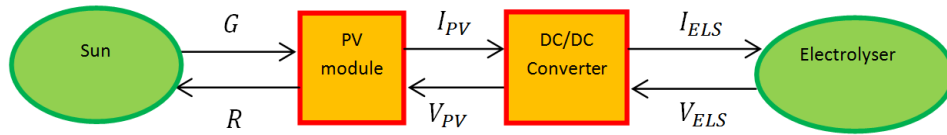


Fig. 3.19: EMR model of the PV panel.

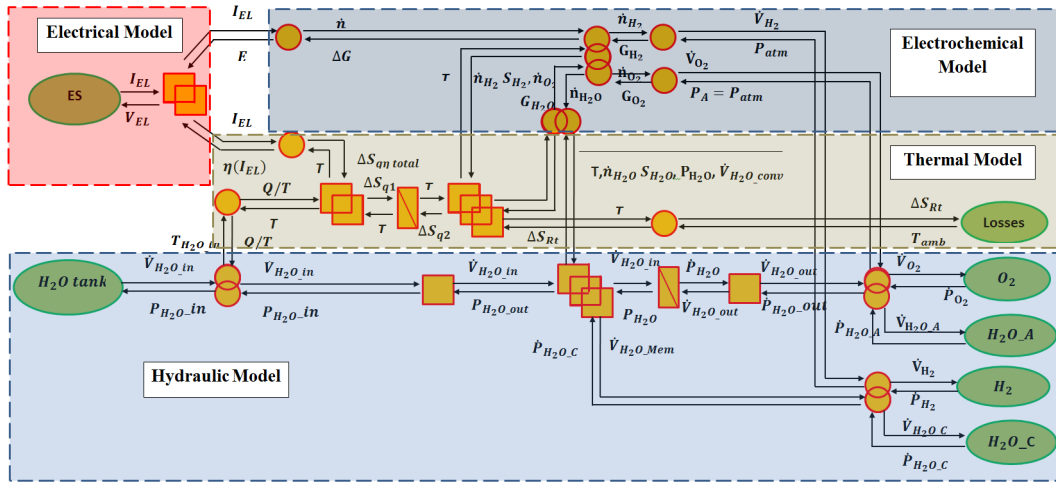


Fig. 3.20: EMR model of PEM electrolyser [Agbl 11a].

Fig. 3.20 shows a global PEM ELS model consisting of electrical, electrochemical, thermic and hydraulic sub-models. The electrical model is concerned with covering the Nernst energy and overcoming over-potential losses. Consequently, the electrochemical reactions can be taken place and the gas flow can be obtained at the electrochemical model output. The electrochemical phenomenon has then induced the temperature and the entropy flow in the thermal model is governed by electrical energy. In the hydraulic model, fluidic and thermal phenomena have taken place simultaneously as water temperature is transferred from the stack and then injected in the tank in order to allow temperature exchange with the surrounding environment. The details of each sub-model in addition to its corresponding equations and parameters are presented in Appendix (Table A.2).

3.3.3.FLC DESIGN

FLC is used for water temperature control as depicted in Fig. 3.21. Two inputs are considered, the first ΔQ_{H_2} is the difference between the hydrogen flow at the electrolyser output at two different temperatures (the measured temperature and the reference one $T_0=288K$). The second input $\partial\Delta Q_{H_2}$ is the difference between two values of ΔQ_{H_2} at two successive moments. The output $T_{H_2O}^{ref}$ (K) is the instantaneous reference water temperature controlled to obtain the hydrogen flow at the electrolyse output. The hydrogen flow at PEM ELS output is proportional to the tank water temperature. The greater the temperature, the more hydrogen flow will be. Therefore, inference rules of FLC are constructed to meet this objective. The inference rules for this FLC are shown in Table 3.5. Hereby, an increase in hydrogen flow is reached by controlling the water temperature emitted by PV panels and injected into PEM ELS and that can be realized by means of FLC.

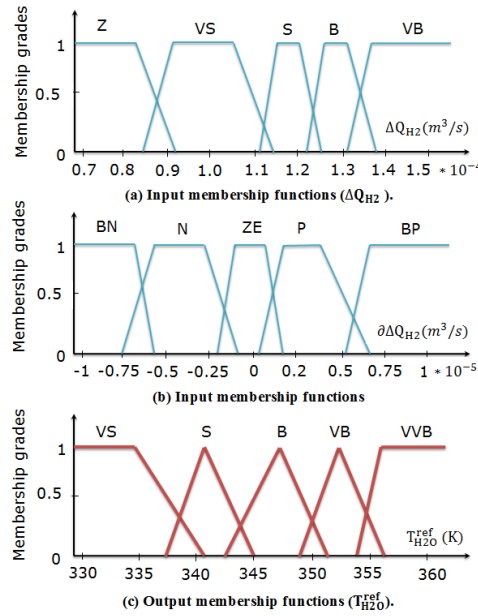


Fig. 3.21: Inputs and outputs membership functions.

Table 3.5: FLC inference rules*.

ΔQ_{H_2}	$\partial\Delta Q_{H_2}$				
	BN	N	ZE	P	BP
ZE	VS	VS	S	S	B
VS	VS	S	S	B	VB
S	S	S	B	VB	VB
B	S	B	VB	VB	VVB
VB	B	VB	VB	VVB	VVB

* ZE: Zero, VS: Very Small, S: Small, B: Big, VB: Very Big, VVB: Very Very Big, BN: Big Negative, N: Negative, P: Positive, BP: Big Positive.

3.3.4.SIMULATION RESULTS OF HYBRID PV-PEM ELS

To obtain different curves of $U=f(I)$ at different temperatures, the current has been injected and the voltage is obtained to represent the electrolyser characteristics.

The ELS voltage curves as a function of the current at different temperatures are given in Fig. 3.22.

At a fixed voltage of 200 V, the corresponding current value has been obtained for different temperature curves as shown in the polarization curves in Fig. 3.22.

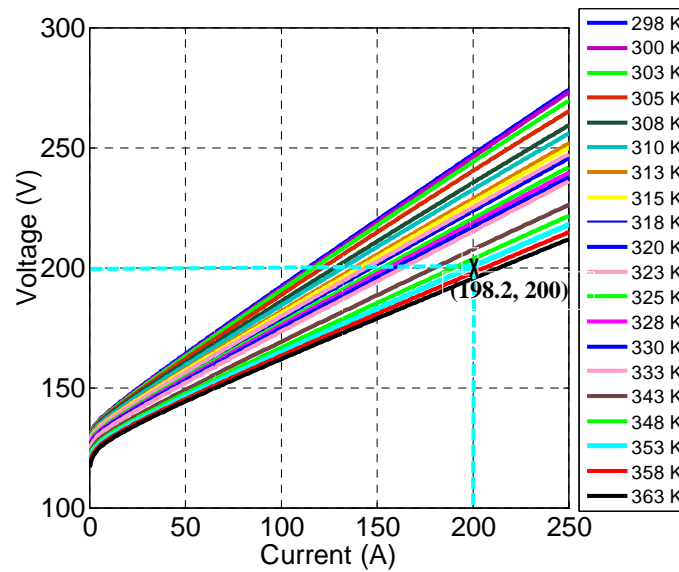


Fig. 3.22: Polarization curves for different water temperature.

The current values at different temperatures are listed in Table 3.6:

Table 3.6: The current values as a function of temperature.

T (K)	I (A)	T (K)	I (A)
298	115.3	323	150.4
300	116.6	325	152.7
303	117.2	328	156
305	121.4	330	159.5
308	127.9	333	163.5
310	132.1	343	179.9
313	138.3	348	190.1
315	140.8	353	198.2
318	144.2	358	206.1
320	146.9	363	213.6

Lookup Table (LUT) uses an array of data to map input values to output values in order to approximate a mathematical function. The LUT has generated outputs that correspond to different inputs. If the inputs match the values of indices specified in breakpoint data sets, the block outputs will be the corresponding values. However, if the inputs fail to match index values in the breakpoint data sets, LUT estimates the output.

LUT has been tested and compared with linear curve fitting method for which $y = 1.5354x - 345.02$. In Fig. 3.23, the results have depicted that both LUT and curve fitting method have the same behaviour within the operating range. Otherwise, the LUT provides more accurate prediction outside the operating range because it fits a line between the first or last pair of breakpoints, depending if the input is less than the first or greater than the last breakpoint, respectively. This method returns an acceptable approximate point on that line corresponding to the input. Therefore, the LUT has been used to estimate the current values as a function of temperature as shown in Fig. 3.24.

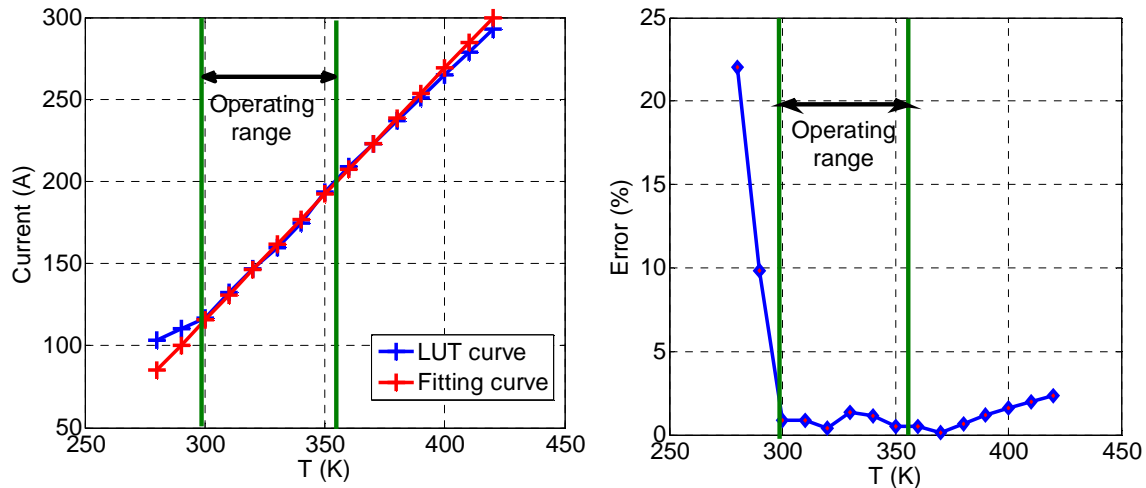


Fig. 3.23: Current-Temperature relation and the error based on LUT and curve fitting approaches.

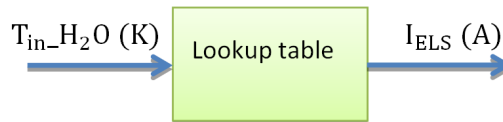


Fig. 3.24: LUT with water temperature input and current electrolyser output.

The changes in water temperature have led to significant changes in the electrolyser current. Thus, the hydrogen flow will vary. The hydrogen generation can be consequently maximized through a water temperature control. The hydrogen flow as function of the water temperature is depicted in Fig. 3.25.

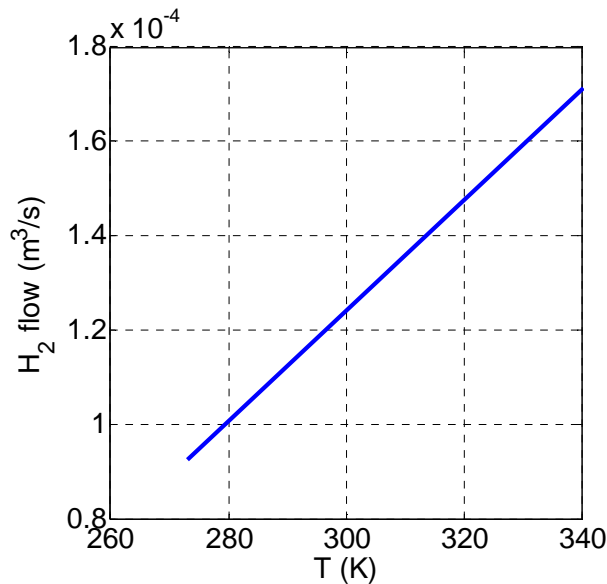


Fig. 3.25: H₂ flow versus water temperature.

As MPPT has been used to maximize the PV electric power output, Fig. 3.26 has demonstrated the uncontrolled operation of the hybrid PV-PEM ELS system. Considering PV-MPPT control, the H₂ flow at PEM ELS output is about $2.1 \times 10^{-4} \text{ m}^3/\text{s}$ at ambient water temperature 288 K. As the water temperature control using PI controller maximizes the electrolyser output H₂ flow, the instantaneous water temperature reference has been determined via FLC technique while considering the physical constraints. The hybrid PV-PEM ELS system has permitted to operate at a water temperature of 358 K. Due to the

physical constraints related to water vaporization and the PEM ELS configuration, the permissible operation time under this high temperature has been limited. Hence, the FLC technique has been used to periodically decrease the temperature reference to 336 K after a specific period as depicted in Fig. 3.27. During the simulation, the “cooling” period is supposed about one third of the overall cycle. Under this condition, the hydrogen behaviour of the hybrid PV-PEM ELS system is investigated in Fig. 3.26. The average flow of hydrogen production at the PEM ELS output is about $3.28 \times 10^{-4} \text{ m}^3/\text{s}$. Consequently, the increased amount of H_2 production using the proposed temperature control estimated as 56 % (referred to the uncontrolled case). This result has shown that the water temperature control is important to increase the H_2 flow at the PEM ELS output particularly when combined with the PV-MPPT.

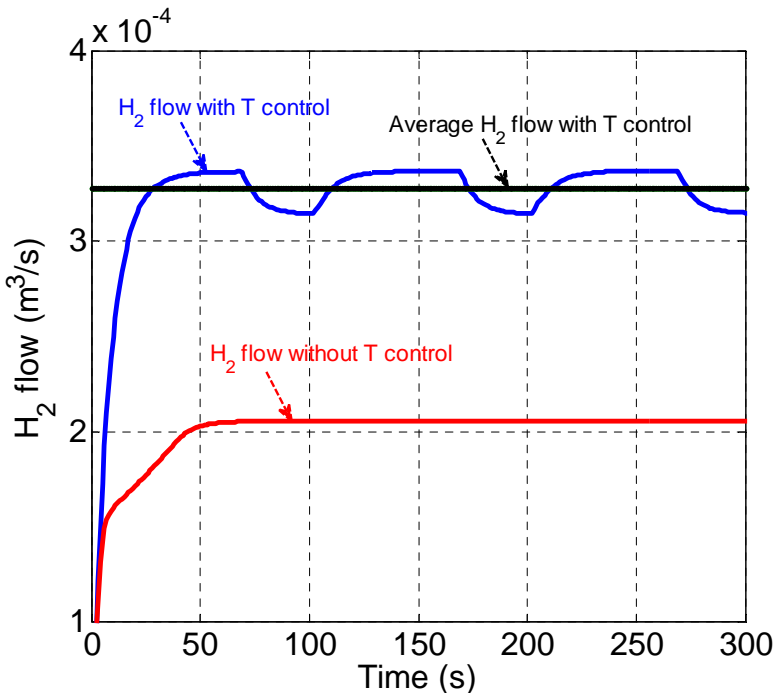


Fig. 3.26: Controlled and uncontrolled hydrogen flow at PEM electrolyser.

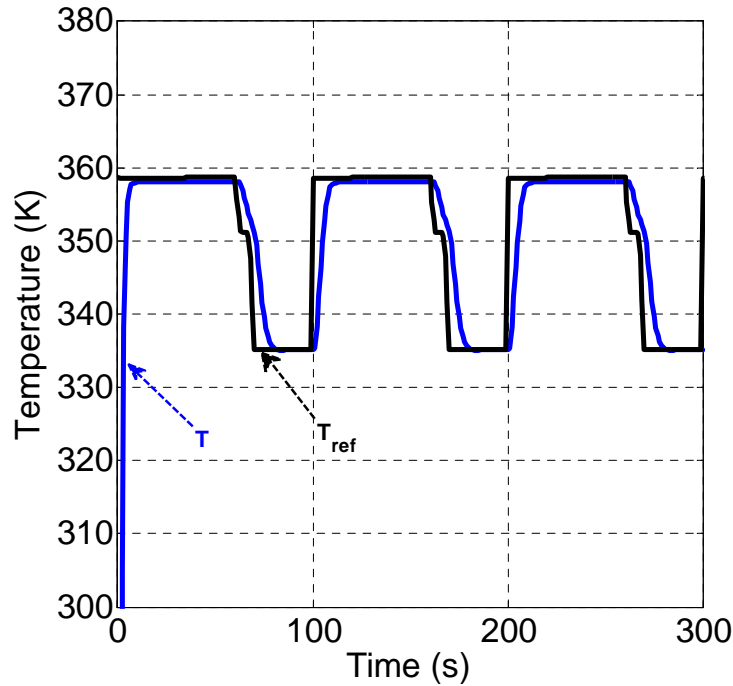


Fig. 3.27: FLC for instantaneous water temperature reference control.

3.4. CONCLUSION

In this chapter, the effect of shading, dust or fault conditions on the PV panels has been studied. Different solutions have been introduced. The MPPT method has been applied to maximize the PV output power. Then, PV panels have been sized, modelled and simulated to fit the experimental test bench of FCLAB laboratory. The impacts of both temperature and shading on the PV panel efficiency have been demonstrated. Then, the PV panel characteristics have been experimentally illustrated. Moreover, FL estimator has been used for identifying the shaded PV panel, estimating the shading percentage and deciding the connection/disconnection of series/parallel PV panels reconfiguration coupling to minimize the total power losses. This relatively simple and cheap method does not request any additional MPPT controllers or sensors. Indeed, it is sufficient to use controlled switches and diodes. This new online reconfiguration has the possibility to be employed to n PV panels ($n \geq 4$). Experimental setup has been built and the proposed solution has been successfully validated.

After overcoming the shading problem, the PV panels have been adapted to provide the PEM ELS with the requested energy. An enhancement of the hybrid PV-PEM ELS system efficiency using the FLC combined with PI control using PV-MPPT has been suggested. The FLC has been developed in order to instantaneously control the water temperature at specific reference values. The PI control has been considered to govern water temperature to its instantaneous optimal value. Moreover, the undesirable temperature surplus of the PV panel can be reused in the hydrogen flow rise in PEM ELS. The hybrid PV-PEM ELS system behaviour has been studied considering the temperature rise from 298 K to 363 K. Using EMR modelling of MATLABTM, simulation results have illustrated that the increase of water temperature at the entrance of the PEM ELS tank leads to considerable rise in the hydrogen flow amount. Therefore, the overall system efficiency has been significantly enhanced.

4. ENERGY MANAGEMENT OF MULTI-SOURCE SYSTEM

4.1. INTRODUCTION

The production of energy is becoming increasingly decentralized. Promoting decentralized energy helps in reconciling the different forms of energy, creating synergies between different energy systems, abolishing the borders between supply and demand. Accordingly, small and medium power producers could use renewable sources of energy for entering the market [Salm 10] through new applications such as: home and office feeding, electric vehicle charging, and energy marketing accompanied with energy fluctuations in power grids and stability problems. The smoothing is the solution of power fluctuations by storing the energy during periods of oversupply and restoring it to the grid during peak load hours [Mash 09] [Mahm 03] [Bach 15].

Therefore, electrical systems are becoming more often powered by hybridized power source (solar panels, WTs ...etc.) connected with auxiliary storage systems [Haes 14]. This is especially true for partially or fully autonomous multi-sources systems.

The energy management is achieved by using one of these strategies [Rigo 13] [Rigo 14a] [Rigo 14b]:

- a. Dynamic programming: is classified as an exact method for solving scheduling problems (global optimization in general). It combines and stores the results of the solution in a matrix that has the same dimensions of the domain of validity [Sing 11];
- b. Adaptive equivalent consumption minimization strategy [Geng 11]: is a control strategy based on the minimization of the equivalent consumption (offline optimization strategy);
- c. Optimal control [Orne 13]: is widely used in conjunction with the principle of Bellman and/or maximum principle of Pontryagin, classified as effective tools for solving global optimization problems.
- d. FL: an AI tool used for energy optimization [Caux 10]. Its difficulty is mainly due to the definition the position of the membership functions which are often defined in non-optimized manner.
- e. Artificial Neural Networks (ANN): an ANN is used for determining the optimal solution of energy storage/consumption decision [Zade 65].

The ANN approach can be described as a mathematical model that reproduces the structure and function of the human biological neuron system. Most mathematical models of NN use learning algorithms. The most popular and effective one is the learning by back propagation algorithm. Typical applications of NN are classification, pattern recognition, input-output and curve fitting, clustering and dynamic time series. These applications are generally non-linear tasks. In power systems, the detection and localization of disruption of power quality [Weil 09] [Liao 10] and the prediction of short-term load [Chog 10] have been employed using NN which is a real-time application. This is an important criterion in instantaneous energy management studies.

In this chapter, a hybrid system including WTs of 800 kW, GMT of 100 kW, PV panels of 63 kW, FCs of 80 kW and PEM ELS of 80 kW has been presented. The aim of this hybridization is to build a reliable system, which is able to supply the load and having the ability to store the excess energy in hydrogen form.

The chapter is organized as: first, the sizing of different multi-source components will be presented. The objective of system sizing is to find out each sub-system dimensions. The strategy of the adopted energy management will be discussed. Then, the energy management

study using NN will be detailed. The simulation results will be introduced and analysed. In addition, the energy management using FL will be presented and comprehensively compared with NN results. An economic study will be carried out to clarify the effectiveness of the proposed energy management strategies. Finally, the conclusion will be shown.

The system sizing comprises not only the RESs but also the BKUSs to overcome the energy shortage during peak loads [Belf 07]. WTs and PVs have been selected to represent the principal sources. During energy shortage, peak load can be fed by RESs and BKUSs such as GMT and FCs simultaneously to conveniently cope with the load dynamic changes. ESS has been considered to store the energy in hydrogen form and restore it when needed. ESS is composed of PEM ELS, tank and FCs as depicted in Fig. 4.1.

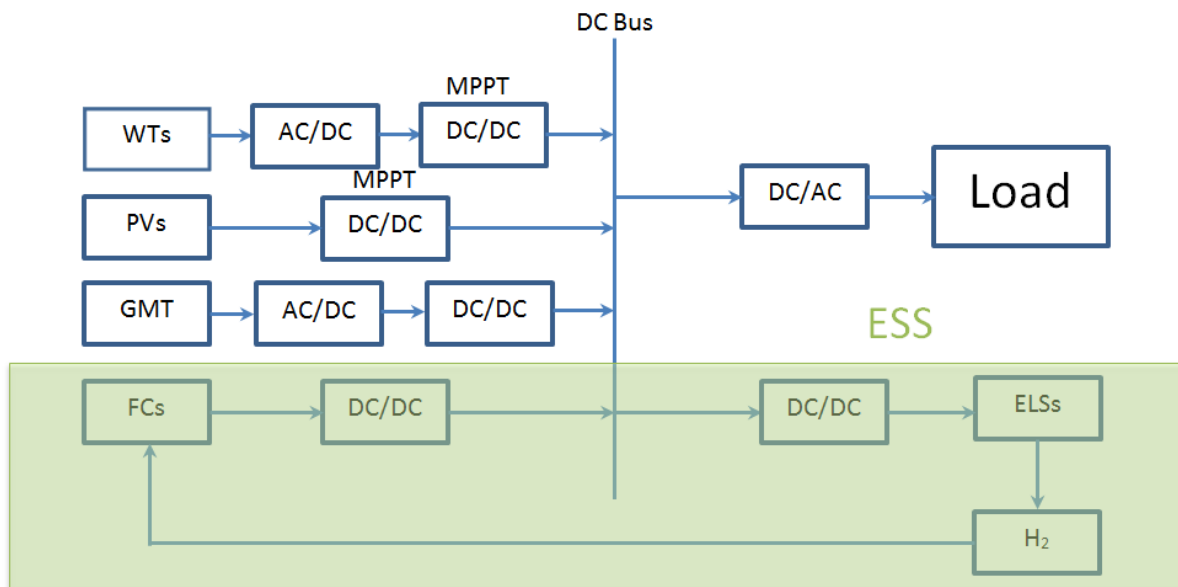


Fig. 4.1: Multi-source system under study.

4.2. SYSTEM SIZING

4.2.1. GAS MICRO-TURBINE SIZING

GMTs are small gas turbines that operate based on the Brayton cycle thermodynamic process [Gold 03]. In this cycle, the inlet air is pressurized in a compressor, to which fuel has been mixed in the combustor and burned. This heated combustion gas is expanded in the turbine section producing rotating mechanical power to drive the compressor and electric generator, mounted on the same shaft. Utilizing a recuperator, or heat exchanger, the overall efficiency of the GMT is 33 to 37%. Without the recuperator, the efficiency is significantly reduced to 15 – 17% [Guda 06]. Depending on the GMT output capacity, the range of rotational speeds varies from 50,000 to 120,000 rpm. Such a high operational frequency must be rectified to DC and inverted to 50 or 60 Hz [Glov 08]. Due to the simple single GMT shaft design without necessity of gearboxes, lubricants, coolants, or pumps, GMTs have simpler installation, higher reliability, reduced noise and vibration, lower maintenance requirements, lower emissions, and continuous combustion [Guda 06].

GMT integration into micro-grids is important because of its lower electricity generation cost and higher efficiency compared to conventional plants. The advantages of GMT are not only financial, but the following merits should be considered: (i) low capacity cost; (ii) possible: pre-packaged, relatively maintenance free, silent; (iii) the wide application range; (iv) low gas

prices; (v) high efficiency (if cogeneration is used); (vi) the reduced impact on the environment.

The considered GMT model of 100 kW has been limited to the study of slow dynamics [Kuma 12]. Fast dynamics related to starting and stopping have not been studied so that the model has been represented only for quasi static conditions.

4.2.2.PV SIZING

The solar module is an association of cells in series n_{cells} with cells in parallel n_{cellp} as shown in Fig. 4.2 [Site 08]. Solar cells are generally very small, and each one may only be capable of generating few watts of electricity. Therefore, the cells have been typically combined into modules of about 40 cells; the modules have been in turn assembled into PV arrays up to several meters on a side as depicted in Fig. 4.2. These *flat-plate* PV arrays can be mounted at a fixed angle facing south of Belfort city in France, or mounted on a tracking device that follows the sun to capture more sunlight. For utility-scale electricity generating applications, hundreds of arrays have been interconnected to form a single large system.

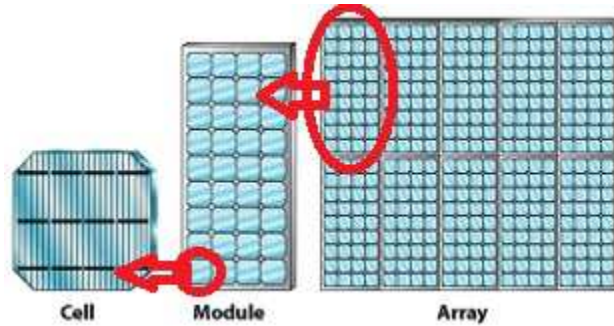


Fig. 4.2: Graphical illustration of cell/module/array photovoltaic.

Given the scale effect, move from PV module parameters “ m ” to PV array parameters “ a ” and vice versa can be done through:

$$I_{pha} = n_{mP} I_{phm} \quad (4.1)$$

$$I_{0a} = n_{mP} I_{0m} \quad (4.2)$$

$$R_{Sa} = \frac{n_{mS}}{n_{mP}} R_{Sm} \quad (4.3)$$

$$R_{Pa} = \frac{n_{mP}}{n_{mS}} R_{Pm} \quad (4.4)$$

$$n_{Sa} = n_{cells} n_{mS} \quad (4.5)$$

$$n_{Pa} = n_{cells} n_{mP} \quad (4.6)$$

The PV model under study allows calculating the PV panel current I_{PVm} and voltage V_{PVm} that include the effects of irradiation level and panel temperature on the output power as follows:

$$I_{PVm} = I_{phm} - I_{0m} \left[\exp \left(\frac{V_{PVm} + I_{PVm} \cdot R_{Sm}}{n \cdot V_T} \right) - 1 \right] - \frac{V_{PVm} + I_{PVm} \cdot R_{Sm}}{R_{Shm}} \quad (4.7)$$

$$I_{PVa} = I_{pha} - I_{0a} \left[\exp \left(\frac{V_{PVa} + I_{PVa} \cdot R_{Sa}}{n \cdot V_T} \right) - 1 \right] - \frac{V_{PVa} + I_{PVa} \cdot R_{Sa}}{R_{Sha}} \quad (4.8)$$

The parameter that mostly affects the relative size of the inverter and the PV array is the efficiency curve of the chosen inverter. For similar PV module technology in the same site, the PV array must be oversized by 30% or undersized 30% compared to the rated capacity of the selected inverter.

The influence of the PV module technology on its sizing is important for amorphous PV modules. Its optimal series resistance $R_{s,opt}$ is always smaller for such technology compared to other PV modules. Consequently, the inverter under-sizing can result in a dramatic decrease of the PV system efficiency more than for the other three PV module types. Therefore, the sizing of a grid-connected PV system using amorphous silicon PV modules must be realized with more attention.

The effect of the inclination on the PV system optimal ratio is low. However, the inclination influence on the PV system performances is more significant for a PV system with an undersized inverter than with an oversized one. The PV module inclination has also an impact on the monthly mean value of its output energy (for example) and efficiency. The site influence, where solar radiation and ambient temperature vary a lot from one site to other, has some effects. In the study, the invested PV array has a maximal output power of 63 kW.

4.2.3. WTs SIZING

WT has the following components : (1) Foundation, (2) electric grid connection, (3) tower, (4) access ladder, (5) wind orientation control, (6) nacelle, (7) generator, (8) anemometer, (9) electric or mechanical brake, (10) gearbox, (11) rotor blade, (12) blade pitch control, (13) rotor hub as depicted in Fig. 4.3.



Fig. 4.3: WT components.

WT installation consists of necessary systems needed to capture the wind's energy, point the turbine into the wind, convert mechanical rotation into electrical power, and other systems to start, stop, and control the turbine.

In the system under study a WT nacelle, composed of turbine of 800 kW, and nominal rotation speed of blades 25 r.p.m. which charges a group of batteries has been used. The group of induction machine (IM) and the controlled static converter allow applying the control on the power conversion from mechanical form into electrical one. The induction generator allows producing alternative electrical voltage and current, the inverter transforms these alternative variables into direct ones for charging the batteries, as shown in Fig. 4.4.

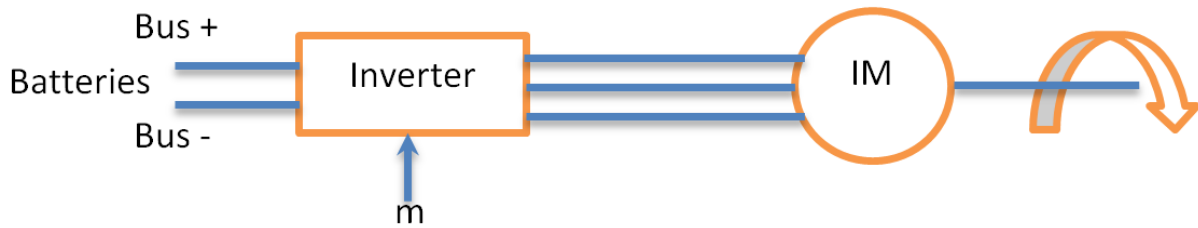


Fig. 4.4: Batteries charging from IM.

WT can produce the electrical power at specific wind speed. The relationship between the wind and the produced power has been presented by the WT power curve that represents its power output at different wind speeds. Normally, the WTs are designed to start at wind speeds of 3 to 5 m/s and to stop automatically when the wind speed exceeds 25 m/s in order to avoid damages to WTs as illustrated in Fig. 4.5.

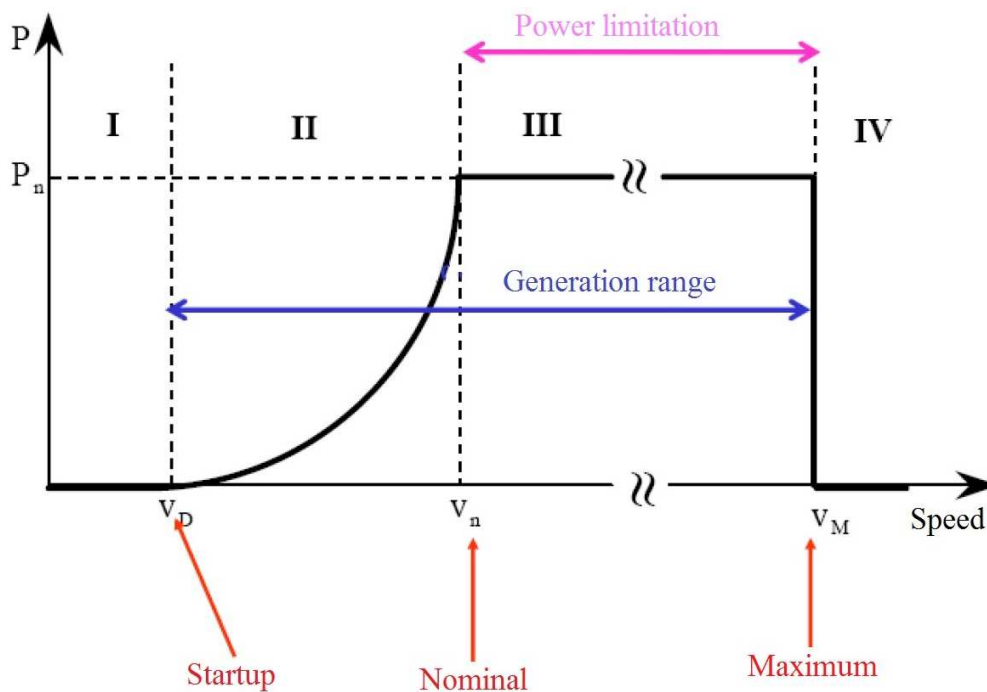


Fig. 4.5: WT operation curve.

WTs are designed to give their maximum performance at wind speed 15 m/s and to produce their maximum power at specific wind speed called survival speed. In addition, all WTs have been designed with power control.

There are three main security control methods in modern WTs:

- Variable pitch system: the principle consists of guiding the WT blades to reduce wind resistance and therefore the power for high wind speeds. Such process, used for power superior 100 kW, is very effective but expensive [Zhan 14b];
- Aerodynamic stall system: the blade profile has been designed in such a way that beyond a certain wind speed, the turbulence presented on the blades has natural drop consequence in the WT power. It is a simple method and reliable but has a poor performance at high wind speeds [Poli 14];

- Active stall system: this system is a combination of the both previous. Generally, systems are mainly used for high power WT's above 1MW. At high wind speeds, instead of reducing the angle of the blades to lower the wind resistance (if the system pitch), the angle is increased to cause the stall of the blades as in Fig. 4.6 [Li 15].

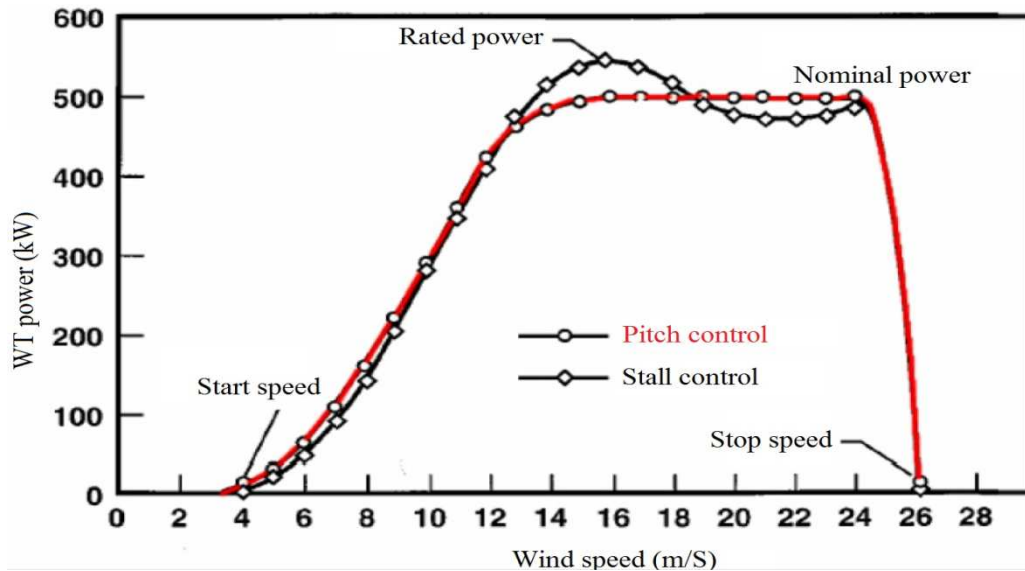


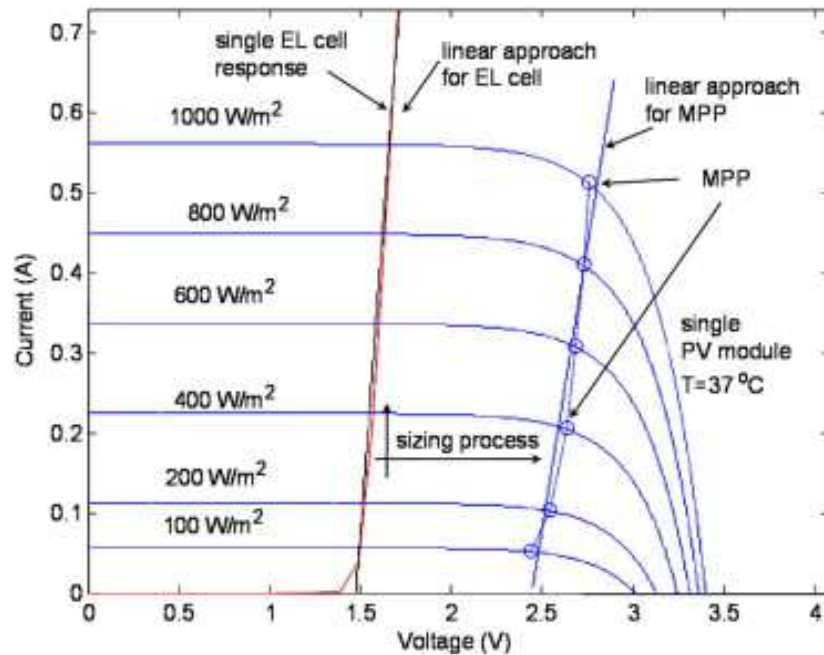
Fig. 4.6: Pitch control and stall control in WT [Blun 11].

4.2.4. PEM ELS SIZING

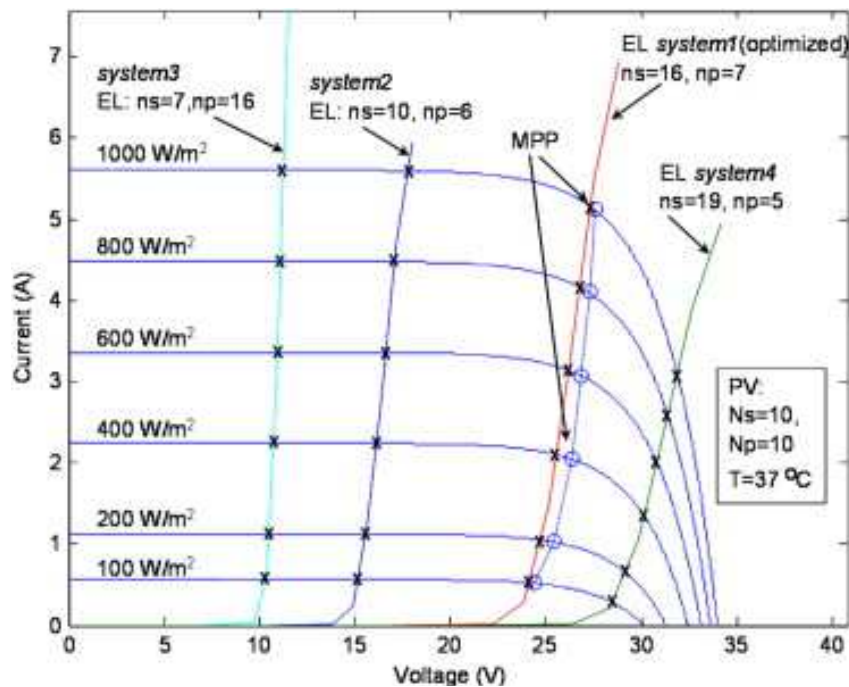
The electrolyser in the system under study is staXX7 of H-TEC with an active area of 16 cm² and a membrane thickness of 130 μm. Tests have been performed on this small electrolyser. Then, the model was extrapolated (80 kW) for realistic parameter values. In the experimental tests, with uncontrolled temperature, the voltage has been imposed and the current has been measured.

The PEM ELS is provided with necessary energy using four different sources. WT's and PV's, as RES's, are considered such as primary sources. However, PEM ELS has a problem of mismatching of the intermittent nature of these primary sources.

One of the important issues in PV-PEM ELS hydrogen generation systems is the maximum power transfer problem between two devices at different irradiance conditions. In direct connected systems, there is usually a mismatch between input PEM ELS's I-V characteristic and output PV's MPPT characteristic. To overcome this problem, PV-ELS systems are usually supported with additional MPPT power electronic control tracker [Zhou 08] [Garc 08] [Cont 07] [Sopi 09]. To operate at the MPPT, the MPPT tracker device sets optimum impedance harmony between the PV and the ELS system in response to irradiance variations. However, this causes additional cost and complexity. Both PV and ELS are modular devices, consisting of a number of smaller units-cells, which can be connected in series and/or in parallel. With appropriate sizing optimization approaches for both PV and ELS, it is possible to directly connect these two systems [Clar 09] [Paul 08] [Gibs 08]. Fig. 4.7(a) presents the I-V characteristics for a single PEM ELS cell and single PV module and the problem of mismatching between them. Under given operating temperature and specified number of PV modules connected in parallel and in series, an optimal ELS size can be obtained with specific number of cells in parallel and in series as depicted in Fig. 4.7(b).



(a) Single PEM electrolyser cell and single PV module



(b) Various ELS systems for the constant PV system.

Fig. 4.7: I-V characteristics of PEM electrolyser and PV module [Alta 11].

4.2.5.FC SIZING

Test has carried out for 20-cell PEMFC stack with 100 cm^2 area of each cell, membrane thickness is $25\mu\text{m}$ and the nominal power is about 400W. The operating conditions of the FC stack are shown in Table A.1 [Bech 10]. Many physical parameters involved in the stack can be measured such as: (i) the inlet/exit measured magnitude are flow rates cathode and anode channel; (ii) inlet/exit air pressures of cathode and anode; (iii) average temperature; (iv) humidity of FC; (v) the stack voltage and current which is traditionally considered as a measurable disturbance to the system. The equivalent electrical circuit model is based on the modelling of anode, membrane and cathode. Moreover, the voltage drops: activation, concentration and ohmic are current-dependent. The hydrogen pressure has been calculated as

an intermediate step for calculating the thermodynamic voltage estimated by Nernst equation. The stack voltage is also the difference between thermodynamic and losses voltages.

During these tests, different current steps are applied to the FC stack to exhibit the steady state and transient behaviour. Firstly, the FC is turned on with a power of about 400W with a load that consumes a current of approximately 30 A. The operating conditions for the FC stack are shown in Table 4.1 [Bech 10].

Table 4.1: PEMFC operation conditions [Bech 10].

Number of single cells	20
Operating temperature °C	20-65
Nominal temperature °C	55
Cell area cm ²	100
Operating pressure	From 1 to 1.5 bar
Differential pressure between anode and cathode compartments	Up to 0.6 bar
Inlet media	Pure hydrogen De-ionized cooling water

For the simulated FC model, it has an output power of 80 kW. So, an extrapolation of FC model has been applied for realistic parameters values as demonstrated in Fig. 4.8.

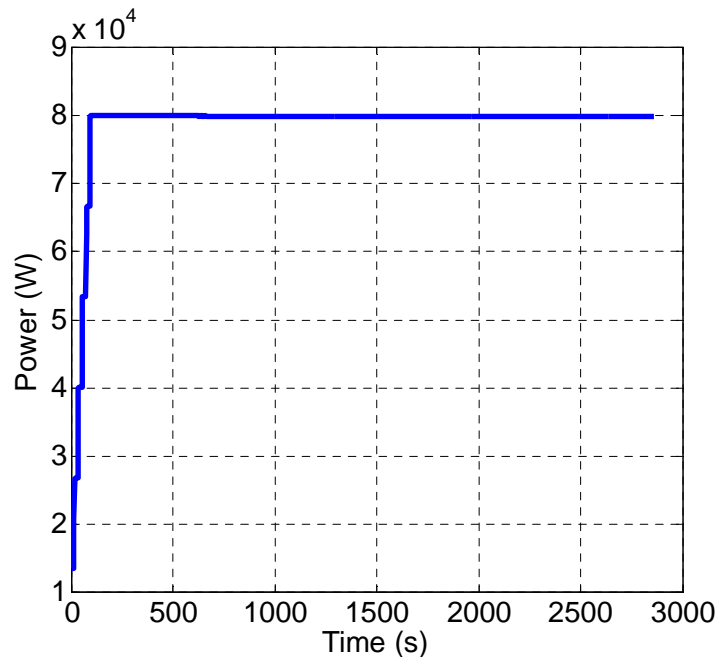


Fig. 4.8: Experimental FC output power.

4.2.6.ENERGY STORAGE SIZING

The electrolyser in the FC/ELS storage system has been used as a part of dump load. When there is excess wind or solar generation, the electrolyser turns on to begin producing hydrogen, which is delivered to the hydrogen storage tanks. If the H_2 storage tanks become full, the excess power will be diverted to another dump load. When there is a deficit in power generation, the FC will begin to produce energy for the load using hydrogen from the reservoir tanks [Shak 05].

The GMT doesn't participate in storage system. It works as BKU generation unit to support the RESs for supplying the peak demands via specific energy management strategy.

The transferred energy from the ELS has been stored in a tank via the hydrogen vector. The hydrogen has been calculated directly at Low Heat Value (LHV). The power requested to obtain one kilogramme of hydrogen is 33.3kWh/kg at LHV. Such power can be calculated from the relationship between the production rates per hour, the number of electrolyser cells η_C and the electrolyser stack current I_{ELS} [Gand 07] [Kell 08]:

$$H_2 \left(\frac{kg}{h} \right) = 7.5816 \frac{\eta_C I_{ELS}}{ZF} \quad (4.9)$$

where Z is the number of electrons per transferred mole of H_2O ($Z=2 e^-$), F is the Faraday constant ($F= 96485 C/mol$), η_C the number of connected cells in series.

The ELS current can be calculated from:

$$I_{ELS} = i \times A_{EL} \quad (4.10)$$

where A_{ELS} is the active area of electrodes which is typically about 100 cm² for the PEM ELS. For 80 kW PEM ELS an extrapolation of model has been applied for realistic parameters values.

4.3. ENERGY MANAGEMENT STRATEGY

The energy management for 24 hours is illustrated in the flowchart of Fig. 4.9. The principle of energy management related to the power availability of RESs outputs and the daily load. Therefore, the difference between the total power and the load power has been checked. If the difference is more than zero, the excess will be stored as hydrogen in hydrogen tanks. Otherwise, the GMT power will be entered in service as an additional source to cover the load.

The new sum of power generation of WT, PV and GMT should cover the load. If the difference between the sum of their powers and the load is positive, the excess power will be stored in the hydrogen tank as in the previous step. Otherwise, the FC will be used for meeting the requested demand. The total power generation from the WT, PV, GMT and FC sources should cover the load. The power that exceeds the load will be stored in hydrogen tanks to be used in the periods of high-peak loads.

This energy management methodology has been applied during the system operation. Consequently, the store/restore process of the hydrogen tanks has been performed.

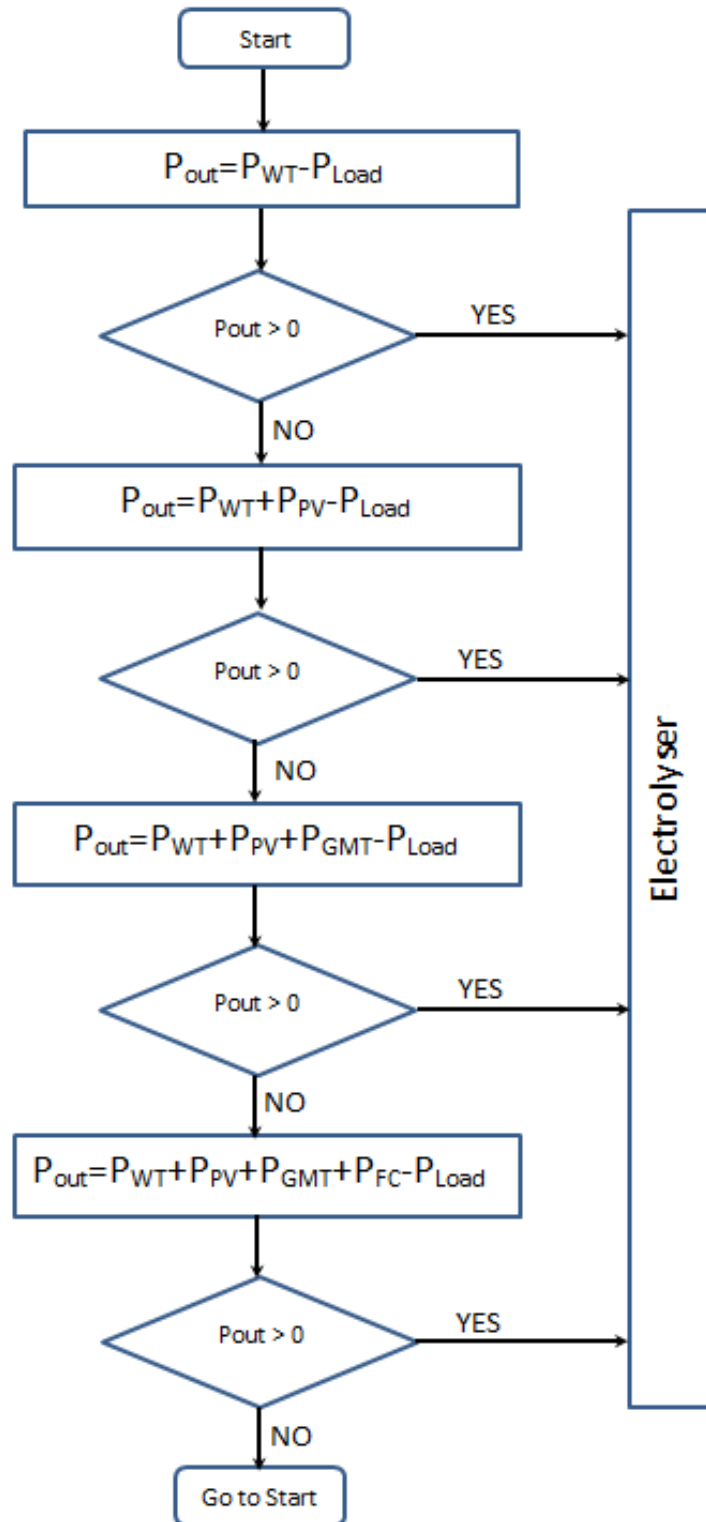


Fig. 4.9: Flowchart for energy storage methodology and energy management strategy.

The WT, PV, GMT and FC hybrid system is an alternative of traditional energy system that in this study can be used for stand-alone power systems applications. WT and PV are the primary power sources of the system, and the FC–ELS combination has been used as BKUSs for long-term storage system. An overall energy management strategy has been designed to manage power flows for the proposed multi-source system and storage systems. Consequently, hybrid RESs of minimum power production price have been considered. In addition, the overall

hydrogen quantity at the end of one cycle of 24 hours of energy stored in/consumed from the hydrogen tank should equal to zero.

These sources and loads have been managed considering the hypothesis that an immediate start of different sources and according to the availability of sources such as:

Case 1: The WT and PVs power have been set to their maximum values. Therefore, if the load is less than 863 kW, the GMT and FCs will be temporary out of service. The power surplus will be stored such as hydrogen in the tanks using ELSs as depicted in Fig. 4.10(a).

Case 2: When the load becomes equal to the power produced from the WT and PV sources, both sources together will continue providing the load with the necessary energy. However, the storage of energy will be stopped and the ELS will be turned off as shown in Fig. 4.10(b).

Case 3: When the load becomes from 863 kW to 963 kW, the GMT will switch on to cover the power deficit. Therefore, the excess energy will be stored in the hydrogen tank as depicted in Fig. 4.10(c).

Case 4: If the load exceeds 963 kW, the FC will turn on and cover the load as illustrated in Fig. 4.10(d).

The role of FC–ELS combination in the four cases is to deliver/store energy when necessary. FC and ELS work alternatively. Obviously, the ELS works when energy storage is requested and FCs work when energy production is needed.

It has been supposed that the WT and PV give their maximum power. However, the power generation of both sources depends on the wind speed and sun irradiation respectively. Accordingly, an in–depth study at different variation of WTs and PVs powers will be done in the forthcoming research. Consequently, a NN and FLC models have been designed to ensure the energy management procedure and a comparison between them has been performed.

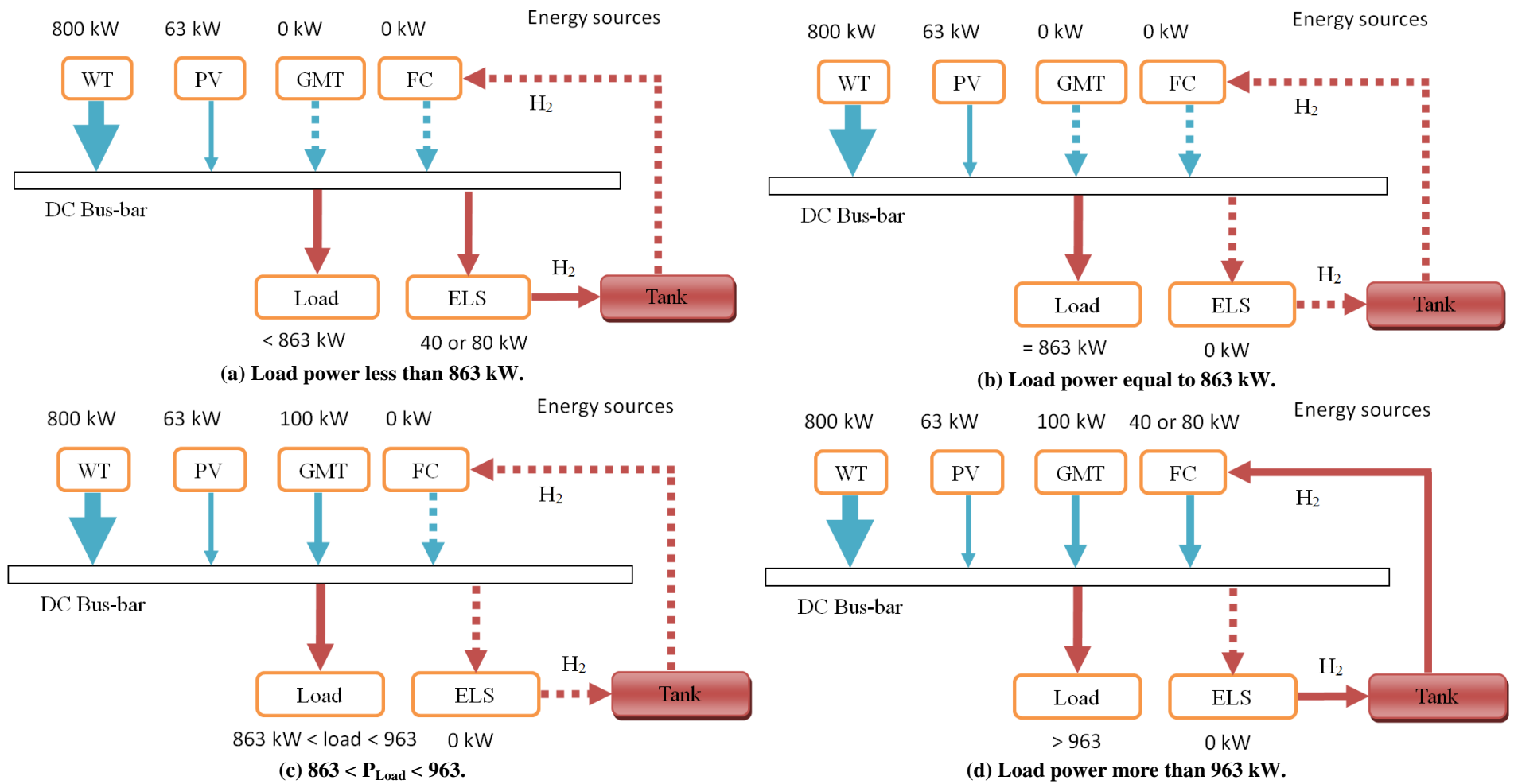


Fig. 4.10: Energy management strategy at different load power values.

4.4. ENERGY MANAGEMENT USING NEURAL NETWORKS

An ANN is a mathematical or computational model that has been inspired by the structure and/or the functional aspects of biological neural networks. A NN consists of an interconnected group of artificial neurons. It processes information using a connection approach to computation. ANN is almost an adaptive system that changes its structure based on external or internal information that flows through the network during the learning phase. A NN is typically defined by three types of parameters as depicted in Fig. 4.11 [Site 09]:

1. the interconnection pattern between different layers of neurons;
2. the learning process for updating the weights of the interconnections;
3. the activation function that converts a neuron's weighted input to its output activation.

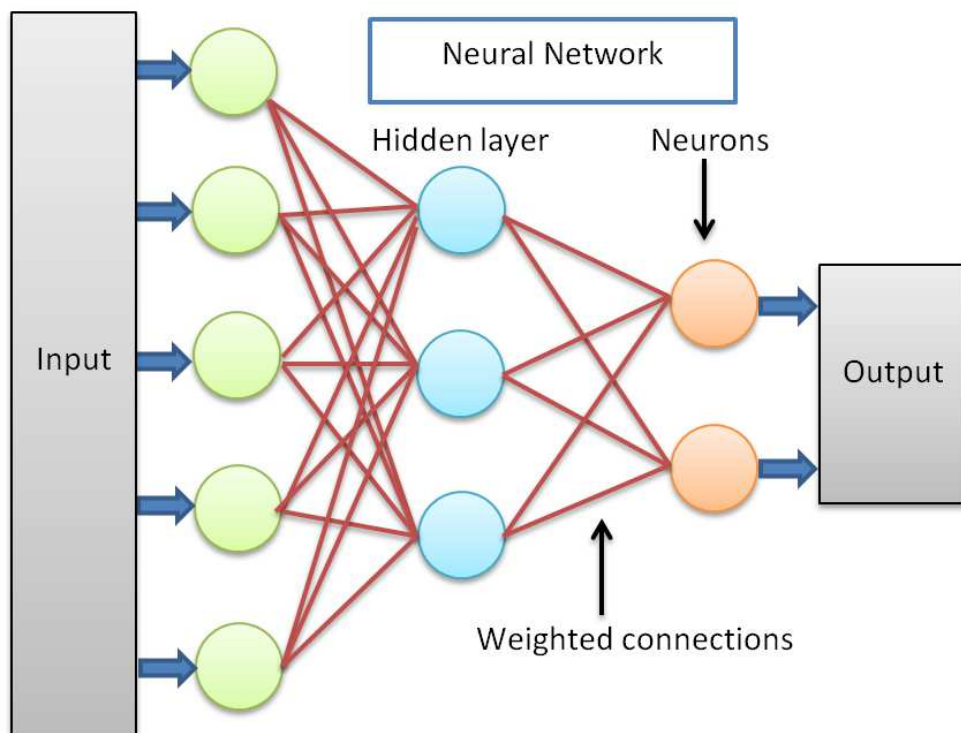


Fig. 4.11: NN general structure.

NN are appropriate at fitting functions and recognizing patterns. To define a fitting problem for the toolbox, a set of X input vectors as columns in a matrix has been arranged. Then, another set of Y target vectors (the correct output vectors for each of the input vectors) into a second matrix has been prepared. Both vector sets have been obtained from calculating the contribution of each traditional sources (GMT and FCs), and RESs (WT and PV) in presence of both wind speed and irradiation intermittency.

More neurons and/or layers require more computation, but they may allow the network to solve efficiently more complicated problems. Once the Network/Data Manager window is up and running, a network can be created, viewed, trained, simulated, and exported the final results to the workspace. Similarly, data can be imported from the workspace for using in the Graphical User Interface (GUI) [Site 09].

A two-layer feed-forward network with sigmoide hidden neurons and linear output neurons (fitnet), can fit multi-dimensional mapping problems arbitrarily well, given consistent data and enough neurons in its hidden layer. The network will be trained with Levenberg-Marquardt

back-propagation algorithm (trainlm), unless there is not enough memory, in which case scale conjugate gradient back propagation (trainscg) will be used.

Feed-forward networks often have one or more hidden layers of sigmoid neurons followed by an output layer of linear neurons as shown in Fig. 4.12 Multiple layers of neurons with nonlinear transfer functions allow the network to learn nonlinear relationships between input and output vectors. The linear output layer is most often used for function fitting (or nonlinear regression) problems [Site 09].

For multiple-layer networks, the layer number determines the superscript on the weight matrix. The appropriate notation is used in the two-layer tansig/purelin network. This network can be used as a general function approximator. It can approximate any function with a finite number of discontinuities arbitrarily well, given sufficient neurons in the hidden layer.

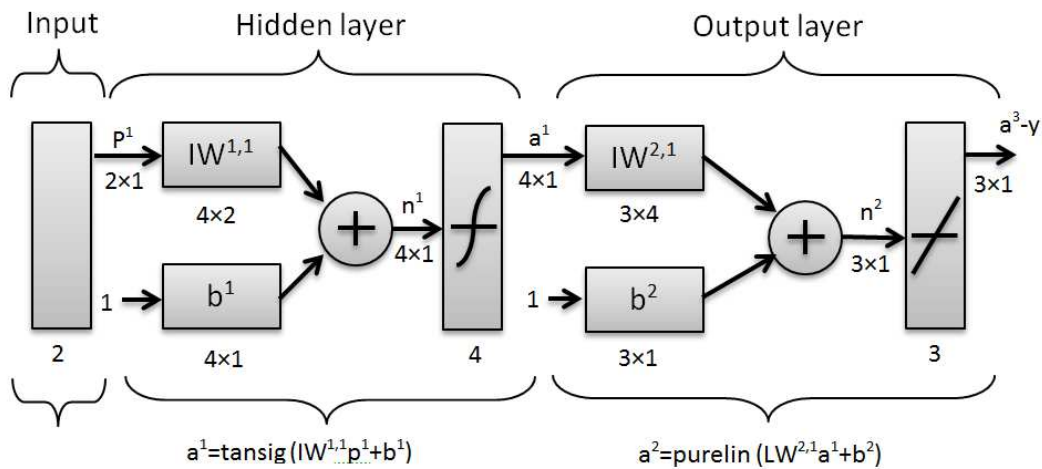


Fig. 4.12: Two layers feed-forward network for energy management.

In this study, (PV and WT) and (GMT and FC) are combined together and operate as main and BKU systems respectively. To conveniently employ the energy management strategy taking into account the intermittency of RESs and load variations alongside with the power generation price of each kind. NN methodology using Fitting tool in MatlabTM-Simulink has been proposed. This tool can fit the power participation of each source depending on sources power availability and load value.

For the system understudy, the input data of NN are the four power sources besides the load at the instant (t). The output data are the participation of the different sources at the instant (t+1) in the covering load depending on RESs contribution conditioned by the hydrogen level in the tank which should equals zero at the end of 24 hours cycle and the cost of energy production have to be at minimum level for the different sources. In addition, the electrolyser data is one part of the ELSs-H₂-FCs combination that is responsible of energy storage for the deficit power situation. Therefore, it has been added to the output data as illustrated in Fig. 4.13.

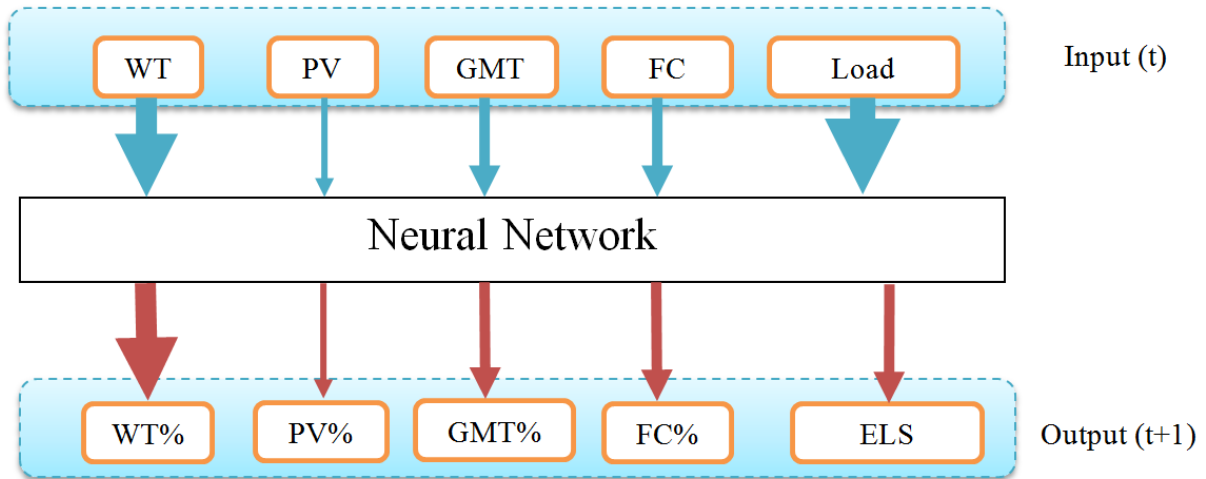


Fig. 4.13: NN inputs and outputs.

4.4.1. NN INPUTS

The power provided by the WTs and PVs for one day depending on the wind speed and the sun irradiance respectively have been demonstrated in Fig. 4.14. The other two sources, GMT and FCs, have provided their maximum power when connected. The load value injected in NN is based on the whole France load on the 15th, November 2012 and matched with the power requirement of a village in the region of Belfort city in France, with maximum load of 1 MW as shown in Fig. 4.15.

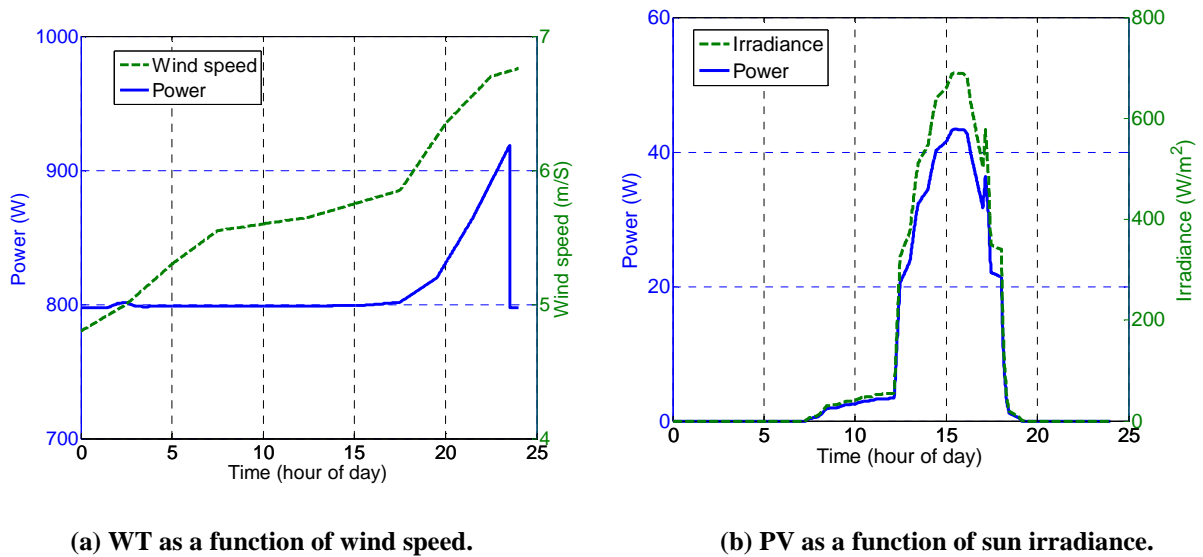


Fig. 4.14: Output power of RESs when MPPT is considered.

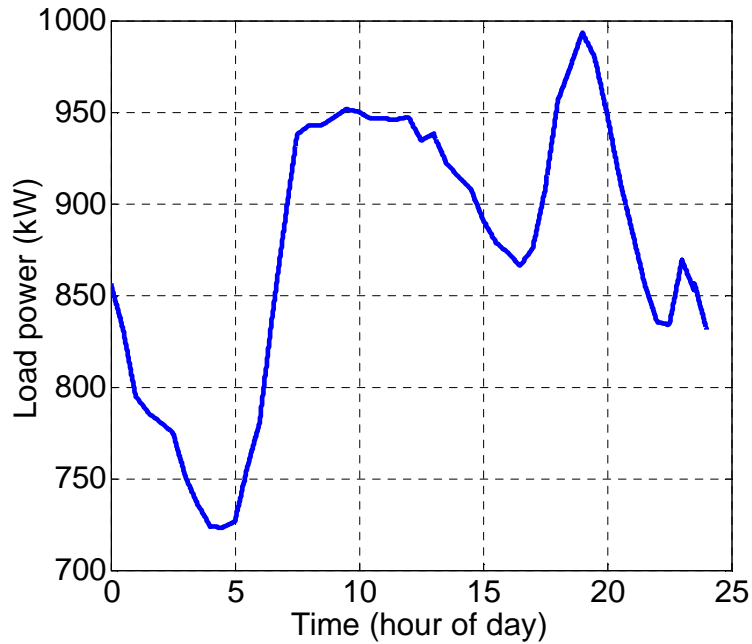


Fig. 4.15: The daily load of one village in region of Belfort.

4.4.2.NN TRAINING, VALIDATION AND TEST

Several points of inputs and outputs data for training, validation and test purposes are obtained by calculating both powers provided by different sources to the NN at the input and suggested power percentages of participation of each source. In NN, the input/output data are injected in the GUI NN. The samples are divided into:

- Training: 70 % of the total samples have been presented to the network during training, and the network has been adjusted according to the error.
- Validation: 15% of the total samples have been used to measure network generalization, and for halt training when generalization stops improving.
- Testing: 15% of total samples have been invested to provide an independent measure of network performance during and after training. It has no effect on the training process.

After injecting the data, the number on hidden neurons in the GUI fitting tool is 10 as depicted in Fig. 4.16.

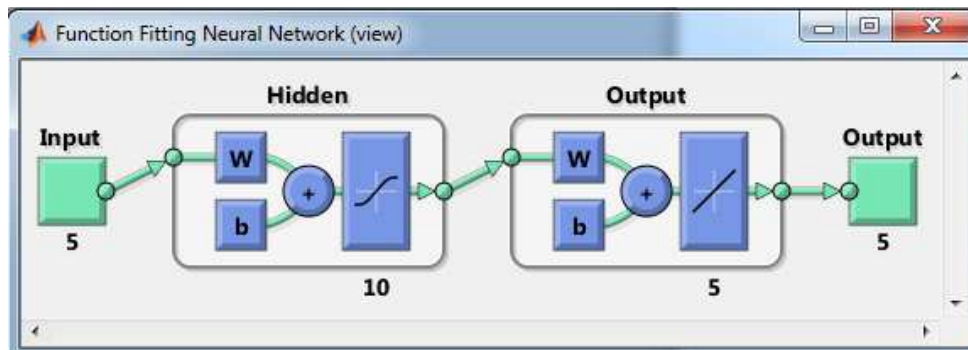


Fig. 4.16: NN GUI for system energy management.

The following regression curves in Fig. 4.17 show the results of the network outputs of the target training, validation and testing. For a perfect fit, the data should fall along a 45 degree

line, where the outputs of the network are equal to targets. The fit is good enough for all data sets, with the values of R (the percentage of data falling along a line 45 degrees) in each case 0.99.

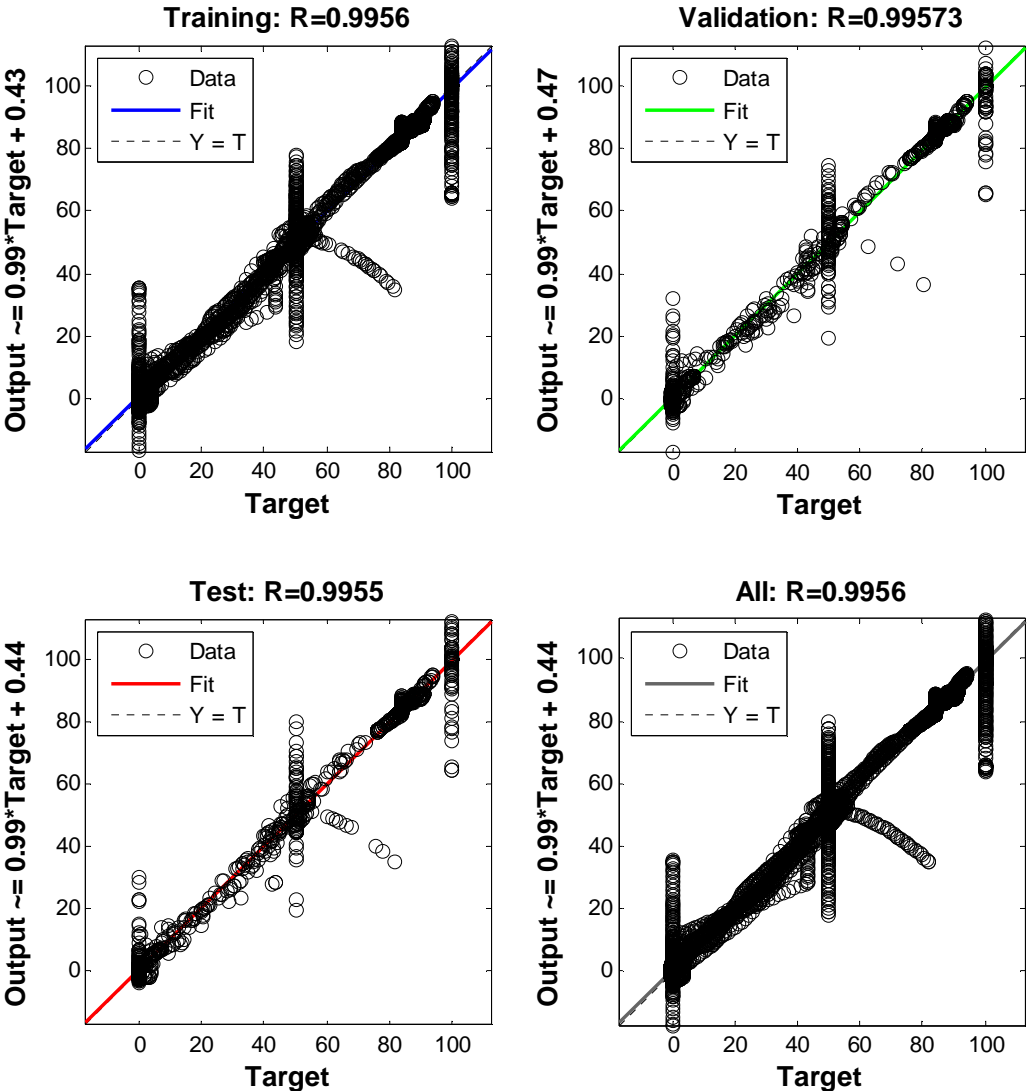


Fig. 4.17: Training, validation and test data fitting for a target.

4.4.3.NN OUTPUTS

After NN training, the percentage of participation of each power sources and the ELS for hydrogen storage are estimated at any time variant load condition as depicted in Fig. 4.18. Considering load variation and/or RESs intermittence, NN will propose the corresponding powers for the different sources taking into account the minimum use of GMT generation, FCs supply and hydrogen storage uses ELS, as shown in Fig. 4.18. Three points of different power sources curves and ELS curve have been chosen to be discussed in Fig. 4.18. Point A presents one instant when the summation of GMT, WT and ELS powers is about 757 kW considering the power negative sign of ELS. The summation of powers for the points B and C are 970 kW and 940 kW respectively. These points represent the total source power at a certain time on the curve presented in Fig. 4.19.

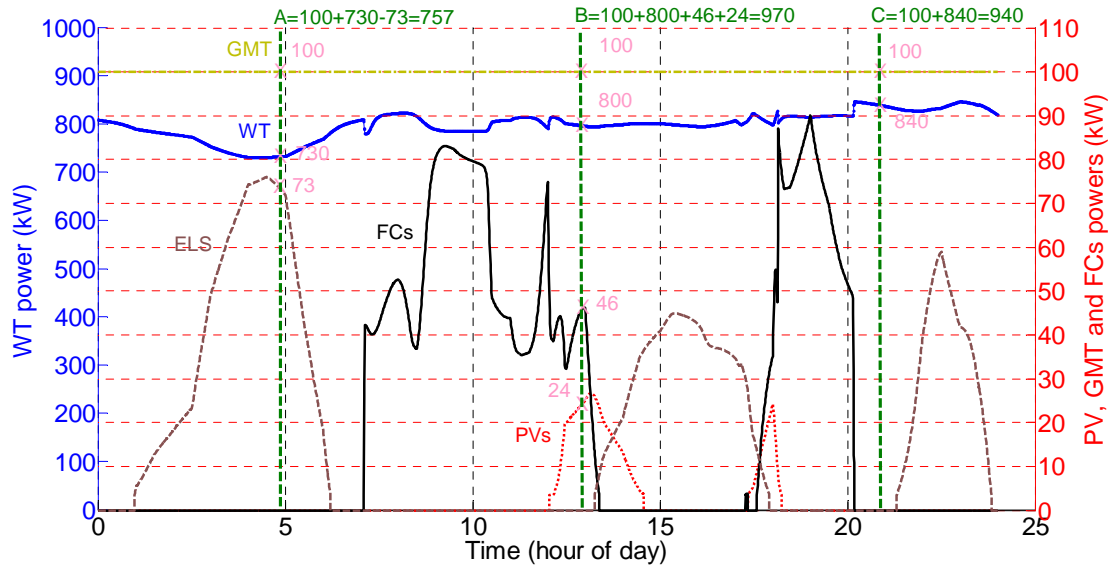


Fig. 4.18: Sources and ELS power for one cycle of 24 hours.

Accordingly, the sources together have a power output capable of providing the necessary power to the load as depicted in Fig. 4.19. This satisfactory result can be applied to any load for all source estimation.

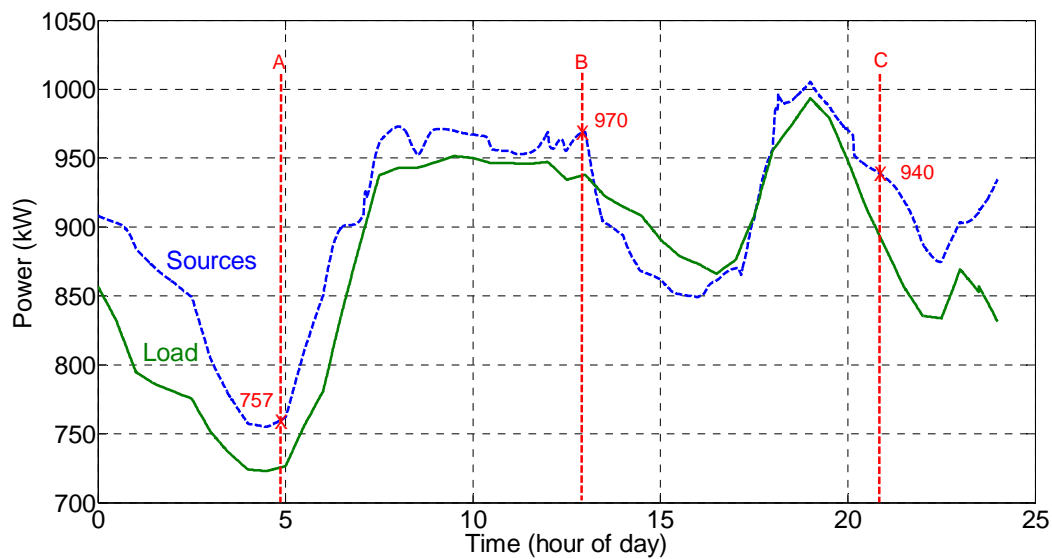


Fig. 4.19: Load tracking by the multi-source power generation.

4.5. ENERGY STORAGE SIMULATION RESULTS

Using NN, the energy generation/storage/consumption have been properly managed. Consequently, the storage system consists of the ELSs, hydrogen tank and FCs can be suitably used when requested. The role of ELS is to convert the power into hydrogen and store it in a tank if there is a surplus power. The task of FCs is totally the inverse of ELS. Obviously, it consumes the hydrogen stored in the tank to overcome the lack of power when the four sources are used together. The tank stores the hydrogen in a buffer stage to realize the objective of this study that is mainly the energy management of multi-source system with minimum cost.

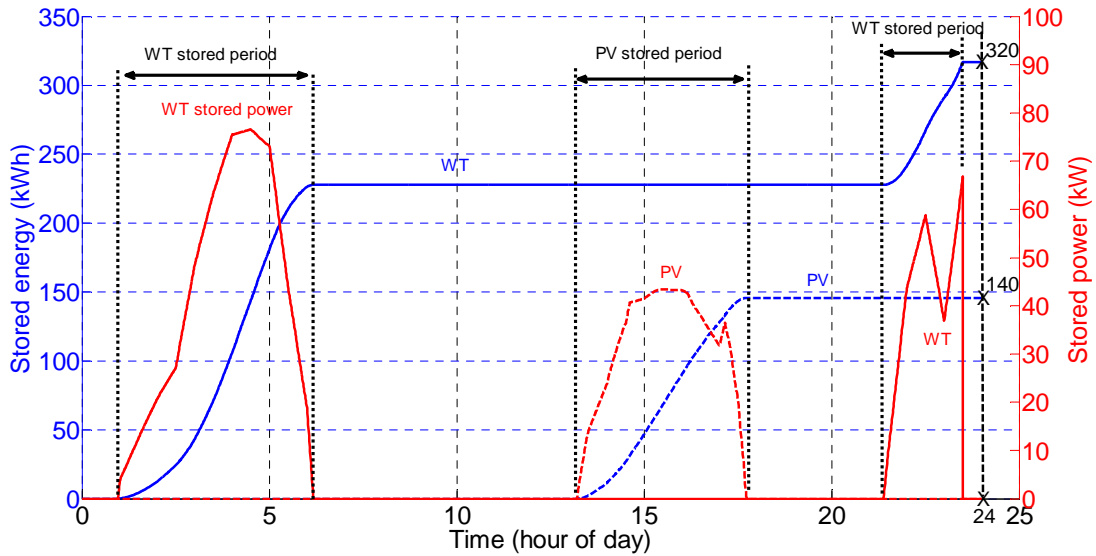


Fig. 4.20: Power and energy stored in the hydrogen tank from RESs.

The stored energy is totally produced by WT and PV sources at low level load values. The over produced energy in the HPS can be discussed through three periods. Two of them are concerned of WT power overproduction and the third one related to PV power source. These periods correspond to maximum wind speed during night and maximum irradiance during day as depicted in Fig. 4.20. The final value of stored energy at the end of 24 hours cycle is about 320 kWh from the WT and about 140 kWh from the PV. On the other side, the consumed energy from the hydrogen tank is supplied to the FCs at high level load value as shown in Fig. 4.21. Obviously, two periods of energy consumption can be observed. They have taken place at maximum load and their total value is about 460 kWh as depicted in Fig. 4.21.

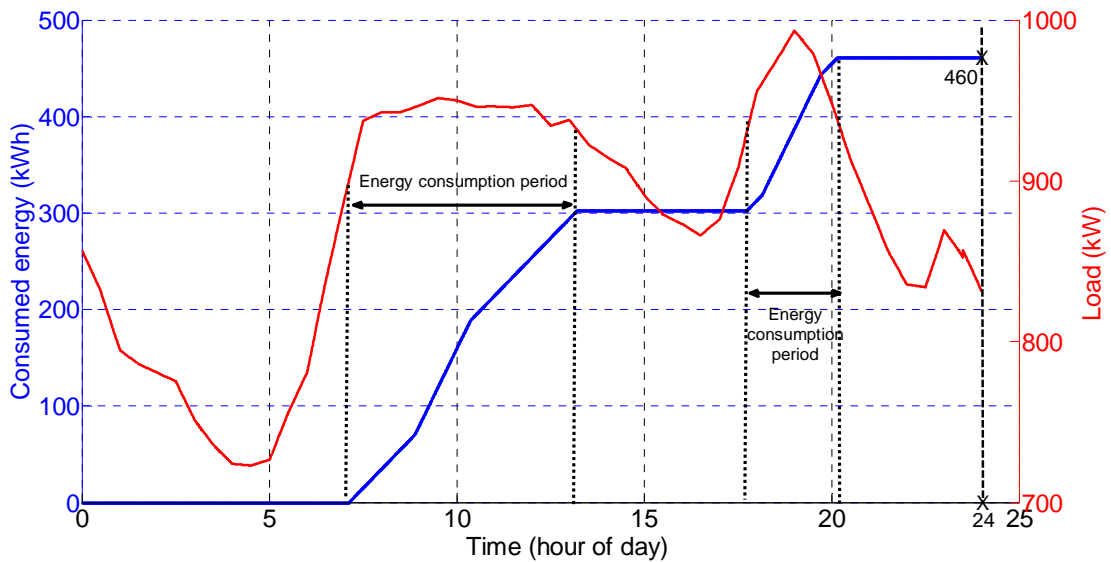


Fig. 4.21: Energy consumption at maximum load values.

The tank is the buffer medium between the stored energy and the consumed one in the studied system. Fig. 4.22 presents the stored energy, consumed energy and the level of total remaining energy in the hydrogen tank during the considered cycle. Accordingly, the hydrogen level in the tank has varied with time and its final value at the end of the cycle should equal zero. The three energy storage periods as well as the two consumption periods mentioned in Fig. 4.20

and 4.21 respectively are clearly demonstrated in Fig. 4.22 and their final values are equal to 460 kWh. Therefore, the total energy level in the hydrogen tank at the end of the considered cycle equal to zero as depicted in Fig. 4.22. Consequently, there is no energy stored at the end of each cycle and the tank has kept its role as a buffer storage element.

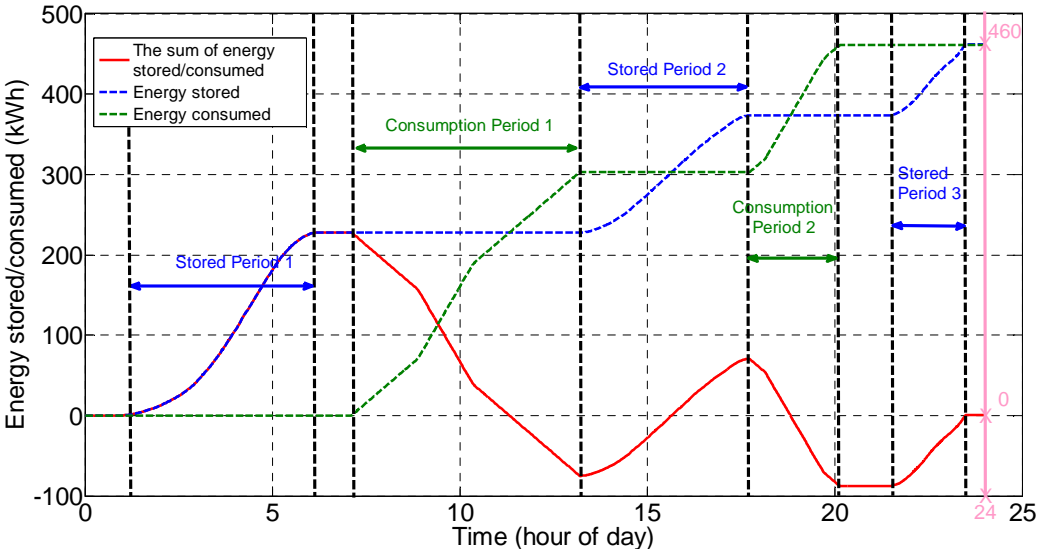


Fig. 4.22: Energy stored in/consumed from the tank and the sum of both during daily operation.

The storage system has correctly performed its energy storage task. Energy has been consumed or stored when necessary. No hydrogen has remained in the tank at the end of the cycle.

4.6. FL FOR ENERGY MANAGEMENT

In Matlab[®] software, GUI tools representing FL toolbox can be used. There are five primary GUI tools for building, editing and observing fuzzy inference systems in the FL toolbox: the Fuzzy Inference System (FIS) Editor, the membership function editor, the rule editor, the rule viewer, and the surface viewer as depicted in Fig. 4.23. These GUIs are dynamically linked. Therefore, the changes made to the FIS using one of them can affect what can be seen on any of the other open GUIs.



Fig. 4.23: GUI tools of FL.

One of two types of fuzzy inference systems can be used in FL [Kaur 12]: the Mamdani and the Sugeno. The Mamdani method has been widely accepted for capturing expert knowledge. It allows describing the expertise in more intuitive, more human-like manner. However, Mamdani-type FIS entails a substantial computational burden. On the other hand, Sugeno method is computationally efficient and works well with optimization and adaptive techniques, which makes it very attractive in control problems, particularly for dynamic nonlinear systems. These adaptive techniques can be used to customize the membership functions so that fuzzy system perfectly models the data. The most fundamental difference between Mamdani-type FIS and Sugeno-type FIS is the way the crisp output has been generated from the fuzzy inputs. While Mamdani-type FIS uses the technique of defuzzification of a fuzzy output, Sugeno-type FIS uses weighted average to compute the crisp output. The expressive power and interpretability of Mamdani output has been lost in the Sugeno FIS since the consequents of the rules are not fuzzy [Kaur 12]. For the energy management using FL, the Mamdani inference system will be used.

FL control method has been applied to set the FCs and ELS power references as shown in Fig. 4.24. These power references represent the ideal powers for which the summation of the produced power of the four sources will track the load. In addition, the second goal is to store the energy according to its cost so that FL will dispatch the energies according to energy cost and its availability as shown in Fig.4.24.

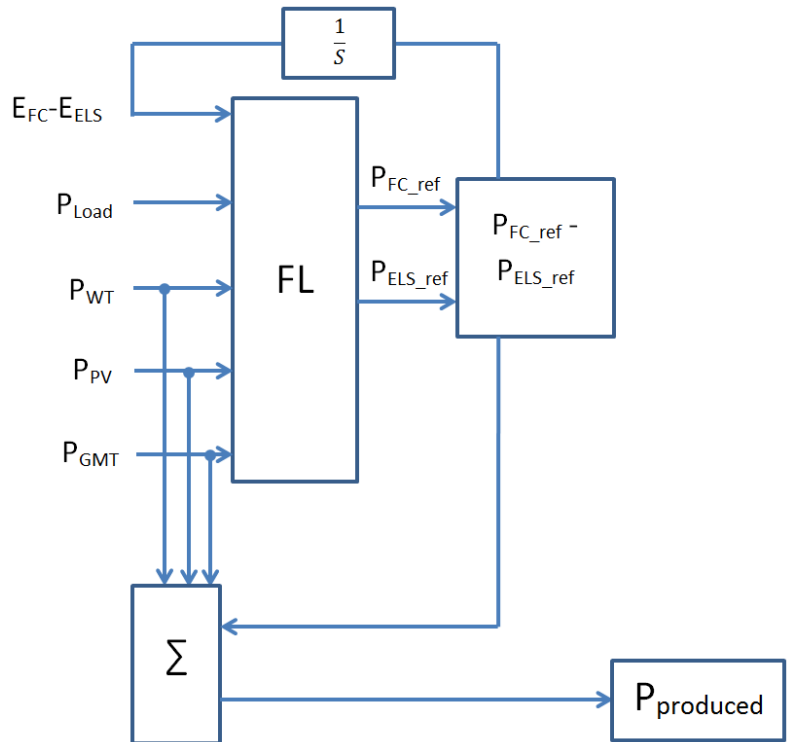


Fig. 4.24: Energy management methodology based on FL.

The FL gives the suitable power references of FC and ELS that depend on the inference rules integrated into the FL. The rules correspond to the minimum cost and the availability of each source. After obtaining the powers of FC and ELS, the subtracting value will be integrated and considered as stored/restored energy in the tank. The sum of this subtracting value with the power values of WT, PV and GMT have been considered as the requested power to cover the load in real time. The FL rules as well as its inputs and outputs have been listed in Appendix (Table A.3 and A.4 respectively).

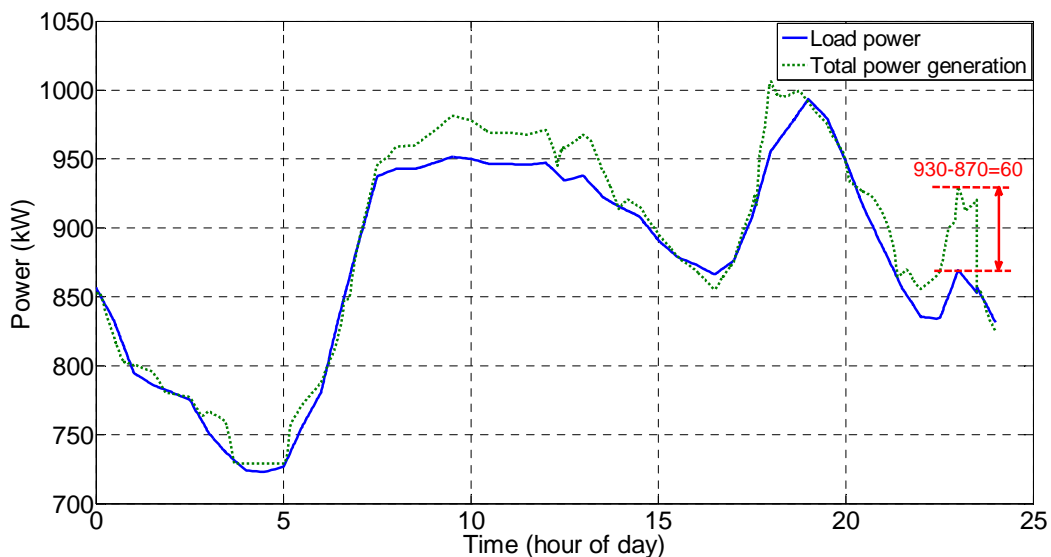


Fig. 4.25: Load tracking by the multi-source power generation using FL.

The comparison between the load and the proposed power from the four sources is illustrated in Fig. 4.25. It is clear that the proposed power management is adequate. The sources total output power is able to track the time variant load with acceptable drift. This last has an

absolute worst-case maximum value referenced to the maximum load of 6%. The stored energy using ELS, the consumed energy using FC and the sum of both stored/consumed energy have been depicted in Fig. 4.26.

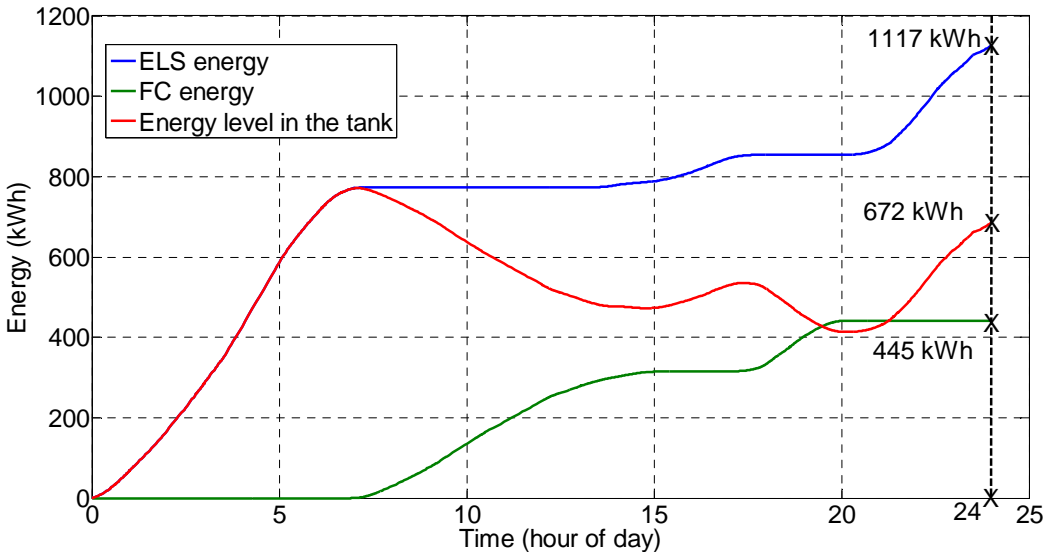


Fig. 4.26: Stored and consumed energies using FL.

From one hand, in the case of energy storage using FL, there is more energy used by ELS compared to NN. Therefore, more energy has been stored in the hydrogen tank. There is about 672 kWh stored in the hydrogen tank after one cycle of 24 hours. This quantity of hydrogen comes from the FL acceptable tracking of the load and the more converting the non-used energy by using ELS. On the other hand, the hydrogen tank at the end of 24 hour cycle was totally empty in case of energy management by using NN.

Consequently, FL is a convenient method for energy management purposes in case of HPSs. It is able to give adequate control to produce a suitable quantity of power to cover the electrical load. In comparison with NN, FL is more appropriate for this task and less stored energy has been achieved. The quantity of hydrogen in the tank at the end of 24 hours cycle is zero and 672 kWh when NN and FL are used respectively.

In this chapter, the economic study has been accomplished using NN for studying the worst case between the two studied techniques and showing the minimum cost reduction. Otherwise, if FL has been used, the obtained result will be better.

4.7. CONCLUSION

In this chapter, the sizing of different sources and the hydrogen storage system has been presented. In addition, the energy management strategy for the multi-source system has been proposed during the 24 hours of load variation. This strategy has considered the intermittence of RESs equipped with BKU generation units and the cost of each. The energy management strategy has been applied using two types of methods: NN and FL. The simulation results have shown that the FL curve conveniently matches the load curve. Obviously, the power generation track the load power with minimum power shifting compared to NN.

GENERAL CONCLUSION

In this thesis a multi-source system including RESs such as PV and WTs as main sources as well as GMT as BKUS was shown. In addition, ESS consisting of PEM ELS, hydrogen tank and PEMFC was injected for enhancing the BKU system. EMR methodology was used for presenting the different sources' models. Different mathematical equations representing the PEM ELS, PEMFC, GMT, PV and WTs models were presented. Moreover, the simulation of each source model has been realized. Consequently, the validation of different models was achieved. Then, the global model of multi-source system was shown. This last one was useful for energy management treated in chapter four.

In addition, the effect of shading, dust or fault conditions on the PV panels was studied. Different solutions were introduced. The MPPT method was applied to maximize the PV output power. Then, PV panels were sized, modelled and simulated to fit the experimental test bench of FCLAB laboratory. The impacts of both temperature and shading on the PV panel efficiency were demonstrated. Then, the PV panel characteristics were experimentally illustrated. Moreover, FL estimator was used for identifying the shaded PV panel, estimating the shading percentage and deciding the connection/disconnection of series/parallel PV panels reconfiguration coupling to minimize the total power losses. This relatively simple and cheap method didn't request any additional MPPT controllers or sensors. Indeed, it was sufficient to use controlled switches and diodes. This new online reconfiguration has the possibility to be employed to n PV panels ($n \geq 4$). Experimental setup has been built and the proposed solution was successfully validated.

After overcoming the shading problem, the PV panels were adapted to provide the PEM ELS with the requested energy. An enhancement of the hybrid PV-PEM ELS system efficiency using the FLC combined with PI control using PV-MPPT was suggested. The FLC was developed in order to instantaneously control the water temperature at specific reference values. The PI control was considered to govern water temperature to its instantaneous optimal value. Moreover, the undesirable temperature surplus of the PV panel could be reused in the hydrogen flow rise in PEM ELS. The hybrid PV-PEM ELS system behaviour was studied considering the temperature rise from 298 K to 363 K. Using EMR modelling of MATLABTM, simulation results illustrated that the increase of water temperature at the entrance of the PEM ELS tank leads to considerably rise in the hydrogen flow amount. Therefore, the overall system efficiency was significantly enhanced.

Moreover, the sizing of different sources and the hydrogen storage system was presented. In addition, the energy management strategy for the multi-source system was proposed during the 24 hours of load variation. This strategy considered the intermittence of RESs equipped with BKU generation units and the cost of each. The energy management strategy was applied using two types of methods: NN and FL. The simulation results showed that the FL curve conveniently matches the load curve. Obviously, the power generation track the load power with minimum power shifting compared to NN.

Hereby, the main scientific contributions of this thesis are:

- using graphical modelling tool EMR for modelling a complex HPS comprising PV, WTs, GMT and FCs;
- the design and experimental implementation of real time PV panels reconfiguration such as shaded PV panels solution;
- the efficiency enhancement of PV-PEM ELS hybrid system by transferring emitted temperature by PV panels to the PEM ELS and control it;

- the proposition of different AI energy management strategies for the studied HPS and conveniently track the load, then comparing the suggested strategies to deduce the most appropriate one.

PERSPECTIVES

- In the studied multi–source sizing, the sources’ volumes were proposed based on the main production of energy via RESs and there were no economic criteria for achieving the ideal point of preference percentage of energy production between conventional power plants and energy storage system. Therefore, the obtained solution was friendly solution but not the most economic one. However, if an optimization method is used for this purpose such as genetic algorithms, the ideal storage volume and power generation from conventional power plants realizing the economic solution will be performed.
- The transferred temperature, emitted from the PVs and injected into PEM ELS in the studied PV–PEM ELS system, had an efficiency enhancement which was verified through the maximization of both the PEM ELS produced H₂ flow and the PV captured energy. However, the ideal temperature for which the balance between the increase in HPS efficiency and the considered physical constraints, especially the temperature limitation to avoid the evaporation, can be founded.
- For the shaded PV panels problem, a reconfiguration PV panels solution based on simple switches and dSPACE electronic card was proposed. The designed FLC program was implemented into the dSPACE because it available in the laboratory. However, PV farm FLC program can be implemented into a PIC microcontroller which is much cheaper than the dSPACE card.
- The proposed shading solution can be compared to the multi–MPPT control’s solution and find out the cost profit percentage.
- The cost of HPS can be calculated and then an economic study comparing the HPS cost with the conventional power plants cost can be performed.
- In the energy management strategy using FL, the membership functions can be modified to perform the appropriate investing of GMT power. In addition, their number can be reduced by combining both provided PV and WT powers such as RES.

REFERENCES

- [Abba 14] Abbasi T, Premalatha M, Abbasi T, Abbasi SA. Wind energy: Increasing deployment, rising environmental concerns. *Int. J. of Renewable and Sustainable Energy Reviews–Elsevier* 2014; 31: 270–288.
- [Abbe 05] Abbey C, Joos G. Energy management strategies for optimization of energy storage in wind power hybrid system. *IEEE 36th Power Electronics Specialists Conf. (PESC'05) 2005*; 2066–2072.
- [Abde 14] Abdelkafi A, Krichen L. Energy management optimization of a hybrid power production unit based renewable energies. *Int. J. of Electrical Power & Energy Systems* 2014; 62: 1–9.
- [Abid 03] Abido MA. Environmental/economic power dispatch using multiobjective evolutionary algorithms. *IEEE Trans. Power Syst.* 2003; 18(4): 1529–1537.
- [Acar 14] Acar C, Dincer I. Comparative assessment of hydrogen production methods from renewable and non-renewable sources. *Int. J. of Hydrogen Energy–Elsevier* 2014; 39(1): 1–12.
- [Adin 13] Adinoyi MJ, Said S. Effect of dust accumulation on the power outputs of solar photovoltaic modules. *Int. J. of Renewable Energy–Elsevier* 2013; 60: 633–636.
- [Agbl 11a] Agbli KS, Péra MC, Hissel D, Rallières O, Turpin C, Doumbia I. Multiphysics simulation of a PEM electrolyser: energetic macroscopic representation approach. *Int. J. of Hydrogen Energy–Elsevier* 2011; 36: 1382–1398.
- [Agbl 11b] Agbli KS, Hissel D, Péra MC, Doumbia I, Turpin C. EMR modelling of PEM electrolyser: real electrical causality approach. (FDfC'2011), Grenoble, France, January 2011; 19–21.
- [Agbl 11c] Agbli KS, Hissel D, Péra MC, Doumbia I. EMR modelling of a hydrogen–based electrical energy storage. *Eur. Phys. J. Appl. Phys.* 2011; 54: 23404–23411.
- [Ahma 08] Ahmad NA, Miyatake M. A novel maximum power point tracking for photovoltaic applications under partially shaded insolation conditions. *Int. J. of Electric Power Systems Research* 2008; 78: 777–784.
- [Ahme 06] Ahmed NA, Miyatake M. A stand–alone hybrid generation system combining solar photovoltaic and wind turbine with simple maximum power point tracking control. *5th Int. Power Electronics and Motion Control Conf. (IPEMC'06) 2006*; 1: 1–7.
- [Alem 14] Alemán-Nava GS, Casiano–Flores VH, Cárdenas–Chávez DL, Díaz-Chavez R, Scarlat N, Mahlknecht J, Dallemard JF, Parra R. Renewable energy research in Mexico: A review. *Int. J. of Renewable and Sustainable Energy Reviews–Elsevier* 2014; 32:140–153.
- [Alon 06] Alonso–Garc MC, Ruizb JM, Chenlo F. Experimental study of mismatch and shading effects in the I–V characteristic of a photovoltaic module. *Int. J. of Solar Energy Materials and Solar Cells* 2006; 90: 329–340.
- [Alta 11] Altam O, Barbir F, Bezmalinovic D. A method for optimal sizing of an electrolyzer directly connected to a PV module. *Int. J. of Hydrogen Energy–Elsevier* 2011; 36: 7012–7018.
- [Arch 07] Archer CL, Jacobson MZ. Supplying base load power and reducing transmission requirements by interconnecting wind farms. *American Metrological Society Journal* 2007; 46(11): 1701–1717
- [Aric 13] Arico AS, Siracusano S, Briguglio N, Baglio V, Di Blasi A, Antonucci V. Polymer electrolyte membrane water electrolysis: Status of technologies and potential applications in combination with renewable power sources. *J. Appl. Electrochem.* 2013; 43: 107–118.
- [Arno 14] Arnone D, Rossi A, Bertoncini N, Proietto R, Moneta D, Tondi G, Garcia–Santiago. Energy management in a smart Grid–integrated hydrogen–based storage. *The 4th Int. Conf. on Smart Grids, Green Communications and IT Energy–aware Technologies: ENERGY 2014*: 86–89.
- [Autt 98] Auttawaitkul Y, Pungsiri B, Chammongthai K, Okuda M. A method of appropriate electric array reconfiguration management for photovoltaic powered car. *IEEE Asia-Pacific Conf. Circuits and Systems (APCCAS'98) 1998*; 201–204.
- [Azmy 05] Azmy AM, Erlich I. Online optimal management of PEM fuel cells using neural networks. *IEEE Trans. Power Del.* 2005; 29(2): 1051–1058.
- [Bach 15] Bacha S, Picault D, Burger B et al. Photovoltaics in microgrids: an Overview of grid integration and energy management aspects. *Industrial Electronics Magazine, IEEE* 2015; 9(1): 33–46.
- [Baer 11] Baert J, Pouget J, Hissel D, Pera MC. Energetic macroscopic representation of a hybrid railway power train. *Vehicle Power and Propulsion Conf. (VPPC'11) 2011*: 1–11.
- [Baer 12] Baert J, Jemei S, Chamagne D, Hissel D, Hibon S, Hegy D. Modeling and energy management strategies of a hybrid electric locomotive. *IEEE Vehicle Power and Propulsion Conf. Oct., 2012*; Seoul, Korea: 9–12.
- [Bahe 06] Baehr HD, Kabelac S. *Thermodynamik*. Volume 13 of Springer, 2006, (in german).
- [Bans 11] Bansal AK, Gupta RA, Kumar R. Optimization of hybrid PV/wind energy system using meta particle swarm optimization (MPSO). *India Int. Conf. on Power Electronics (IICPE'11) 2011*.

- [Bari 09] Barin A, CanhaL N, da Rosa Abaide A, Faverzani Magnago K. Selection of storage energy technologies in a power quality scenario – the AHP and the fuzzy logic. 35th Annual Conf. (IECON'09) 2009; 3115–3120.
- [Bech 10] Becherif M, Hissel D, Gaagat S, Wack M. Three order state space modeling of proton exchange membrane fuel cell with energy function definition. *Int. J. of Power Sources* 2010; 195: 6645–6651.
- [Bech 11] Becherif M, Ayad MY, Hissel D, Mkahl R. Design and sizing of a stand-alone recharging point for battery electrical vehicles using photovoltaic energy. *IEEE Vehicle Power and Propulsion Conf. (VPPC'11)* 2011.
- [Belf 07] Belfkira R, Hajji O, Nichita C et al. Optimal sizing of stand-alone hybrid wind/PV system with battery storage. *European Conference on Power Electronics and Applications* 2007: 1–10.
- [Beni 08] Benitez LE, Benitez PC, van Kooten GC. The economics of wind power with energy storage. *Int. J. of Energy Economics* 2008; 30(4): 1973–1989.
- [Biak 08] Biaku CY, Mann MD, Salehfar H, Peters AJ, Han T. A semiempirical study of the temperature dependence of the anode change coefficient of a 6 kW PEM electrolyser. *Int. J. of Hydrogen Energy–Elsevier* 2008; 33: 4247–4254.
- [Bidr 12] Bidram A, Davoudi A, Balog RS. Control and circuit techniques to mitigate partial shading effects in photovoltaic arrays. *IEEE Journal of Photovoltaics* 2012; 2(4): 532–546.
- [Bitt 06] Bitterlin IF. Modeling a reliable wind/PV/storage power system for remote radio base station sites without utility power. *Int. J. of Power Sources* 2006; 162: 906–912.
- [Blun 11] Blunier B. Lectures ER54 of Master courses at UTBM.
- [Boda 04] Bodansky D. *Nuclear energy: principles, practices, and prospects*. Springer, Oxford, 2004.
- [Boss 07] Bossmann T, Bouscayrol A, Barrade P, Lemoufouet S, Rufer A. Energetic macroscopic representation of a hybridstorage system based on supercapacitors and compressed air. *Int. Conf. on Industrial Electronics* 2007; 2691–2696.
- [Bous 09] Bouscayrol A, Guillaud X, Delarue Ph, Lemaire–Semail B. Energetic macroscopic representation and inversion–based control illustrated on a wind–energy–conversion system using hardware–in–the–loop simulation. *IEEE Conf. on Transactions on Industrial Electronics* 2009; 4826–4835.
- [Boui 13] Bouilouta A, Mellit A, Kalogirou SA. New MPPT method for stand-alone photovoltaic systems operating under partially shaded conditions. *Int. J. of Energy* 2013; 55: 1172–1185.
- [Boul 08] Boulon L, Hissel D, Bouscayrol A, Péra MC, Delarue P. Multi physics modelling and representation of power and energy sources for hybrid electric vehicles. *IEEE Vehicle Power and Propulsion Conf. (VPPC'08)* 2008: 1–6.
- [Bous 00] Bouscayrol A, Davat B, Fornel B, Francois B, Hautier JP, Meibody-Tabar F, Pietrzak-David M. Multi-converter multi-machine systems: application for electrochemical drivers. *The European Physical Journal – Applied Physics* 2000; 10: 13–147.
- [Bous 02] Bouscayrol A, Delarue P, Semail E, Hautier J, Verhille J. Energetic macroscopic representation (EMR) application to a system of multimachine traction: MMS representation of VAL 206. *Revue Int. de Génie Electrique* 2002; 5(3–4): 431–53 [In French].
- [Bous 03a] Bouscayrol A, Delarue P, Tounzi A, Guillard X, Lancigu G. Modelling, control and simulation of an overall wind energy conversion system. *Int. J. of Renewable Energy–Elsevier* 2003; 28: 1169–1185.
- [Bous 03b] Bouscayrol A, Davat B, Fornel B, Françoise B, Hautier JP, Meibody-Tabar E, Monmasson F, Pietrzak-David M, Razik H, Semail E, Benkhoris MF. Control structures for multi-machine multiconverter systems with upstream coupling. *Int. J. of Mathematics and Computers in Simulation–Elsevier* 2003; 63(3-5): 261–270.
- [Bous 05a] Bouscayrol A, Schoenfeld R, Dauphin–Tangy G, Geitner GH, Guillaud X, Pennamen A, Hautier JP. Different energetic descriptions for electromechanical systems. *IEEE Power Electronics and Applications Conf.* 2005.
- [Bous 05b] Bouscayrol A, Delarue P, Guillaud X. Power strategies for maximum control structure of a wind energy conversion system with a synchronous machine. *Int. J. of Renewable Energy–Elsevier* 2005; 30: 2273–2288.
- [Bous 06] Bouscayrol A, Pietrzak David M, Delarue P, Pena-Eguiluz R, Vidal PE, Kestelyn X. Weighted control of traction drives with parallel connected ac machines. *IEEE Transactions on Industrial Electronics* 2006, 53(6): 1799–1806.
- [Bowe 03] Bowen AJ, Zakay N, Ives RL. The field performance of a remote 10 kW wind turbine. *Int. J. of Renewable Energy–Elsevier* 2003; 28(1): 13–33.
- [Brec 11] Brecl K, Topic M. Self-shading losses of fixed free-standing PV arrays. *Int. J. of Renewable Energy–Elsevier* 2011; 36: 3211–3216.
- [Brka 14] Brka A, Al-Abdeli YM, Kothapalli G. The interplay between renewables penetration, costing and

- emissions in the sizing of stand-alone hydrogen systems. *Int. J. of Hydrogen Energy-Elsevier* 2015; 40(1): 125-135.
- [Cau 14] Cau G, Cocco D, Petrollese M, Kaer SK, Milan C. Energy management strategy based on short-term generation scheduling for a renewable microgrid using a hydrogen storage system. *Int. J. of Energy Conversion and Management-Elsevier* 2014; 87: 820-831.
- [Caux 10] Caux S, Hankache W, Fadel M, Hissel D. On-line fuzzy energy management for hybrid fuel cell systems. *Int. J. of Hydrogen Energy-Elsevier* 2010; 35: 2134-2143.
- [Ceng 01] Çengel YA, Turner RH. *Fundamentals of thermal fluid sciences*. McGraw-Hill, New York, 2001.
- [Char 13] Charabi Y, Gastli A. Integration of temperature and dust effects in siting large PV power plant in hot arid area. *Int. J. of Renewable Energy-Elsevier* 2013; 57: 634-644.
- [Ched 97] Chedid R, Rahman S. Unit sizing and control of hybrid wind-solar power systems. *IEEE Trans. Energy Convers.* 1997; 12(1): 79-85.
- [Ched 00] Chedid RB, Karaki SH, El-Chamali C. Adaptive fuzzy control for wind-diesel weak power system. *IEEE Trans. Energy Convers.* 2000; 15(1): 71-78.
- [Chen 03] Chen Z, Hu Y. A hybrid generation system using variable speed wind turbines and diesel units. *The 29th Annual Conf. of the IEEE Industrial Electronics Society (IECON'03)* 2003; 3: 2729-2734.
- [Chen 07] Chenni R, Makhlouf M, Kerbache T, Bouzid A. A detailed modeling method for photovoltaic cells. *Int. J. of Energy* 2007; 32: 1724-30.
- [Chen 13] Chena CC, Changa HC, Kuob CC, Linc CC. Programmable energy source emulator for photovoltaic panels considering partial shadow effect. *Int. J. of Energy* 2013; 54: 174-183.
- [Cher 07] Chrenko D, Péra MC, Hissel D. Fuel cell modeling and control with energetic macroscopic representation. *Int. IEEE Symposium on Industrial Electronics* 2007; 169-174.
- [Chna 05] Chnani M, Maker H, Candusso D, Péra MC, Hissel D. Electrical analogy modelling of pefc system fed by a compressor. *European Fuel Cell Forum, Lucerne, Switzerland, 2005*.
- [Chog 10] Chogumaira EN, Hiyama T, Elbaset AA. Short-term load forecasting using dynamic neural networks. *Proc. Of the Asia-Pacific Power and Energy Engineering Conf. (APPEEC'10)* 2010; 28-31.
- [Chou 15] Choudar A, Boukhetala D, Barkat S, Brucker JM. A local energy management of a hybrid PV-storage based distributed generation for microgrids. *Int. J. of Energy Conversion and Management-Elsevier* 2015; 90: 21-33.
- [Chow 10] Chowdhury SR, Saha H. Maximum power point tracking of partially shaded solar photovoltaic arrays. *Solar Energy Materials and Solar Cells Journal* 2010; 94: 1441-1447.
- [Chre 08] Chrenko D, Péra MC, Hissel D. Inversion based control of a diesel fed low temperature fuel cell system. *The 13th IEEE Power Electronic and Motion Control Conf. (EPE-PEMC'08)* 2008: 2156-2163.
- [Chre 09] Chrenko D, Péra MC, Hissel D, Bouscayrol A. Inversion-based control of a proton exchange membrane fuel cell system using energetic macroscopic representation. *Int. J. of Fuel Cell Science and Technology* 2009; 6: 024501-024505.
- [Cimu 06] Cimuca GO, Saudemont C, Robyns B et al. Control and performance evaluation of a flywheel energy-storage system associated to a variable-speed wind generator. *Industrial Electronics, IEEE Transactions* 2006; 53(4): 1074-1085.
- [Clar 09] Clarke RE, Giddey S, Ciacchi FT, Badwal SPS, Paul B, Andrews J. Direct coupling of an electrolyzer to a solar PV system for generating hydrogen. *Int. J. of Hydrogen Energy-Elsevier* 2009; 34: 2531-2542.
- [Cont 07] Contreras A, Guirado R, Veziroglu TN. Design and simulation of power control system of a plant for the generation of hydrogen via electrolysis, using photovoltaic solar energy. *Int. J. of Hydrogen Energy-Elsevier* 2007; 32: 4635-4640.
- [Dai 15] Dai K, Bergot A, Liang C, Xiang W-N, Huang Z. Environmental issues associated with wind energy-A review. *Int. J. of Renewable Energy-Elsevier* 2015; 75: 911-921.
- [Dali 08] Dali M, Belhadj J, Roboam X. Design of a stand-alone hybrid photovoltaic-wind generating system with battery storage. *Int. J. of Electrical Systems* 2008; 4(3): 25.
- [Degeo 06] Degobert Ph, Kreuawan S, Guillaud X. Use of super capacitors to reduce the fast fluctuations of power of a hybrid system composed of photovoltaic and micro turbine. *Int. Symposium on Power Electronics, Electrical Drives, Automation and Motion (SPEEDAM'06)* 2006; 1223-1227.
- [Dela 03] Delaruea Ph, Bouscayrola A, Tounzia A, GuillaudaX, Lancigub G. Control and simulation of an overall wind energy conversion system. *Int. J. of Renewable Energy-Elsevier* 2003; 28: 1169-1185.
- [Demi 06] Demirel Y, Ozturk HH. Thermoeconomics of seasonal heat storage system. *Int. J. of Energy* 2006; 30: 1001-1012.

- [Dept 11] Dept. of Electr. Eng. King Mongkut's Inst. of Technol. Ladkrabang, Bangkok, Thailand. The efficiency improvement of series connected PV panels operating under partial shading condition by using per-panel DC/DC converter. The 8th Electrical Engineering, Electronics, Computer, Telecommunications and Information Technology (ECTI) Association of Thailand Conference 2011.
- [Diaz 11] Díaz-Dorado E, Suárez-García A, Carrillo JC, Cidrás J. Optimal distribution for photovoltaic solar trackers to minimize power losses caused by shadows. *Int. J. of Renewable Energy* 2011; 36: 1826–1835.
- [Dime 05] Dimeas AL, Hatziaargyriou ND. Operation of a multiagent system for microgrid control. *IEEE Trans. Power Syst.* 2005; 20(3): 1447–1455.
- [Dire 01] Directive 2001/77/EC of the European parliament and of the council of 27 september 2001 on the promotion of electricity produced from renewable energy sources in the internal electricity market. *Official Journal of the European Communities*, L 283/33.
- [DOE 01] A Study by Sandia National Laboratories in USA for the DOE energy storage systems program. *Characteristics and Technologies for Long vs. Short-Term Energy Storage* 2001.
- [Doun 13] Dounis AI, Kofinas P, Alafodimos C, Tseles D. Adaptive fuzzy gain scheduling PID controller for maximum power point tracking of photovoltaic system. *Int. J. of Renewable Energy* 2013; 60: 202–214.
- [Drog 09] Dorgan BL. The case for a 21st century electricity transmission system, Democratic Policy Committee, 2009.
- [Ehte 14] Ehteshami SMM, Chan SH. The role of hydrogen and fuel cells to store renewable energy in the future energy network—potentials and challenges. *Int. J. of Energy Policy* 2014; 73: 103–109.
- [El-Sh 01] El-Shater TF, Eskander M, El-Hagry M. Hybrid PV/fuel cell system design and simulation. 36th Intersociety Energy Conversion Engineering Conference 2001; 112–121.
- [EWEA 09] The European Wind Energy Association. *Wind energy—the facts: a guide to the technology, economics and future of wind power*. 1st edition, Earthscan, 2009.
- [Famo 03] Famouri P, Gemmen RS. Electrochemical circuit model of a pem fuel cell. *Power Engineering Society General Meeting*, Toronto, Canada, 2003.
- [Fero 14] Feroldi D, Zumoffen D. Sizing methodology for hybrid systems based on multiple renewable power sources integrated to the energy management strategy. *Int. J. of Hydrogen Energy—Elsevier* 2014, 39: 8609–8620.
- [Form 05] *Formalismes graphiques de modélisation et de commande de systèmes électromécaniques*. Ecole d'été, July 2005, (in french).
- [Four 06] Fournier M, Agbossou K, Poulin A, Dubé Y, Simard G. Dynamic model of a PEMFC stack suitable for component level modelling of a fuel cell based generator. The 16th World Hydrogen Energy Conference (WHEC'16), Lyon, France 2006; 16: 13–16.
- [Gand 07] Gandía LM, Oroz R, Ursúa A, Sanchis P, Diéguez PM. Renewable hydrogen production: performance of an alkaline water electrolyzer working under Emulated wind conditions. *Int. J. of Energy & Fuels* 2007; 21(3): 1699–1706.
- [Gao 14] Gao D, Jiang D, Liu P, Li Z, Hu S, Xu H. An integrated energy storage system based on hydrogen storage: Process configuration and case studies with wind power. *Int. J. of Energy* 2014; 66: 332–341.
- [Garc 08] Garcia-Valverde R, Miguela C, Martinez-Béjar R, Urbina A. Optimized photovoltaic generator–water electrolyser coupling through a controlled DC-DC converter. *Int. J. of Hydrogen Energy—Elsevier* 2008; 33: 5352–5362.
- [Garc 14] Garcia P, Torreglosa JP, Fernandez LM, Jurado F. Improving long–term operation of power sources in off–grid hybrid systems based on renewable energy, hydrogen and battery. *Int. J. of Power Sources* 2014; 265: 149–159.
- [Garr 07] Garrigos A, Blanesa JM, Carrasco JA, Ejea JB. Real time estimation of photovoltaic modules characteristics and its application to maximum power point operation. *Int. J. of Renewable Energy* 2007; 32: 1059–1076.
- [Geng 11] Geng B, Mills JK, Sun D. Energy management control of micro–turbine–powered plug–in hybrid electric vehicles using telemetry equivalent consumption minimization strategy. *IEEE Transactions on Vehicular Technology* 2011; 60: 4238–4248.
- [Ghaz 14a] Ghazi S, Ip K. The effect of weather conditions on the efficiency of PV panels in the southeast of UK. *Int. J. of Renewable Energy—Elsevier* 2014; 69: 50–59.
- [Ghaz 14b] Ghazi S, Sayigh A, IP K. Dust effect on flat surfaces—Areview paper. *Int. J. of Renewable and Sustainable Energy Reviews* 2014; 33: 742–751.
- [Ghri 13] Ghribi D, Khelifa A, Diaf S, Belhamel M. Study of hydrogen production system by using PV solar energy and PEM electrolyser in Algeria. *Int. J. of Hydrogen Energy—Elsevier* 2013; 38:

- 8480–8490.
- [Gibs 08] Gibson TL, Kelly NA. Optimization of solar powered hydrogen production using photovoltaic electrolysis device. *Int. J. of Hydrogen Energy–Elsevier* 2008; 33: 5931–5940.
- [Glov 08] Glover JD, Sarma MS, Overbye TJ. *Power System Analysis and Design*, 4th ed, Thomson, USA, 2008.
- [Gold 03] Goldstein L, Hedman B, Knowles D, Freedman FI, Woods R, Schweizer T. Gas-fired distributed energy resource technology characterizations. NREL, NREL/TP-620-34783, November 2003.
- [Gonz 04] Gonzalez A, Gallachóir BO, Mckeogh E, Lynch K. Final report of study of electricity storage technologies and their potential to address wind energy intermittency. UCC sustainable Energy Research Group in Ireland, 2004.
- [Goun 09] Gounden NA, Peter SA, Nallandula H, Krithiga S. Fuzzy logic controller with MPPT using line-commutated inverter for three-phase grid-connected photovoltaic systems. *Int. J. of Renewable Energy–Elsevier* 2009; 34: 909–915.
- [GRID 03] GRID 2030: A national vision for electricity's second 100 years, US Department of Energy, 2003.
- [Grim 08] Grimes CA, Varghese OK, Ranjan S. *Light, water, hydrogen; The solar generation of hydrogen by water photoelectrolysis*. New York: Springer, 2008.
- [Guda 06] Guda SR, Wang C, Nehrir MH. Modeling of microturbine power generation system. *Int. J. of Electric Power Components and System* 2006; 34: 1027–1041.
- [Gyuk 04] Gyuk IP, Eckroad S, Key T, Kamath H. EPRI–DOE Handbook supplement of energy storage for grid connected wind generation applications. US Department of Energy, 2004.
- [Haes 14] Haessig P, Multon B, Ahmed HB et al. Quelle importance du choix de la loi de gestion pour dimensionner un système de stockage d'énergie?. *Symposium de Génie Électrique* 2014.
- [Haji 09] Hajizadeh A, Golkar MA. Fuzzy neural control of a hybrid fuel cell/battery distributed power generation system. *IET Renewable Power Generation* 2009; 3(4): 402–414.
- [Hann 93] Hannet LN, Khan A. Combustion turbine dynamic model validation. *IEEE Transactions on Power Systems* 1993; 8(1): 152–158.
- [Harr 05] Harrison KW, Hernandez–Pacheco E, Mann M, Salehfar H. Semiempirical model to determining PEM electrolyseur stack characteristics. *Int. J. of Fuel Cell Science and Technology* 2005; 3(2): 220–223.
- [Haut 96] Hautier JP, Faucher J. Le Graphe Informationnel Causal. *Bulletin de l'Union des Physiciens*, (text in French) 1996; 90: 167–189.
- [Haut 04] Hautier JP, Barre PJ. The causal ordering graph–A tool for modelling and control law synthesis. *Studies in Informatics and Control Journal* 2004; 13(4): 265–283.
- [Hayo 10] Hayoun LP, Arrigoni A. *Les installations photovoltaïques*. 1st ed. Paris: Groupe Eyrolles, 2010.
- [Hern 05] Hernandez A, Hissel D, Outbib R. Electric equivalent model for a hydrogen fuel cell (pefc). In CD-ROM, editor, *Electrimacs Conference, Hammamet, Tunisia*, 2005.
- [Heyd 13] Heydari-doostabada H, Keypoura R, Khalghanib MR, Hassan Khoobanc M. A new approach in MPPT for photovoltaic array based on extremum seeking control under uniform and non-uniform irradiances. *Int J of Solar Energy–Elsevier* 2013; 94: 28–36.
- [Hino 04] Hino R, Haga K, Aita H, Sekita K. R&D on hydrogen production by high-temperature. *Int. J. of Nuclear Engineering and Design–Elsevier* 2004; 233: 363–375.
- [Hiss 08] Hissel D, Péra MC, Bouscayrol A, Chrenko D. Energetic macroscopic representation of a fuel cell. *Revue internationale de génie électrique* 2008; 11(4–5): 603–623.
- [Hohm 03] Hohm DP, Ropp ME. Comparative study of maximum power point tracking algorithms. *Int. J. of Progress in Photovoltaics: Research and Applications* 2003; 11: 47–62.
- [Huan 09] Huang W, Wang X, Guo J, Zhang J, Yang J. Discussion on application of super capacitor energy storage system in microgrid. *Int. Conf. on Sustainable Power Generation and Supply (SUPERGEN'09)* 2009.
- [Ibra 08] Ibrahim H, Iinca A, Perron J. Energy storage systems–characteristics and comparisons. *Int. J. of Renewable and Sustainable Energy Reviews* 2008; 12: 1221–1250.
- [Iwas 94] Iwasaki Y, Simon HA. Causality and model abstraction. *Int. J. of Artificial Intelligence–Elsevier* 1994; 67(1): 143–194.
- [Jian 08] Jiang Z, Dougal R. Hierarchical microgrid paradigm for integration of distributed energy resources. *Proc. IEEE Power Engineering Society General Meeting, Pittsburgh*, 2008: 20–24.
- [Jose 14] Joseline Herbet GM, Iniyani S, Amutha D. A review of technical issues on the development of wind farms. *Int. J. of Renewable and Sustainable Energy–Elsevier* 2014; 32: 619–341.
- [Kako 11] Kakosimos PE, G. Kladas A. Implementation of photovoltaic array MPPT through fixed step predictive control technique. *Int. J. of Renewable Energy–Elsevier* 2011; 36: 2508–2514.
- [Kanc 11] Kanchev H, LU Di, COLAS F et al. Energy management and operational planning of a microgrid with a PV-based active generator for smart grid applications. *Industrial Electronics, IEEE*

- Transactions 2011; 58(10): 4583–4592.
- [Kara 06] Krautier S. *Solar Electric Power Generation*. Springer Berlin Heidelberg, 2006.
- [Kara 07] Karatepe E, Boztepe M, Colak M. Development of a suitable model for characterizing photovoltaic arrays with shaded solar cells. *Int. J. of Solar Energy–Elsevier* 2007; 81: 977–992.
- [Kara 08] Karatepe E, Hiyama T, Boztepe M, Colak M. Voltage based power compensation system for photovoltaic generation system under partially shaded insolation conditions. *Energy Conversion and Management* 2008; 49(8): 2307–2316.
- [Kare 14] Karellas S, Tzouganatos N. Comparison of the performance of compressed–air and hydrogen energy storage systems: Karpathos island case study. *Int. J. of Renewable and Sustainable Energy Reviews* 2014; 29: 865–882.
- [Karn 90] Karnopp D, Margolis DL, Rosenberg RC. *System Dynamics: A Unified Approach*. John Wiley & Sons Inc., 1990.
- [Kasi 13] Kasisomayajula SR. Compressive study on importance of wind power in India. *American Journal of Engineering Research (AJER)* 2013; 2(3): 27–35.
- [Kaur 12] Kaur A, Kaur A. Comparison of mamdani–type and sugeno–type fuzzy inference systems for air conditioning system. *Int. J. of Soft Computing and Engineering (IJSCE)* 2012; 2(2).
- [Kell 08] Kelly NA, Gibson TL, Ouwerkerk DB. A solar powered, high–efficiency hydrogen refuelling system using high–pressure electrolysis of water: Design and initial results. *Int. J. of Hydrogen Energy* 2008; 33: 2747–2764.
- [Ko 07] Ko H, Jatskevich J. Power quality control of wind–hybrid power generation system using fuzzy–LQR control. *IEEE Trans. Energy Convers.* 2007; 22(2): 516–527.
- [Koba 06] Kobayashi K. A study of a two stage maximum power point tracking control of a photovoltaic system under partially shaded insolation conditions. *Solar Energy Materials & Solar Cells* 2006; 90: 2975–2988.
- [Kous 14] Kouskous T, Bruel P, Jamil A, El Rhafiki T, Zeraouli Y. Energy storage: Applications and challenges. *Int. J. of Solar Energy Materiels and Cells* 2014; 120: 59–80.
- [Kuma 12] Kumaravela S, Ashoka S. An optimal stand–alone biomass/solar–PV/pico– hydel hybrid energy system for remote rural area electrification of isolated village in western–ghats region of India. *Int. J. of Green Energy* 2012; 9(5): 398–408.
- [Kusa 15] Kusakana K, Vermaak HJ. Hybrid renewable power systems for mobile telephony base stations in developing countries. *Int. J. of Renewable Energy–Elsevier* 2015; 51: 419–425.
- [Lago 09] Lagorse J, Simoes M, Miraoui A. A multiagent fuzzy–logic–based energy management of hybrid systems. *IEEE Trans. Ind. Appl.* 2009; 45(6): 2123–2129.
- [Lali 13] Lalili D, Mellit A, Lourci N, Medjahed B, Boubakri C. State feedback control and variable step size MPPT algorithm of three–level grid–connected photovoltaic inverter. *Int. J. of Solar Energy* 2013; 98: 561–571.
- [Larm 03] Larminie J, Dicks A. *Fuel cell systems explained*, 2nd edition 2003. Wiley, New York.
- [Lebb 09] Lebbal ME, Lecoche S. Identification and monitoring of a PEM electrolyser based on dynamical modelling. *Int. J. of Hydrogen Energy–Elsevier* 2009; 34: 5992–5999.
- [Lhom 08] Lhomme W, Trigui R, Delarue P, Jeanneret B, Bouscayrol A, Badin F. Switched causal model of transmission with clutch in hybrid electric vehicles. *IEEE Transactions on Vehicular Technology* 2008; 57(4): 2081– 2088.
- [Li 15] Li P, Song YD, Li DY, Cai WC, Zhang K. Control and monitoring for grid–friendly wind turbines: research overview and suggested approach. *IEEE Transaction on Power Electronics* 2015; 30(4): 1979–1986.
- [Liao 10] Liao W, Wang H, Han P. Application of neural network combined with improved algorithm in distorted waveform analysis. *Proc. Of the Chinese Control and Decision Conference (CDCC’10)* 2010; 26–28.
- [Lim 14] Lim YS, Lo CK, Kee SY, Ewe HT, Faidz AR. Design and evaluation of passive concentrator and reflector systems for bifacial solar panel on a highly cloudy region e A case study in Malaysia. *Int. J. of Renewable Energy* 2014; 63: 415–425.
- [Lind 01] Linden D, Reddy TB. *Handbook of batteries*. McGraw–Hill, New York, 2001.
- [Locm 10] Locment F, Sechilariu M. Energetic macroscopic representation and maximum control structure of electric vehicles charging photovoltaic system. *Vehicle Power and Propulsion Conf. (VPPC’10)*, 2010 IEEE; 1–6.
- [Luci 14] Lucia U. Overview on fuel cells. *Int. J. of Renewable and Sustainable Energy Reviews* 2014; 30: 164–169.
- [Luim 09] Luimnigh O, Connolly D. An investigation into the energy storage technologies available, for the integration of alternative generation techniques, 2009; University of Limerick.
- [Mahm 03] Mahmoud MS, Ismail A. Robust decentralized stabilization of thermal–power plants. *Control*

- Applications CCA Proc. IEEE Conf. 2003; 1: 628–632.
- [Male 14] Maleki A, Askarzadeh A. Comparative study of artificial intelligence techniques for sizing of a hydrogen-based stand-alone photovoltaic/wind hybrid system. *Int. J. of Hydrogen Energy* 2014; 39(19): 9973–9984.
- [Manw 10] Manwell JF, McGowan JG, Rogers AL. *Wind energy explained: theory, design application*, 2nd edition 2010; Wiley, New York.
- [Mark 07] Markel A. *Plug-in hybrid-electric vehicle analysis*. NREL, Golden, 2007.
- [Mash 09] Mashhour E, Moghaddas-Tafreshi SM. The opportunities for future virtual power plant in the power market, a view point. *Int. Conf. on Clean Electrical Power* 2009; 448–452.
- [Mass 15] Masson JJ. Comparative impacts of wind and photovoltaic generation on energy storage for small islanded electricity systems. *Int. J. of Renewable Energy* 2015; 80: 793–805.
- [Medi 14] Medina P, Bizuayehu AW, Catalao JPS, Rodrigues EMG, Contreras J. Electrical energy storage systems: technologies' state-of-the-art, techno-economic benefits and applications analysis. 47th Hawaii International Conference on System Science 2014; 2295–2304.
- [Meen 14] Meena N, Baharawani V, Dubey A, Brighu U, Mathur J. Need and comparison of energy storage technologies –a review. *Int. J. of Applied Engineering Research* 2014; 9(2): 177–184.
- [Miet 98] Miettinen K. *Nonlinear Multiobjective Optimization*. Springer, 1998.
- [Moha 14] Mohammed OH, Amirat Y, Benbouzid M, Feld G, Tang T, Elbaset AA. Optimal design of a stand-alone hybrid PV/fuel cell power system for the city of Brest in France. *Int. J. on Energy Conversion* 2014; 2(1): 1–7.
- [Mokr 10] Mokri A, Emziane M. Evaluation of a CPV system with beam-splitting features for hydrogen generation. 35th IEEE Photovoltaic Specialists Conf. (PVSC'10) 2010; 3055–3058.
- [Monn 14] Monnerie N, Roeb M, Houaijia A, Sattler C. Coupling of wind energy and biogas with a high temperature steam electrolyser for hydrogen and methane production. *Int. J. of Scientific Research* 2014; 4: 60–69.
- [Mori 10] Moriana I, San Martin I, Sanchis P. Wind-photovoltaic hybrid systems design. *Proc. of the Int. Symposium on Power Electronics, Electrical Drives, Automation and Motion (SPEEDAM'10)* 2010; 610–615.
- [Mult 13] Multon B, Aubry J, Haessig P et al. *Systèmes de stockage d'énergie électrique*. *Technique de l'Ingénieur* 2013; BE8100.
- [Nguy 08] Nguyen D, Lehman B. An adaptive solar photovoltaic array using model-based reconfiguration algorithm. *IEEE Trans. Ind. Electron.* 2008; 55(17): 2644–2654.
- [Ni 07] Ni M, Leung MKH, Leung DYC. Parametric study of solid oxide steam electrolyzer for hydrogen production. *Int. J. of Hydrogen Energy-Elsevier* 2007; 32: 2305–2313.
- [Ohun 14] Ohunakin OS, Adaramola MS, Oyewola OM, Fagbenle RO. Solar energy applications and development in Nigeria: Drivers and barriers. *Int. J. of Renewable and Sustainable Energy Reviews* 2014; 32: 294–301.
- [Onar 06] Onar OC, Uzunoglu M, Alam MS. Dynamic modeling, design and simulation of a wind/fuel cell/ultra-capacitor-based hybrid power generation system. *Int. J. of Power Sources* 2006; 161(1): 707–722.
- [Onda 04] Onda K, Kyakuno T, Hattori K, Ito K. Prediction of production power for high-pressure hydrogen by high-pressure water electrolysis. *Int. J. of Power Sources* 2004; 132: 64–70.
- [Orne 13] Ornelas-Tellez F and Jesus Rico-Melgoza J. Optimal tracking control for energy management system in micro-grids. *Int. Midwest Symposium on Circuits and Systems (MWSCAS'13)* 2013; 489–492.
- [Pank 04] Pankow Y. *Etude de l'intégration de la production décentralisé dans un réseau basse tension. Application au Générateur Photovoltaïque*. Ph. D. of Ecole National Supérieure d'Arts et Metiers, 2004.
- [Park 04] Park SJ, Kang BB, Yoon JP, Cha IS, Lim JY. A study on the stand-alone operating or photovoltaic wind power hybrid generation system. 35th Annual IEEE Power Electronics Specialists Conference; 2004: 2095–2099.
- [Parr 14] Parra D, Walke GS, Gillott M. Modeling of PV generation, battery and hydrogen storage to investigate the benefits of energy storage for single dwelling. *Int. J. of Sustainable Cities and Society* 2014; 10: 1–10.
- [Paul 08] Paul B, Andrews J. Optimal coupling of PV arrays to PEM electrolyzers in solar-hydrogen systems for remote area power supply. *Int. J. of Hydrogen Energy* 2008; 33: 490–498.
- [Payn 06] Paynter H. *Analysis and design of engineering systems*. MIT Press, 1961.
- [Pére 10] Pérez-Herranz V, Pérez-Page M, Beneito R. Monitoring and control of a hydrogen production and storage system consisting of water electrolysis and metal hydrides. *Int. J. of Hydrogen Energy-Elsevier* 2010; 35: 912–919.

- [Pers 14] Persola A, Serkkola A, Lahdelma R, Salminen P. Multicriteria evaluation of alternatives for remote monitoring systems of municipal buildings. *Int. J. of Energy and Buildings–Elsevier* 2014; 72: 229–237.
- [Peti 14] Petipas F, Brisse A, Bouallou C. Benefits of external heat sources for high temperature electrolyser systems. *Int. J. of Hydrogen Energy* 2014; 5505–5513.
- [Pica 09] Picault D, Raison B, Bacha S. Guidelines for evaluating grid connected PV system topologies. *Int. Conf. on Industrial Technology (ICIT'09)* 2009, 1–5.
- [Pier 07] Pierre M. Electrolysers of water with membrane. *Tech de l'ingenieur* September 2007; J4810: 16 [In French].
- [Poli 14] Polinder H, Bang, D, van Rooij RPJOM, McDonald AS, Mueller MA . 10 MW wind turbine direct-drive generator design with pitch or active speed stall control. *Electrical Machines & Drives Conf. (IEMDC'07)* 2007; 2: 1390–1395.
- [Polo 14] Polonsky J, Mazu P, Paidar M, Christensen E, Bouzek K. Performance of a PEM water electrolyser using a TaC-supported iridium oxide electrocatalyst. *Int. J. of Hydrogen Energy* 2014; 3072–3078.
- [Qi 14] Qi J, Zhang Y, Chen Y. Modeling and maximum power point tracking (MPPT) method for PV array under partial shade conditions. *Int. J. of Renewable Energy* 2014; 66: 337–345.
- [Raba 14] Rabady RI. Solar spectrum management for effective hydrogen production by hybrid thermo-photovoltaic water electrolysis. *Int. J. of Hydrogen Energy* 2014 ;1–10.
- [Rau 14] Rau S, Vierrath S, Ohlmann J, Fallisch A, Lackner D, Dimroth F, Smolinka D. Highly efficient solar hydrogen generation–An integrated concept joining III–V solar cells with PEM electrolysis cells. *Int. J. of Energy Technology* 2014; 2(1): 43–53.
- [Redd 07] Reddy KN, Agarwal V. Utility interactive hybrid distributed generation scheme with compensation feature. *IEEE Trans Energy Convers* 2007; 22(3): 666–673.
- [Ren 15] Ren G, Ma G, Cong N. Review of electrical energy storage system for vehicular applications. *Int. J. of Renewable and Sustainable Energy Reviews* 2015; 41: 225–236.
- [Riff 09] Riffonneau Y, Bacha S, Barruel F, Delaille A. Energy flow management in grid connected PV systems with storage–A deterministic approach. *Int. Conf. On Industrial Technology (ICIT'09)* 2009: 1–6.
- [Rigo 13] Rigo-Mariani R, Sareni B, Roboam X. A fast optimization strategy for power dispatching in a microgrid with storage. *Industrial Electronics Society, IECON 2013-39th Annual Conference of the IEEE* 2013: 7902–7907.
- [Rigo 14a] Rigo-Mariani R, Rigo Sareni B, Roboam X. Optimization methodologies for the power management and sizing of a microgrid with storage. *Symposium de Génie Électrique* 2014.
- [Rigo 14b] Rigo-Mariani R, Rigo Sareni B, Roboam X et al. Optimal power dispatching strategies in smart-microgrids with storage. *Renewable and Sustainable Energy Reviews*, 2014; 40: 649–658.
- [Riha 14] Riahy GH, Khalilnejad A. A hybrid wind–PV system performance investigation for the purpose of maximum hydrogen production and storage using advanced alkaline electrolyzer. *Int. J. of Energy Conversion and Management* 2014; 398–406.
- [Ross 10] Ross TJ. *Fuzzy logic with engineering applications*. 3rd ed., Wiley & Sons, 2010.
- [Rowe 83] Rowen I. Simplified mathematical representations of heavy-duty gas. *ASME Journal of Engineering for Power* 1983; 105(4): 865–869.
- [Roy 06] Roy A, Watson S, Infield D. Comparison of electrical energy efficiency of atmospheric and high-pressure electrolysers. *Int. J. of Hydrogen Energy–Elsevier* 2006; 31: 1964–1979.
- [Sala 90a] Salameh ZM, Liang C. Optimum switching point for array reconfiguration controller. *IEEE 21th Photovoltaic Specialist Conf.* 1990, Kissimmee.
- [Sala 90b] Salameh ZM, Dagher F. The effect of electrical array reconfiguration on the performance of a PV-powered volumetric water pump. *IEEE Trans. Energy Convers* 1990; 5(2): 653–658.
- [Sala 09] Salas V, Alonso-Abella M, Chenlo F, Olias E. Analysis of the maximum power point tracking in the photovoltaic grid inverters of 5 kW. *Int. J. of Renewable Energy* 2009; 34: 2366–2372.
- [Salm 10] Salmani MA, Anzalchi A, Salmani S. Virtual power plant: new solution for managing distributed generation in decentralized power system. *Int. Conf. of Management and Service Science (MASS'10)* 2010; 1–6.
- [Sama 06] Samantaray AK, Medjaher K, Bouamama O, Staroswiecki M, Dauphin–Tanguy G. Diagnostic bond graphs for online fault detection and isolation. *Int. J. of Simulation Modelling Practice and Theory–Elsevier* 2006; 14: 237–262.
- [Sant 05] Santilli M, Moutinho P, Schwartzman S, Nepstad, D, Curran L, Nobre C. *Tropical deforestation and the Kyoto protocol*. Springer, 2005; 71: 267–276.
- [Sara 10] Saravana Ilango G, Srinivasa Rao P, Karthikeyan A, Nagamani C. Single-stage sine wave inverter for an autonomous operation of solar photovoltaic energy conversion system. *Int. J. of*

- Renewable Energy 2010; 35: 275–282.
- [Scho 96] Schoenung SM, Eyer JM, Joseph J. Iannucci, Susan A. Energy storage for a competitive power market. Horgan, 1996.
- [Scib 83] Scibona G, Fabiani C, Scuppa B. Electrochemical behaviour of Nafion type membrane. *Int. J. of Membrane Science* 1983; 16: 37–50.
- [Sema 13] Semaoui S, Arab AH, Bacha S et al. The new strategy of energy management for a photovoltaic system without extra intended for remote-housing. *Solar Energy* 2013; 94: 71–85.
- [Senj 06] Senjyu T, Hayashi D, Urasaki N, Funabashi T. Optimum configuration for renewable generating systems in residence using genetic algorithm. *IEEE Trans Energy Convers* 2006; 21(1): 459–467.
- [Shaa 10] Shaahid SM, El-Amin I, Rehman S, Al-Shehri A, Ahmad F, Bakashwain J, et al. Techno-economic potential of retrofitting diesel power systems with hybrid wind-photovoltaic-diesel systems for off-grid electrification of remote villages of Saudi Arabia. *Int. J. of Green Energy* 2010; 7(6): 632–646.
- [Shah 13] Shahzad A, Kanwal T, He M-G. Design and development of efficient domestic electric cum solar oven. *Int. J. of Basic & Applied Sciences* 2013; 9: 296–301.
- [Shak 05] Shakya BD, Aye L, Musgrave P. Technical feasibility and financial analysis of hybrid wind-photovoltaic system with hydrogen storage for Cooma. *Int. J. of Hydrogen Energy* 2005; 30: 9–20.
- [Sham 13] Shams El-Dein MZ, Kazerani M, Salama MMA. Optimal photovoltaic array reconfiguration to reduce partial shading losses. *IEEE Transactions on Sustainable Energies* 2013; 4(1): 145–153.
- [Sher 02] Sherif RA, Boutros KS. Solar module array with reconfigurable tile. U.S. Patent 6 350 944 B1 2002.
- [Shin 07] Shin Y, Park W, Chang J, Park J. Evaluation of the high temperature electrolysis of steam to produce hydrogen. *Int. J. of Hydrogen Energy* 2007; 32: 1486–1491.
- [Sica 06] Sicard P, Bouscayrol A. Extension of energetic macroscopic representation to time varying systems. *Int. Symposium of Industrial Electronics (ISIE'06)* 2006; 1370–1375.
- [Sing 11] Singhal PK, Sharma RN. Dynamic programming approach for solving power generating unit commitment problem. *Int. Conf. on Computer & Communication Technology (ICCT'11)* 2011; 298–303.
- [Sinh 14] Sinha S, Chandel SS. Review of software tools for hybrid renewable energy systems. *Int. J. of Renewable and Sustainable Energy* 2014; 32: 192–205.
- [Skop 09] Skoplaki K, Palyvos JA. Operating temperature of photovoltaic modules: a survey of pertinent correlations. *Int. J. of Renewable Energy–Elsevier* 2009; 34: 23–29.
- [Sola 09] Solano-Martinez J, Boulon L, Hissel D, Pera MC, Amiet M. Energetic macroscopic representation of a multiple architecture heavy duty hybrid vehicle. *Vehicle Power and Propulsion Conference* 2009; 1322–1329.
- [Sopi 09] Sopian K, Ibrahim MZ, Daud WRW, Othman MY, Yatim B, Amin N. Performance of a PV-wind hybrid system for hydrogen production. *Int. J. of Renewable Energy* 2009; 34: 1973–1978.
- [Spro 09] Sprooten J, Courtecuisse V, Robyns B, Deuse J. Méthodologie de développement de superviseurs à logique floue de centrales multisources à base d'énergie renouvelable. *Revue Internationale de Génie Electrique* 2009; 12(5): 553–583.
- [Stig 14] Stigka EK, Paravantis JA, Mihalakakou GK. Social acceptance of renewable energy sources: A review of contingent valuation applications. *Int. J. of Renewable and Sustainable Energy Reviews* 2014; 32: 100–106.
- [Subk 11] Subkhan M, Komori M. New concept for flywheel energy storage system using SMB and PMB. *IEEE Transactions on Applied Superconductivity* 2011; 21: 1485–1488.
- [Sudo 01] Sudoworth JL. The sodium/nickel chloride (ZEBRA) battery. *J. of Power Sources–Elsevier* 2001; 100: 149–163.
- [Syaf 09] Syafaruddin, Karatepe E, Hiyama T. Polar coordinated fuzzy controller based real time maximum power point control of photovoltaic system. *Int. J. of Renewable Energy–Elsevier* 2009; 34: 2597–2606.
- [Taba 12] Tabanjat A, Becherif M, Hissel D. Hybrid renewable energy system connected to the grid: The hydrogen storage solution. *Int. Conf. on Renewable Energy: Generation and Applications (ICREGA'12)* 2012.
- [Taba 13] Tabanjat A, Becherif M, Emziane M, Hissel D, Mahmah B. Water heating control for efficiency enhancement of proton exchange membrane electrolyser using photovoltaic panels and MPPT. *Int. Conf. on Fundamentals and Development of Fuel Cells (FDFC'13)* 2013.
- [Taba 15] Tabanjat A, Becherif M, Emziane M, Hissel D, Ramadan HR, Mahmah B. Fuzzy logic-based water heating control methodology for the efficiency enhancement of hybrid PV-PEM electrolyser systems. *Int. J. of Hydrogen Energy–Elsevier* 2015; 40(5): 2149–2161.

- [Tali 13] Talin AA, Esposito D, Levin I, Moffat T. Hydrogen Evolution at Si-based metal-insulator-semiconductor photoelectrodes enhanced by inversion channel charge collection and hydrogen spillover. Renewable Energy and the Environment Congress 2013; Tucson, Arizona.
- [Thom 06] Thoma J, Mocellin G. Simulation with entropy in engineering thermodynamics- understanding matter and systems with bondgraphs. Springer, 2006.
- [Torr 08] Torres-Hernandez ME. Hierarchical control of hybrid power systems. Power Electronics Congress (CIEP'2008) 2008; 169–176.
- [Torr 15] Torreglosa JP, Garcia P, Fernandez LM, Jurado F. Energy dispatching based on predictive controller on an off-grid wind turbine/photovoltaic/hydrogen/battery hybrid system. Int. J. of Renewable Energy 2015; 74: 326–336.
- [Trif 14] Trifkovic M, Sheikhzadeh M, Nigim K, Daoutidis P. Modeling and control of a renewable hybrid energy system with hydrogen storage. IEEE Transaction on Control System Technology 2014; 22(1): 169–179.
- [Tyag 07] Tyagi VV, Buddhi D. PCM thermal storage in buildings: a state of art. Int. J. of Renewable and Sustainable Energy 2007; 11: 1146–1166
- [Ubis 09] Ubisse A, Sebitosi A. A new topology to mitigate the effect of shading for small photovoltaic installations in rural sub-Saharan Africa. Energy Conversion and Management 2009; 50: 1797–1801.
- [Ulle 03] Ulleberg Ø. Modeling of advanced alkaline electrolyzers: a system simulation approach. Int. J. of Hydrogen Energy 2003; 28: 21–33.
- [Ural 14] Ural Z, Gencoglu MT. Design and simulation of a solar-hydrogen system for different situations. Int. J. of Hydrogen Energy 2014; 39(16): 8833–8840.
- [Vaid 13] Vaidya V, Wilson D. Maximum power tracking in solar cell arrays using time-based reconfiguration. Int. J. of Renewable Energy 2013; 50: 74–81.
- [Vale 05] Valenciaga F, Puleston PF. Supervisor control for a stand-alone hybrid generation system using wind and photovoltaic energy. IEEE Trans Energy Convers 2005; 20(2): 398–440.
- [Vela 05] Velasco G, Negroni JJ, Guinjoan F, Piqué R. Energy generation in PV grid-connected systems: A comparative study depending on the PV generator configuration. IEEE Int. Symp. Industrial Electronics (ISIE'05) 2005; 3: 1025–1030.
- [Vela 08] Velasco G, Negroni JJ, Guinjoan F, Piqué R. Grid-connected PV systems energy extraction improvement by means of an electric array reconfiguration (EAR) strategy: operating principle and experimental results. IEEE 39th Power Electronics Specialists Conf. (PESC 08) 2008; Rhodes, Greece.
- [Vela 09] Velasco-Quesada G, Guinjoan-Gispert F, Pique-Lopez R, Roman-Lumbreras M, Conesa-Roca A. Electrical PV array reconfiguration strategy for energy extraction improvement in grid-connected PV systems. IEEE Trans. Ind. Electron 2009; 56(11): 4319–4331.
- [Veli 14] Velik R, Nicolay P. Grid-price-dependent energy management in microgrids using a modified simulated annealing triple-optimizer. Int. J. of Applied Energy-Elsevier 2014; 130: 384–395.
- [Verh 04] Verhille JN, Bouscayrol A, Barre PJ, Hautier JP, Semail E. The use of energetic macroscopic representation for control of traction systems: application to subway val 206. In IEEE-VPPC, Paris, France, 2004.
- [Viel 09] Vielstich W, Gasteinger HA, Yokokawa H. Handbook of fuel cells: advances in electrocatalysis, materials, diagnostics and durability. Wiley, New York, 2009.
- [Vina 08] Vinatoru M. Level control of pumped-storage hydro power plants. IEEE Int. Conf. on Automation, Quality and Testing, Robotics (AQTR'08) 2008; 43–47.
- [Walk 04] Walker GR. Cascaded DC-DC converter connection of photovoltaic modules. IEEE Trans. Power Electronics 2004; 19(4): 1130–1139.
- [Wang 08] Wang C, Nehrir MH. Power management of a stand-alone wind/photovoltaic/fuel-cell energy system. IEEE Trans. Energy Convers 2008; 23(3): 957–967.
- [Weil 09] Weili H, Wei D. Wavelet neural network applied to power disturbance Signal in distributed power system. Proc. Of the Chinese Control and Decision Conference (CDCC'09) 2009; 17–19.
- [Yang 07] Yang HX, Lu L, Zhou W. A novel optimization sizing model for hybrid solar-wind power generation system. Int. J. of Solar Energy 2007; 81(1): 76–84.
- [Yang 08] Yang HX, Zhou W, Lu L, Fang ZH. Optimal sizing method for stand-alone hybrid solar-wind system with LPSP technology by using genetic algorithm. Int. J. of Solar Energy 2008; 82(4): 354–67.
- [Yu 04] Yu S, Yuvarajan S. A novel circuit model for pem fuel cells. Applied Power Electronics Conference and Exposition IEEE 2004; 1: 362–366.
- [Zade 65] Zadeh LA. Fuzzy sets. Information and Control 1965; 8, 338–353.
- [Zhan 14a] Zhang L, Gari N, Hmurcik LV. Energy management in a microgrid with distributed energy

- resources. *Int. J. of Energy Conversion and Management* 2014; 78: 297–305.
- [Zhan 14b] Zhang Y, Chen Z, Hu W, Cheng M. Flicker mitigation by individual pitch control of variable speed wind turbines with DFIG. *IEEE Transactions on Energy Conversion* 2014; 29: 20–28.
- [Zhen 14] Zheng H, Li S, Chaloo R, Proano J. Shading and bypass diode impacts to energy extraction of PV arrays under different converter configurations. *Int. J. of Renewable Energy* 2014; 68: 58–66.
- [Zhou 07] Zhou T, Francois B. Modeling and control design of hydrogen production process by using a causal ordering graph for wind energy conversion System. *IEEE Int. Symposium on Industrial Electronics (ISIE'07)* 2007.
- [Zhou 08] Zhou K, Ferreira JA, de Haan SWH. Optimal energy management strategy and system sizing method for standalone photovoltaic-hydrogen systems. *Int. J. of Hydrogen Energy* 2008; 33: 477–489.
- [Zhu 02] Zhu Y, Tomsovic K. Development of models for analyzing the load-following performance of microturbines and fuel cells. *J. of Electric Power* 2002; 62(2): 1–11.
- [Zhu 14] Zhu HY, Yao J, Jiang R, Fu YQ, Wu YH, Zeng GM. Enhanced decolorization of azo dye solution by cadmium sulfide/multi-walled carbon nanotubes/polymer composite in combination with hydrogen peroxide under simulated solar light irradiation. *Ceramics International* 2014; 40: 3769–3777.
- [Zou 14] Zou JP, Lei SL, Yu J, Luo SL, Luo XB, Tang XH, Dai WL, Sun J, Guo GC, Aua CT. Highly efficient and stable hydrogen evolution from water with CdS as photosensitizer—A noble-metal-free system. *Int. J. of Applied Catalysis B: Environmental* 2014; 150–151: 466–471.

Website references

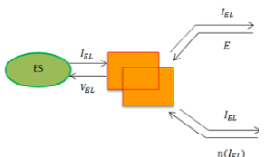
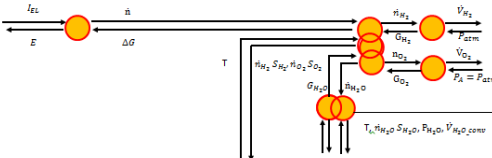
- [Site 01] <http://www.csiro.au/science/Ultra-Battery.html>
- [Site 02] <http://www.bydit.com/doce/products/li.asp>
- [Site 03] http://www.electricitystorage.org/site/technologies/li-ion_batteries/
- [Site 04] http://forschung-energiespeicher.info/en/project-showcase/industrial_processes/project-single-view//Stacks_auf_Herz_und_Nieren_testen/
- [Site 05] Bond graph information. www.bondgraph.info.
- [Site 06] <http://www.emrwebsite.org/energetic-macroscopic-representation.html>
- [Site 07] http://cp.literature.agilent.com/litweb/pdf/ads2008/optstat/ads2008/Summary_of_Optimizers.html
- [Site 08] <http://solareis.anl.gov/guide/solar/pv/index.cfm>
- [Site 09] <http://fr.mathworks.com/products/neural-network/>

APPENDIX

Table A.1: PEMFC operation conditions.

Number of single cells	20
Operating temperature (°C)	20-65
Nominal temperature (°C)	55
Cell area (cm²)	100
Operating pressure (bar)	1 - 1.5
Differential pressure between anode and cathode compartments	Up to 0.6
Inlet media	Pure hydrogen De-ionized cooling water

Table A.2: PEM electrolyser EMR sub-models [Agbl 11].

	EMR	General formula
Electrical sub-model		1) $V_{EL} = E + \eta(I_{EL})$
Electrochemical and thermodynamic sub-model		2) $E = \frac{\Delta G}{nF}$ 3) $\dot{n} = \dot{n}_{H_2O} = \dot{n}_{H_2} = 2 \dot{n}_{O_2} = \eta_F \frac{I_{EL}}{2F} N_{cell}$ 4) $\Delta S_{H_2O, H_2, O_2} = A \cdot \ln(t) + B \cdot t + C \frac{t^2}{2} + D \frac{t^3}{2} - \frac{E}{2t^2} + G$ 5) $\Delta H_{H_2O, H_2, O_2} = At + B \frac{t^2}{2} + C \frac{t^3}{3} + D \frac{t^4}{4} - \frac{E}{t} + F - H$ 6) $\Delta G = \Delta H + T\Delta S$

Thermal sub-model		<p>7) $T\Delta S = 2F(\eta_{EL} + \eta_{diff} + R_ej)$</p> <p>8) $\Delta S_{\eta_{Total}} = \dot{n} \Delta S = I_{EL} \frac{(\eta_{EL} + \eta_{diff} + R_ej)}{T}$</p> <p>9) $\eta_{EL} = E_{act-anod} + E_{act-cath} = \frac{RT}{2\alpha_A F} \sinh^{-1}\left(\frac{I}{2j_{0,A}A}\right) + \frac{RT}{2\alpha_C F} \sinh^{-1}\left(\frac{I}{2j_{0,C}A}\right)$</p> <p>10) $E_{ohm} = R_ej = \frac{\phi}{\sigma_m} j$</p> <p>11) $C_p \frac{dT}{dt} = T \left[\sum (\Delta S_q)_{in} - \sum (\Delta S_q)_{out} \right]$</p> <p>12) $\Delta S_{q_{H_2O_Mem}} = \left(\frac{\dot{Q}_{H_2O_Mem}}{T} \right)$</p> <p>13) $\Delta S_{q_{H_2,O_2}} = \frac{\dot{Q}_{H_2,O_2}}{T}$</p> <p>14) $\Delta S_{q_{H_2O,H_2,O_2}} = \sum_{i=H_2O,H_2,O_2} \dot{n}_i \Delta S_i$</p> <p>15) $\Delta S_{q_{losses}} = \frac{\dot{Q}_{losses}}{T}$</p> <p>16) $\Delta S_{q2} = \Delta S_{q_{H_2O_Mem}} + \Delta S_{q_{H_2,O_2}} + \Delta S_{q_{H_2O,H_2,O_2}} (\sum_{i=H_2O,H_2,O_2} \dot{n}_i \Delta S_i) + \Delta S_{q_{losses}} (\Delta S_{q_conv})$</p> <p>17) $\dot{Q}_{losses} = \frac{1}{R_t} (T - T_{amb}) \Delta S_{q_{losses}} = \frac{\dot{Q}_{losses}}{T}$</p>
Hydraulic sub-model		<p>18) $\dot{V}_{H_2O} = \frac{\delta P}{R_h}$</p> <p>19) $\rightarrow \delta P = \dot{V}_{H_2O} \cdot R_h$</p> <p>20) $\dot{V}_{Liq} = \dot{V}_{Liq_In} - (\dot{V}_{react} + \dot{V}_{Mem})$</p> <p>21) $C_h \frac{dP_A}{dt} = \dot{V}_{Liq} - \dot{V}_{Liq_Gaz}$ $\dot{V}_{Liq} = \dot{V}_{Liq_In} - (\dot{V}_{react} + \dot{V}_{Mem})$</p> <p>22) $\dot{Q}_{H_2O} = \dot{m}_{H_2O} C_{PH_2O} (T - T_{amb})$</p> <p>23) $\dot{m}_{H_2O} = \dot{V}_{H_2O} \rho_{H_2O}$</p> <p>24) $\Delta S_{q_{H_2O}} = \left(\frac{\dot{Q}_{H_2O}}{T} \right)$</p>

Table A.3: Fuzzy logic rules used for the energy management*.

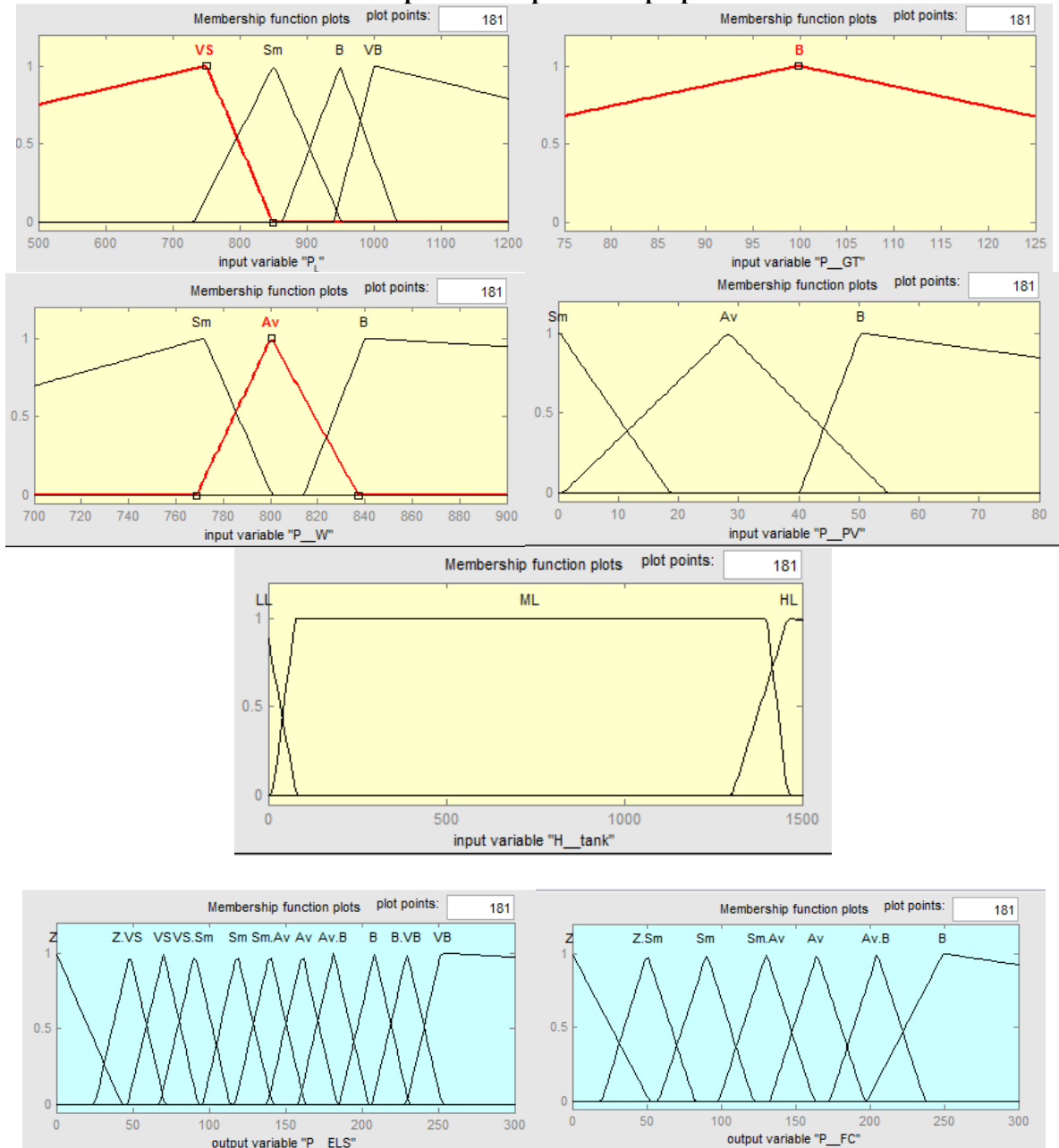
Rules	P _{Load}	P _{GMT}	P _{WT}	P _{PV}	H ₂ tank level	P _{ELS}	P _{FC}
1	VS	B	Sm	Sm	LL	Sm.AV	Z
2	VS	B	Sm	Sm	ML	Sm.AV	Z
3	VS	B	Sm	Sm	HL	Z	Z
4	VS	B	AV	Sm	LL	AV	Z
5	VS	B	AV	Sm	ML	AV	Z
6	VS	B	AV	Sm	HL	Z	Z
7	VS	B	B	Sm	LL	B	Z
8	VS	B	B	Sm	ML	B	Z
9	VS	B	B	Sm	HL	Z	Z
10	Sm	B	Sm	Sm	LL	Z	Z
11	Sm	B	Sm	Sm	ML	Z	Z
12	Sm	B	Sm	Sm	HL	Z	Z
13	Sm	B	AV	Sm	LL	Z.VS	Z
14	Sm	B	AV	Sm	ML	Z.VS	Z
15	Sm	B	AV	Sm	HL	Z	Z
16	Sm	B	B	Sm	LL	VS.Sm	Z
17	Sm	B	B	Sm	ML	VS.Sm	Z
18	Sm	B	B	Sm	HL	Z	Z
19	B	B	Sm	Sm	LL	Z	Z

20	B	B	Sm	Sm	ML	Z	Sm
21	B	B	Sm	Sm	HL	Z	Sm
22	B	B	AV	Sm	LL	Z	Z
23	B	B	AV	Sm	ML	Z	Z.Sm
24	B	B	AV	Sm	HL	Z	Z.Sm
25	B	B	B	Sm	LL	Z	Z
26	B	B	B	Sm	ML	Z	Z
27	B	B	B	Sm	HL	Z	Z
28	VB	B	Sm	Sm	LL	Z	Z
29	VB	B	Sm	Sm	ML	Z	Sm.AV
30	VB	B	Sm	Sm	HL	Z	Sm.AV
31	VB	B	AV	Sm	LL	Z	Z
32	VB	B	AV	Sm	ML	Z	Sm
33	VB	B	AV	Sm	HL	Z	Sm
34	VB	B	B	Sm	LL	Z	Z
35	VB	B	B	Sm	ML	Z	Z.Sm
36	VB	B	B	Sm	HL	Z	Z.Sm
37	VS	B	Sm	AV	LL	Sm.AV	Z
38	VS	B	Sm	AV	ML	Sm.AV	Z
39	VS	B	Sm	AV	HL	Z	Z
40	VS	B	AV	AV	LL	AV.B	Z
41	VS	B	AV	AV	ML	AV.B	Z
42	VS	B	AV	AV	HL	Z	Z
43	VS	B	B	AV	LL	B	Z
44	VS	B	B	AV	ML	B	Z
45	VS	B	B	AV	HL	Z	Z
46	Sm	B	Sm	AV	LL	Z.VS	Z
47	Sm	B	Sm	AV	ML	Z.VS	Z
48	Sm	B	Sm	AV	HL	Z	Z
49	Sm	B	AV	AV	LL	VS	Z
50	Sm	B	AV	AV	ML	VS	Z
51	Sm	B	AV	AV	HL	Z	Z
52	Sm	B	B	AV	LL	Sm	Z
53	Sm	B	B	AV	ML	Sm	Z
54	Sm	B	B	AV	HL	Z	Z
55	B	B	Sm	AV	LL	Z	Z
56	B	B	Sm	AV	ML	Z	Z.Sm
57	B	B	Sm	AV	HL	Z	Z.Sm
58	B	B	AV	AV	LL	Z	Z
59	B	B	AV	AV	ML	Z	Z.Sm
60	B	B	AV	AV	HL	Z	Z.Sm
61	B	B	B	AV	LL	Z	Z
62	B	B	B	AV	ML	Z	Z
63	B	B	B	AV	HL	Z	Z
64	VB	B	Sm	AV	LL	Z	Z

65	VB	B	Sm	AV	ML	Z	Sm
66	VB	B	Sm	AV	HL	Z	Sm
67	VB	B	AV	AV	LL	Z	Z
68	VB	B	AV	AV	ML	Z	Sm
69	VB	B	AV	AV	HL	Z	Sm
70	VB	B	B	AV	LL	Z	Z
71	VB	B	B	AV	ML	Z	Z.Sm
72	VB	B	B	AV	HL	Z	Z.Sm
73	VS	B	Sm	B	LL	AV	Z
74	VS	B	Sm	B	ML	AV	Z
75	VS	B	Sm	B	HL	Z	Z
76	VS	B	AV	B	LL	B	Z
77	VS	B	AV	B	ML	B	Z
78	VS	B	AV	B	HL	Z	Z
79	VS	B	B	B	LL	B.VB	Z
80	VS	B	B	B	ML	B.VB	Z
81	VS	B	B	B	HL	Z	Z
82	Sm	B	Sm	B	LL	VS	Z
83	Sm	B	Sm	B	ML	VS	Z
84	Sm	B	Sm	B	HL	Z	Z
85	Sm	B	AV	B	LL	VS.Sm	Z
86	Sm	B	AV	B	ML	VS.Sm	Z
87	Sm	B	AV	B	HL	Z	Z
88	Sm	B	B	B	LL	Sm.AV	Z
89	Sm	B	B	B	ML	Sm.AV	Z
90	Sm	B	B	B	HL	Z	Z
91	B	B	Sm	B	LL	Z	Z
92	B	B	Sm	B	ML	Z	Z.Sm
93	B	B	Sm	B	HL	Z	Z.Sm
94	B	B	AV	B	LL	Z	Z
95	B	B	AV	B	ML	Z	Z
96	B	B	AV	B	HL	Z	Z
97	B	B	B	B	LL	Z.VS	Z
98	B	B	B	B	ML	Z.VS	Z
99	B	B	B	B	HL	Z	Z
100	VB	B	Sm	B	LL	Z	Z
101	VB	B	Sm	B	ML	Z	Sm
102	VB	B	Sm	B	HL	Z	Sm
103	VB	B	AV	B	LL	Z	Z
104	VB	B	AV	B	ML	Z	Z.Sm
105	VB	B	AV	B	HL	Z	Z.Sm
106	VB	B	B	B	LL	Z	Z
107	VB	B	B	B	ML	Z	Z
108	VB	B	B	B	HL	Z	Z

* **VS:** Very Small, **Sm:** Small, **B:** Big, **VB:** Very Big, **AV:** Average, **LL:** Low level, **ML:** Medium Level, **HL:** High Level, **Z:** Zero, **Z.VS:** Zero Very Small, **VS.Sm:** Very Small Small, **Sm.AV:** Small Average, **AV.B:** Average Big, **Z.Sm:** Zero Small, **Sm. AV:** Small Average.

Table A.4: Inputs and outputs of the proposed FLC.



Explication the membership function selection

The numeric values of membership functions inputs and outputs are given depending on the power value of each.

The FL maximum power inputs of P_L , P_{GMT} , P_W and P_{PV} are 1000, 100, 800 and 63 kW respectively. Its maximum power outputs of P_{ELS} and P_{FC} are 250 kW for each. One membership function is selected to present the GMT power as it works during the whole cycle. Several membership functions are indicated to present the ELS and FC powers as their

role of storing and reuse the stored energy requests the accuracy of tracking the sources and the load power changes.

The proposed tank can store up to 1300 kWh of energy. The excess energy will be considered as stored energy at high level in the hydrogen tank, then it cannot be stored and the ELS will be stopped.

The inputs and outputs achieve the following equation all the time:

$$P_L = P_{GMT} + P_W + P_{PV}$$

Each disorder on this equation will require the operation of FC or ELS and the change of the applied rule from Table A.3 as well. This algorithm is considered when the membership functions are established.

MY PUBLICATIONS

1. A. Tabanjat, M. Becherif, D. Hissel. Reconfiguration solution for shaded PV panels using switching control. *International Journal of Renewable Energy-Elsevier* 2014; 82: 4–13.
2. A. Tabanjat, M. Becherif, M. Emziane, D. Hissel, H. S. Ramadan, B. Mahmah, Fuzzy logic-based water heating control methodology for the efficiency enhancement of hybrid PV-PEM electrolyser systems. *International Journal of Hydrogen Energy* 2015; 40(5): 2149–2161.
3. F.Z. Aouali, M. Becherif, A. Tabanjat, M. Emziane, K. Mohammedi, S. Krehi, A. Khellaf. Modelling and experimental analysis of a PEM electrolyser powered by a solar photovoltaic panel. *International Journal of Energy Procedia* 2014; 62: 714–722.
4. A. Tabanjat, M. Becherif, D. Hissel. Reconfiguration solution for shaded PV panels using fuzzy logic. *ICREGA'14- Renewable Energy: Generation and Applications 2014; Chapter 13 Springer: 161–177.*
5. A. Tabanjat, M. Becherif, D. Hissel. Reconfiguration solution for shaded PV panels using fuzzy logic. *The 3rd International Conference on Renewable Energy: Generation and Applications 2014 (ICREGA'14).*
6. A. Tabanjat, M. Becherif, D. Hissel. Hybrid renewable Energy system connected to the grid: the hydrogen storage solution. *The 2nd International Conference on Renewable Energy: Generation and Applications 2012 (ICREGA'12).*
7. A. Tabanjat, M. Becherif, M. Emziane and D. Hissel. Water heating control for efficiency enhancement of proton exchange membrane electrolyser using photovoltaic panels and MPPT. *The 5th International Conference of the fundamentals and development of fuel cells 2013 (FDGC'13).*
8. F. Bandou, M. Becherif, P.O. Logerais, A. Hadj Arab, M.S. Belkaid, A.Tabanjat. Détection et localisation des échauffements dans un module photovoltaïque. *2^{ème} Conférence Internationale des Energies Renouvelables 2014 (CIER'14).*
9. Fatima Zohra Aouali, Mohamed Becherif, Mahieddine Emziane, Serge Krehi, Kamal Mohammedi, Abdulkader Tabanjat. Modelling and experimental analysis of a PEM electrolyser powered by a solar photovoltaic panel. *International conference on sustainable in Energy and Buildings 2014 (SEB–14).*
10. A. Tabanjat. Amélioration du rendement d'un système hybride basé sur une double commande MPPT et logique floue. *Journées des Jeunes Chercheurs en Génie Electrique 2015 (JCGE'15).*

ABSTRACT

The limited reserves of fossil fuel and the pollution gases produced pave the way to promising alternative Renewable Energy Sources (RESs) such as Solar Energy Sources (SESs) and Wind Energy Sources (WESs). SESs and WESs are freely available and environmentally friendly. However, RESs are intermittent in nature. Therefore, the smoothing of power fluctuations by storing the energy during periods of oversupply and restore it to the grid when demand becomes necessary. Accordingly, Energy Storage Systems (ESSs) can be appropriately used for this purpose.

Using several energy sources for constructing HPSs alongside with ESS will require an energy management strategy to achieve minimum HPS cost and optimal balance between energy generation and energy consumption. This energy management method is a mechanism to achieve an ideal energy production and to conveniently satisfy the load demand at relatively high efficiency.

In this thesis, a Hybrid Power System (HPS) including Renewable Energy Sources (RESs) such as main sources combined with Gas Micro-Turbine (GMT) and hydrogen storage system such as Back-up Sources (BKUSs) has been presented. The aim of this hybridization is to build a reliable system, which is able to supply the load and having the ability to store the excess energy in hydrogen form and reuse it later when demanded. Consequently, the stored energy at the end of each cycle will be zero and a minimum generated power cost is achieved. In addition, partial shading problem of Photovoltaic (PV) panels is comprehensively studied and a new solution based on simple switches and Fuzzy Logic Control (FLC) integrated into dSPACE electronic card is created. Consequently, a real time PV panels reconfiguration and disconnecting shaded ones is performed and minimum power losses is achieved. Then, the PV panels are connected to a Proton Exchange Membrane Electrolyser (PEM ELS). The emitted temperature by the PV panels is transferred to the endothermic element PEM ELS. Consequently, an efficiency enhancement of the hybrid system PV-PEM ELS is realized.

RESUME

Les réserves limitées de combustibles fossiles et la pollution entraînée par les gaz produits ouvrent la voie à des ressources énergétiques renouvelables (RER) alternatives et prometteuses telles que les ressources solaires (RS) et les ressources éoliennes (RE). Ces ressources sont librement disponibles et respectueuses de l'environnement. Cependant, les RER sont de nature intermittente. Par conséquent, il existe un besoin de lissage des fluctuations de puissance en stockant l'énergie pendant les périodes de surproduction pour la restituer au réseau lorsque la demande énergétique devient importante. Les systèmes de stockage de l'énergie (SSE) peuvent alors être utilisés de manière appropriée à cette fin.

L'utilisation de plusieurs sources d'énergie et de stockeurs pour construire des systèmes de puissance hybrides (SPH) exige une stratégie de gestion de l'énergie pour atteindre le minimum de coût des SPH et un équilibre entre la production et la consommation de l'énergie. Cette méthode de gestion de l'énergie est un mécanisme pour obtenir une production d'énergie idéale et pour satisfaire convenablement la demande de charge à rendement relativement élevé.

Dans cette thèse, un SPH intégrant production électrique photovoltaïque, éolienne, une micro-turbine à gaz ainsi qu'un système de stockage de l'électricité par le vecteur hydrogène est considéré. Le but de cette hybridation est de construire un système fiable, qui est en mesure de fournir la charge et qui a la capacité de stocker l'énergie excédentaire sous forme hydrogène et de la réutiliser plus tard. En outre, le problème d'ombrage partiel de Panneaux Photovoltaïques est étudié de manière approfondie. Une nouvelle solution basée sur des interrupteurs simples et un contrôle par logique floue intégré dans une carte électronique dSPACE a été proposée. Une reconfiguration des panneaux photovoltaïques en temps réel et de déconnexion de ceux ombragés est également effectuée en cherchant à minimiser les pertes de puissance. Le couplage thermique entre ces panneaux photovoltaïques et un électrolyseur à membrane polymère est également étudié, à l'échelle système. En récupérant une partie de l'énergie thermique reçue par les panneaux, une amélioration du rendement du système hybride PPV-ELS MEP est réalisée.

The logo for SPIM (École doctorale SPIM) features a blue horizontal bar on the left, followed by the letters 'S', 'P', 'I', and 'M' in a large, white, sans-serif font.

■ École doctorale SPIM - Université de Technologie Belfort-Montbéliard

F - 90010 Belfort Cedex ■ tél. +33 (0)3 84 58 31 39

■ ed-spim@univ-fcomte.fr ■ www.ed-spim.univ-fcomte.fr

